AD-A182 590

AMPLIFIED SPONTANEOUS EMISSION OF THE

IODINE $B^3\Pi(0_u^+) - X^1\Sigma(0_g^+)$ SYSTEM

DISSERTATION

AFIT/DS/PH/87-2          John W. Glessner
                        Captain      USAF

DEPARTMENT OF THE AIR FORCE
AIR UNIVERSITY
# AIR FORCE INSTITUTE OF TECHNOLOGY

Wright-Patterson Air Force Base, Ohio

87    22 082

AMPLIFIED SPONTANEOUS EMISSION OF THE

IODINE $B^3\Pi(0_u^+)$ - $X^1\Sigma(0_g^+)$ SYSTEM

DISSERTATION

AFIT/DS/PH/87-2          John W. Glessner
                        Captain     USAF

# AMPLIFIED SPONTANEOUS EMISSION OF THE
# IODINE $B^3\Pi(0_u^+) - X^1\Sigma(0_g^+)$ SYSTEM

## DISSERTATION

Presented to the Faculty of the School of Engineering

of the Air Force Institute of Technology

Air University

in Partial Fulfillment of the

Requirements for the Degree of

Doctor of Philosophy

by

John W. Glessner, B.S., M.S.

Captain                            USAF

| Accession For | |
| --- | --- |
| NTIS GRA&I | ☒ |
| DTIC TAB | ☐ |
| Unannounced | ☐ |
| Justification | |

| By | |
| --- | --- |
| Distribution/ | |

| Availability Codes | |
| --- | --- |
| Dist | Avail and/or Special |
| A-1 | |

April 1987

# AMPLIFIED SPONTANEOUS EMISSION OF THE
## IODINE $B^3\Pi(0_u^+)$ – $X^1\Sigma(0_g^+)$ SYSTEM

by

John W. Glessner, B.S., M.S.

Captain                              USAF

Approved:

_Ernest K. Darko_     _27 MAR. 87_
Chairman

_____     _27 MAR 87_

_Steve J. Davis_     _31 March 87_

_Robert J. Carel_     _10 APR 87_

_Won B. Roh_     _27 Mar 87_

Accepted:

_JS Przemieniecki_     _8 June 1987_

Dean, School of Engineering

# ACKNOWLEDGEMENTS

## Table of Contents

# Table of Contents

## List of Figures

## List of Figures

## List of Figures

# List of Figures

# List of Tables

## Abstract

Amplified spontaneous emission (ASE) via optical excitation of the $B^3\Pi(0_u^+) - X^1\Sigma(0_g^+)$ system of molecular iodine has been studied. Rotationally resolved excitation and emission spectroscopy over the entire B-X manifold was investigated. The relative reduction of ASE output energy through collisional losses was studied for various buffer gases. A parametric study of output performance, including gain and conversion efficiency, was also performed.

ASE was observed for the pump wavelength range 604-514 nm. This wavelength range produced excited $I_2$(B) with vibrational excitation of $v' = 7-44$. Subsequent emission to the $I_2$(X) state occured to the vibrational levels $v'' = 38-84$. Emission for these transitions occured in the wavelength range of 1.07-1.34 micro $\mu$m.

The rotational dependence of the ASE showed two distinct regions. The normal emission intensity varied with the rotational Boltzmann population distribution with a threshold requirement, with emission over the region of $25 \lesssim J \lesssim 85$. The spike emission displayed an abnormally strong signal near the pump bandhead. Also, spike emission consisted of a single line rather than doublet emission.

The spike is the result of a cooperative stimulated emission (CSE) of several, simultaneously populated rotational levels whose emission occurs within the Doppler

width of any one of the levels involved (called a
superlevel). A superlevel is formed of rotational levels
that emit at the emission bandhead in the R branch. Through
stimulated emission, independent rotational levels combine
their subthreshold populations to exceed threshold and emit
as one "super" level. The CSE hypothesis was verified by
use of computer modeling.

Through a simple model, the superlevel was observed to
be remarkably immune to collisional quenching. This was
verified by using buffer gases (He, Ar, Xe, and $N_2$) to study
the relative quenching of the ASE in both the spiked and
normal band regions.

The ASE output energy was studied as a function of
iodine pressure, gain cell length, and pump energy. Output
powers as high as 60 $\mu$Joules per pulse were recorded at 320
mTorr pressure and 204 cm cell length. Using the model that
a single photon initiates ASE, a total gain of 33.6, or
16.5 % per cm, was calculated from the above conditions.
Energy conversion efficiencies of 2% were calculated, with
4.5% quantum efficiency.

ASE performance was greatly increased when the iodine
cell was heated. Output energies of 0.5 mJoules per pulse
were realized at $65^{\circ}$c for a 98 cm cell. Iodine ASE has
potential application for a simple visible to near-infrared
wavelength converter for various spectroscopic uses.

# I. INTRODUCTION

## A. Background

The subject of optically pumped lasers (OPL) has grown
into an important new field of research, largely due to the
availability of suitable pump lasers. Optical pumping with
lasers has numerious advantages over other sources
(flashlamps, arc lights, atomic lamps). These include high
pump powers, narrow spectral bandwidth, wavelength
tuneability, and both pulsed and continuous wave (CW)
operation. Gas phase, electronic transition, diatomic OPL's
have held the most interest within three general areas of
exploration: spectroscopy, kinetics, and new laser devices
[1,2].

The general procedure for OPL's is to pump at a set
wavelength and spectrally analyzed the resultant stimulated
emission. The fundamental operating principle of these
OPL's is shown by the potential energy curves in Figure 1.1.
A fraction of the ground state thermal population is
optically pumped to the excited state, where a population
inversion is created relative to the thermally unpopulated
high lying vibrational levels of the electronic ground
state. If a sufficient population can be excited, and the
gain is high enough to overcome losses (radiative and
collisional), then lasing can be achieved. Because of gain

1
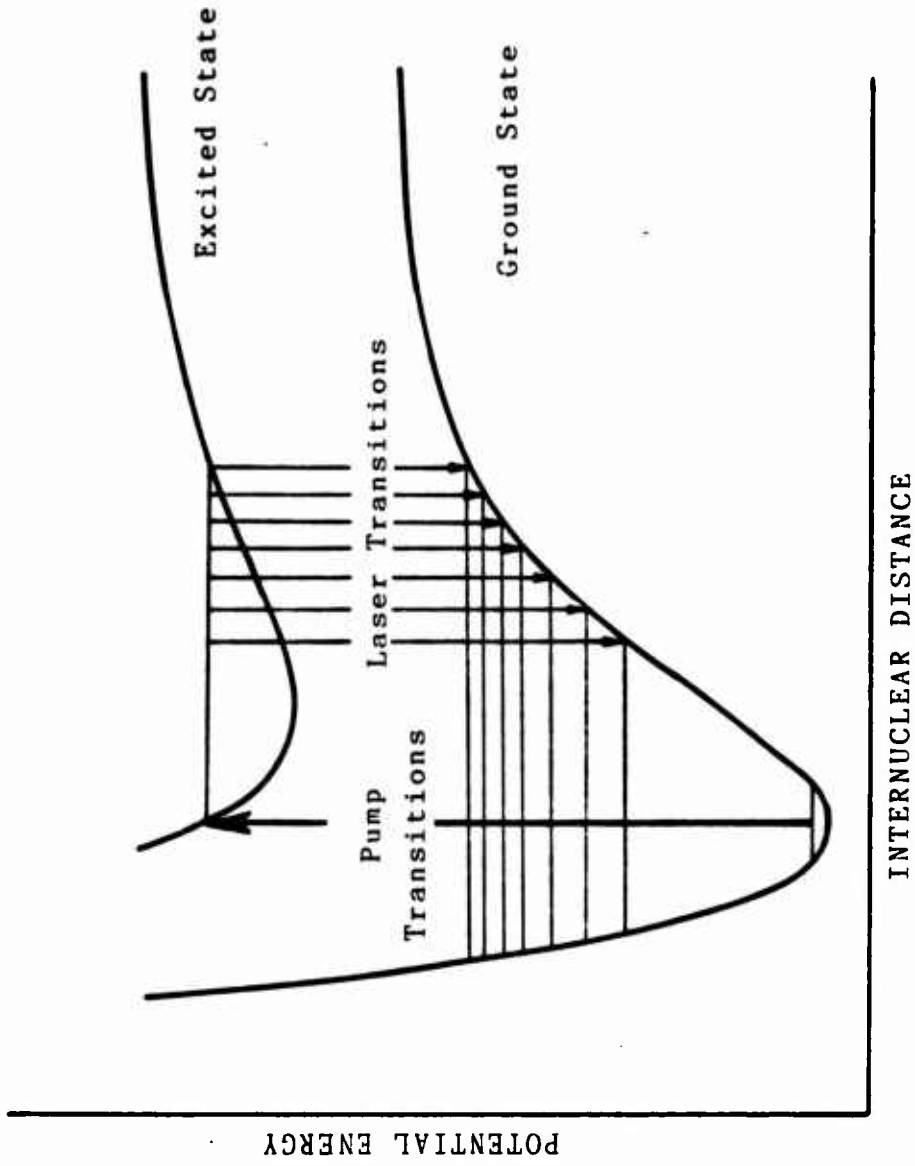
Figure 1.1 Optical Pumped Laser Molecular Transitions.

2

competition amoung the many radiative transitions and threshold population requirements, the intensity of the laser lines may only approximately follow the Franck-Condon transition intensity factors [1,3]. Indeed, by using intra-cavity etalons, prisms, gratings, or filters, a laser cavity can be tuned to a specific transition frequency, allowing selectivity of normally weak transitions. The use of lasers as optical pumping sources allows single, selective energy levels to be populated, greatly simplifing the emission spectrum which aids in spectroscopic and kinetic studies.

The development of electronic transition OPL's progressed rapidy after molecular iodine was shown to lase [4]. A brief review of OPL demonstrations is shown in Table 1.1. As shown, many molecules have been lased, using both pulsed and CW pump sources, and laser emission from the ultra-violet to the infra-red has been observed. The $I_2$ OPL is perhaps the best studied and most understood system yet demonstrated [4-7]. Gains of 3 %cm$^{-1}$ have been calculated with a power conversion efficiency of < 1%. For halogen molecules, $Br_2$ exhibits a very high gain of 11 %cm$^{-1}$ [9]. The only interhalogen OPL yet demonstrated is IF [10-12]. This species is unique in that lasing from collisionally pumped vibrational levels has been observed [11]. Both $Na_2$ and $S_2$ have been lased at high temperatures, 500$^{\circ}$c and 240$^{\circ}$c respectively, with "superfluorescent gain" observed on the

3

Table 1.1

Optical Pumped Laser Development Summary

| Species | Date | Pump Source | Lasing Range | Remarks | Ref |
|---|---|---|---|---|---|
| $I_2$ $B^3\Pi(0^+)-X^1\Sigma_g^+$ | Jun 1972 | Pulsed-doubled Nd:YAG | 544-1335 nm | gain=2.4%cm⁻¹ eff=0.5% | [4] |
| | Apr 1977 | Pulsed-flashlamp dye | 890-1300 nm | Applied to atmospheric absorption | [5] |
| | Nov 1977 | CW-Ar⁺ | 570-1027 nm | gain=3%cm⁻¹ eff=0.14% | [6] |
| | Nov 1977 | CW-Ar⁺ | 583-1338 nm | Ar and He collisional quenching | [7] |
| $Br_2$ $B^3\Pi(0^+)-X^1\Sigma_g^+$ | Nov 1977 | Pulsed-doubled Nd:YAG | 550-750 nm | gain>5%cm⁻¹ eff=0.2% | [8] |
| | Mar 1986 | Pulsed-pulsed dye laser | Not Reported | detailed modeling | [9] |
| $IF$ $B^3\Pi(0^+)-X^1\Sigma^+$ | Oct 1980 | Pulsed-flashlamp dye | 650-720 nm | gain=1.8%cm⁻¹ v'=2,3,4 | [10] |
| | Jan 1983 | Pulsed-flashlamp dye | 650-723 nm | v'=1-5 Thermalized lasing | [11] |
| | Jun 1985 | CW-ring dye laser | Not Reported | Hyperfine structure analyzed | [12] |
| $Na_2$ $B^1\Pi_u -X^1\Sigma_g^+$ | Apr 1976 | Pulsed-doubled Nd:YAG | 526-549 nm | gain=407%cm⁻¹ eff=0.067% | [13] |
| $A^1\Sigma_u^+ -X^1\Sigma_g^+$ | Apr 1976 | Pulsed-doubled Nd:YAG | 785-808 nm | 2.35x10⁻³ wJ output energy | [13] |
| $D^1\Pi_u -X^1\Sigma_g^+$ | Aug 1976 | Pulsed-flashlamp dye | 790-810 nm | Output intensity peaks at 550°c | [14] |
| $S_2$ $B^3\Sigma_u^- -X^3\Sigma_g^-$ | Apr 1977 | Pulsed-doubled dye & $N_2$ | 365-570 nm | eff=2% | [15] |
| $Bi_2$ $A\ 0_u^+ -X\ 0_g^+$ | Sep 1978 | CW-Ar⁺ | 592-755 nm | gain=1%cm⁻¹ eff=10% | [16] |
| $Te_2$ $B/A\ 0_u^+ -X\ 0_g^+$ | Sep 1978 | CW-Ar⁺ | 550-660 nm | gain=0.85%cm⁻¹ eff=2% | [16] |
| $Li_2$ $B^1\Pi_u -X^1\Sigma_g^+$ | 1977 | CW-Ar⁺ | Not Available | | [1] |
| $K_2$ $B^1\Pi_u -X^1\Sigma_g^+$ | 1978 | CW-Kr⁺ | 696-709 nm | 3mW output power | [2] |
| $NO$ $A^2\Sigma^+ -X^2\Pi$ | Jun 1985 | Pulsed-doubled dye | 237-248 nm | eff=15% Output energy 13 wJ | [17] |
| $I^*$ $^2P_{1/2} -^2P_{3/2}$ | May 1978 | Pulsed-flashlamp dye | 1315 nm | Photodissociation of $I_2$ | [18] |
| $HgBr$ $B^2\Sigma_u^+ -X^2\Sigma$ | 1977 | Pulsed-ArF | Not Available | Photodissociation of $HgBr_2$ | [19] |

4

stronger transitions [13-15]. The molecules of $Bi_2$, $Te_2$, $Li_2$, and $K_2$ have been lased, demonstrating conversion efficiency of greater than 1% [16,1,2]. The A-X system of NO has recently been lased, with a very high 15 % conversion efficiency [17]. Although not true dimer OPL's, $I^*$ and HgBr have lased through laser photodissociation of their parent molecules, $I_2$ and $HgBr_2$ respectively [18,19].

Of all the OPL's, the halogen and interhalogen B-X systems have received the greatest attention with both pulsed and CW studies to produce large amounts of kinetic and spectroscopic data [4-12]. This interest results from the extensive information already availiable for $I_2$ [20-38], $Br_2$ [39,40], $Cl_2$ [41-44], IF [45-48], ICl [49-52], IBr [53,54], BrF [55-58], and BrCl[59-61]. This class of molecules has displaced potential curves where the equilibrium internuclear separation of the B state is much larger than that of the X state. This allows for high transition probabilities between vibration levels of the B and X states. High lying vibrational levels of the X state are thermally unpopulated facilitating population inversions necessary for lasing.

Of the halogen and interhalogen molecules, the $I_2$ B-X system is probably the most extensively studied. Mulliken gives an excellent review of iodine in his landmark 1971 paper [20]. The $I_2$ B-X system has been examined to high precision, with the rovibronic energy levels known to better

5

than 0.01 cm$^{-1}$ over a majority of the B-X manifold [21-23].

As described earlier, the first lasing of $I_2$ was reported by Byer, et al. in 1972 [4]. They used the 532 nm second harmonic of a Q-switched Nd:YAG laser as the pump source (190 ns pulses). Lasing was observed from 544 to 1335 nm with output energies of up to 54 nJ per pulse and a 0.5 % maximum power conversion efficiency. A gain of 19 % was calculated for an 8 cm cell.

The first CW optically pumped molecular iodine laser was reported in 1977 [6]. Koffend and Field used an Ar$^{+}$ laser at 514.5 nm to pump v'= 43, J'= 12 and 16. Laser emission was observed from 570 to 1027 nm oscillating on a single (v'=43,v") band for as long as 200 ms. Conversion efficiency of 0.14 % with a maximum output power of 3 mW with a 3 % single pass gain was achieved. Later, Koffend et al. used gain measurements in an $I_2$ OPL to determine the electronic transition moment of the B-X system over a range of R-centroid from 2.8-4.6 Å [62].

In a novel application, Truesdell et al. locked a CW dye laser emission onto wavelengths corresponding to $I_2$ fluorescence by placing iodine samples inside the dye laser cavity [63]. The sensitivity of the dye laser to intracavity gains is analogous to its sensitivity to intracavity loses. Iodine fluorescence introduces gain into the optical cavity at the iodine B-X transition frequencies. When the dye laser is tuned near one of the fluorescence

6

frequencies, the dye laser locks onto the corresponding wavelength. Single pass gain as low as 0.0001 was sufficient to lock the dye laser output onto $I_2$ B-X fluorescence frequencies.

Despite the considerable work on the $I_2$ B-X system, there has been only one brief study on optically pumped mirrorless lasing of this system [64]. In that study, Hanko et al. observed mirrorless lasing or amplified spontaneous emission (ASE) for several pumping wavelengths (510 to 600 nm) of a broadband (5 Å), flashlamp pumped dye laser. The spectral content of this ASE covered 1150 to 1343 nm. For the pump wavelengths of 5154 and 5161 Å, only single line emission was observed. This was unusual since $I_2$ B-X rovibronic emission typically occurs in two lines, consistent with the transition selection rules [65]. The researchers could not resolve this issue and no further work was reported.

Later, Hanko accumulated excitation spectrum of $I_2$ B-X ASE [66]. Excitation spectroscopy is where the total unrsolved emission is observed as a function of the pump laser wavelength. Hanko used a doubled Nd:YAG pumped dye laser (10 ns pulses at 10 Hz) as the pump source covering the excitation wavelengths of 510 to 550 nm. The ASE emission was not spectrally resolved. A typical excitation spectrum of both normal side fluorescence and end-on fluorescence, or ASE, is shown in Figure 1.2. The two

7
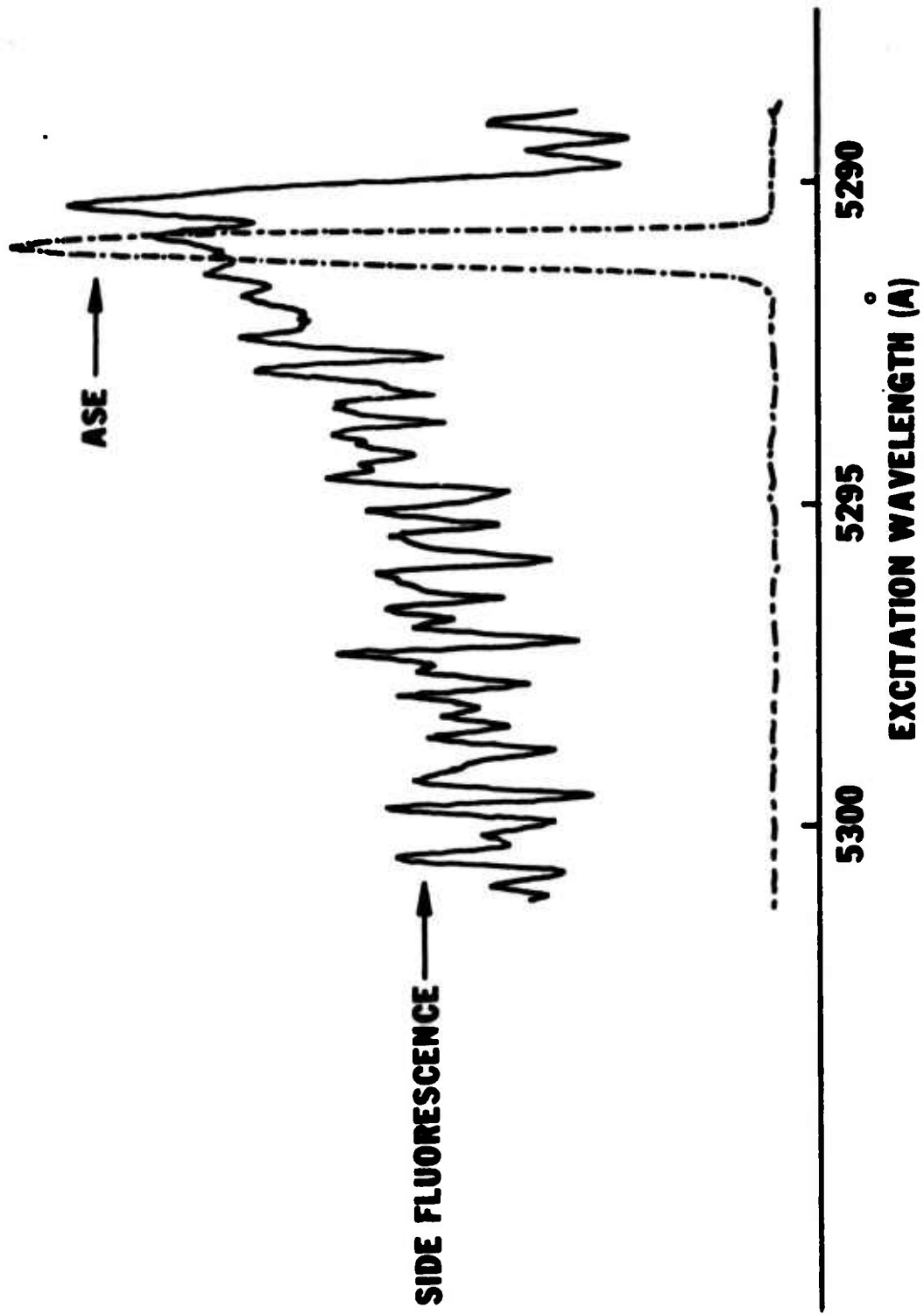
Figure 1.2  I$_2$ (B-X) Excitation Spectrum of the (33,0) Band [64].

8

traces were taken simultaneously using a two-pen stripchart recorder. The cause of the ASE trace could not causually be explained, and the spontaneous fluorescence trace reveals no hint of the very unusual behavior of the ASE trace. No further work was done, and the unusual excitation and emission behavior of $I_2$ B-X ASE remained unexplained. The detailed investigation and understanding of $I_2$ B-X ASE forms the basis for this dissertation.

B.Objective

The primary objective of this work was to investigate and understand the excitation and emission spectroscopy of $I_2$ $B^3\Pi(0_u^+)-X^1\Sigma(0_g^+)$ amplified spontaneous emission (ASE). This included examining the vibrational extent of ASE behavior for the B-X system and resolving the questions raised by the work of Hanko et al. [64], as discussed above.

The approach was to use a pulsed dye laser to optically pump gas phase molecular iodine in a sealed cell. Resolved and unresolved laser induced fluorescence (LIF) of the spontaneous and stimulated emission was extensively employed. Computed modeling was used to generate synthetic spectra, to aid in the analysis and understanding of the observed spectra.

Additionally, energy output performance of $I_2$ B-X ASE was examined. Performance parameters investigated included

9

gain and conversion efficiency. These parameters were parametrically studied by varing the gain cell length and the iodine pressure, while monitoring the total ASE energy output.

Unique collisional energy transfer properties of the iodine ASE were investigated through the use of He, Ar, Xe, and $N_2$ buffer gases. The effects were observed using unresolved LIF and monitoring the total ASE energy output.

Also, the gain cell was heated well above room temperature, with spectroscopic and energy performance information collected and compared to room temperature data.

C.Presentation

Chapter II develops the relevant theortical background for understanding this thesis. This includes molecular spectroscopy, principles of optically pumped lasers, and amplified spontaneous emission.

Chapter III gives detailed descriptions of the various experiments performed. This section includes the excitation sources, gas handleing, and signal processing.

Chapter IV presents the results and discussion. Basic and detailed spectroscopy, buffer gas studies, and performance investigations are presented.

Chapter V gives the summary and conclusions of this effort as well as outlining future work in this area.

10

# II.THEORY

## A. Spectroscopy

### 1. Molecular Energy Levels and Electronic Transitions

Diatomic molecules are free to vibrate along their internuclear axis and to rotate in space [3]. The electronic absorption or emission spectra for bound-bound transitions for diatomic molecules generally consists of a series of individual lines, which may or may not be resolvable. The wavelength of these lines corresponds to the transition energy between the individual rotational and vibrational energy levels of the two electronic states of the molecule. The energy levels of the molecule are given in terms of the vibrational and rotational quantum numbers, v and J. An important part of spectroscopy is to characterize a molecule with constants, such that any specific v,J energy level can be accurately determined. The Dunham equation [67] is a conveinient expression for the energy levels

$$F(v,J) = \sum Y_{jn} (v+0.5)^j J^n (J+1)^n \qquad (2.1)$$

The $Y_{jn}$'s are called Dunham coefficients. The development of spectroscopic constants from the Dunham equation is given

in Appendix A.

The molecular rovibronic transition energy $\nu$, can be related phenomenologically to the rotational $F_J$ and vibrational $G_v$ term symbols of the molecule as shown in Equation 2.2.

$$\nu = \nu_0 + (G_{v'} - G_{v''}) + (F_{J'} - F_{J''}) \qquad (2.2)$$

where $\nu_0$ (the band origin) is the transition energy between the electronic states of the molecule with no rotational or vibrational energy. The primed values correspond to the higher energy level, and the double primed values to the lower energy level of the transition. Inclusion of rotation and vibration produces a spectrum consisting of many lines grouped into vibrational bands, which under high resolution reveal rotational fine structure. To illustrate the spectroscopic nomenclature, an energy level schematic is shown in Figure 2.1. This figure shows the band origin transition for $v' = 0 - v'' = 0$, or simply the (0,0) band. The rotational fine structure is split into P, Q, or R branches based on the change in the rotational quantum number as shown:

P Branch for $\Delta J = -1$

Q Branch for $\Delta J = 0$

R Branch for $\Delta J = +1$

12
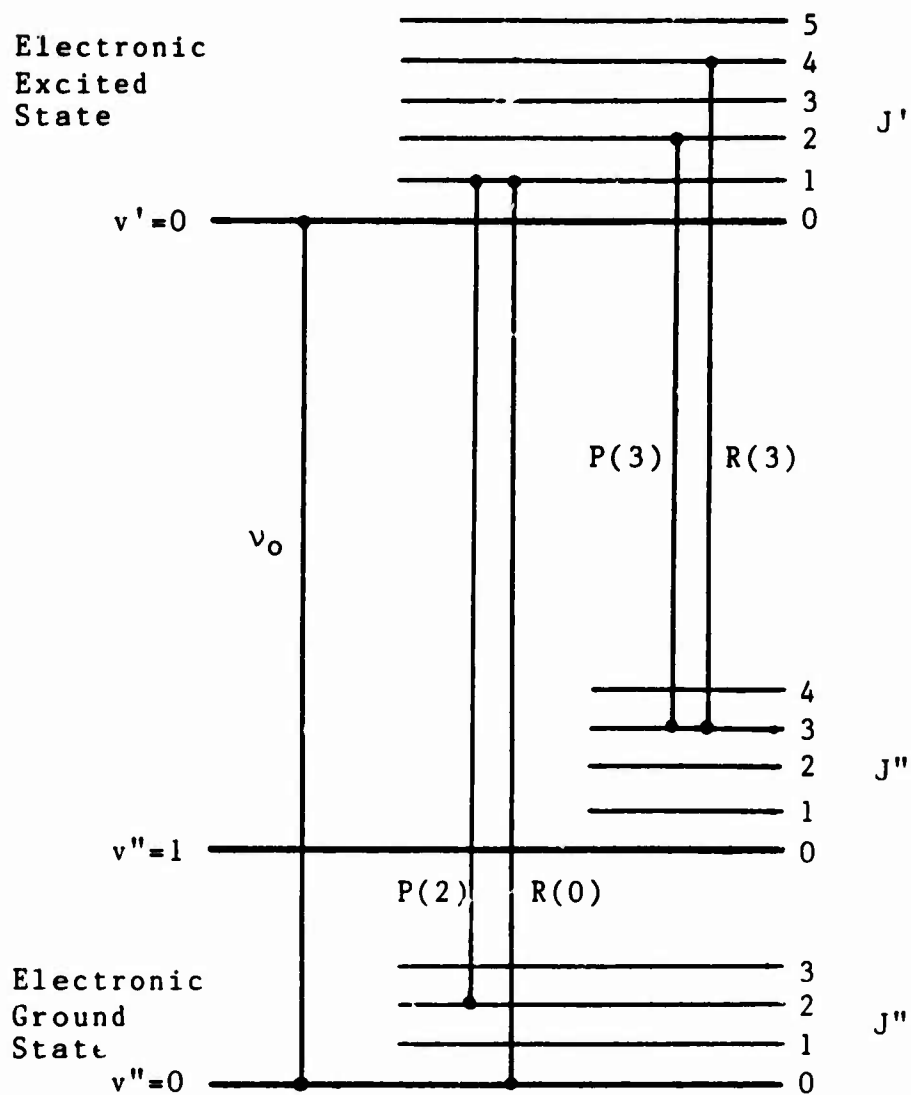
Figure 2.1 Energy Level Schematic Diagram.

where the change in J, $\Delta J$ is defined in absorption as $\Delta J = J' - J''$. The rotational transitions are labeled according to the $J''$ value. Figure 2.1 shows the R(0) and P(2) transitions of the (0,0) band and the R(3) and P(3) transitions of the (0,1) band. For the iodine $B(0_u^+) - X(0_g^+)$ transition, the Q branch is forbidden because the following selection rule restriction applies [3]

$$\Delta J \neq 0 \text{ for } \Omega = 0 \rightarrow \Omega = 0 \text{ transitions} \qquad (2.3)$$

Therefore, discussions of the Q branch will not be included here.

It is possible to express the rovibronic transition energy as the function of a single variable, m:

$$\nu = \nu_o + [B_{v'} m(m+1) - B_{v''} m(m-1)] - [D_{v'} m^2 (m+1)^2 - D_{v''} m^2 (m-1)^2] + [H_{v'} m^3 (m+1)^3 - H_{v''} m^3 (m-1)^3] + \ldots \qquad (2.4)$$

where

$$m = -J \quad \text{for the P Branch} \quad P(J)$$
$$m = J+1 \quad \text{for the R Branch} \quad R(J)$$
$$m = 0 \quad \text{for the band origin } \nu_o$$
$$J = J'' \quad \text{the lower quantum state [28]}$$

14

An instructive way to graphically portray the various
rotational transitions is in a plot of rotational number m
versus transition energy . Such a figure is called a
Fortrat Diagram [3]. An example of a Fortrat Diagram is
shown in Figure 2.2. This figure shows that rotational
lines are more closely spaced at lower m, and the R branch
"turns around", forming a "bandhead" at low m. A bandhead
may also occur in the P branch rather than the R branch.
Bandhead formation is a result of differences between
rotational constants and the $J(J+1)$ factor in rotational
energy. A more detailed discussion about bandhead formation
is given in Appendix B.

2. Potential Energy Curves

During vibration, a diatomic molecule undergoes
nonuniform variation of the internuclear separation about
the equilibrium value. When the nuclei approach one
another, repulsive Coulomb forces between the electrons
prevent close approach of the nuclei [65]. When the nuclei
recede from one another, the momentum of the nuclei tend to
increase the internuclear separation. This is why
molecules are described as anharmonic oscillators (Appendix
A). As can be seen, the internulcear motion of the molecule
and its relationship to molecular energy is very important.

15
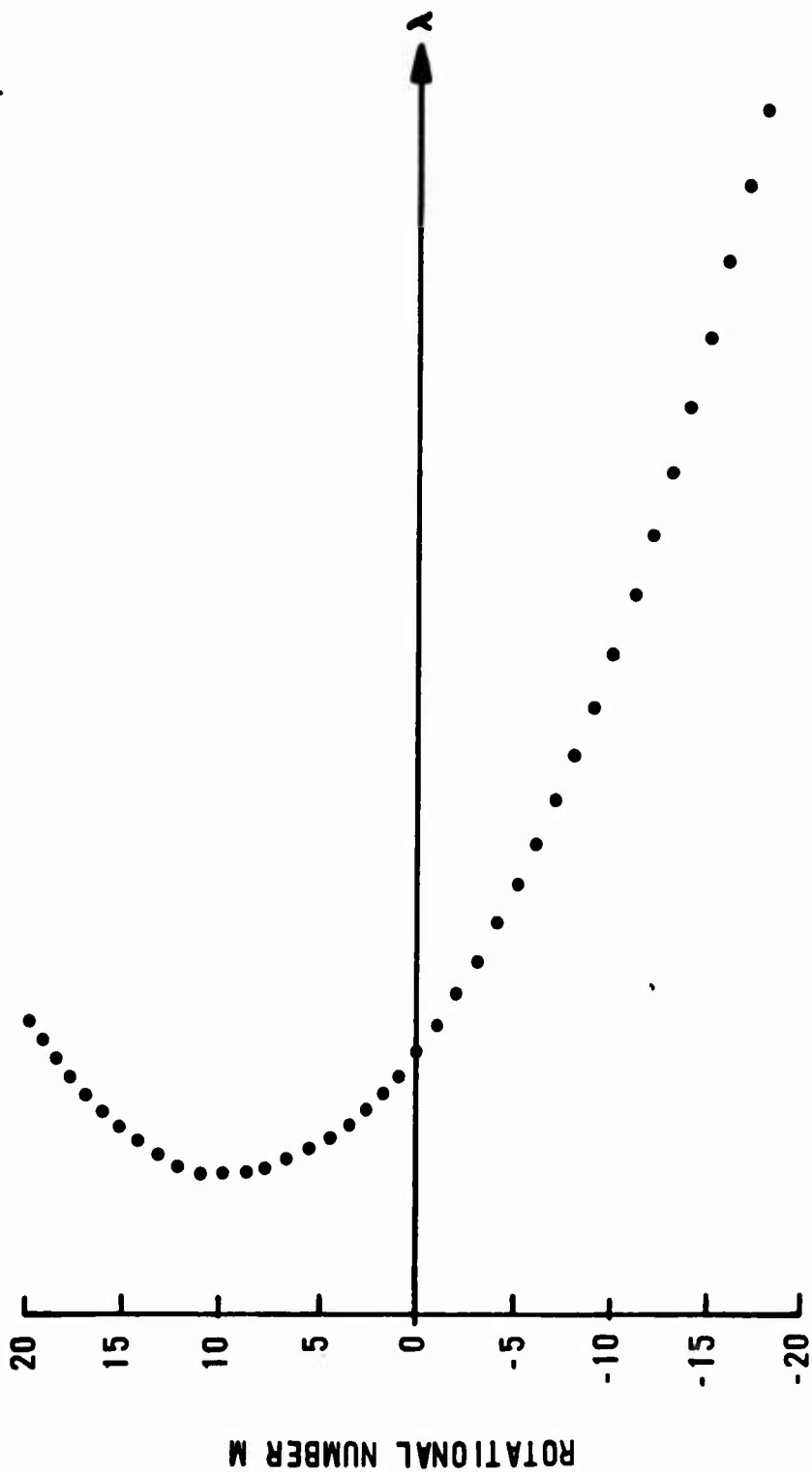
Figure 2.2 Fortrat Diagram.

ROTATIONAL NUMBER M

The variation of energy with internuclear separation can be shown by a potential energy curve, as shown in Figure 1.1. Determination of potential energy curves is a major concern in spectroscopy [66-73].

In a potential curve such as this, one nucleus is considered fixed, and the vibration of the reduced mass is plotted [65]. As the potential energy increases, the anharmonicity becomes apparent. With sufficient energy, the molecule dissociates into its parent atoms.

Besides displaying the motion of the nuclei, a potential energy curve can illustrate the variation of transition probabilities between electronic states of a molecule. Transition probabilities are proportional to the Franck-Condon factors (FCF), which are the square of the overlap integral between vibrational wave functions of the two states involved [3]. With electronic transitions represented by vertical lines on a potential energy diagram, as Figure 1.1 shows, and since a vibrator spends more time at the classical turning points, rather the midpoints, during its motion, the probability is greatest for transitions to occur at the extremes of a potential curve, as shown in Figure 1.1. For a more detailed treatment of transition probabilities, see Appendix C.

A potential energy diagram which includes some of the lowest energy electronic states is shown in Figure 2.3. The B and X states of iodine have received the most interest

17
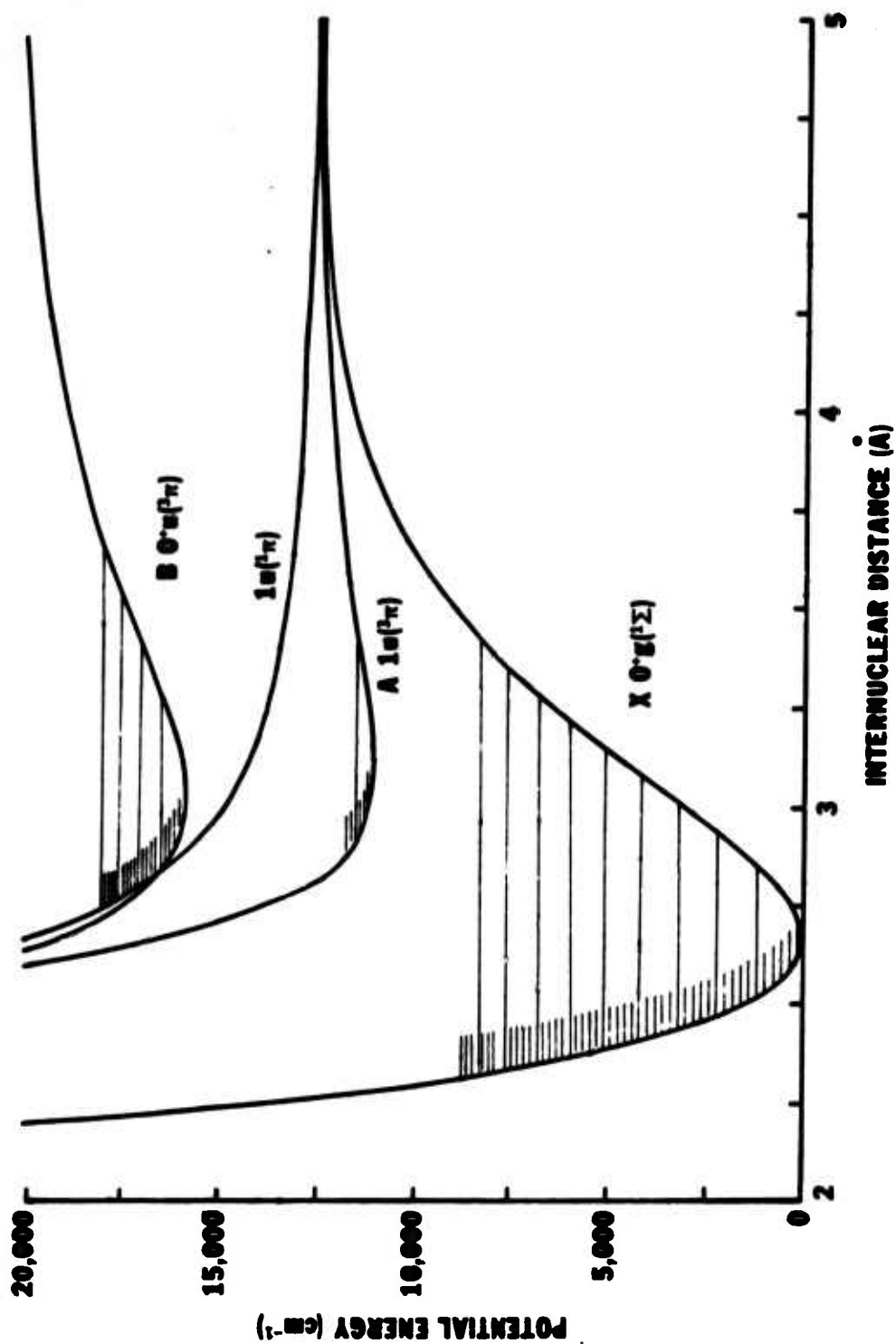
Figure 2.3 Iodine Potential Energy Curves.

18

from researchers, largely because it is relatively easy to populate the B state due to the strong absorption transition intensities, X →B, brought about by the large difference in the equilibrium internuclear separation of the X and B states.

### 3.Laser Induced Fluorescence

Laser induced fluorescence (LIF) has become a common technique to investigate molecular systems [74]. In LIF a laser is used to optically pump molecules from the ground state to the desired excited state. The molecules then spontaneously de-excite through various mechanisms such as predissociation, collisional quenching, or fluorescence. Using narrow bandwidth lasers, specific energy levels can be populated for detailed spectroscopic or kinetic investigation. LIF was first used by Zare and co-workers to measure internal state distributions of reaction products [75].

Consider a three level LIF system as shown in Figure 2.4. Also consider the following processes: optical pumping, spontaneous emission, and collisions. The rate equation describing the upper state population $N_2$ is

$$dN_2/dt = R_{12}N_1 - A_{23}N_2 - KN_2 \qquad (2.5)$$
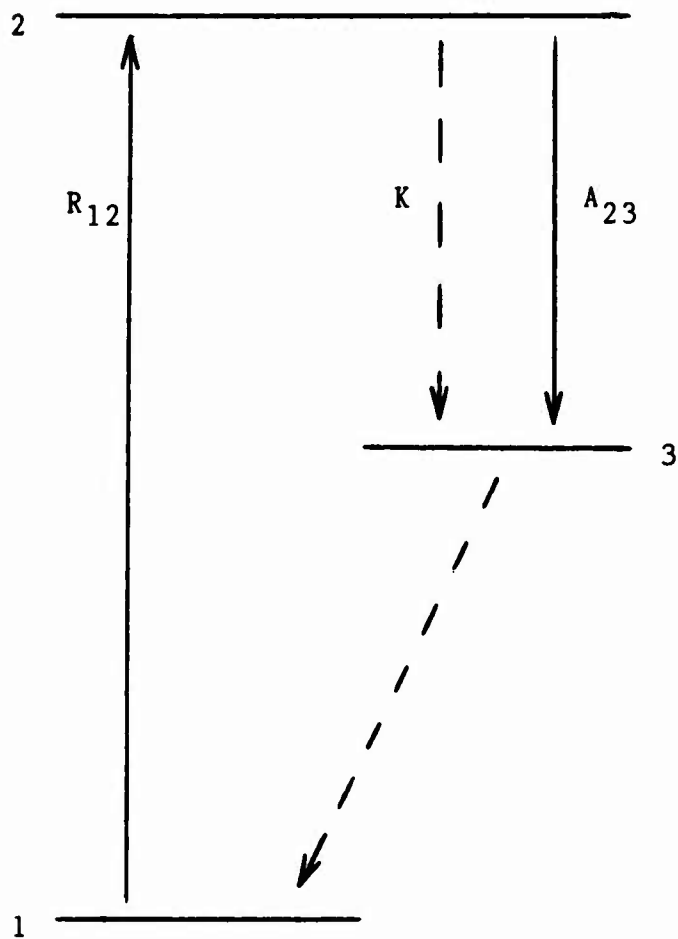
Figure 2.4 Three Level LIF System. Optical transitions are shown by solid lines. Non-radiative transitions are shown by broken lines.

where $R_{12}$ is the optical pumping rate from level 1 to 2, $A_{23}$ is the Einsteinn A coefficient for spontaneous emission (or the inverse radiative lifetime) from level 2 to 3, and K is the collisional removal rate from level 2. After termination of optical pumping, $R_{12} = 0$, the upper state expodentially decays since

$$dN_2/dt = -(A_{23} + K)N_2 \qquad (2.6)$$

leads to

$$N_2(t) = N_2(0)\exp(-(A_{23}+K)t) \qquad (2.7)$$

or

$$N_2(t) = N_2(0)\exp(-\Gamma t) \qquad (2.8)$$

where $N_2(0)$ is the upper state population at the termination of optical pumping and $\Gamma$ is the total decay rate.

There are two techniques that are employed with LIF. Emission spectroscopy uses a fixed frequency laser as the pump, and the resulting emission is spectrally resolved. The pump wavelength may coincide with more than one absorption transition, so the emission spectrum may contain $v''$ progressions from many excited vibrational levels. Transitions from one excited vibrational level $v'$ to many

21

ground state levels is called a v" progression [65].
Through LIF, very detailed information about the $I_2$ B-X
system has been learned [20-38,62,63]. Spectroscopic and
kinetic details about the $I_2$ B-X system is given in
Appendix D.

Excitation spectroscoy is a complementary procedure,
where the total unresolved spontaneous fluorescence is
monitored as a function of the pump laser wavelength.
Narrow band dye lasers are generally used for excitation
spectroscopy. Their output can be easily tuned with
moveable dispersive elements, such as prisms or gratings, to
cover a broad wavelength range [76]. Excitation
spectroscopy has the advantage of strong signals so one can
generally use a simple detection system. In an excitation
spectrum, the wavelength scale corresponds to the pump
wavelength, which corresponds to the absorption transitions.
The observed intensity is proportional to the number of
molecules pumped and those excited molecules that generate
detectable fluorescence. So the intensity yields informtion
about the pump and emission processes.

B. Principles of Optically Pumped Lasers

1.Gain

The quantity of fundanmental importance in a system

22

involving optical gain is the gain coefficient. The gain coefficient is related to the stimulated emission cross section $\sigma$ by

$$g = \sigma \Delta n \qquad (2.9)$$

where $\Delta n$ is the inversion density, $\Delta n = n_u - \frac{g_l}{g_u} n_l$, where u refers to the upper state and l refers to the lower state and the g's are the degenercies. The stimulated emission cross section for a diatomic molecule is developed in Appendix F, and the result for a Doppler broadened transition on line center is

$$\sigma = \frac{2\pi^2}{3\varepsilon_o hc} \sqrt{\frac{4\ln 2}{\pi}} \; \frac{\nu_o}{\Delta\nu} \; |R_e|^2 q_{v',v''} \frac{S_{J',J''}}{2J'+1} \qquad (2.10)$$

where $\nu_o$ is the transition frequency, $\Delta\nu$ is the Doppler broadened FWHM linewidth, $|R_e|^2$ is the average electronic transition moment, $q_{v',v''}$ is the Franck-Condon factor for the vibrational transition $(v',v'')$, and $S_{J',J''}$ is the Hönl-London factor for rotational line strength [87]. The calculation of $\sigma$ requires detailed knowledge of the molecular transition. Fortunately, for $I_2$ B-X all these quantities are fairly well known [37,38,62,78].

A laser is a device which generates a coherent, highly directional beam of light from an optical gain medium. In a laser, light is amplified by stimulated emission of

23

radiation using optical feedback. Figure 2.5 shows a schematic of a laser. A gain medium with a gain coefficient of $\sigma\Delta n$ of length $\ell$ is placed between two highly reflective mirrors of reflectivity $R_1$ and $R_2$ respectively. These mirrors are a distance L apart and form an optical resonator or laser cavity.

Consider a radiation wave of intensity $I_0$ completing one roundtrip along the laser cavity axis. The final intensity is

$$I(2L/c) = I_0 R_1 R_2 \exp(2(\sigma\Delta n - \gamma)\ell) \qquad (2.11)$$

where $\gamma$ is the losses within the gain medium. Losses would include spontaneous emission, absorption, scattering, and collsional deactivation.

When $I(2L/c) = I_0$, the system is at threshold and the threshold gain is

$$g_{TH} = \gamma - (2L)^{-1}\ln(R_1 R_2) \qquad (2.12)$$

For the intensity to increase after a roundtrip, the gain must exceed the losses

$$\sigma\Delta n > \gamma - (2L)^{-1}\ln(R_1 R_2) \qquad (2.13)$$

When the above condition is satisfied, laser amplifiation

24
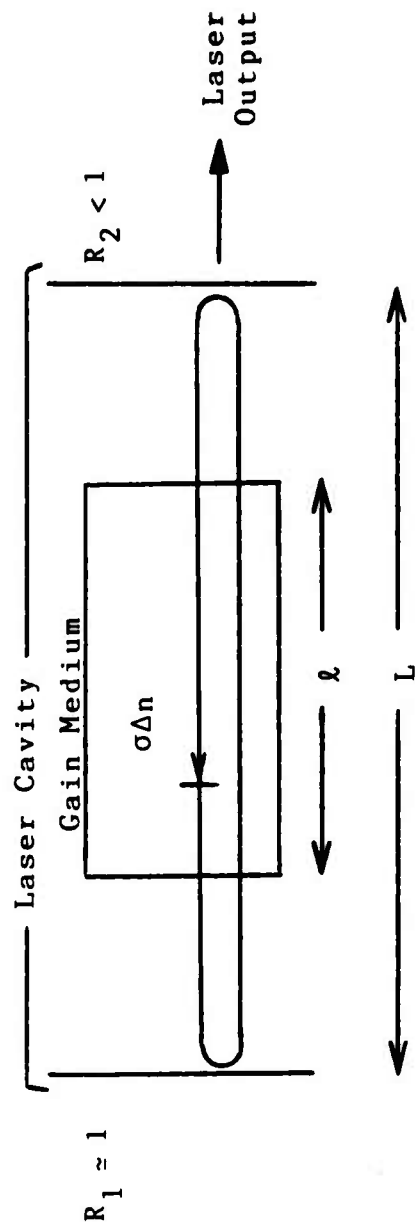
Figure 2.5 Laser Schematic Diagram.

25

results.

Generally, one cavity mirror is highly reflective, $R_1 \approx 1$, and one mirror is partially transmissive, $R_2 < 1$. This allows a useful output to be extracted from the laser cavity, via the transmissive mirror.

2.Molecular Laser Cycles

In a laser using molecules for the gain medium, excitation of a rovibronic level in an excited state generally results in a three or four level laser cycle, as shown in Figure 2.6(a) and (b). The optical pump transition initiates the cycle. Optical radiation at the desired pump transition frequency is absorbed by molecules in the lower state, thereby exciting them to the upper state. The available population to be pumped is dependent upon the rotational and vibrational transition(s) accessed and the temperature of the gas phase species. Generally, for room temperature gases, practically all the population lies in the ground electronic state (see Appendix E). This is not the case for high temperature OPLs such as $S_2$ and $Na_2$ [13-15]. Within an electonic state, the population is partitioned vibrationally, according to vibrational energy, and rotationally, according to the Boltzmann distribution (refer to Appendix E). Additional variations in population distributions may occur, such as those that result from
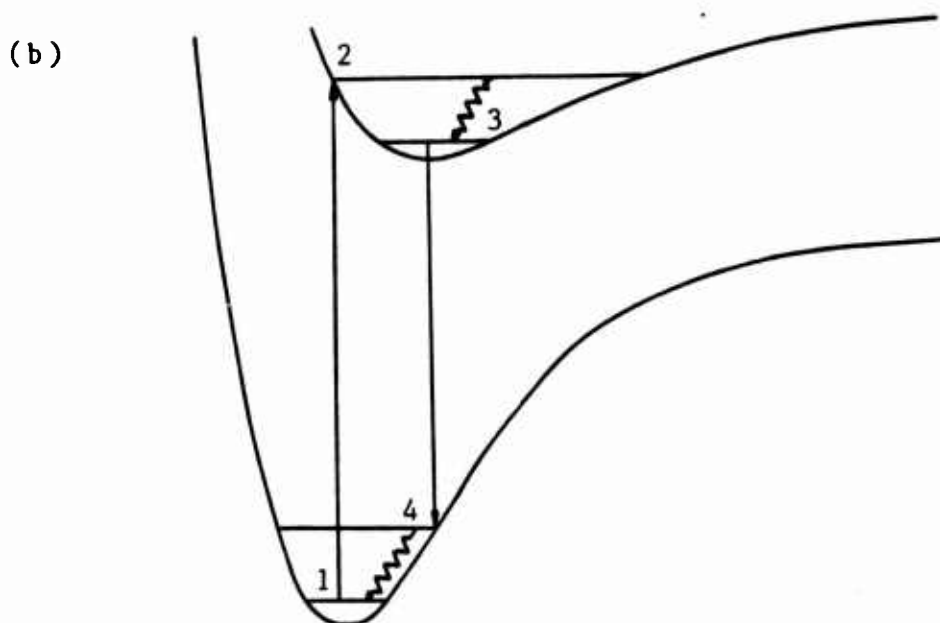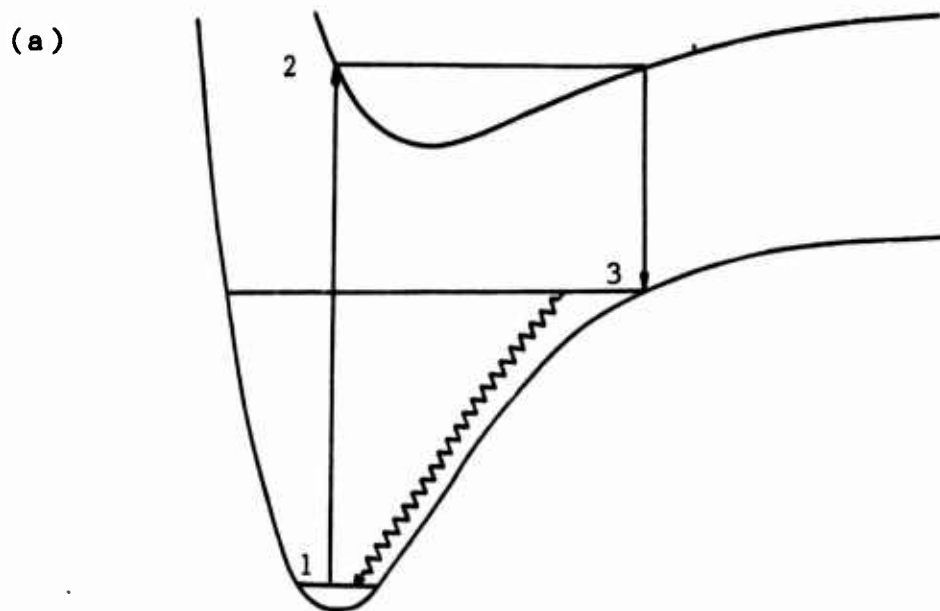
Figure 2.6 Molecular Laser Cycles.  A three level system
is shown in (a) and a four level system in (b).  Relaxation
is shown by zig-zag lines.  Optical transitions are shown
by verticle lines.

nuclear spin statistics [65]. Generally, a significant fraction of the population of the ground electronic state resides in the ground vibrational state, $v''=0$. The rotational population distribution maximizes for the rotational quantum number $J_{max}$ where $J_{max}$ is the integer nearest to $0.348T(^OK)/B_v(cm^{-1})$ [65].

Up to half the population of any individual rovibronic level may by optically pumped. This restriction is due to the competition between absorption and stimulated emission of the same transition. With infinite pump energy, the two processes compete equally, with the populations of the two levels equal. The transition is then said to be completely saturated [76,84]. For a saturated pump transition, the population distribution in the upper state will correspond to the population of the lower state. Therefore, it is at $J_{max}$ where the largest excited state population occurs, hence the strongest lasing intensity.

Once in the excited state rovibronic level, a population inversion is created between the pumped level and sparcely populated vibrational levels high in the ground electronic state. The molecules can lase directly from the pumped level to the ground state, as show in Figure 2.6(a). There is competition to lasing though. Spontaneous fluorescence to many ground state levels, collisional quenching, radiative and collisional relaxation, and predissociation are some competing processes, all of which

28

tend to dilute the population of the upper laser level by reducing the population of the pumped level. The three level laser cycle is completed by transitions within the ground electronic state. Either radiative or collisional relaxation cascades the population back to the lower vibrational levels, regaining the origional equilibrium distribution.

Besides the three level scheme described above, a four level cycle is possible, as shown in Figure 2.6(b). The upper laser level no longer is the same as the initially pumped level. Rather, relaxation processes (as described above) populate lower levels of the excited state. Lasing is possible from these lower levels. For example, lasing of IF(B:v'=0) via collisional pumping has been demonstrated [11]. Since the relaxed population is distributed over many adjacent rotational-vibrational levels, the population in the upper laser level will always be lower in a four-level scheme than in a three-level scheme. Therefore four-level lasing is more difficult to achieve.


3.Fluorescence and Stimulated Emission Spectra


The Einstein A and B coefficients are used to describe spontaneous and stimulated emission respectively. In a radiating system, both processes are present, since

$$A/B = 8\pi h(\nu/c)^3 \qquad (2.14)$$

Although stimulated emission is always present, threshold gain must be exceeded for laser oscillation to commence. In a molecular rovibronic gain system, the threshold condition results in marked differences in the observed side fluorescent and stimulated emission spectra.

As developed earlier, the population in a vibrational band is distributed amoung the rotational levels according to the Boltzman distribution (see Appendix E). The rotational population varies as shown in Figure 2.7(a). In a pulsed three-level system, if this represents the population in the ground state, and a strong pump is used, it will also represent the initial population distribution of the excited state (according to the rotational level pumped).

Fluorescence results in vibrational bands, as shown in Figure 2.7(b). The sharp rise of intensity is due to overlap of rotational transitions near the band origin, as the P and/or R branch forms a bandhead (as discussed earlier). The intensity drops off as the density of rotational transitions is reduced, and as the populations decrease with increasing J.

Now consider an inverted system where a threshold population level is required to achieve optical gain. Figure 2.7(a) marks a threshold level such that only a

30
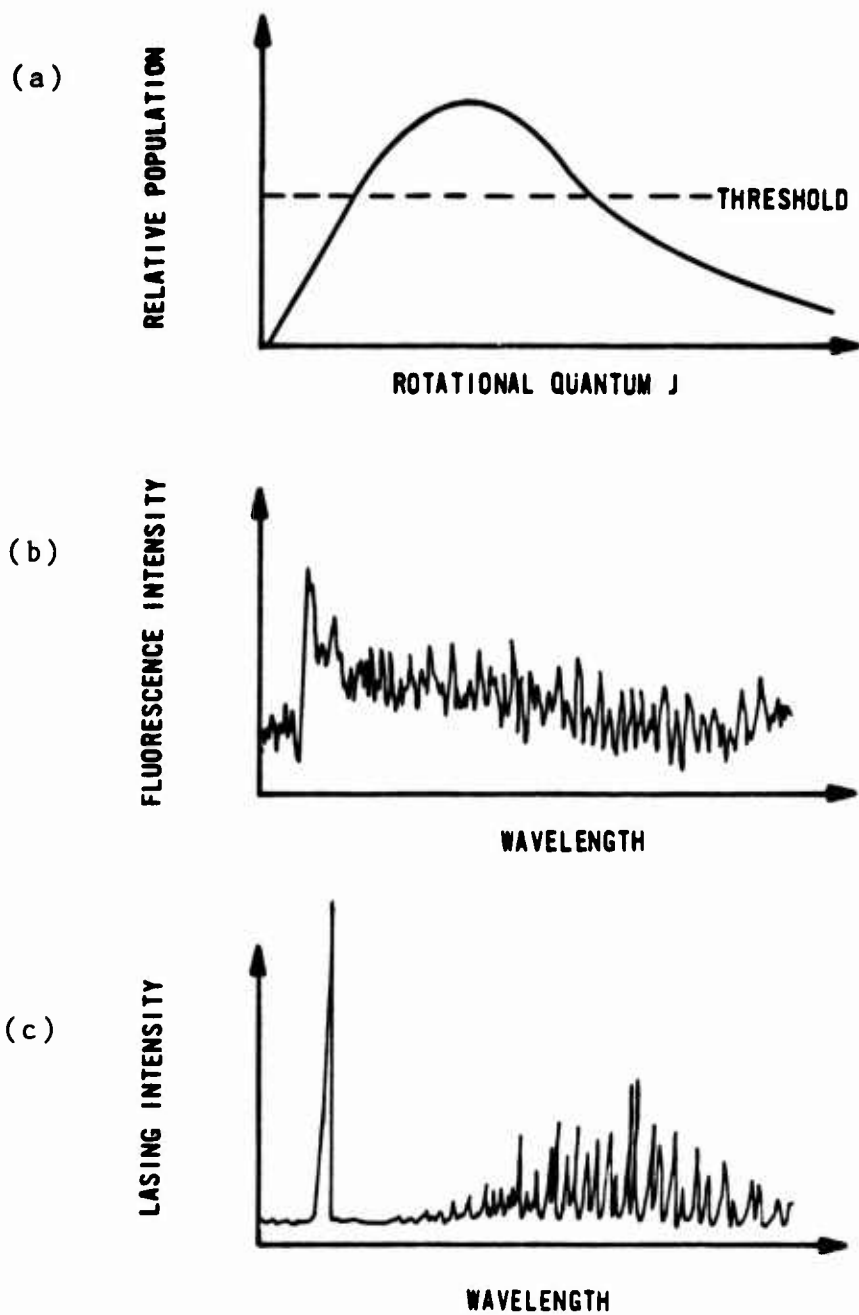
Figure 2.7 Fluorescence and Stimulated Emission Spectra. Relative rotational population (a) resulting in fluorescence (b) and stimulated emission (c) are shown. The large spike structure in (c) is explained in the Results section of this dissertation.

portion of the rotational levels exceed the threshold. For this condition, a resulting stimulated emission spectrum is shown in Figure 2.7(c). The region of emission is restricted to include only those rotational levels above threshold. There is no bandhead because all those transitions near the band origin fall below threshold. The intensity envelope follows the curve of the Boltzmann populations above threshold.

When observing stimulated emission in an excitation spectrum, an apparent resolution enhancement may occur. Since not all transitions are active, the spectrum is simplified, with only the actual gain transitions observed. An example of this is shown in Figure 2.8 for a $Br_2$ excitation scan of the (14,0) band [9]. The superior resolution of the stimulated emission spectrum is evident.

## C. Amplified Spontaneous Emission

### 1.Mirrorless Lasing

The above discussions consider a gain system contained in an optical cavity to reach lasing threshold. But if a system has very high gain, such that optical feedback is not necessary to reach "lasing" threshold then the spontaneous emission noise is amplified through stimulated emission, and mirrorless lasing results [88]. Such amplified spontaneous

32
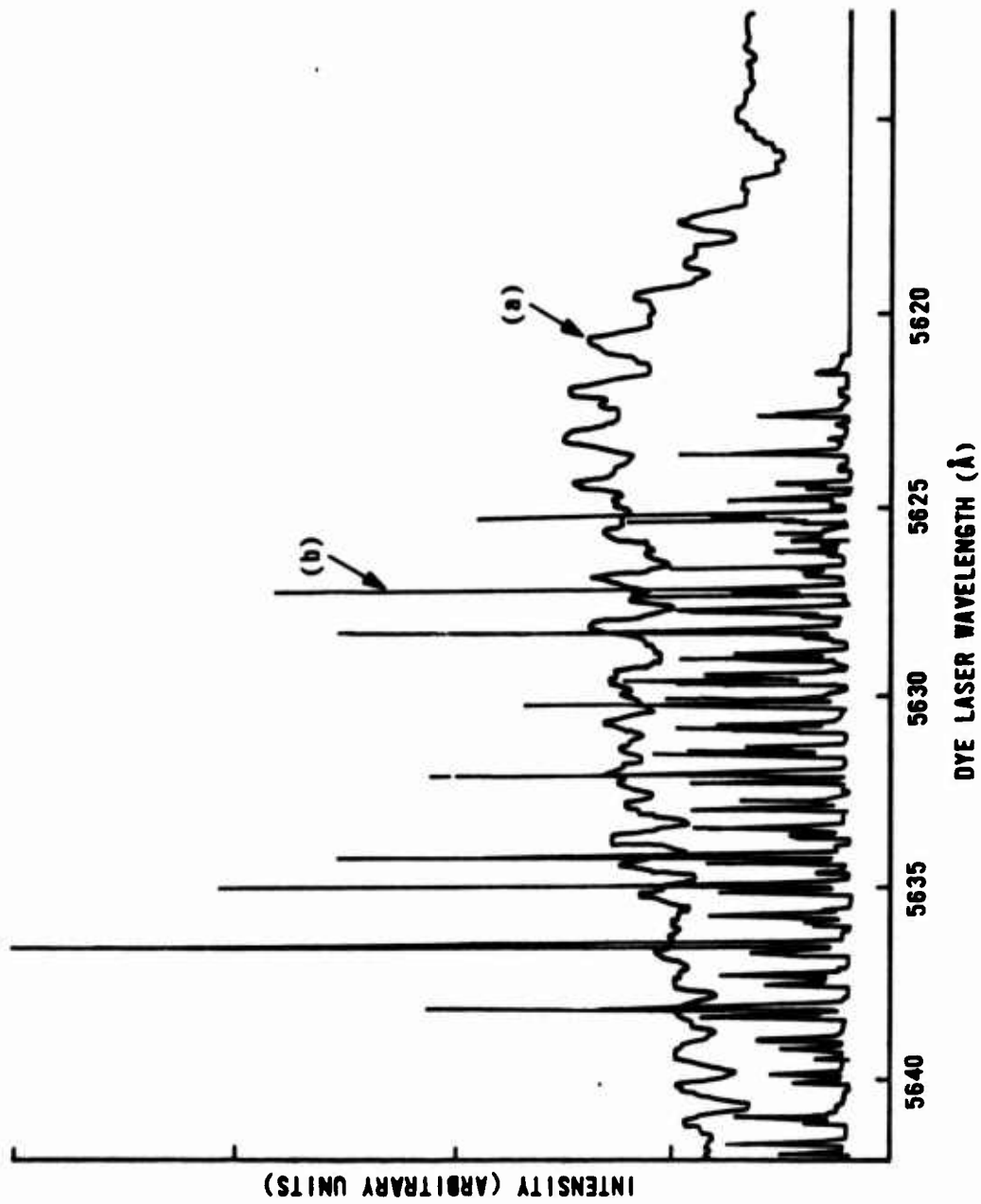
Figure 2.8 Br$_2$ (B-X) Excitation Spectrum. Side fluorescence (a) and laser excitation (b) is shown.

33

emission (ASE) has been observed for $I_2$ and $Br_2$ [64,9].
Quite generally though, ASE is considered a nuisance, and a
process to be avoided in high gain laser systems, such as
dye lasers [76,87].

The wavelength dependence of the reflectivity of the
laser resonator mirrors, as well as the presence of
intracavity tuning elements, and the absence of such for
ASE, can result in drastic differences in the spectral
content of a laser output and an ASE output. In a laser,
the resonator can be designed and tuned to generate
oscillation at practically any desired wavelength and
bandwidth. In ASE, the experiment has practically no
control over the spectral content of the output, other than
simply dispersing the output and using a portion of it. In
ASE, the gain of the particular transitions control the
output, with ASE action likely on only the highest gain
transitions. This self selection can have practical
applications. In a molecular gain medium, only the highest
Franck-Condon factor (FCF) transitions are likely to reach
ASE threshold. So ASE can be a good test of FCF's. The
fact that the medium is responding to the excitation with no
external influence, allows the system's spectroscopy and
kinetics to be investigated.


2.Comparison of ASE to Coherent Processes


34

In the work of Hanko, et al. [64], there exists a problem in terminology. The mirrorless lasing they observed was referred to as superfluorescent emission, amplified spontaneous emission, and superradiance. The problem is that these terms describe different physical processes.

The term "superradiance" was coined by Dicke in his 1954 paper entitled "Coherence in Spontaneous Radiation Processes" [89]. Dicke described how a neutron placed in a uniform magnetic field in its excited spin state, will spontaneously radiate a photon via magnetic dipole transition and decay to the lower energy state. The radiation process is strongly effected if a second, ground state neutron is nearby the first excited neutron. This leads to considering a radiating gas as a single quantum mechanical system with energy levels corresponding to correlations between individual molecules. Spontanoeus emission of radiation in a transition between two such levels results in the emission of coherent radiation, with the radiation rate proportonal to the square of the number of radiating molecules. Dicke's best known result states that the radiating intensity I is

$$ I = \tfrac{1}{2} N ( \tfrac{1}{2} N + 1 ) I_{o} \qquad (2.15) $$

where N is the number of molecules and $I_{o}$ is the radiation rate of a gas composed of one molecule in its excited state

35

[89].   Dicke called this process superradiance.

Dicke's origional definition of superradiance was very broad and has been taken to mean different things by different authors.  For reasons not quite clear, many authors began to use the new term "superfluorescence" interchangeably with superradiance [90,91].  This practice has become so common that in an extensive review article on superradiance [92], these two terms are defined to be used interchangeably.  So there exists no distinction between superradiance and superfluorescence and both terms describe coherent spontaneous emission as described by Dicke.

The process of light amplification through stimulated emission of radiation, or lasing, usually makes use of optical feedback via mirrors to form an optical cavity.  Such stimulated emission reguires a population inversion between the lasing states and the intensity of radiation is set by the gain of the system.  When the system gain is very high such that feedback via the cavity mirrors is not required for laser action to commence, the process is called mirrorless lasing, or amplified spontaneous emission (ASE) [88].  ASE is a stimulated emission process quite different from the superradiance

A question arises of how does one distinguish between superradiance from ASE?  In both cases the output would be intense, directional radiation.  The distinguishing differences are in time scales and intensity.

Superradiance is characterized by a delay time $T_D$ and the superradiance time $T_R$. The delay time is the time between the inversion of the medium and the peak of the output pulse. The superradiance time is the characteristic radiation damping time of the collective system [93]. These times are defined as [93]

$$T_R = T_{sp}(8\pi / n\lambda^2 L)$$

$$T_D = 100 T_R$$

$$\left.\begin{array}{r}\\ \\ \\ \\ \\ \end{array}\right\} \quad (2.16)$$

With the following typical values for iodine B-X

$$T_{sp} = 1 usec$$
$$n = 10^{12}/cc$$
$$\lambda = 1300nm$$
$$L = 200cm$$

these times are

$$T_R = 0.007nsec$$
$$T_D = 0.7nsec$$

Although Hanko does not report an ASE pulse width, the ASE was observed to begin 40nsec after the onset of the pump pulse (which was 200nsec long) [64].

Superradiance produces a ringing structure called Burnham-Chiao ringing [94]. This ringing is due to the medium, immediately after the leading edge of the pulse and therefore in the ground state, absorbing energy from the trailing part of the pulse, then re-radiating.

The peak intensity of the superradiant pulse was first shown by Dicke to be proportional to the number of radiators squared [89]. ASE intensity, on the other hand, would depend on the gain (as per the gain equation, Equation 2.7). For $gl \ll 1$, a gain system's intensity is linear with respect to the number of inverted radiators, since

$$I = I_o \exp(\sigma \Delta n \ell) \simeq I_o (1 + \sigma \Delta n \ell) \qquad (2.17)$$

So there exist many measurable differences between ASE and coherent processes, such that an exact determination can be made.

3. Simplified Kinetic Model

If one were to model the kinetic processes of a pulsed, optically pumped ASE in a molecular system, the populations of the various levels involved would be functions of vibration, rotation, position along the gain length, and time. In addition, ASE can be initiated randomly in space and time with a random number of source locations. Gain

38

depletion due to ASE which is not in the proper solid angle and in various directions is also random.

Because of these complications, a total model of the kinetic process in ASE will not be attempted in the present study. However, a model which adaquately describes the total loss from the upper state can be developed relatively simply. The proposed model contains the following features:

1) The gain medium is an optically pumped three level system as shown in Figure 2.9a.

2) Both the pump and ASE pulses are considered instantaneous and copropagating.

3) Only the total energy per pulse is considered.

4) There is a time delay between the pump and ASE pulse as shown in Figure 2.9b.

5) Only collisional loses are considered with radiative and other non-radiative, non-collisional processes ingored.

Losses from the prepared level due to collisions are described by the following kinetic equation
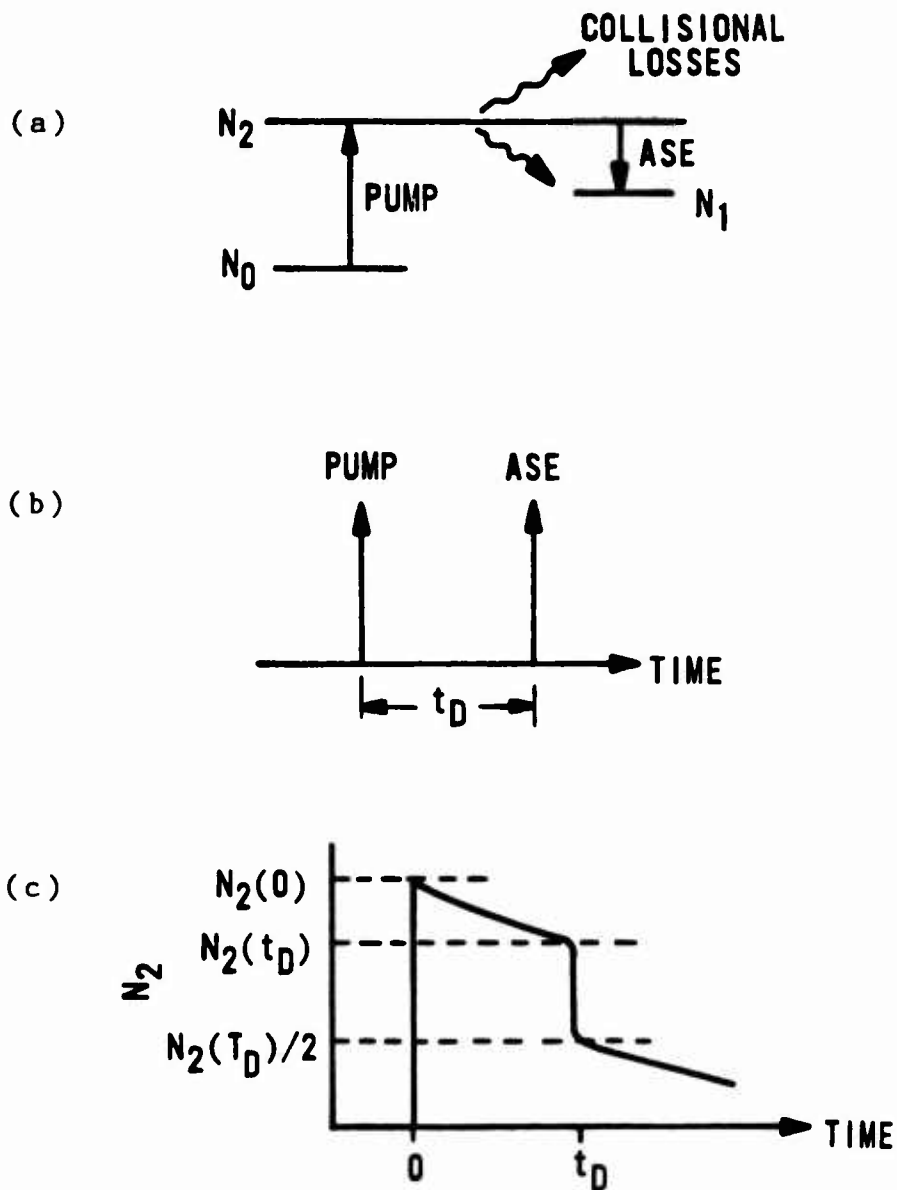
Figure 2.9 ASE Kinetic Model. Schematic energy level diagram (a), time history of transitions (b), and the upper state population (c) are shown.

40

$$I_2(B{:}v',J') + M \overset{k}{\to} I_2 + M \qquad (2.18)$$

where $I_2(B{:}v',J')$ is the prepared level, M is any collision partner, $I_2$ is any state other than the prepared one, and k is the collisional rate constant. It follows from the above equation that

$$d[I_2(B{:}v',J')]/dt = -k[I_2(B{:}v',J')][M] \qquad (2.19)$$

If one defines $[I_2(B{:}v',J')]{=}N_2$ amd $[M]{=}P$ then

$$dN_2/dt = -kN_2P \qquad (2.20)$$

Solving for $N_2$ as a function of time yields

$$N_2(t) = N_2(0)\exp(-tkP) \qquad (2.21)$$

where k is the collisional rate constant for all losses out of the pumped level and P is redefined as the buffer pressure. The population of $N_2$ after a time $t_D$ is

$$N_2(t_D) = N_2(0)\exp(-t_D kP) \qquad (2.22)$$

According to the model, ASE occurs after a delay time $t_D$. The time history of $N_2$ is shown in Figure 2.9c. As shown, the upper state population at time t=0 decays due to

41

collisions for a time $t_D$, when ASE occurs. Note that only half of the available molecules can contribute to ASE because the population inversion drops to zero at that point.

The initial population inversion depends on the number of molecules available for pumping. If the pumping pulse saturates the pump transition, the initial inversion will be half of the number of molecules in the ground rovibronic state. Therefore, knowledge of the ground state population distribution is vital to accurately describing the initial population inversion. A complete discussion of the ground state population distribution for molecular iodine is given in Appendix E.

# III.EXPERIMENTAL

## A. Excitation Sources

Two excitation sources were used to provide tuneable
radiation for the experiments.  The bulk of the work was
done with a Quanta-Ray Nd:YAG pumped dye laser system.  The
1064nm output from the Q-switched Nd:YAG (DCR-1) was
frequency doubled to 532nm or tripled to 353nm using
potassium dihydrogen phosphate (KDP) crystals in an harmonic
generator (HG-1).  A prism harmonic separator (PHS-1)
dispersed the output from the harmonic generator, allowing
only the desired wavelength to pump the dye laser (PDL-1).
The dye laser consisted of an oscillator-amplifier
combination with wavelength selection via a stepping motor
controlled grating.  Various dyes were used depending on the
wavelength coverage desired.  Table 3.1 lists the dyes used,
dye laser pump wavelengths, dye laser output wavelength
range and peak output wavelength, and accesible $I_2$ pump
transitions.

The dye laser produced 10ns pulses (FWHM) at a 10Hz
rate.  The linewidth was $0.5cm^{-1}$ as measured with a
Fabry-Perot spectrum analyzer.  Absolute output wavelength
was displayed on a dial mechanically linked to the dye
oscillator grating.  This dial was accurate only to $\pm 0.5\text{Å}$
due to zero error and gear lash.  The dial reading was used

43

Table 3.1

Dyes Used with Quanta-Ray Dye Laser

| Dye | Pump (nm) | Output (nm) | Peak (nm) |
|------|-----------|-------------|-----------|
| C500 | 355 | 485-545 | 506 |
| F548 | 532 | 540-567 | 550 |
| R590 | 532 | 550-575 | 565 |
| KR620 | 532 | 572-591 | 582 |
| R640 | 532 | 592-617 | 603 |

only as a rough wavelength guide and not for actual recording. Dye laser output energy was generally below 20mJ per pulse, and typically in the range of 1-5 mJ, depending on the dye used.

For a small portion of work, a Phase-R DL 1400 flashlamp pumped dye laser was employed. This laser generated 200ns pulses at a typical pulse rate of 0.1Hz. Coumarine 504 dye was used to pump at 510-520nm with output energies as high as 100mJ per pulse.

The wavelength of the Phase-R laser was monitored using a P.A.R. optical multichannel analyzer (OMA Model 120A) whose detector head (1205DE) was mounted on a McPhereson 0.3m momochrometer (1200gr/mm, 6000A blazed grating). The OMA was calibrated using cadmium and rubidium standard lamps.

The Phase-R laser used two 60-60-60 dispersing prisms to spectrally line-narrow the dye laser output to $\pm 4\overset{\circ}{A}$ FWHM as measured by the OMA with 10μ slits (giving a $1\overset{\circ}{A}$ system

44

resolution).

## B. Gas Handling System

Iodine and buffer gases were handled using a gas handling system as shown in Figure 3.1. The gain cell was constructed of modular glass components for easy modification and fabrication. Pyrex glass tube of 13mm diameter was joined using Cajon Ultra-Torr® stainless steel O-ring connectors to insure vacuum tightness. Brewster-angled pyrex precision flats were used for the end windows. The gain cell length was varied from 20cm to 400cm, depending on the particular experiment. All valves were glass Kontes HI-VAC valves with Viton O-ring seals.

Iodine crystals were stored in a valved side finger and exposed to liquid nitrogen freeze-thaw-pumping cycles to reduce impurities. Pressures were monitored using MKS Baratron Type 222 capacitance manometers (10, 100, and 1000 Torr pressure transducers were employed) with PDR-D-1 digital readouts. An Alcatel M2004A direct connect 3.2 CFM mechanical vacuum pump was used to evacuate the gain cell to a base pressure of approximately 1mTorr. The vacuum pump was connected to the gain cell via a liquid nitrogen cold trap using flexible Teflon hose.

Helium, argon, xenon, and nitrogen buffer gases (Matheson Ultra High Purity Research Grade) were stored,
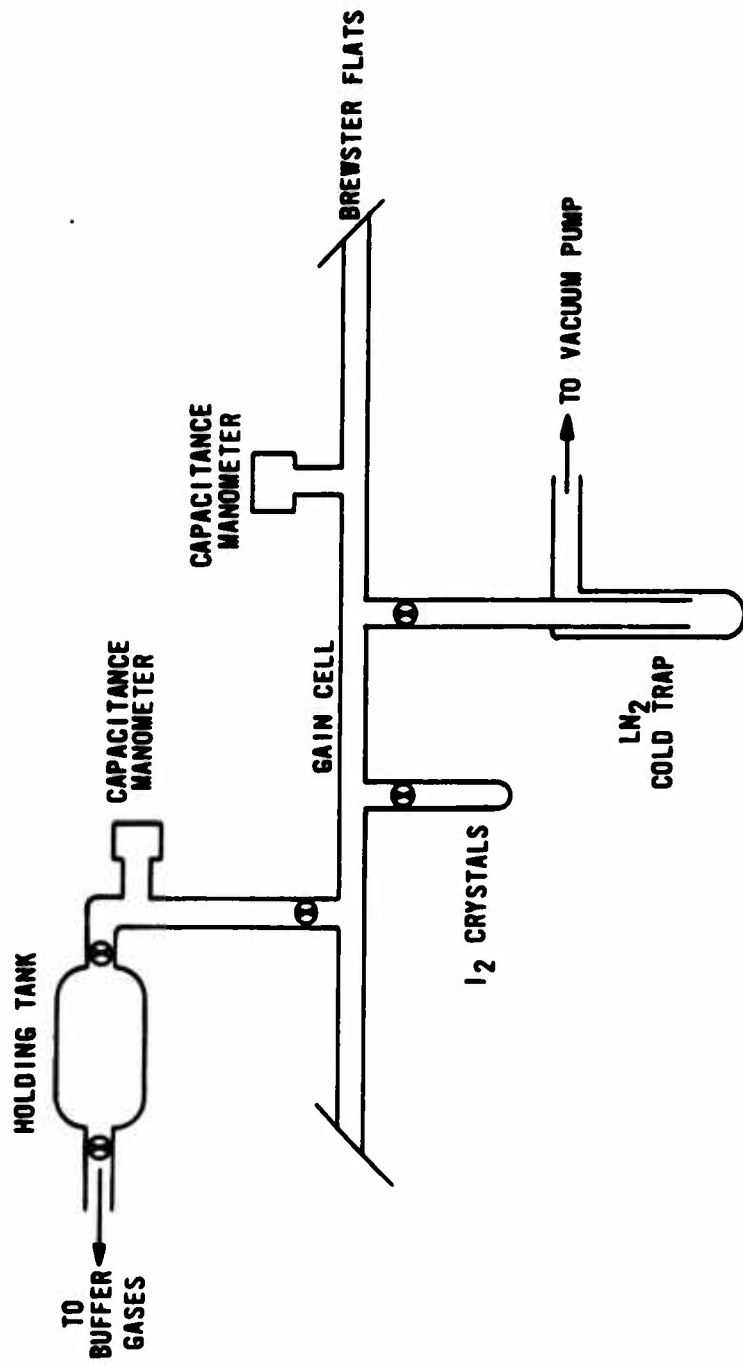
Figure 3.1 Gas Handling System.

46

when used, in a 10cm by 50cm glass holding tank at 100Torr and metered into the gain cell with a stainless steel vernier valve.

An additional 98cm long cell, with Brewster angled windows, was made from material as described earlier. Iodine crystals were placed inside the cell. The iodine was then frozen out by using a liquid nitrogen cooled cold finger. While the iodine was frozen, the cell was evacuated via a thin hollow tube attached to the cell. This tube was subsequently heated with a torch such that it sealed the cell. This cell was placed in an oven for heated cell experiments to be described later.

C. Data Aquisition

The experiments consisted of optically pumping a long iodine cell, then observing the resolved or unresolved end fluorescence with various detection systems. The fundamental experimental set-up is shown in Figure 3.2. This figure depicts an excitation experiment, where the total unresolved end fluorescence intensity is measured as a function of the pump laser wavelength. The pump laser beam was focused with a 1 to 2 meter focal length lens to pass through the gain cell. Pump laser power was monitored by catching the reflection off a Brewster window or by using a beam splitter. The energy per pulse was measured with a

47
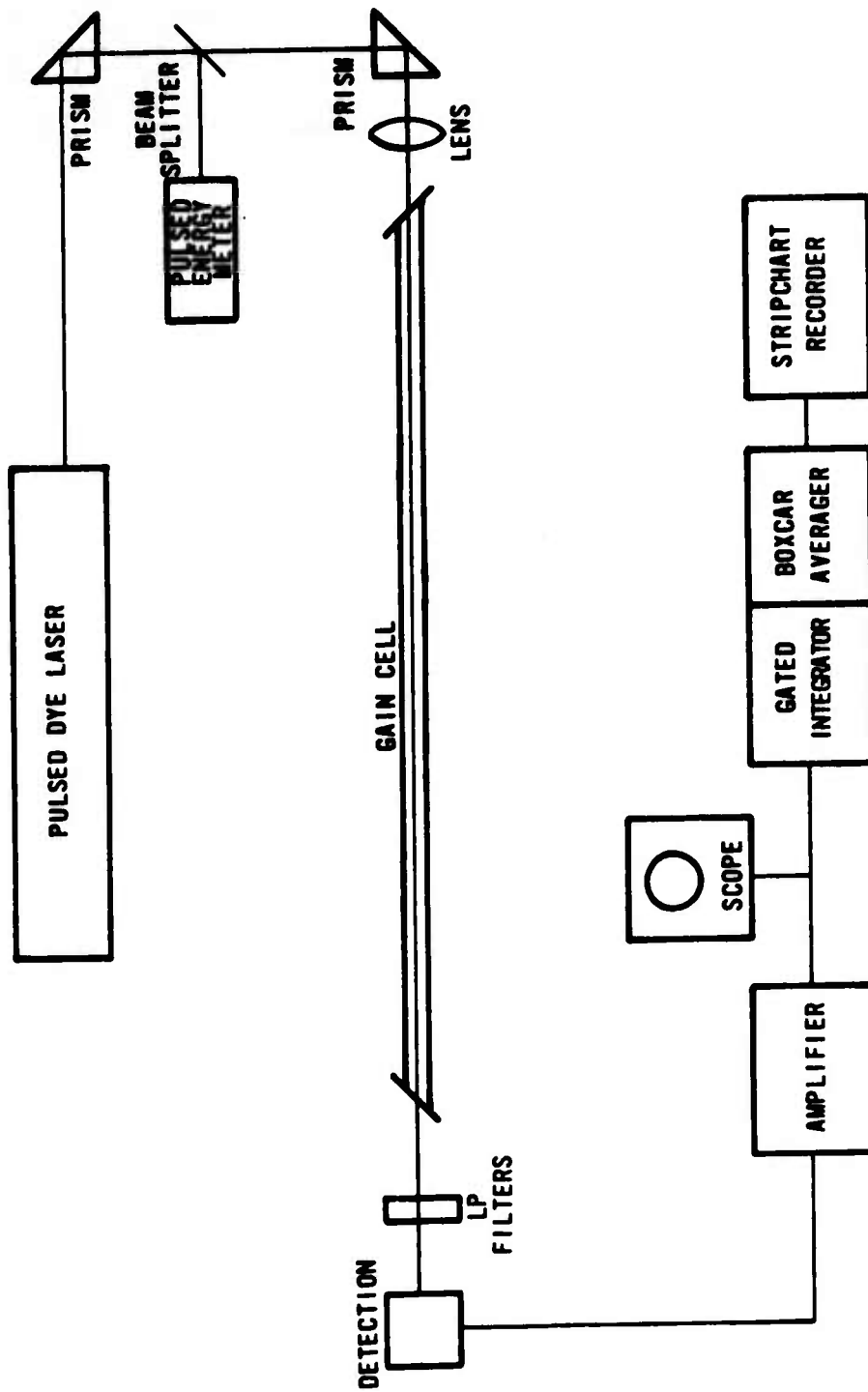
Figure 3.2 Experimental Set-Up.

Laser Precision RJP 735 probe and displayed with a RJ 7100 energy meter. After passing through the gain cell, the pump beam was attenuated with Corian® glass and interference band pass filters. No detectable pump beam intensity was observed to pass through the filters. An unbiased germanium photodiode ($1cm^2$ active area) detected the signal. The output from the diode was fed into an HP 462A amplifier. The output signal was then fed into a P.A.R. 162/164 boxcar averager and gated integrator. This averages the 10Hz signal, giving a voltage proportional to the fluorescent intensity. This voltage was used to drive a HP 7100BM stripchart recorder. Neutral density filters were usually employed to prevent the fluorescant signal from overloading the detection electronics.

When experiments to spectrally resolve the fluorescent signals were also performed, the fluorescent signal was directed into a scanning monochromator/photodiode detector system or an optical multichannel analyser/photomultiplier tube system. Both 0.3 and 1 meter McPherson monochromators were used with grating specifications of 600gr/mm, blazed at 1.6μ and 600gr/mm, blazed at 1.85μ respectively. The monochromators were calibrated using an Oriel argon calibration lamp.

The PAR model 1205A OMA used a McPhereson 0.3 meter monochromator with a 1200gr/mm grating, blazed at 600nm. The output of the 1205DE detection head was displayed on a

49

Textronix 7844 oscilloscope and subsequently passed to a HP
7044A X-Y plotter for a plot. The OMA was calibrated using
various calibration lamps.

During the course of this work many additional
experiments were performed. The photodiode detector was
replaced with a pulsed energy meter, as described earlier,
for performance measurements. Side fluorescent excitation
spectra were taken. Buffer gases were introduced into the
gain cell, and performance or spectroscopic studies were
performed. An iodine laser was assembled from two CVI laser
mirrors (R=99% @ 1.3μ, 5m fl). A 20 to 40 cm gain cell was
used, and excitation and emission spectra recorded. Also,
one mirror ASE was studied using one of the mirrors
described above.

Finally, a sealed cell, as described earlier, was used
in an oven for high temperature excitation, emission and
output energy experiments. The oven was constructed from a
2 inch OD steel pipe 130 cm long which was wrapped with
flexible heat tape. The temperature in the cell was
controlled by varying the AC power to the tapes with an
autotransformer. A small hole in the pipe allowed an
alumel-chromel thermocouple to touch the glass cell at it's
center. An Omega 2166A digital thermometer displayed the
temperature to within $1^{\circ}$c. The temperature measurement was
used to calculate the iodine vapor pressure using the
expression

$$LogP = 12.1891 - 0.001301T - 0.3523LogT - 3410.71/T$$

where P is the vapor pressure in Torr and T is the
temperature in degrees Kelvin [95].

# IV.RESULTS and DISCUSSION

## A. Basic Spectroscopic Understanding

### 1.Complete Excitation Spectra.

To understand and expand upon the data of Hanko et al.
[64], a thorough spectroscopic survey of iodine ASE was
initiated.  The spontaneous fluorescent excitation spectrum
over the Rhodamine 590 dye region is a convienient starting
point.  It is shown in Figure 4.1.  The familiar red
degraded vibrational bands of the v"= 0,1 progressions are
shown.

An ASE excitation spectrum over this region is shown in
Figure 4.2.  Comparing this figure with the previous one
reveals dramatic differences in the spectra.  Figure 4.2
shows the stimulated emission spectrum.  The figure shows
pumping from v"= 0.  This spectrum appears to be simpler
than the spontaneous fluorescence spectrum because of the
threshold requirement for ASE gain.  In addition to the
resolution enhancement, there are drastic differencs between
the overall shapes of the ASE and the spontaneous
fluorescence.  Within each ASE pump band, there are two
regions: an isolated narrow "spike" (shown as feature A of
the (23,0) band in Figure 4.2) and a region corresponding to
more regular banded excitation (shown as feature B).  For
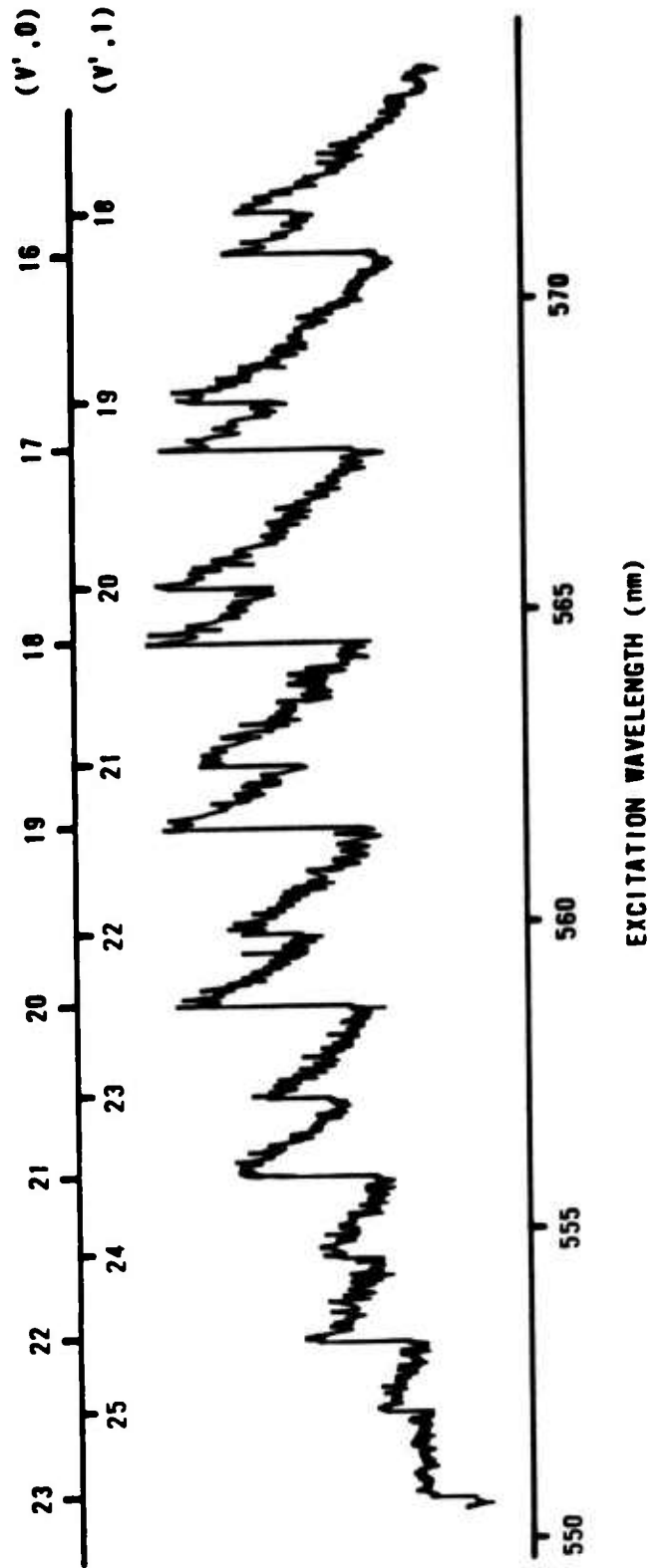
Figure 4.1 Side Fluorescence Excitation Spectrum over the Rhodamine 590 Dye Region.

53
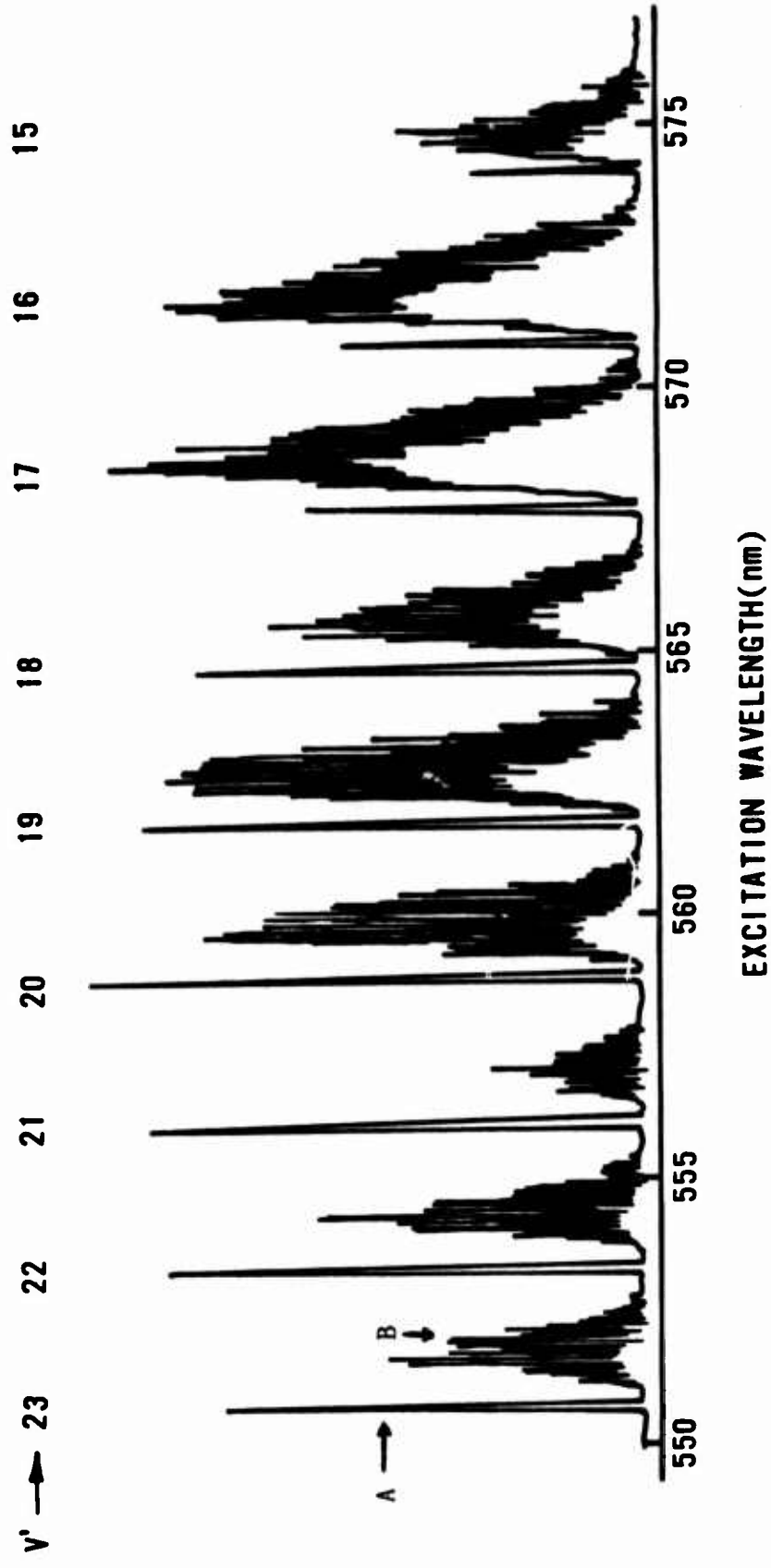
Figure 4.2 ASE Excitation Spectrum over the Rhodamine 590 Dye Region.

54

reference, we define the narrow isolated emission as "spiked" and the regular banded region as "normal".

A more detailed examination of this ASE spectrum is shown in Figures 4.3 to 4.6. These spectra show the spike to be wider than the features in the normal region. The spike is asymetric with multiple excitation features observed for the $v'$= 18, 17, 16, and 15 bands. These figures also show a zero signal level between the spiked and normal region.

To continue the excitation summary, consider Figures 4.7 and 4.8. These figures show ASE excitation out to the long wavelength limit using Kitton Red 620 and Rhodamine 640 dyes. ASE excitation ceases after the (7,0) band. This termination point probably has no real significance, other than that at this point the pump laser can just bring the (7,0) band to ASE threshold. When comparing these figures with the Rhodamine 590 excitation region, Figure 4.2, note that the ratio of the spike peak-to-band peak intensity decreases as the pump band decreases. Only normal excitation is observed for the R640 region.

ASE excitation to shorter pump wavelengths is shown in Figures 4.9 to 4.11. Figure 4.9 shows excitation with Fluorescein 548 dye out to the (27,0) pump band. Note that the peak for the spike feature for the $v'$= 23, 24, and 25 pump bands have saturated the detection electronics, so the

55
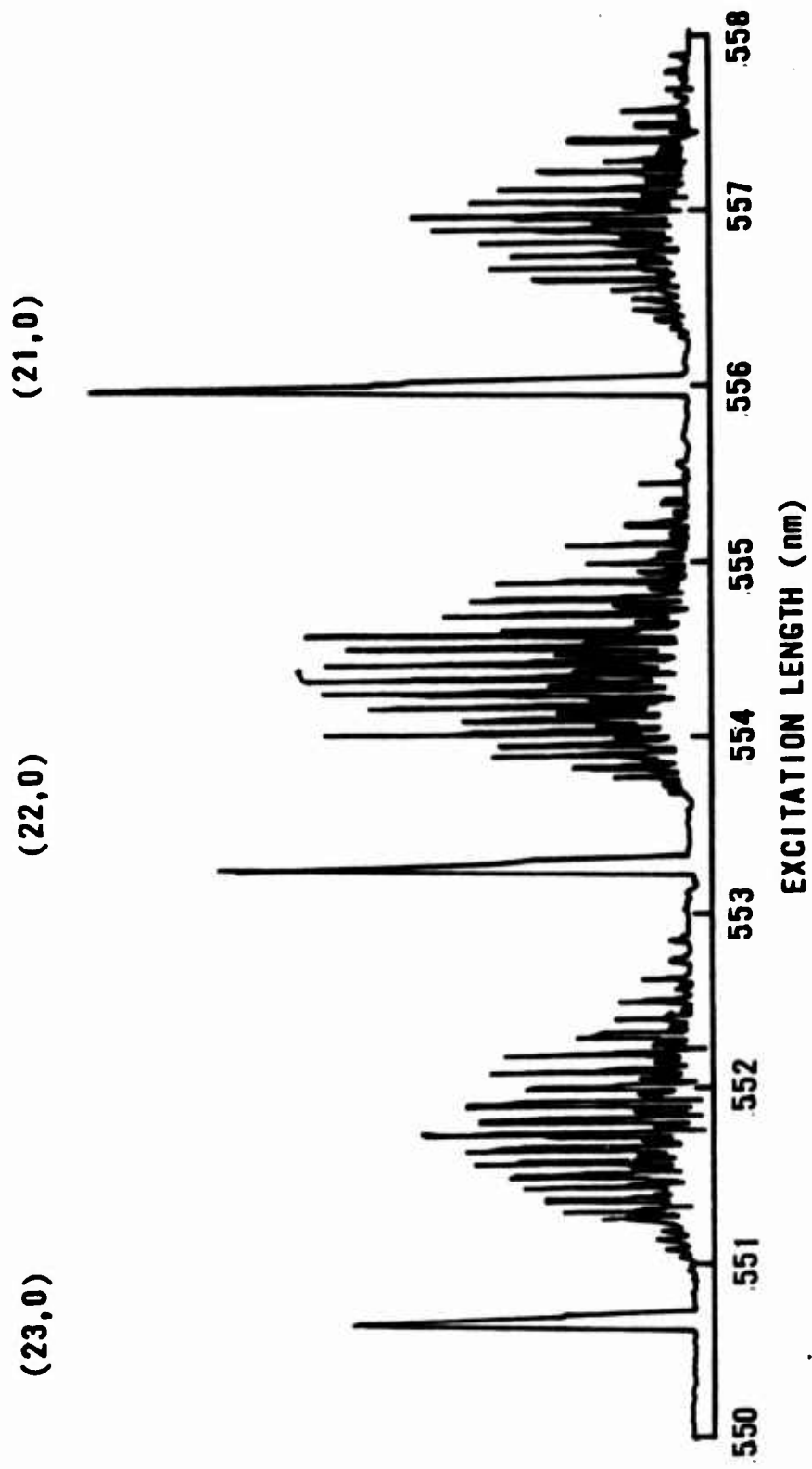
Figure 4.3 ASE Excitation of v' = 23, 22, and 21.
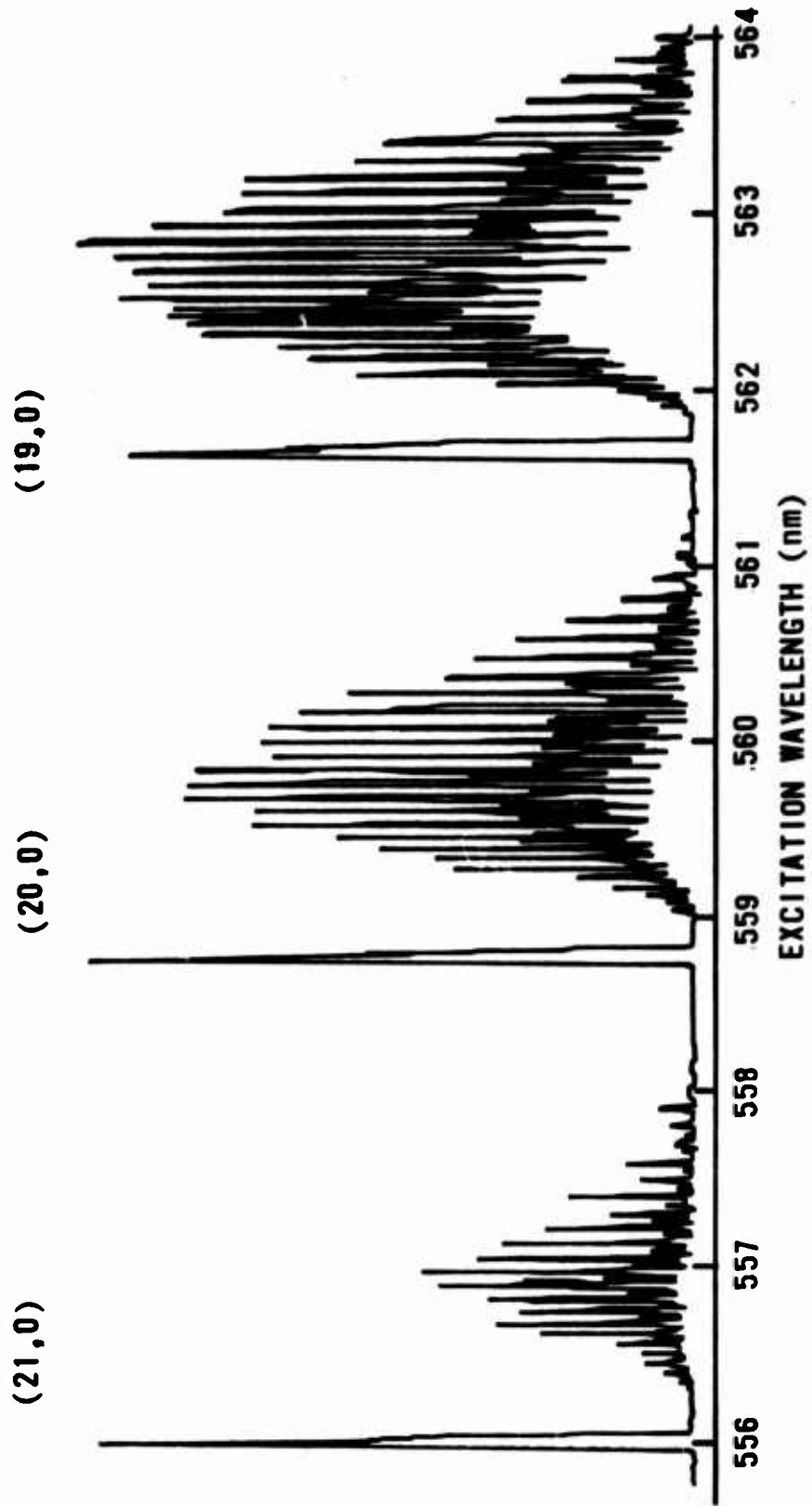
Figure 4.4 ASE Excitation of v' = 21, 20, and 19.

57
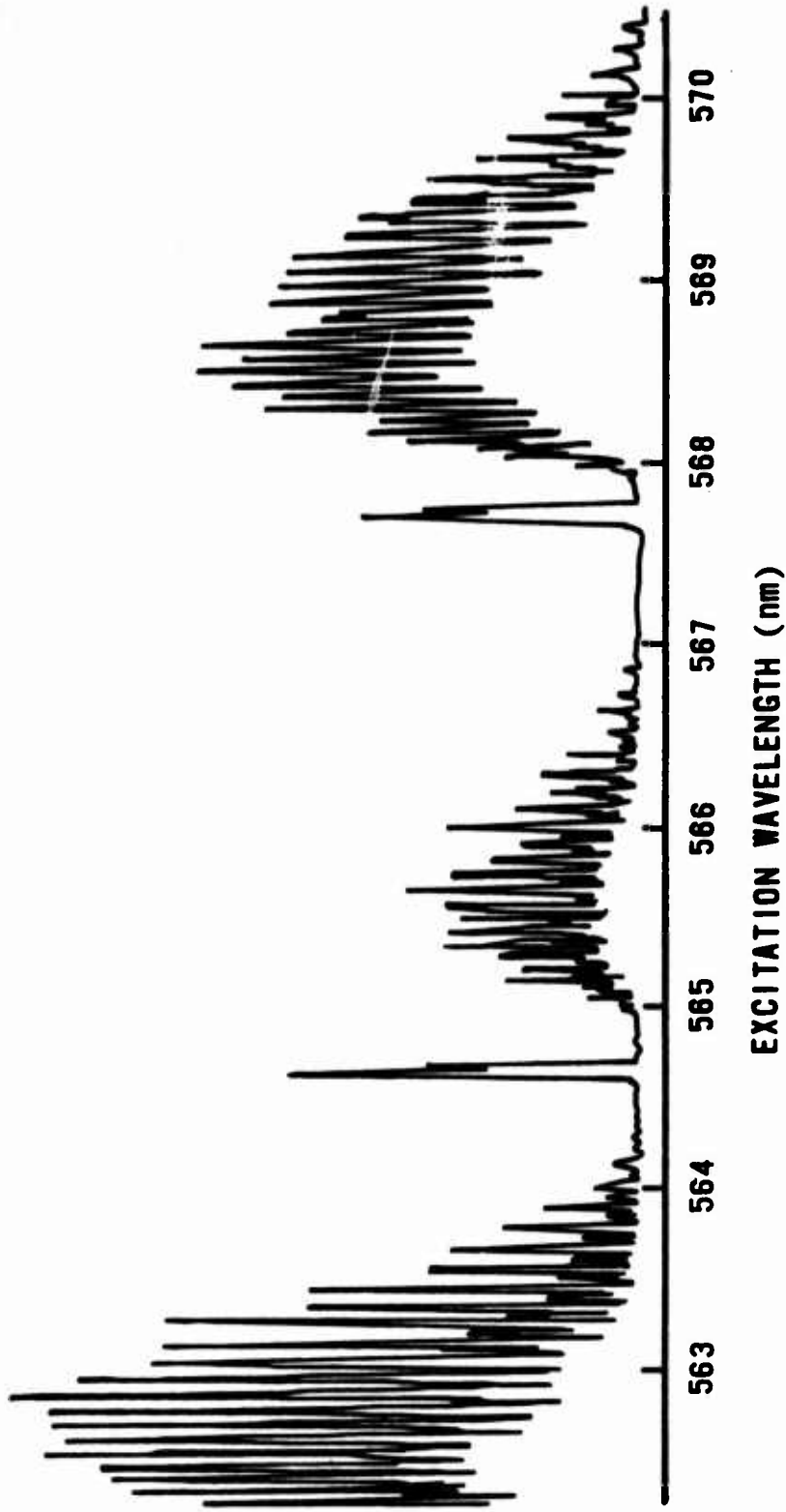
Figure 4.5 ASE Excitation of v' = 18 and 17.
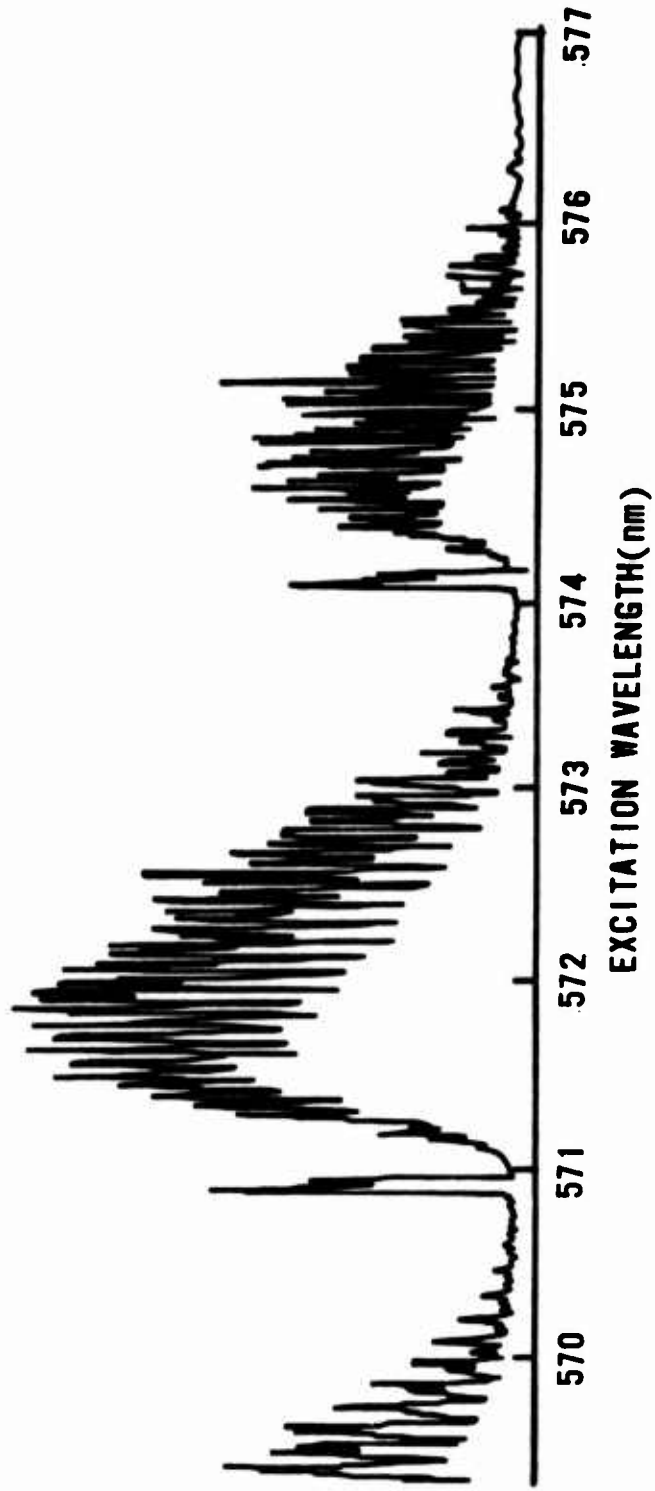
Figure 4.6 ASE Excitation of v' = 16 and 15.

59
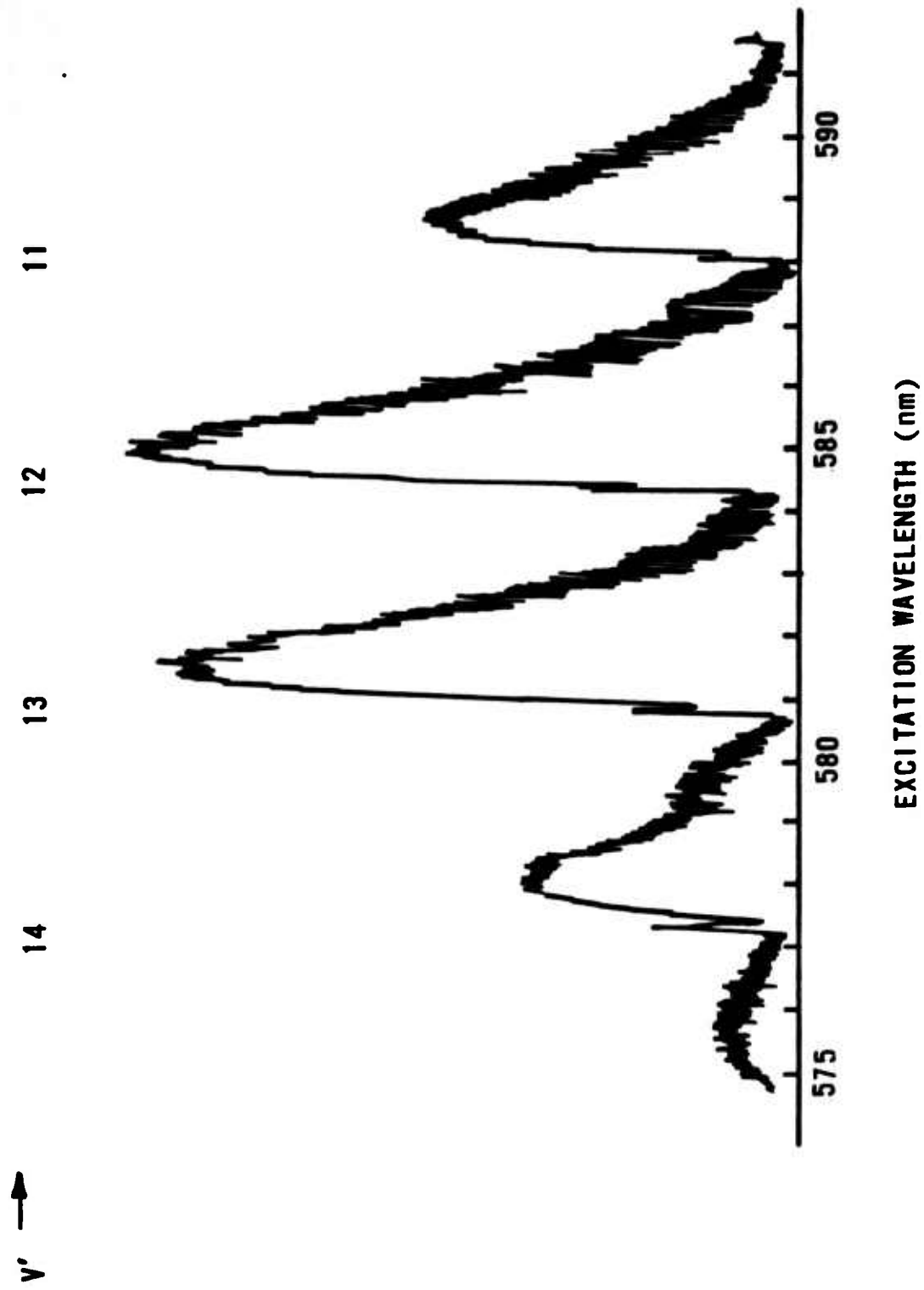
Figure 4.7 ASE Excitation Spectrum over the Kitton Red 620 Dye Region.
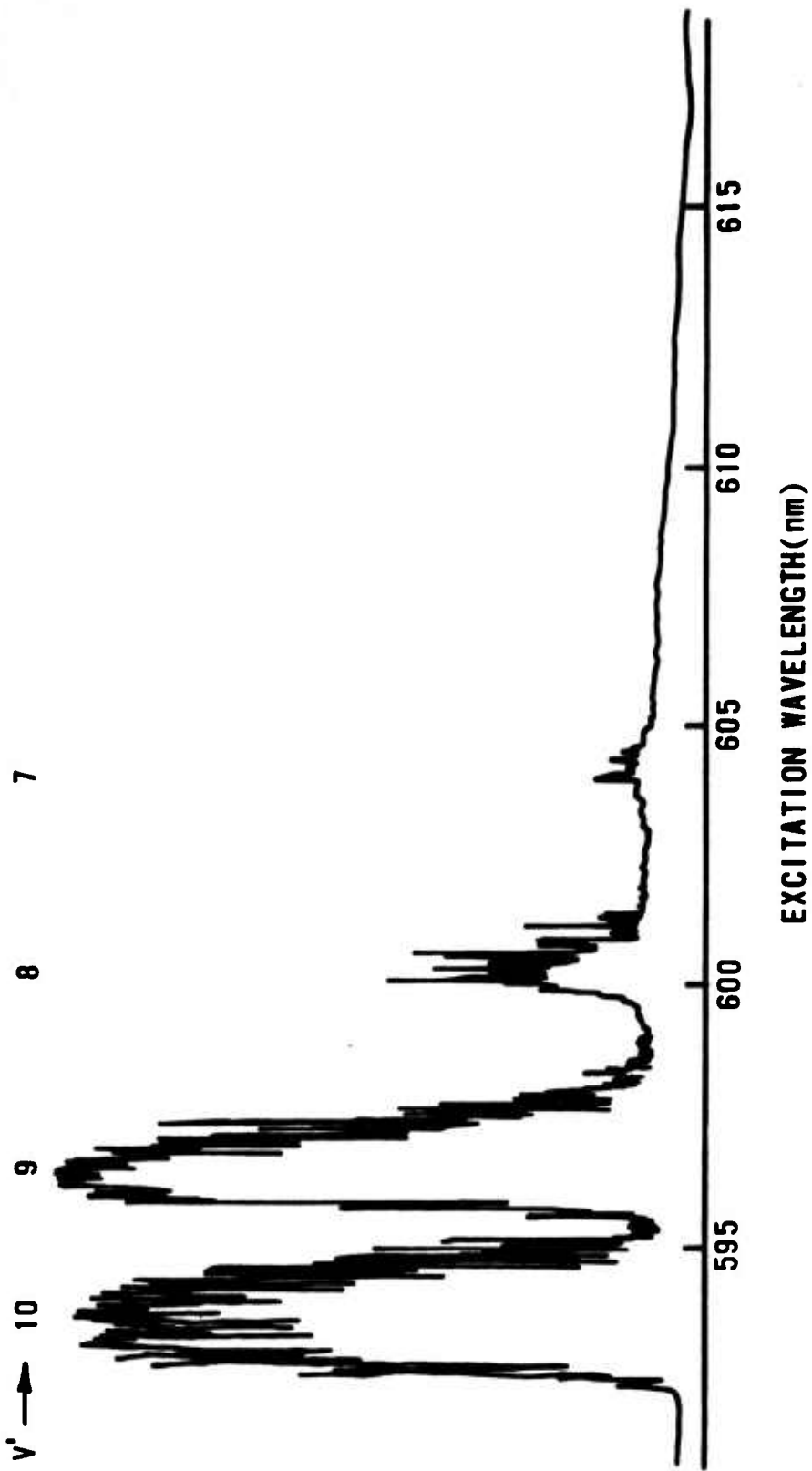
Figure 4.8 ASE Excitation Spectrum over the Rhodamine 640 Dye Region.

61
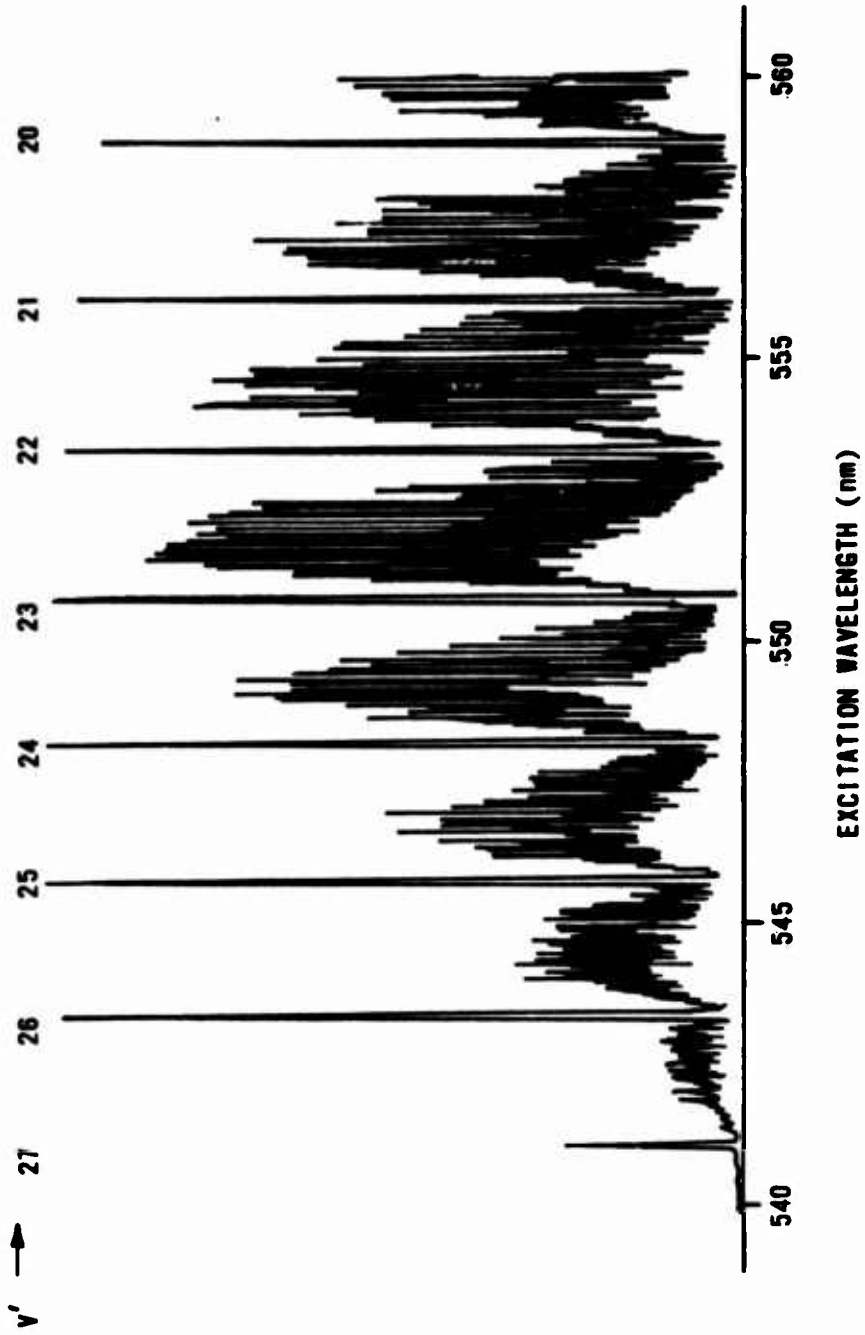
Figure 4.9 ASE Excitation Spectrum over the Fluorescein 548 Dye Region.

62
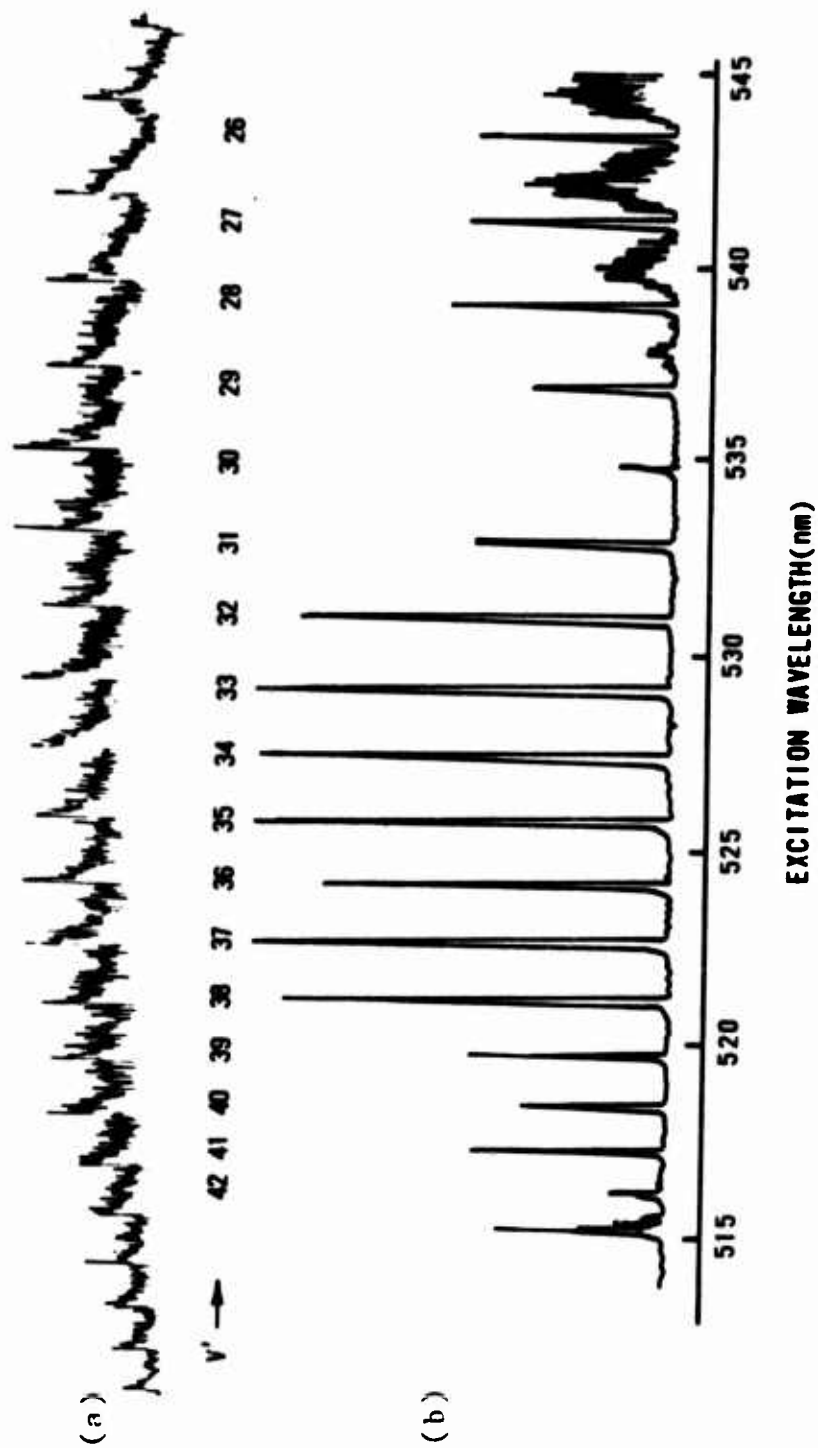
Figure 4.10 ASE Excitation Spectrum over the Coumarine 500 Dye Region. Side fluorescence (a) and ASE (b) is shown.

63

EXCITATION WAVELENGTH(Å)

5150    5155    5160
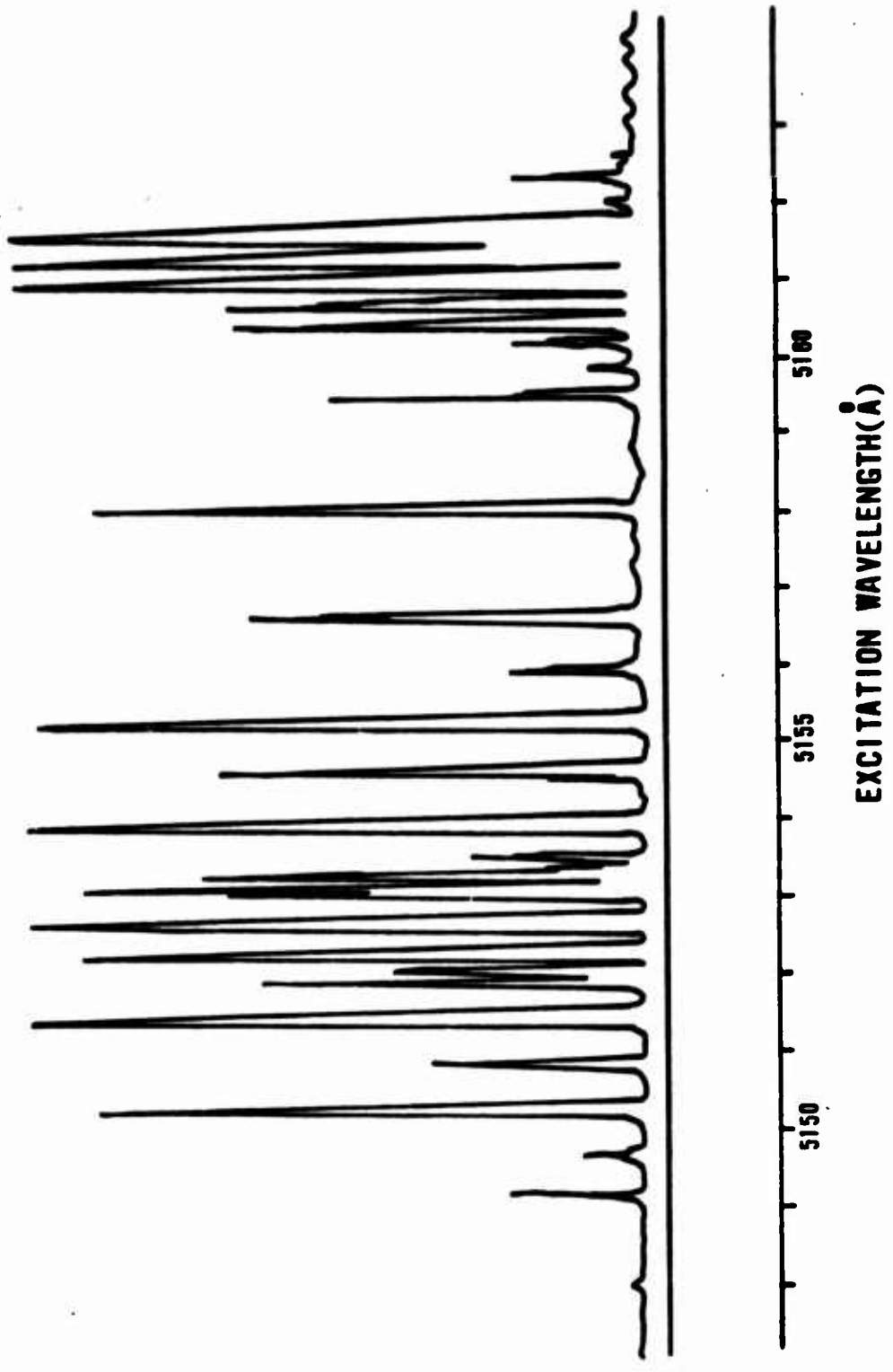
Figure 4.11 High Resolution ASE Excitation Spectrum Near 515nm.

spectra at various resolution levels taken under various conditions throughout the ASE excitation region.

## 2.Emission Spectra

A complete and detailed emission survey was crucial to the understanding of the ASE excitation spectra and its assignment. The wavelength of the ASE depended upon the B state vibrational level excited. Figure 4.12 shows a typical resolved emission spectrum for excitation within the normal region, in this case for the (21,0) pump band. Emission was to the (21,59) band. Observed was the normal P-R doublet consistant with the selection rule $\Delta J = \pm 1$ [3]. Four lines are present because two rotational levels in the ground state are simultaneously pumped.

Figure 4.13 shows an emission spectrum for the spiked region of the (21,0) pump band. Only a single emission line is observed. A single emission line is always observed when optically pumping within any of the spiked regions, including the 515 nm region that displays abnormal spike behavior. The emission behavior for the spiked regions is significant to aid in the understanding the spiked excitation, and will be discussed in following sections.
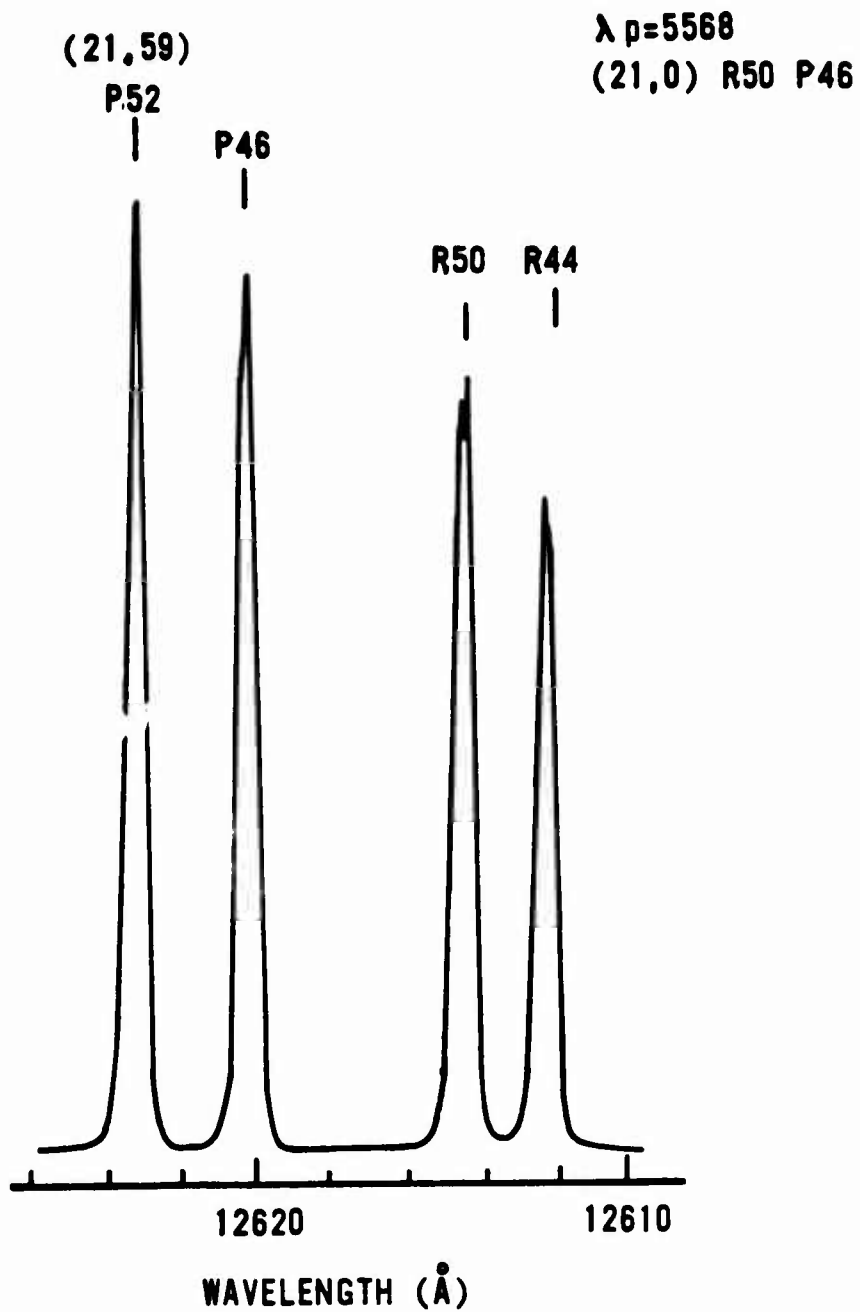
Figure 4.12 Typical Band Emission Spectrum.
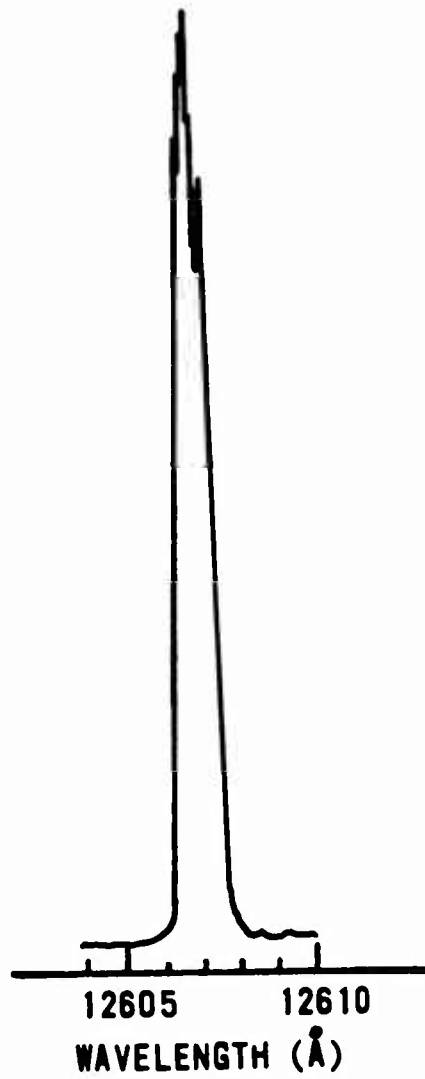
Figure 4.13 Typical Spike Emission Spectrum.

### 3.Summary of Vibrational Spectra

A complete vibrational summary of the ASE is given in Table 4.1. As presented, excitation occurs in the visible region and emission is in the near-infrared region. This suggests the possibility of using this process as a "wavelength converter". The range of operation is shown in Figure 4.14. The usefulness of ASE as a wavelength converter depends upon the efficiency of converting visible photons to infrared photons. This point is discussed in a later section.

Table 4.1 reveals that ASE generally terminates to multiple ground state vibrational levels for excitation $v' \leq 30$. For $v' \geq 31$, all emission occurs to a single vibrational level, terminating on very high $v''$ with large $\Delta v$ transitions. In a paper by Tellinghuisen [38] are published Franck-Condon Factors (FCF) for $v'-v''$ transitions for $v' = 6, 21, 43,$ and 62. He shows that some transitions have FCF that are much larger than any others. As an example, for $(v',v'') = (43,83)$, the FCF is 0.45. Table 4.1 does indeed show that ASE occurs on this transition. In general then, the transitions reported in Table 4.1 should be an indication of the highest FCF for B-X transitions occuring in the infrared.

At this point, consider what is actually happening to the sample of iodine molecules, as depicted by Figure 4.15.

69

**Table 4.1**

**Vibrational Summary of ASE Transitions**

| Excitation | | Emission | | |
| Wavelength (Å) | Band | Wavelength (Å) | Band | Strength[1] |
|---|---|---|---|---|
| 6041.0 | ( 7,0) | 10747 | ( 7,38) | – |
| 6005.5 | ( 8,0) | 10519 | ( 8,38) | 3 |
|  |  | 10695 | ( 8,39) | 1 |
| 5970.9 | ( 9,0) | 10755 | ( 9,40) | 3 |
|  |  | 10935 | ( 9,41) | 1 |
| 5944.4 | (10,0) | 11008 | (10,42) | 6 |
|  |  | 11200 | (10,43) | 1 |
| 5889.6 | (11,0) | 11027 | (11,43) | 1 |
|  |  | 11220 | (11,44) | 11 |
| 5855.0 | (12,0) | 11271 | (12,45) | 2 |
|  |  | 11455 | (12,46) | 1 |
| 5821.1 | (13,0) | 11323 | (13,46) | 1 |
|  |  | 11507 | (13,47) | 3 |
|  |  | 11699 | (13,48) | 73 |
| 5774.8 | (14,0) | 11541 | (14,48) | 1 |
|  |  | 11728 | (14,49) | 4 |
| 5747.2 | (15,0) | 11787 | (15,50) | 8 |
|  |  | 11975 | (15,51) | 1 |
| 5708.6 | (16,0) | 11823 | (16,51) | 1 |
|  |  | 12013 | (16,52) | 4 |
| 5672.5 | (17,0) | 12059 | (17,53) |  |
|  |  | 12247 | (17,54) | 1 |
| 5647.0 | (18,0) | 12107 | (18,54) | 1 |
|  |  | 12294 | (18,55) | 2 |
| 5617.1 | (19,0) | 12155 | (19,55) | 1 |
|  |  | 12337 | (19,56) | 83 |
| 5588.0 | (20,0) | 12384 | (20,57) | 3 |
|  |  | 12567 | (20,58) | 1 |

1. Strength indicates relative intensity between multiple
emission lines.

Table 4.1, continued

Vibrational Summary of ASE Transitions

| Excitation | | Emission | | |
| Wavelength (Å) | Band | Wavelength (Å) | Band | Strength[1] |
|---|---|---|---|---|
| 5560.2 | (21,0) | 12426 | (21,58) | 1 |
| | | 12608 | (21,59) | 8 |
| 5535.2 | (22,0) | 12653 | (22,60) | - |
| 5506.9 | (23,0) | 12689 | (23,61) | 38 |
| | | 12865 | (23,62) | 1 |
| 5482.2 | (24,0) | 12727 | (24,62) | 1 |
| | | 12903 | (24,63) | 2 |
| 5457.7 | (25,0) | 12767 | (25,63) | 1 |
| | | 12935 | (25,64) | 2 |
| 5434.6 | (26,0) | 12976 | (26,65) | - |
| 5411.8 | (27,0) | 13008 | (27,66) | - |
| 5389.8 | (28,0) | 13038 | (28,67) | - |
| 5368.6 | (29,0) | 13070 | (29,68) | 8 |
| | | 13220 | (29,69) | 1 |
| 5348.1 | (30,0) | 13099 | (30,69) | 2 |
| | | 13246 | (30,70) | 1 |
| 5328.6 | (31,0) | 13268 | (31,71) | - |
| 5309.6 | (32,0) | 13289 | (32,72) | - |
| 5291.5 | (33,0) | 13308 | (33,73) | - |
| 5274.1 | (34,0) | 13326 | (34,74) | - |
| 5257.3 | (35,0) | 13343 | (35,75) | - |
| 5241.1 | (36,0) | 13359 | (36,76) | - |
| 5225.9 | (37,0) | 13372 | (37,77) | - |
| 5211.4 | (38,0) | 13385 | (38,78) | - |
| 5197.6 | (39,0) | 13390 | (39,79) | - |

71

Vibrational Summary of ASE Transitions

| Excitation | | Emission | | |
|---|---|---|---|---|
| Wavelength (Å) | Band | Wavelength (Å) | Band | Strength[1] |
| 5184.3 | (40,0) | 13395 | (40,80) | - |
| 5172.5 | (41,0) | 13401 | (41,81) | - |
| 5165.2 | (42,0) | 13402 | (42,82) | - |
| 5154.0 | (43,0) | 13412 | (43,83) | - |
| 5149.7 | (44,0) | 13414 | (44,84) | - |

The molecules are pumped from the ground state level into the excited state due to the high degree of wavefunction overlap at the inner classical turning points of the potential curves. ASE occurs to the high lying vibrational levels of the X state due to the large wavefunction overlap at the outer turning points of the vibration. This figure in a convienient way to express the dynamics of the process. This explains why pumping is in the visible, and ASE is in the infrared.

4.Spectra of the 515 nm Excitation Region

Recall, that in excitation, the region around 515 nm showed an irregular behavior. Also note that Figure 4.11 contains no assignments. The excitation of this region was impossible to assign without knowledge of the emission wavelengths. Assignment in this region was a severe test of
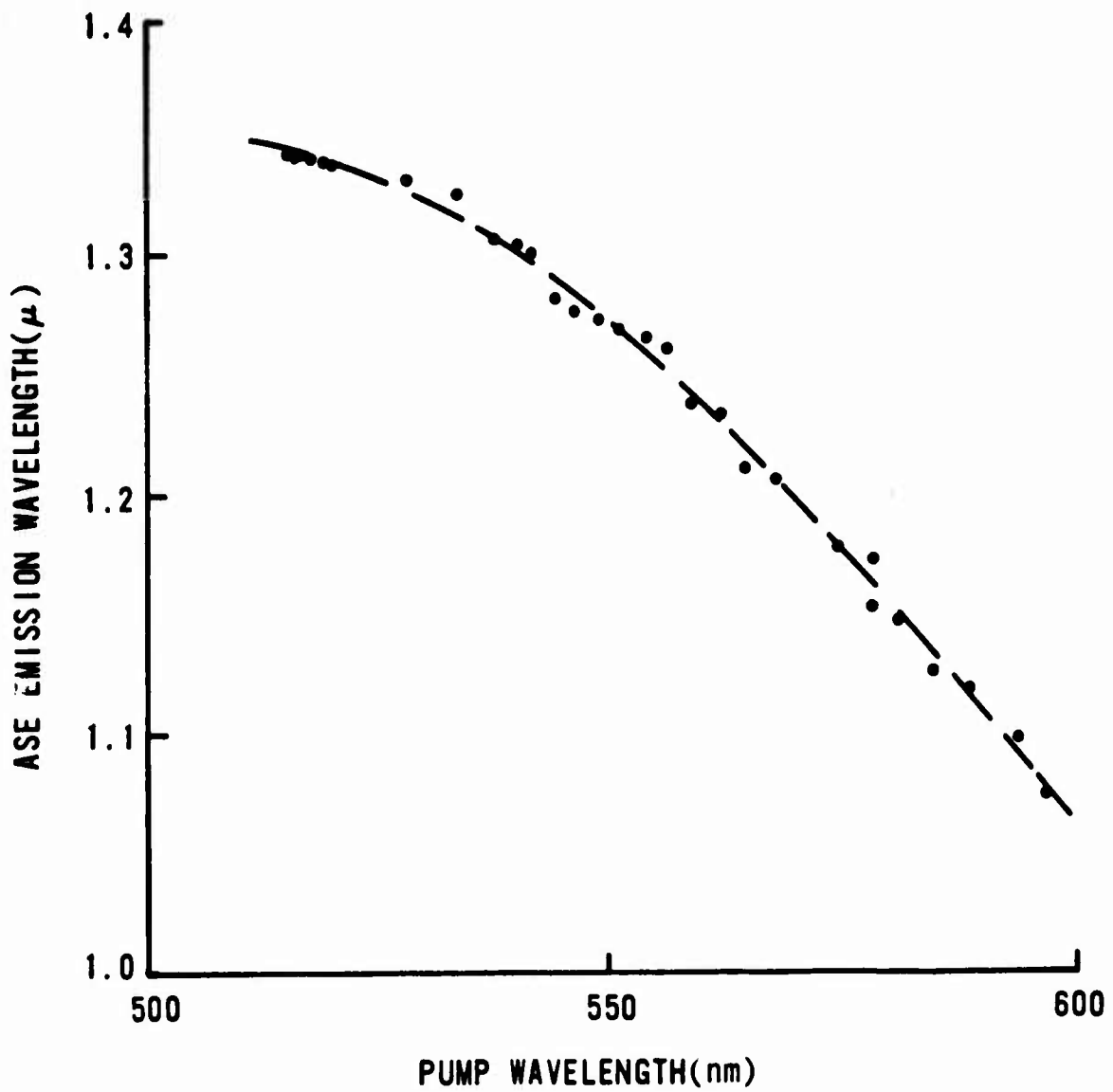
Figure 4.14 ASE as a Wavelength Converter.
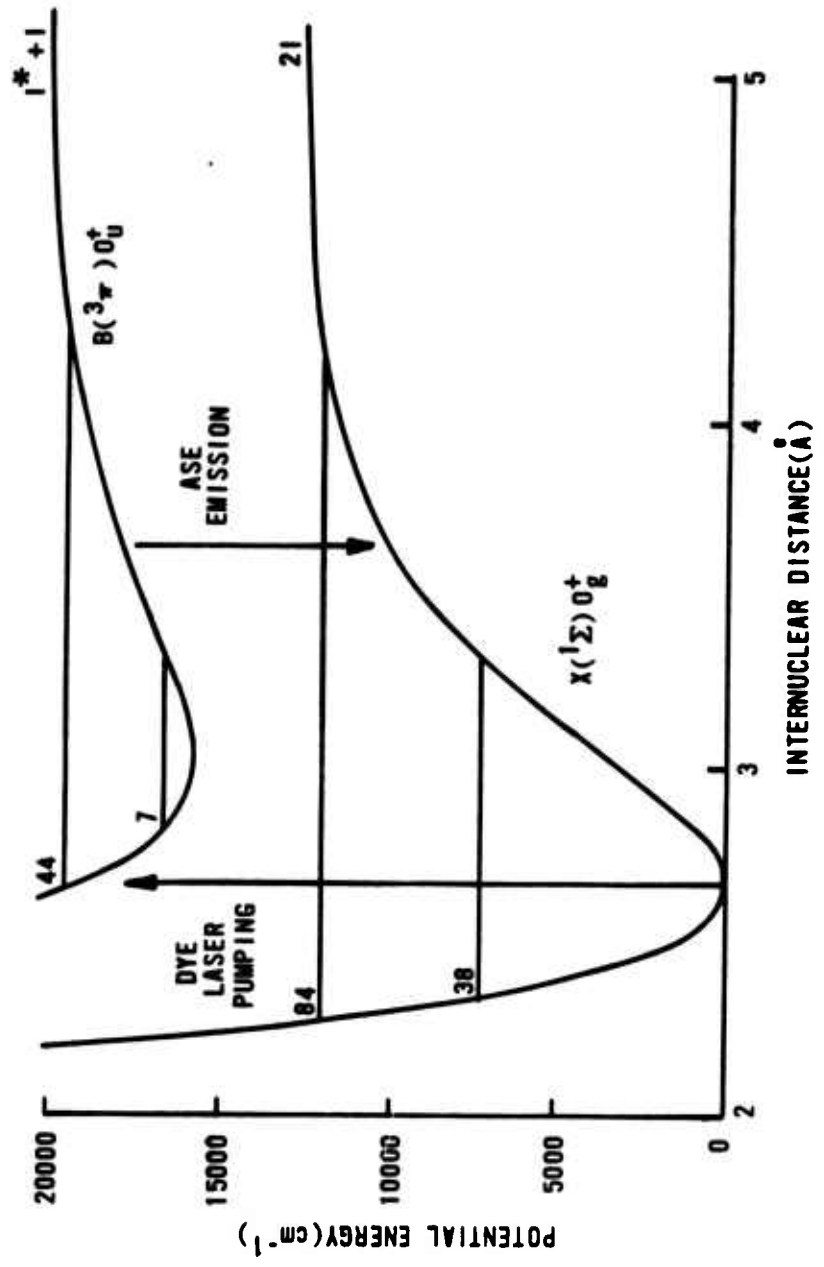
Figure 4.15 ASE Molecular Cycles.
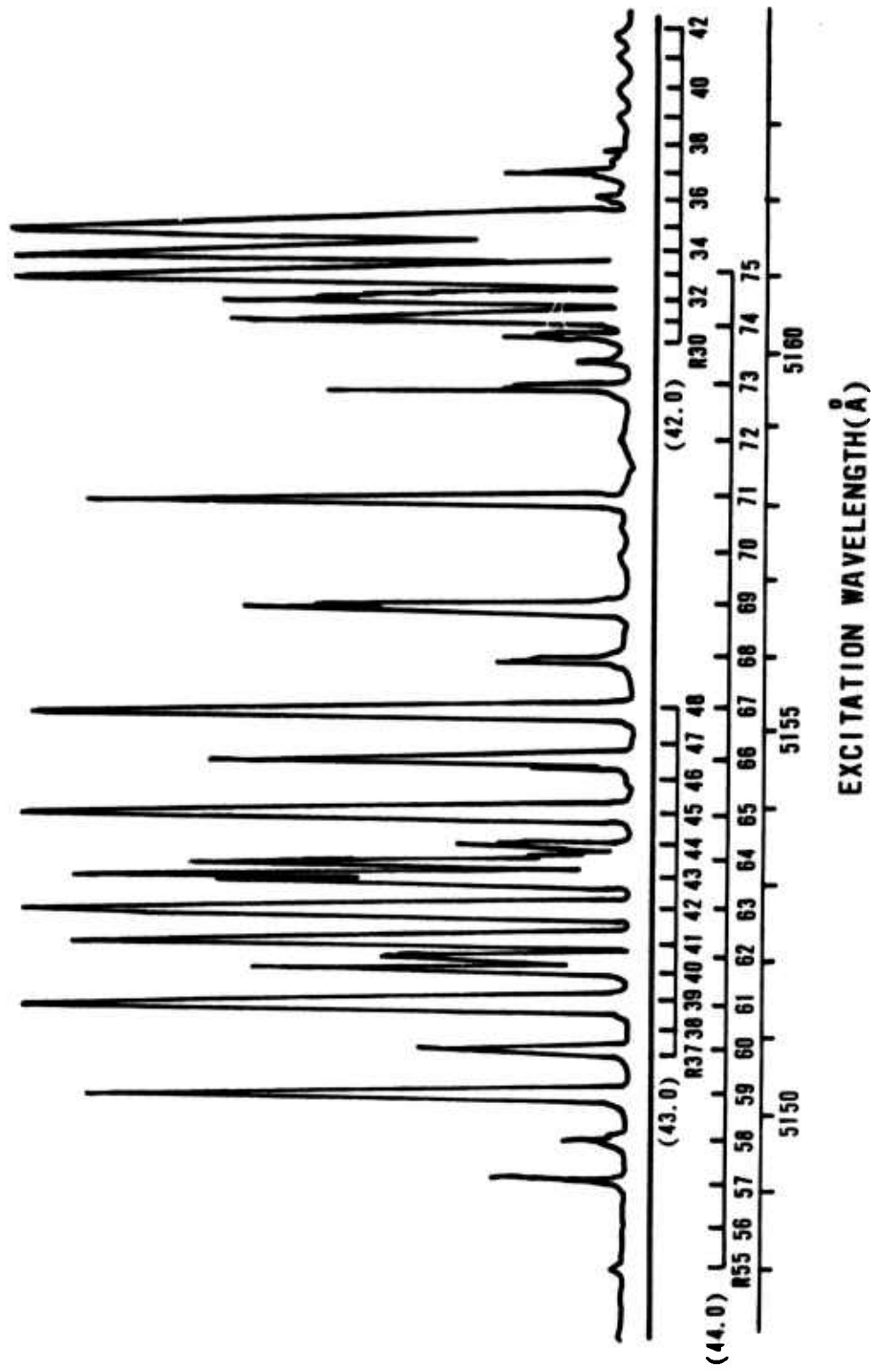
Figure 4.16 Excitation Assignments for the 515 nm Region.

Table 4.2

Spectroscopic Summary for the 515 nm Pump Region

| Excitation | | Emission | | Delta[2] |
|---|---|---|---|---|
| Wavelength (Å) | Transition | Wavelength (Å) | Transition[1] | |
| 5161.8 | (42,0) R35 | 13407.2 | (42,82) R35  13408.8 | 1.6 |
| 5161.5 | (42,0) R34 | 13406.8 | (42,82) R34  13408.8 | 2.0 |
| 5161.1 | (42,0) R33 | 13407.2 | (42,82) R33  13408.8 | 1.6 |
| 5159.7 | (44,0) R73 | 13414.0 | (44,84) R73  13415.8 | 1.8 |
| 5158.2 | (44,0) R71 | 13414.5 | (44,84) R71  13415.8 | 1.3 |
| 5156.6 | (44,0) R69 | 13414.0 | (44,84) R69  13415.8 | 1.8 |
| 5155.4 | (44,0) R67 | 13414.0 | (44,84) R67  13415.8 | 1.8 |
| 5154.7 | (44,0) R66 | 13414.4 | (44,84) R66  13415.8 | 1.4 |
| 5154.1 | (43,0) R45 | 13412.1 | (43,83) R45  13413.2 | 1.4 |
|  | (44,0) R65 | 13414.4 | (44,84) R65  13415.8 | 1.1 |
| 5153.4 | (44,0) R64 | 13411.6 | (44,84) R64  13415.8 | 4.2 |
| 5152.8 | (43,0) R42 | 13411.6 | (43,83) R42  13413.2 | 1.8 |
|  | (44,0) R63 | 13414.0 | (44,84) R63  13415.8 | 1.6 |
| 5152.4 | (43,0) R41 | 13412.0 | (43,83) R41  13413.2 | 1.2 |
| 5151.6 | (43,0) R39 | 13411.0 | (43,83) R39  13413.2 | 1.0 |
|  | (44,0) R61 | 13414.8 | (44,84) R61  13415.8 | 2.2 |
| 5150.9 | (44,0) R60 | 13414.0 | (44,84) R60  13415.8 | 1.8 |
| 5150.3 | (44,0) R59 | 13414.5 | (44,84) R59  13415.8 | 1.3 |
| 5149.7 | (44,0) R58 | 13414.3 | (44,84) R58  13415.8 | 1.5 |
| 5149.2 | (44,0) R57 | 13414.1 | (44,84) R57  13415.8 | 1.7 |
| 5148.6 | (44,0) R56 | 13414.0 | (44,84) R56  13415.8 | 1.8 |
| 5148.0 | (44,0) R55 | 13414.5 | (44,84) R55  13415.8 | 1.3 |

1. Transition wavelength reported in this column is based upon calculauted values using spectroscopic constants [22,23].
2. Delta is defined as the difference between the calculated value and the observed value of the emission wavelength.

77
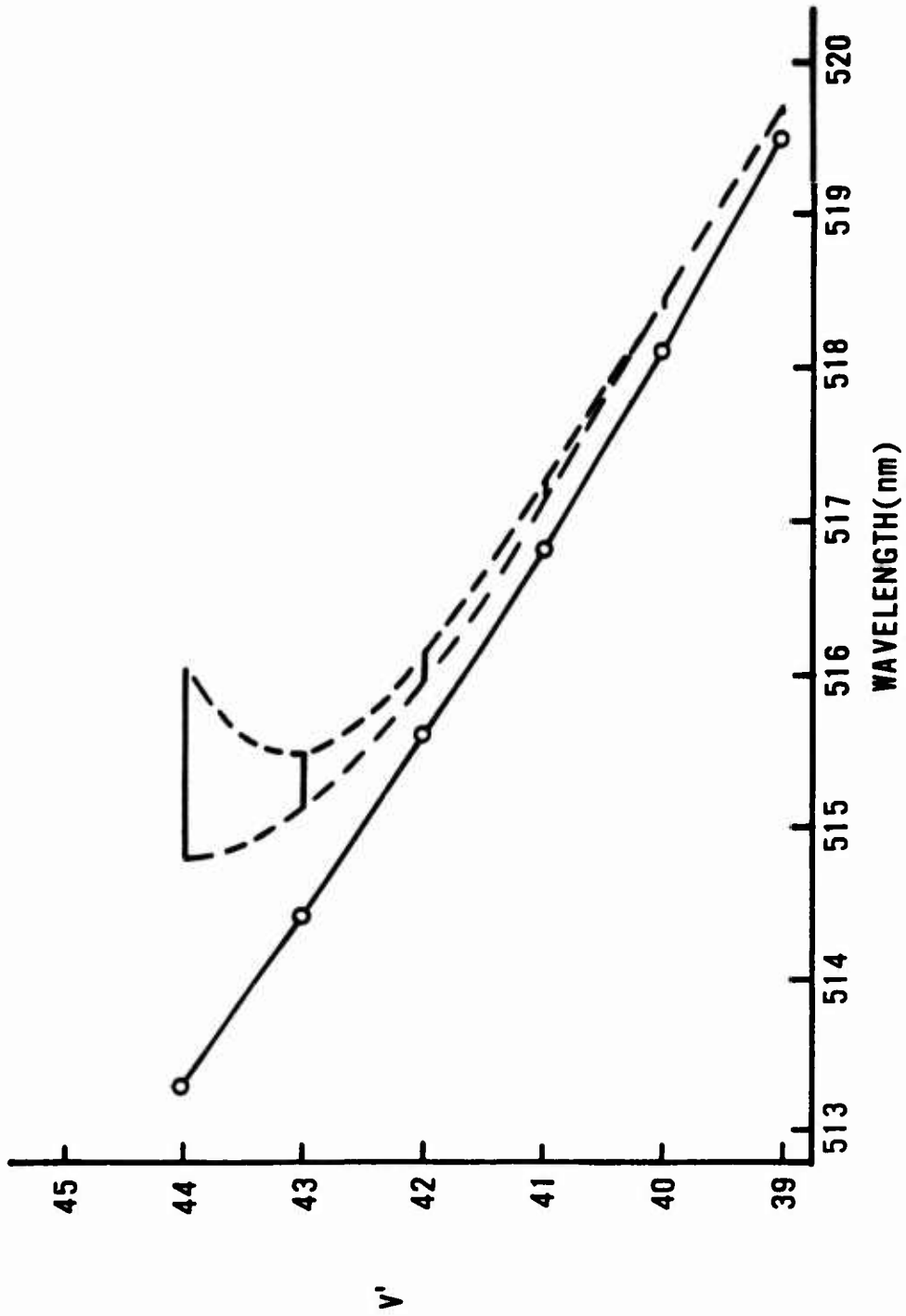
Figure 4.17 ASE Spike Envelope Trend. The pump band origins are indicated by the circles. The spike envelope is given as a horizontal line.

78

## 5.Summary of Important Facts

Reviewing the important facts of the ASE excitation and emission:

1) Excitation was observed from $v'$= 7-44 in the visible region of the spectrum.

2) Emission occured to $v''$= 38-84 in the infrared region of the spectrum.

3) The spiked ASE within any band consisted of a single emission line.

4) The spiked excitation spectra were wider than the pump laser, and the excitation envelope expands rapidly at $v'$= 44.

5) The spiked excitation normally occured near the band origin, but rapidly moved to higher rotational levels at $v'$= 44.

A close examination of the excitation spectra, Figure 4.18, showed that the width of the spikes to be much greater than the width of any single rotational line within the band, suggesting that the dye laser was simultaneously

79

exciting more than one rotational line when pumping the spike. One might conclude that simultaneous excitation of several adjacent rotational levels in $I_2(B)$ could explain the spiked behavior. However, as shown below, independent emissions from a few simultaneously excited levels is inadequate to explain the observed behavior. The explanation is more subtle.

## 6. Cooperative Stimulated Emission

Consider pumping of the (21,0) band and subsequent ASE on the (21,59) band. Table 4.3 presents the relevant line positions and normalized line strengths of $(J',J")$ transitions using the spectroscopic constants of Luc [22] and Tellinghuisen et al. [23]. The line strength factor $\theta_{J',J"}$ is proportional to the Boltzmann population of $J"$ (see Appendix E). The rotational line strengths $S_{J',J"}$ are neglected because under the conditions of the present example all $J',J"$ pump transitions were saturated. The $\theta_{J',J"}$ were normalized to the Boltzmann maximum at $J"= 53$. When pumping a $(v',J'-v",J")$ band, the population in $J'$, and hence the ASE gain, will be proportional to the population in $J"$. For the conditions shown in Figure 4.18, normal ASE ceases for $\lambda_{pump}$ shorter than that for P(25) $(\theta_{J',J"}=0.70)$. This is the threshold condition. Spiked ASE first occurs for excitation near R(16) $(\theta_{J',J"}=0.36)$. Thus there will be
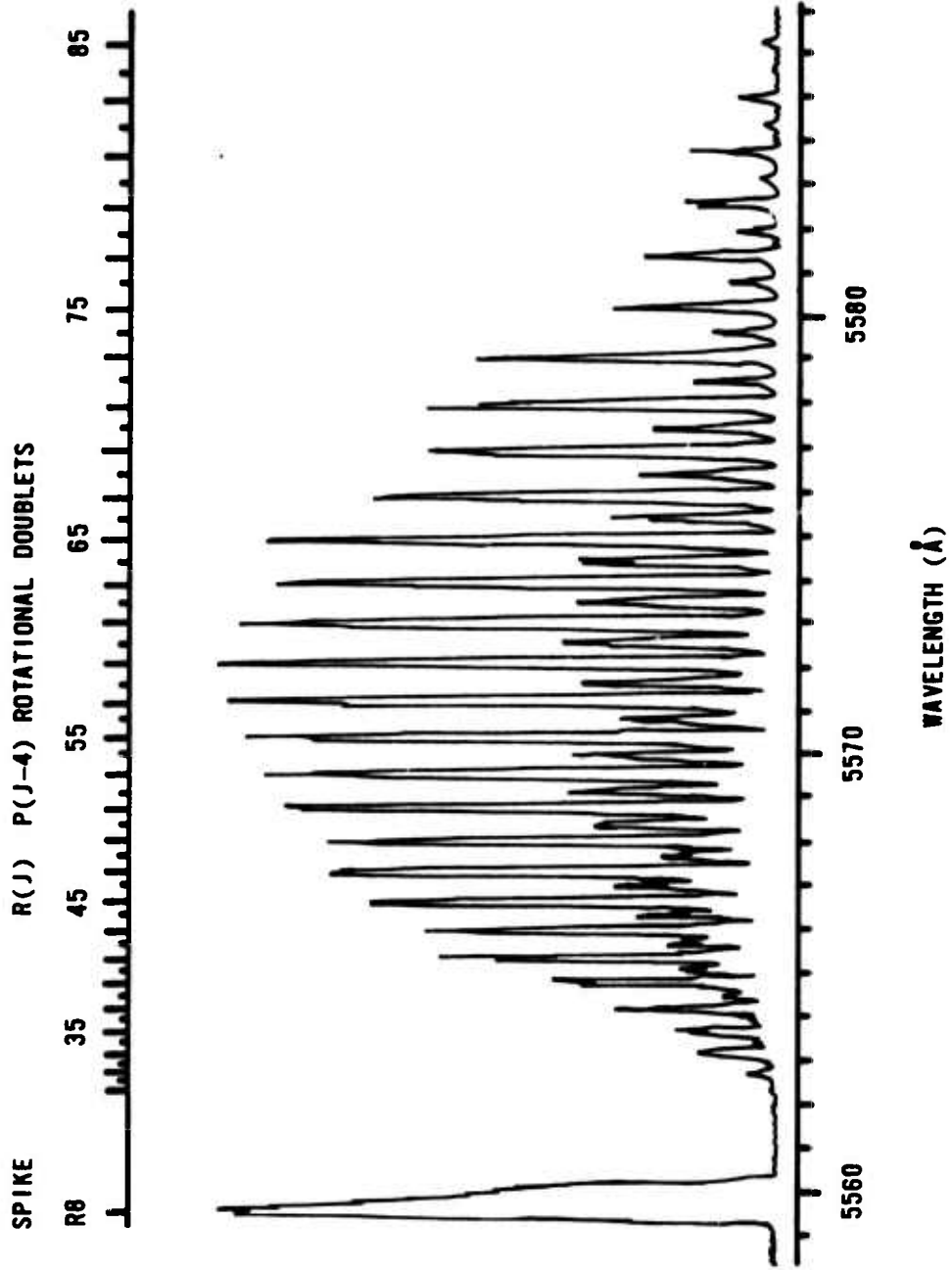
Figure 4.18 High Resolution ASE Excitation Spectrum of the (21,0) Band.

82

anomalously wide rovibronic lines for the $I_2$ (B-X) system.
At room temperature, Doppler broadening blends these lines
to produce relatively large linewidths and Fabry-Perot
absorption measurements have shown that these widths can be
as large as 0.03 cm$^{-1}$ [96]. From Table 4.3 note that near
the emission bandhead of (21,59), the R(5)-R(12) lines lie
within this 0.03 cm$^{-1}$ range. There are no such overlaps for
the P branch emission lines. This is the reason that no P
branches are observed in spectrally resolved spiked
emission.

Recall that for the present example $J \leq 25$ levels are
too sparsely populated to be brought to ASE threshold as
individual levels. However, near the absorption transition
bandhead in absorption several levels are simultaneously
populated. In addition there is a near coincidence of P(J)
and R(J+4) for the (21,0) band. For example P(10) and R(14)
are only 0.03 cm$^{-1}$ apart and well within the dye laser
bandwidth of 0.5 cm$^{-1}$. They also have a combined intensity
factor greater than that for pumping J'= 25. Even though
these simultaneously excited J' levels are separated by
approximately ten times the doppler width of any one
emission line, they emit in an extremely narrow frequency
range that is smaller than the inhomogeneous linewidth of a
single $I_2$(B-X) rovibronic emission line. Spontaneous
emission originating from any one of these levels (J'=6-13)
can cause stimulated emission from several other adjacent

84

levels.  These adjacent levels act as a single state in that if several are simultaneously excited, they can subsequently emit cooperatively.

The observation of cooperative lasing in molecular lasers has been reported in connection in systems with densely overlapped discrete spectra, such as XeF, HgCl, HgI, and HgBr [97-100].  But very little has been concluded about the physics of the process.  Therefore it is not clear that the cooperative emission described here is the same process as described in the literature.

The following is a summary explanation of the cooperative stimulated emission process.  Several adjacent rotational levels of the excited state are simultaneously populated via optical pumping.  Individually, these energy levels have insufficient population to excede ASE threshold. Their emission frequencies are coincident, so these discreet energy levels contribute photons to a common radiation field.  The stimulated emission intensity is therefore enhanced.  The system of levels act as a "super level" with a population that is the sum of the individual levels.  This "super" population is well above ASE threshold, hence strong ASE is observed.  One can say that the levels cooperate in the stimulated emission at a common frequency.  The process described above will be defined as Cooperative Stimulated Emission (CSE).  The system of adjacent, independent rotational levels involved will be defined as a

"superlevel". These superlevels excede the normal threshold requirement, and the spiked excitation results.

The above discussion clearly explains the forked structure observed for spikes in the R590 pump region, such as the (17,0) band whose spiked region is shown in Figure 4.19. Also shown is an energy level schematic. Table 4.4 contains the transition wavelength and Boltzmann intensity $\theta_{J',J''}$ values. Refer to this table during the following discussion.

The separation between the peak of the forks of the (17,0) spike is 0.4 $\overset{\circ}{A}$. This separation coincides with the difference between the (17,0) R7 and P9 transitions. These transitions both populate J'= 8 in the B state. The emission band of (17,53) contains a bandhead at R7. The CSE superlevel is centered at J'= 8, with CSE centered on the (17,53) R7 transition at 12059.29 $\overset{\circ}{A}$. When the dye laser is centered on the (17,0) P9 transition, the P8 and P11 transitions are also pumped. These transition populate J'= 7, 8, and 9 forming a three level superlevel which excedes ASE threshold and CSE is observed.

When the dye laser is centered on the (17,0) R7 transition, R0 through R9 are pumped, populating J'= 1-10. Only the states J'= 6-10 are a superlevel though. The R branch pumps a five level superlevel, yielding a cooperative population, which results in stronge CSE (as Figure 4.19 shows). Only the (17,53) R5-R10 transitions are close

86
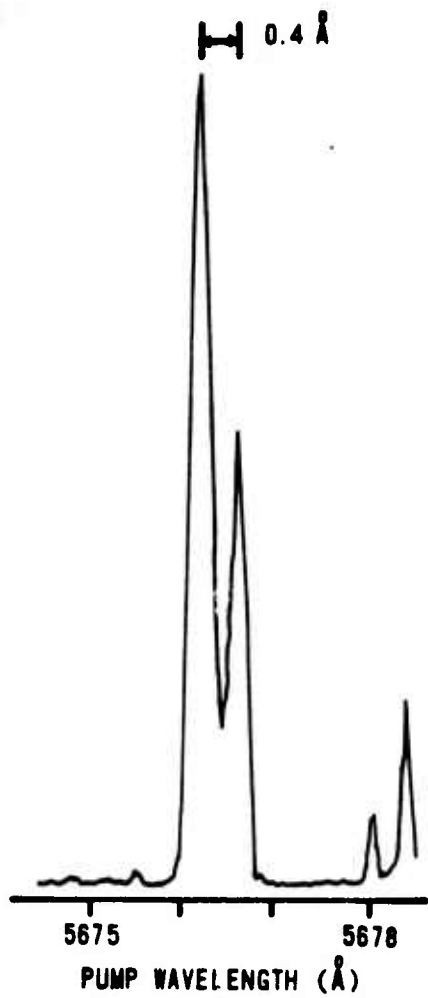
**(a) ASE (17,0) SPIKE EXCITATION**
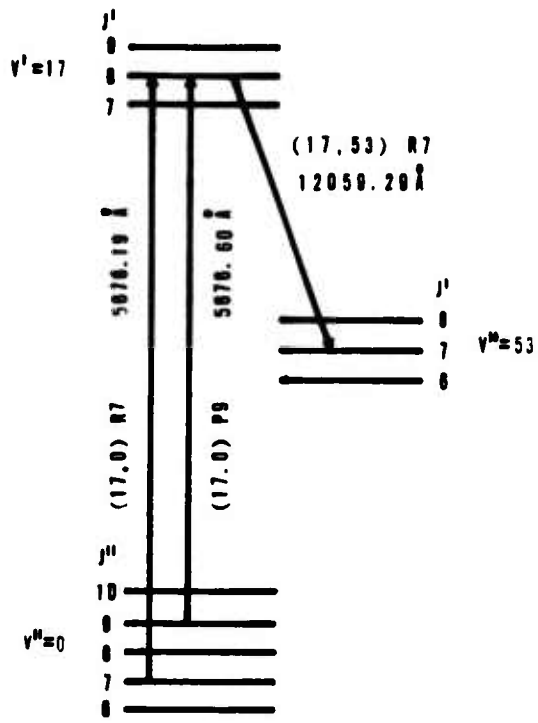
**(b) SCHEMATIC**

Figure 4.19 ASE (17,0) Spike Excitation. Spectrum (a) and energy level schematic (b) is shown.

Table 4.4

Transition Wavelengths for the (17,0) and (17,53) Bands

| | (17,0) Band | | | | (17,53) Band | | |
|---|---|---|---|---|---|---|---|
| | Wavelength (Å) | $\theta_{J',J''}$ | | Wavelength (Å) | Wavelength (Å) | | Wavelength (Å) |
| P 1 | 5676.14 | 0.032 | R 0 | 5676.10 | 12059.71 | R 0 | 12059.55 |
| P 2 | 5676.18 | 0.045 | R 1 | 5676.09 | 12059.80 | R 1 | 12059.48 |
| P 3 | 5676.21 | 0.094 | R 2 | 5676.09 | 12059.91 | R 2 | 12059.42 |
| P 4 | 5676.26 | 0.090 | R 3 | 5676.10 | 12060.02 | R 3 | 12059.38 |
| P 5 | 5676.31 | 0.16 | R 4 | 5676.11 | 12060.15 | R 4 | 12059.34 |
| P 6 | 5676.38 | 0.13 | R 5 | 5676.13 | 12060.28 | R 5 | 12059.32 |
| P 7 | 5676.44 | 0.22 | R 6 | 5676.16 | 12060.43 | R 6 | 12059.30 |
| P 8 | 5676.52 | 0.18 | R 7 | 5676.19 | 12060.58 | R 7 | 12059.29 |
| P 9 | 5676.60 | 0.28 | R 8 | 5676.23 | 12060.75 | R 8 | 12059.30 |
| P10 | 5676.69 | 0.22 | R 9 | 5676.28 | 12060.92 | R 9 | 12059.31 |
| P11 | 5676.79 | 0.34 | R10 | 5676.34 | 12061.11 | R10 | 12059.34 |
| P12 | 5676.89 | 0.26 | R11 | 5676.40 | 12061.30 | R11 | 12059.37 |
| P13 | 5677.01 | 0.40 | R12 | 5676.48 | 12061.51 | R12 | 12059.41 |
| P14 | 5677.12 | 0.30 | R13 | 5676.55 | 12061.72 | R13 | 12059.47 |
| P15 | 5677.25 | 0.45 | R14 | 5676.64 | 12061.94 | R14 | 12059.53 |
| P16 | 5677.39 | 0.34 | R15 | 5676.73 | 12062.18 | R15 | 12059.60 |
| P17 | 5677.53 | 0.51 | R16 | 5676.83 | 12062.42 | R16 | 12059.69 |
| P18 | 5677.68 | 0.38 | R17 | 5676.94 | 12062.68 | R17 | 12059.78 |
| P19 | 5677.83 | 0.56 | R18 | 5677.06 | 12062.94 | R18 | 12059.88 |
| P20 | 5678.00 | 0.42 | R19 | 5677.18 | 12063.21 | R19 | 12060.00 |
| P21 | 5678.17 | 0.61 | R20 | 5677.31 | 12063.50 | R20 | 12060.12 |

1. The $\theta_{J',J''}$ values are normalized Boltzmann populations.

enough in emission frequencies to allow CSE to take place.

7.Computer Modeling of CSE

In an attempt to test the above explanation, a synthetic excitation spectrum was produced using the simple model described below. Positions of the absorption lines were calculated from the constants of Luc [22] and Tellinghuisen et al. [23]. The dye laser linewidth was modeled as a Gaussion with $\Delta\nu = 0.5$ cm$^{-1}$. At a fixed laser frequency, convolution of $\Delta\nu$ with the absorption line positions gave a relative population for each pumped rotational level J'. Emission from each J' was given a 0.03 cm$^{-1}$ Gaussian linewidth. For pumping at any particular wavelength, a complete emission spectrum was internally computer calculated, with careful attention to overlaps between adjacent rotational levels' emissions. Contributions of adjacent levels were calculated by summing the emission intensities every 0.005 cm$^{-1}$ from all emissions for that particular pump spectral location. A composite emission spectrum for that particular pump wavelength is produced. The threshold emission intensity was set from the observed beginning of normal ASE. This value of threshold $\theta_{J',J''}$ defined a new zero intensity level for the composite emission spectrum. The total area of the new emission spectrum was calculated, and this was used as the intensity

for that pump wavelength. Synthetic excitation spectra were
produced by incrementing the model's excitation wavelength
in 0.005 Å increments, and repeating the above process. The
computer code for the above model is reproduced in Appendix
H.

Figure 4.20 shows the excitation spectrum for the
(17,0) spiked region produced by calculation using this
model. A similar synthetic spectrum was produced for the
(21,0) excitation band, both the spiked region and the
entire band, Figures 4.21 and 4.22. Compare them with
Figure 4.18. While not accounting for all spectral details,
this simple model does give a satisfactory "synthetic"
spectral reproduction of the data.


8.Explanation of the 515 nm Excitation Region


The excitation spectra for $\lambda_{pump}$ ≤517 nm can also be
explained by the above model in association with knowledge
of the emission band characteristics. Initially, consider
the (44,0) pump band and the (44,84) emission band. The
energies for selected rotational transitions of these bands
and the normalized Bolzmann populations for the pump band
are given in Table 4.5. In excitation, the 0.5 cm$^{-1}$
bandwidth dye laser can at most populate two rotational
levels simultaneously from a R(J)P(J-2) pair of transitions.
Therefore the superlevel is restricted to two levels, J' and
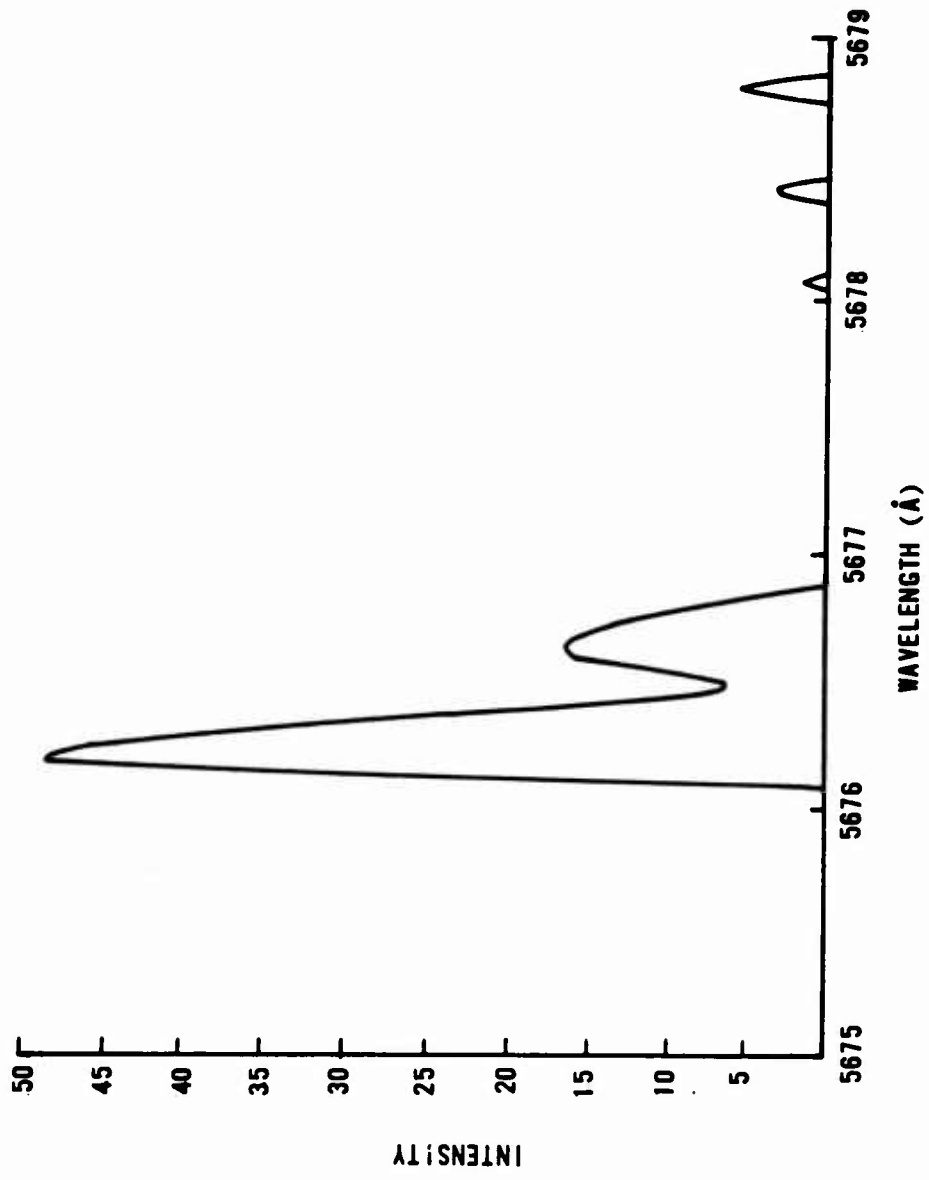
Figure 4.20 Synthetic Excitation Spectrum for the (17,0) Spike.
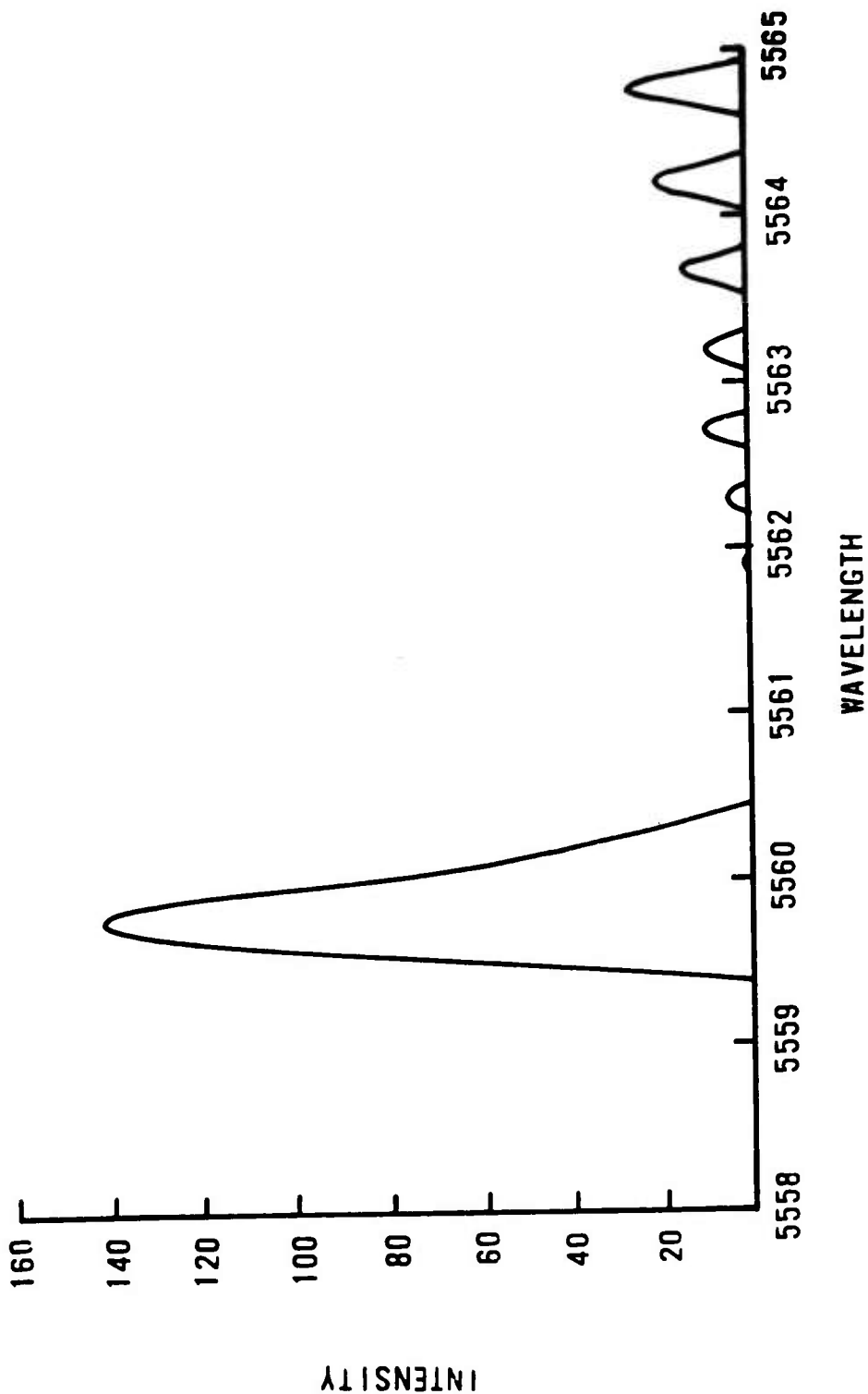
Figure 4.21 Synthetic Excitation Spectrum for the (21,0) Spike.
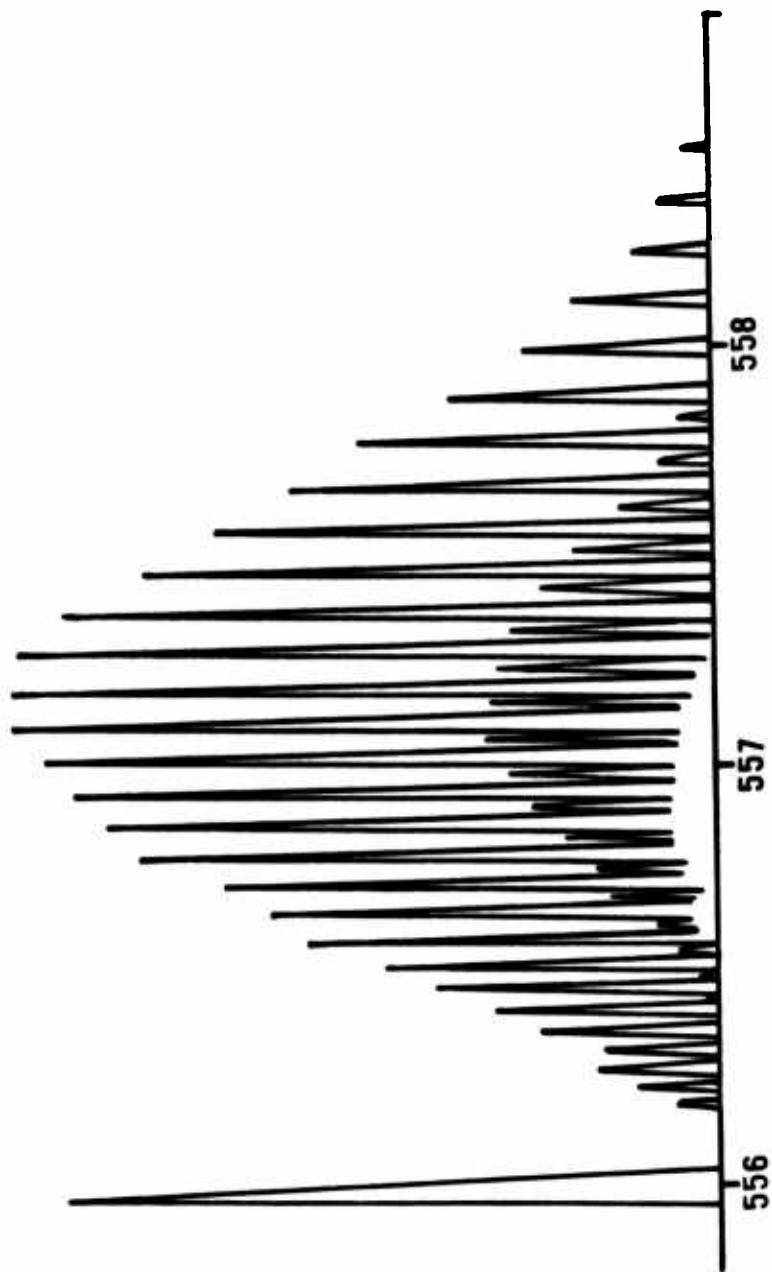
**EXCITATION WAVELENGTH (nm)**

Figure 4.22 Synthetic Excitation Spectrum for the (21,0) Band.

Table 4.5

Transition Energies for the (44,0) and (44,84) Bands

| | (44,0) Band | | | | | (44,84) Band | | | |
|---|---|---|---|---|---|---|---|---|---|
| Line | Energy (cm⁻¹) | $\theta_{J',J''}$ | Line | Energy (cm⁻¹) | $\theta_{J',J''}$ | Line | Energy (cm⁻¹) | Line | Band Energy (cm⁻¹) |
| P61 | 19401.87 | 0.70 | R60 | 19408.63 | 0.70 | P61 | 7447.40 | R60 | 7451.87 |
| P62 | 19399.46 | 0.97 | R61 | 19406.34 | 0.97 | P62 | 7447.33 | R61 | 7451.87 |
| P63 | 19397.02 | 0.69 | R62 | 19404.01 | 0.69 | P63 | 7447.26 | R62 | 7451.87 |
| P64 | 19394.54 | 0.96 | R63 | 19401.63 | 0.96 | P64 | 7447.19 | R63 | 7451.87 |
| P65 | 19392.02 | 0.68 | R64 | 19399.22 | 0.68 | P65 | 7447.12 | R64 | 7451.87 |
| P66 | 19389.46 | 0.94 | R65 | 19396.77 | 0.95 | P66 | 7447.05 | R65 | 7451.87 |
| P67 | 19386.86 | 0.67 | R66 | 19394.23 | 0.67 | P67 | 7446.98 | R66 | 7451.88 |
| P68 | 19384.22 | 0.93 | R67 | 19391.75 | 0.93 | P68 | 7446.91 | R67 | 7451.88 |
| P69 | 19381.54 | 0.65 | R68 | 19389.19 | 0.66 | P69 | 7446.84 | R68 | 7451.88 |
| P70 | 19378.83 | 0.91 | R69 | 19386.58 | 0.91 | P70 | 7446.77 | R69 | 7451.88 |
| P71 | 19376.07 | 0.64 | R70 | 19383.93 | 0.64 | P71 | 7446.70 | R70 | 7451.88 |
| P72 | 19373.28 | 0.87 | R71 | 19381.25 | 0.89 | P72 | 7446.63 | R71 | 7451.88 |
| P73 | 19370.44 | 0.63 | R72 | 19378.52 | 0.63 | P73 | 7446.56 | R72 | 7451.88 |
| P74 | 19367.57 | 0.86 | R73 | 19375.76 | 0.87 | P74 | 7446.49 | R73 | 7451.88 |
| P75 | 19364.65 | 0.61 | R74 | 19372.95 | 0.61 | P75 | 7446.42 | R74 | 7451.88 |
| P76 | 19361.70 | 0.84 | R75 | 19370.11 | 0.85 | P76 | 7446.35 | R75 | 7451.88 |
| P77 | 19358.71 | 0.59 | R76 | 19367.23 | 0.60 | P77 | 7446.29 | R76 | 7451.88 |
| P78 | 19355.68 | 0.82 | R77 | 19364.30 | 0.82 | P78 | 7446.22 | R77 | 7451.88 |
| P79 | 19352.61 | 0.57 | R78 | 19361.34 | 0.58 | P79 | 7446.15 | R78 | 7451.88 |
| P80 | 19349.50 | 0.79 | R79 | 19358.34 | 0.80 | P80 | 7446.08 | R79 | 7451.88 |
| P81 | 19346.34 | 0.56 | R80 | 19355.30 | 0.56 | P81 | 7446.01 | R80 | 7451.88 |
| P82 | 19343.15 | 0.76 | R81 | 19352.22 | 0.77 | P82 | 7445.94 | R81 | 7451.88 |
| P83 | 19339.92 | 0.54 | R82 | 19349.09 | 0.54 | P83 | 7445.88 | R82 | 7451.88 |
| P84 | 19336.65 | 0.74 | R83 | 19345.93 | 0.75 | P84 | 7445.81 | R83 | 7451.89 |
| P85 | 19333.34 | 0.52 | R84 | 19342.73 | 0.52 | P85 | 7445.74 | R84 | 7451.89 |
| P86 | 19329.99 | 0.71 | R85 | 19339.49 | 0.72 | P86 | 7445.68 | R85 | 7451.89 |
| P87 | 19326.60 | 0.50 | R86 | 19336.21 | 0.50 | P87 | 7445.61 | R86 | 7451.89 |
| P88 | 19323.17 | 0.68 | R87 | 19332.89 | 0.69 | P88 | 7445.54 | R87 | 7451.89 |
| P89 | 19319.70 | 0.48 | R88 | 19329.52 | 0.48 | P89 | 7445.48 | R88 | 7451.89 |
| P90 | 19316.70 | 0.66 | R89 | 19326.12 | 0.66 | P90 | 7445.42 | R89 | 7451.90 |
| P91 | 19312.64 | 0.46 | R90 | 19322.68 | 0.46 | P91 | 7445.35 | R90 | 7451.90 |

1. The $\theta_{J',J''}$ values are normalized Boltzmann populations.

J'+4. The fact that these levels are not adjacent, and cooperative emission is observed results from the unique emission band characteristics. As shown in the table, the R60 to R90 transitions of the (44,84) band occur within 0.03 cm$^{-1}$. Therefore, populating two or more $61 \leq J' \leq 92$ levels will result in cooperative emission. In the present experiment, a pair of levels, J' and J'+4, are simultanously populated, resulting in the observed CSE as shown in Figure 4.11 and 4.16. Although only two levels form the superlevel, these levels are strongly populated since the pump transitions occur near the Boltzmann population maximum, not near the bandhead as generally the case.

The anomalous behavior of the excitation spectrum of the 515 nm region is a direct result of the superlevel forming at increasingly higher J', as shown for the case of v' = 44 above. As J' increases, the separation between rotational transitions increases, which allows the rotational transitions to become more easily resolved. This effect is easily observed in the high resolution spectrum of the (21,0) band, Figure 4.18. The "break-up" of the spikes in the 515 nm region is a result of CSE occuring at high J' such that the individual transitions are resolved and CSE occuring over a broad range of J'. The wide J' range of possible CSE for this region is a result of changes is the bandhead characteristics of the emission bands.

An instructive way to illustrate these emission

properties is by use of Fortrat diagrams. Figure 4.23 gives Fortrat diagrams for the (43,83), (44,84), and (45,85) bands. Note that multiple bandheading occurs for (43,83). The (43,83) bandhead at $J = 41$ gives rise to CSE over the range $38 \leq J \leq 49$ as Figure 4.16 shows.

The (44,84) band has an R brranch "shoulder", that allows over 30 rotational transitions to emit within the Doppler width of one another. The shoulder transitions have been presented in Table 4.5. The transitions of this shoulder give rise to the very broad CSE envelope shown in Figure 4.16, and explained above.

Figure 4.23 displays a trend in the Fortrat curves. The values of the spectroscopic constants for $I_2$ B-X are such that the two bandheads of (43,83) "merge" to form a shoulder in (44,84) and "coalesce" to form the smooth curve of (45,85). Since (45,85) has no band head or shoulder in the R branch, no CSE is possible. Indeed, no ASE has been observed from $v' = 45$, although a careful search for any such emission was conducted.

Each of the bands of Figure 4.23 also possess a bandhead in the P branch at very high J. These are not shown in the figure, but as v' increases, the J value of the P branch beadhead location decreases. The location of the lowest J value bandhead for all the ASE bands is shown in Figure 4.24. One sees the gradual, then dramatic shift of the bandhead away from the band origin. The CSE follows
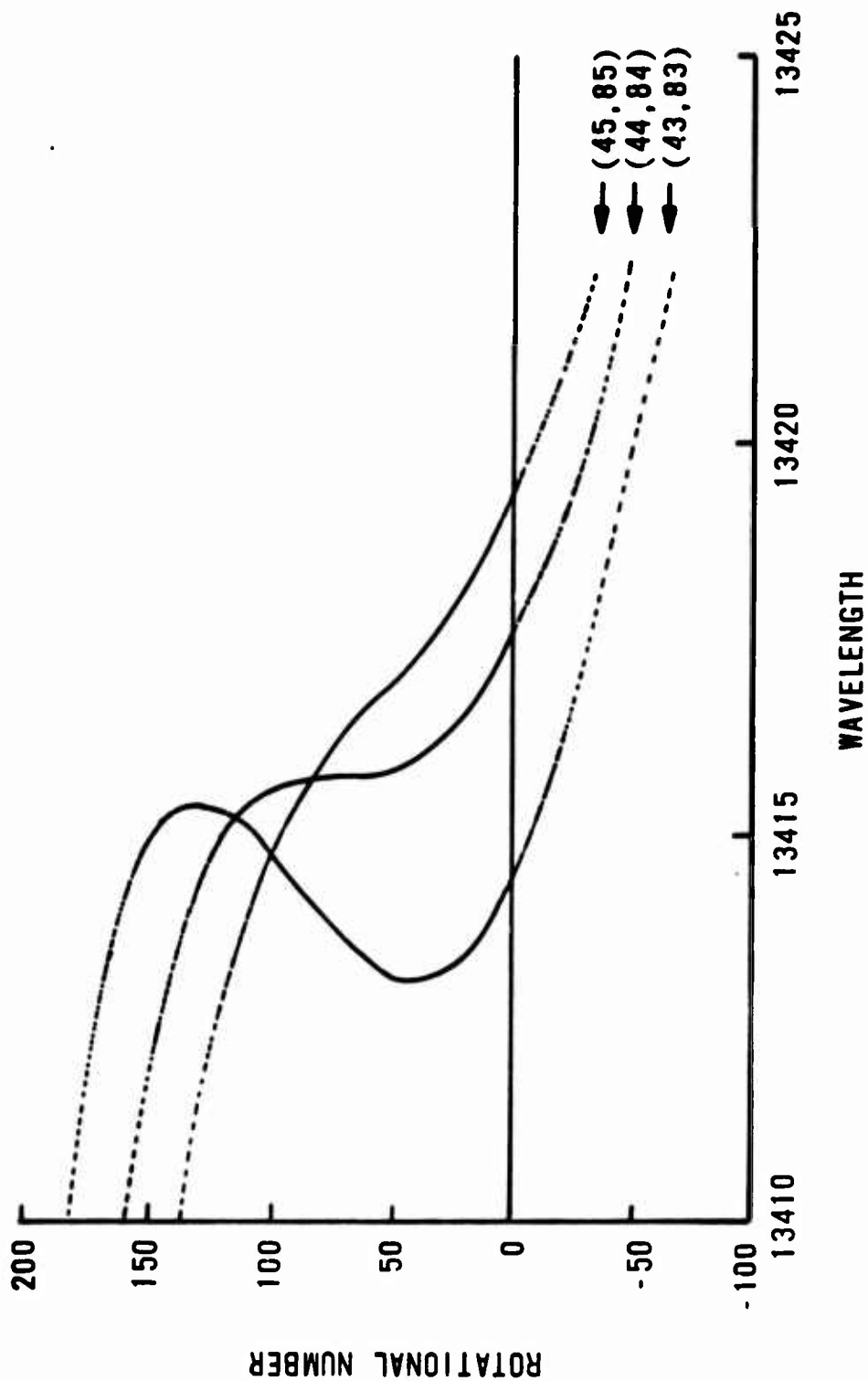
Figure 4.23 Fortrat Diagrams for the (43,83), (44,84), and (45,85) Bands.

Figure 4.24 Bandhead Transitions for the ASE Bands. For those transitions of $v' \geq 45$ the emission band is taken to be $v''=v'+40$.
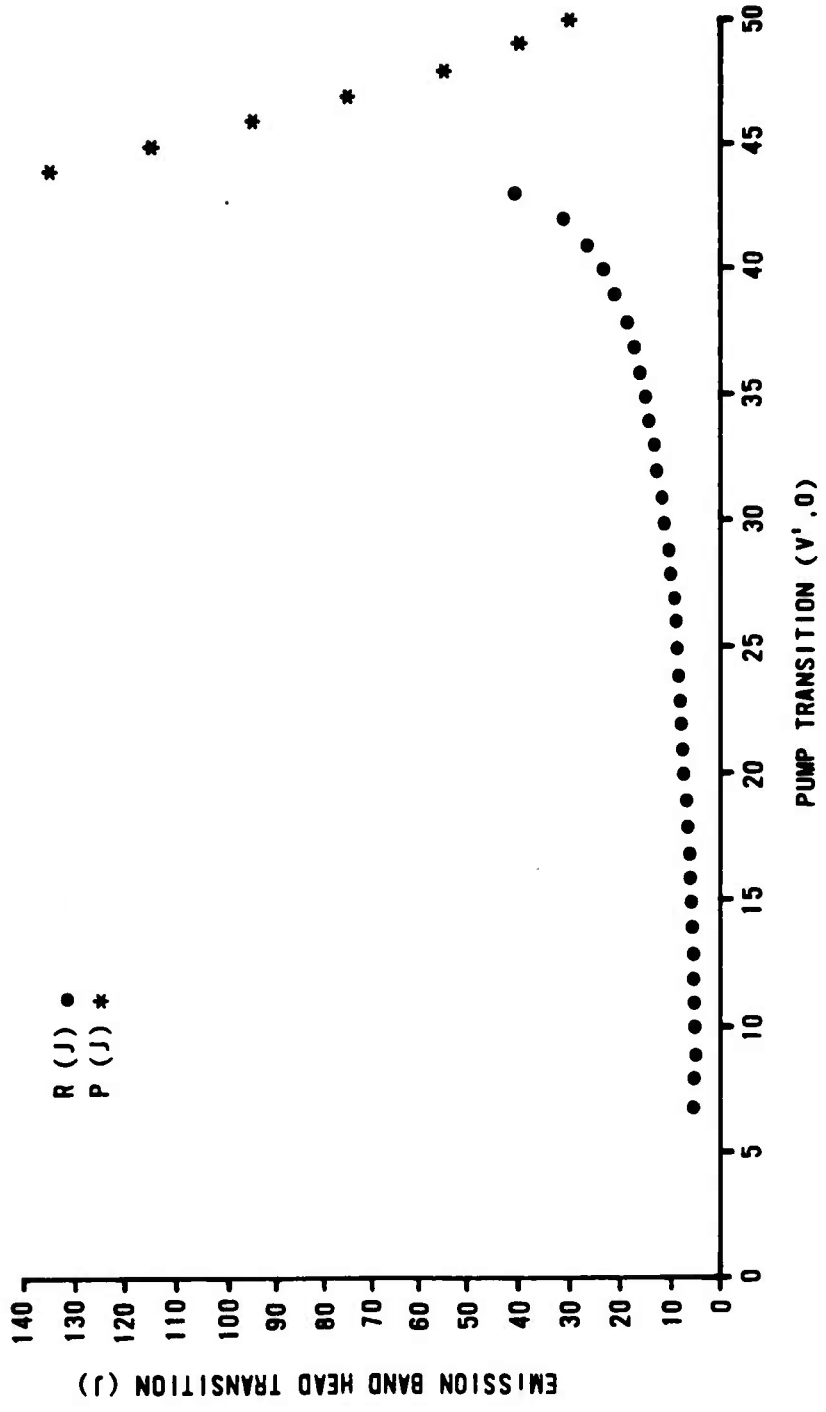
this trend. The apparent irregular appearence of the excitation spectra for $\lambda_{pump} \leq 517$ nm is a direct consequence of the bandhead behavior shown by this figure.

B.Expanded Spectroscopic Studies

1.Gain Variation

The preceding section presented a fundemental survey of the $I_2$ (B-X) ASE spectroscopy and explained the earlier work of Hanko et al. and expanded upon it. The spiked behavior is readily observed in a laser cavity, as Figure 4.25 shows. With an understanding of the spiked excitation in hand, various properties of CSE can be explored with a variety of experiments thay will lend additional support to the validity of the CSE theory presented earlier.

Consider Figure 4.26, which shows excitation of the (21,0) spike region with different gain cell pressures. Figure 4.26(a) is very near ASE threshold and only the R branch contributes to the excitation. In Figure 4.26(b) the R branch pumped signal has overloaded the detection electronics while the P branch pumped signal has just reached threshold. This shows that the R branch is indeed far more efficient than the P branch when competing for pump photons. The reason being that the R branch forms a bandhead so has a higher density of absorption lines,
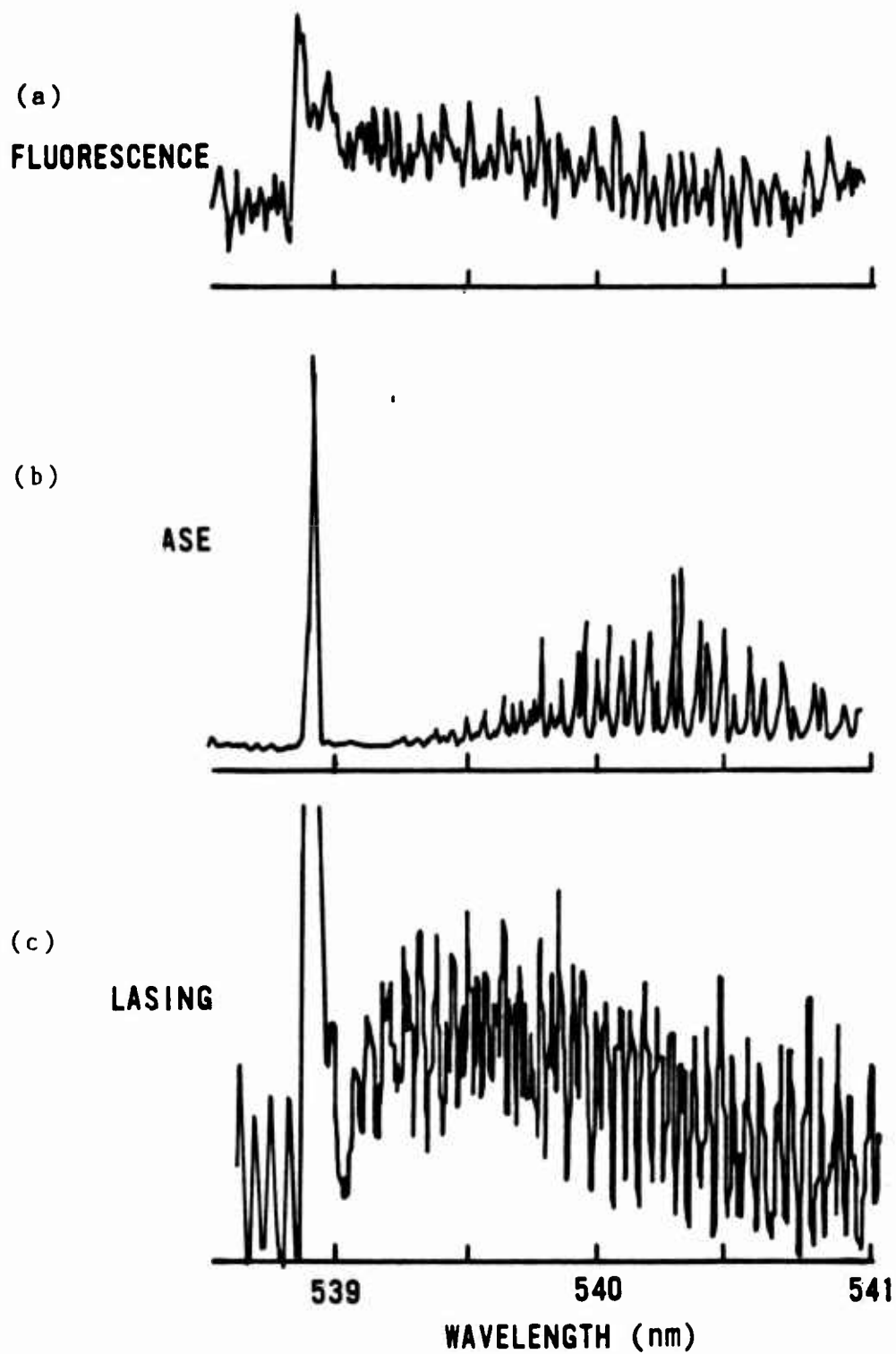
Figure 4.25 Excitation Spectra for the (28,0) Band. Side fluorescence (a), ASE (b), and lasing (c) spectra are shown.

100
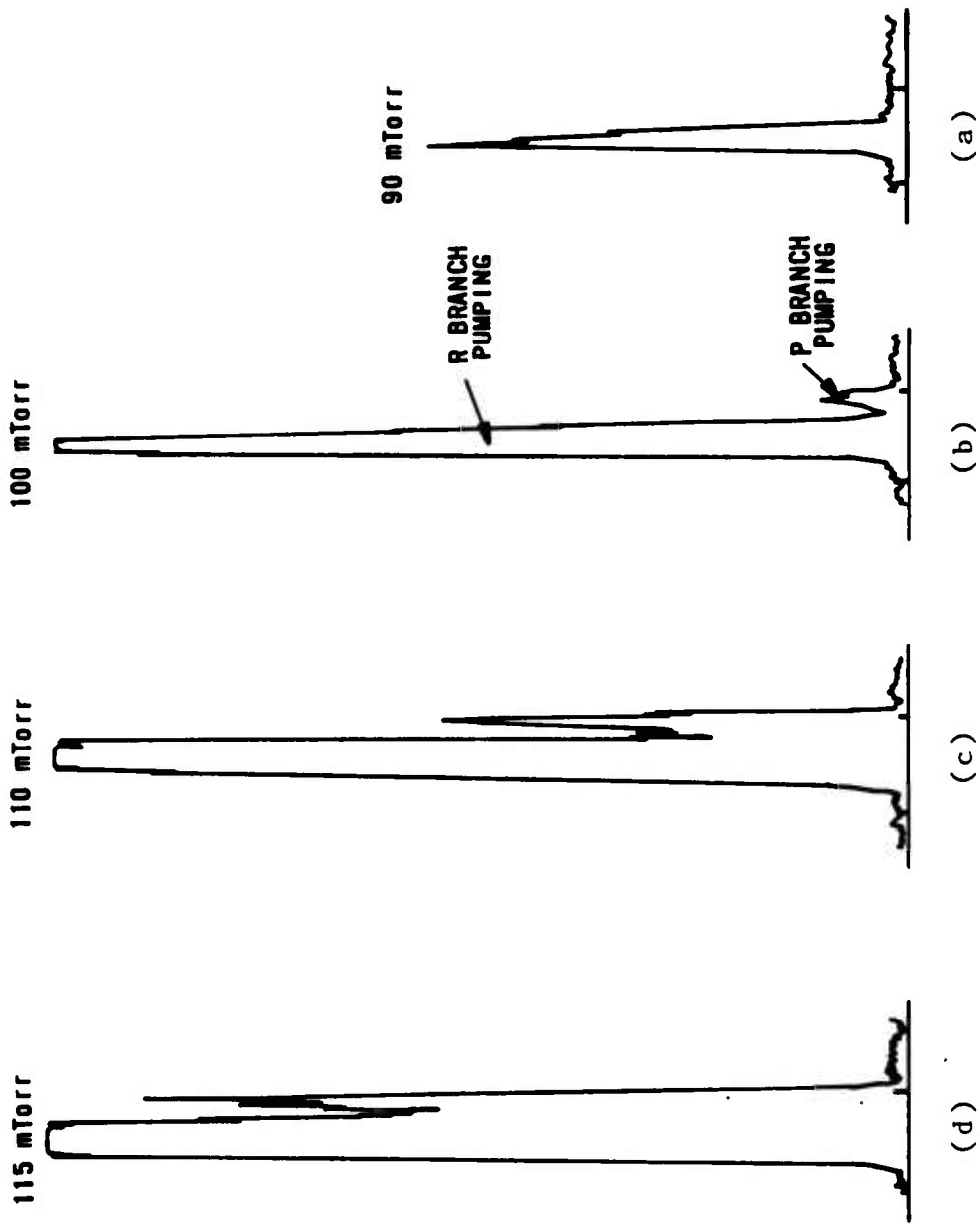
Figure 4.26 Excitation of the (21,0) Spike at Various Gain Cell Pressures.

allowing more levels to be pumped simultaneously yielding a
stronger CSE signal.

## 2.Threshold Gain Spectra

As shown above, excitation spectra taken under
conditions of various gain reveal much qualitative
information about the system under study.  Of interest is
the excitation spectrum taken near the threshold gain level.
Figure 4.27 shows the excitation spectrum for the R590 dye
region at very low gain cell iodine pressure.  The pressure
was varied by varing the temperature of a sealed cell and
the vapor pressure was calculated with the aid of
Equation 3.1.  No signal attenuation (neutral density
filters) was used here.  The spontaneous fluorescence
signal, which is always present but usually insignificantly
small, is observed with the ASE signal just reaching
threshold for some transitions.  Observe that the normal
excitation is very strong for the v'= 16 and 17 pump bands,
while the spiked excitation is strongest for the v'= 22
and 23 pump bands.  Very little spike excitation is observed
for the (16,0) band.

The situation changes greatly when the iodine pressure
is increased from 153 to 182 mTorr, Figure 4.28.  Here the
signal level has been attenuated by a factor of two when
compared to the previous figure.  So the v'= 16 and 17
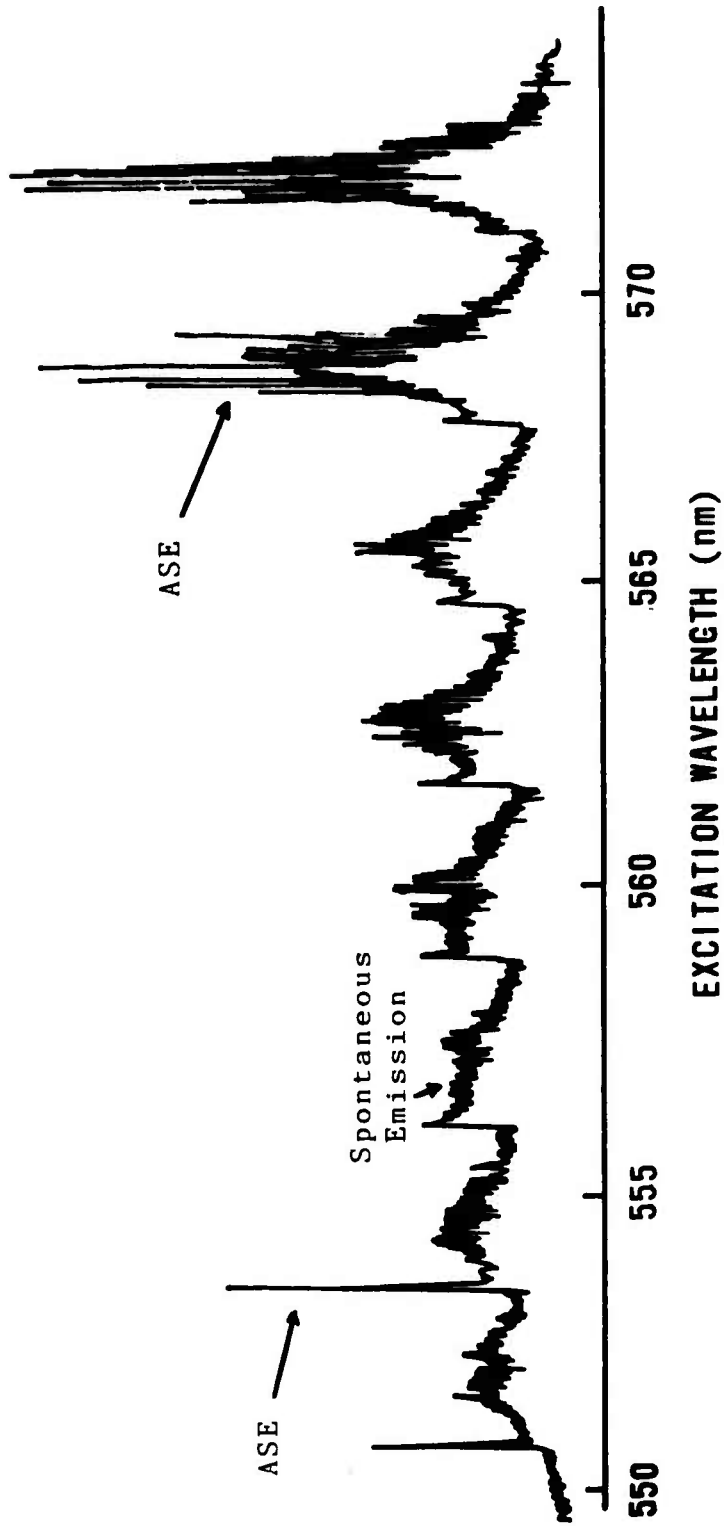
Figure 4.27 Excitation Spectrum for Low ASE Gain. Spectrum was taken with a 98 cm cell at 17°c corresponding to 153 mTorr vapor pressure.
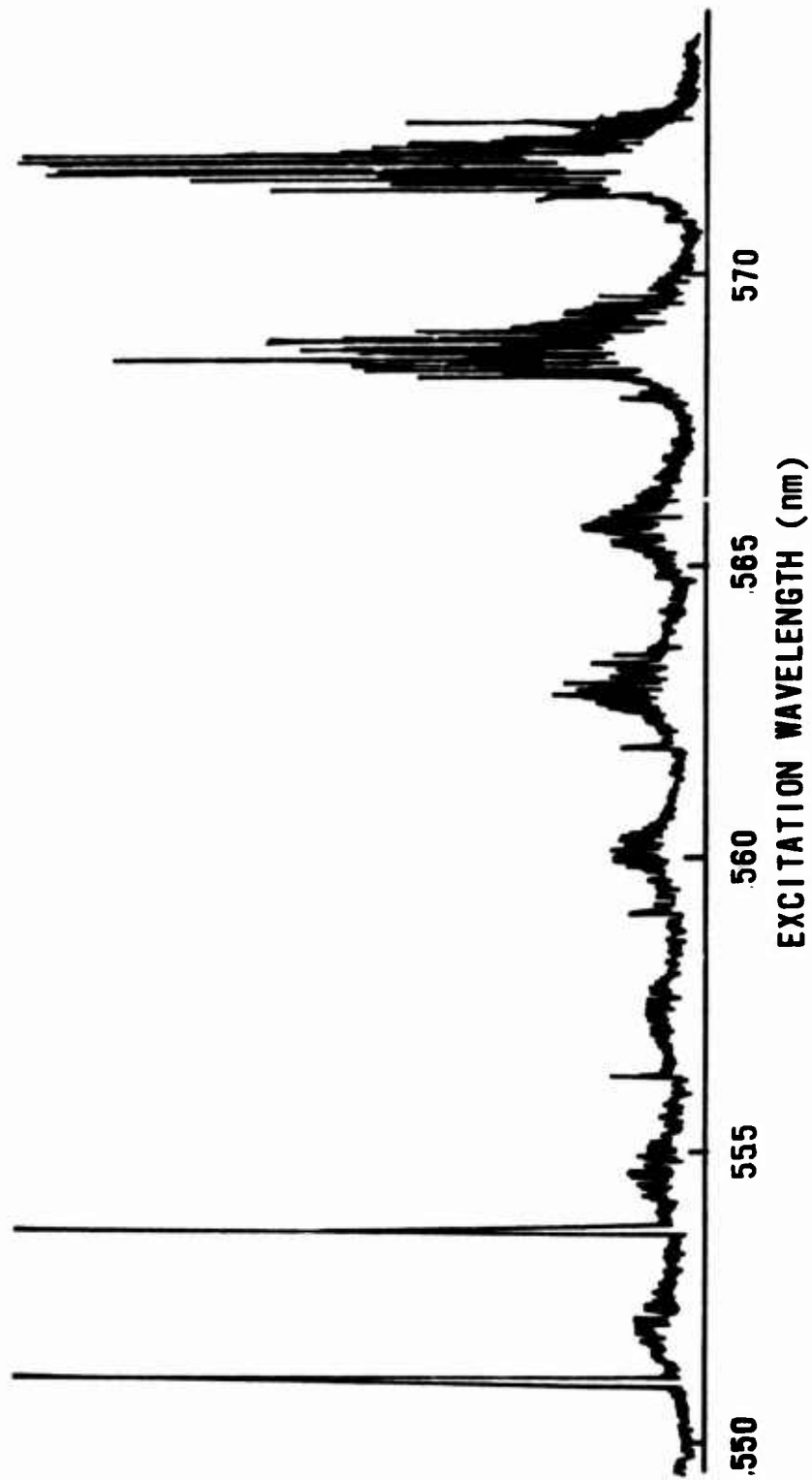
Figure 4.28 Excitation Spectrum for 182 Torr Iodine Vapor Pressure.

EXCITATION WAVELENGTH (nm)

normal excitation has increased by about a factor of 2 or 3 over the previous figure, but the v'= 23 and 22 spike excitation has so greatly increased as to overload the detection electronics. The intermediate pump bands have not greatly changed their character. This is odd when one considers that the pump power is greatest at 565 nm. To see the true signal levels, refer to Figure 4.29, which is a repeat of Figure 4.28 but taken at higher signal attenuation. The (23,0) spike dominates the spectrum, followed by the (22,0) spike. The normal excitation at (16,0) and (17,0) is far weaker than the spiked excitation. The small increase in gain has generated a large increase in CSE, as the figure shows. This behavior near threshold gain will be quantitatively investigated in a later section.

### 3.Buffer Gases

A very interesting property of CSE and the formation of a superlevel is revealed by Figure 4.30. Here 7000 mTorr of helium gas has been added to 200 mTorr of iodine in the gain cell. It has been reported that the addition of 1 torr of helium has quenched laser action of iodine OPL's [7]. The quenching has been attributed to upper state population losses due to collisional transfer with the buffer gas. Figure 4.30 shows a strong overall ASE signal. But the normal excitation is rapidly quenched as v' increases, with
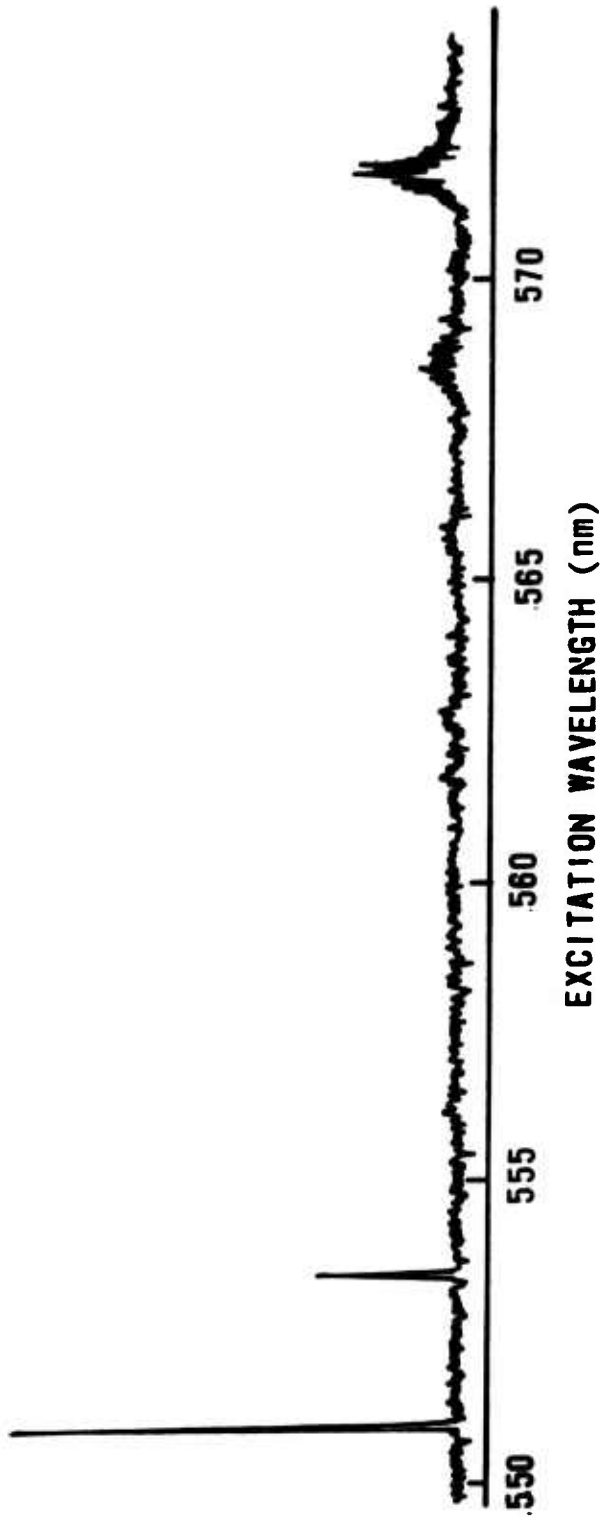
Figure 4.29 Excitation Spectrum for 182 mTorr Iodine Vapor Pressure Showing True Signal Strengths.
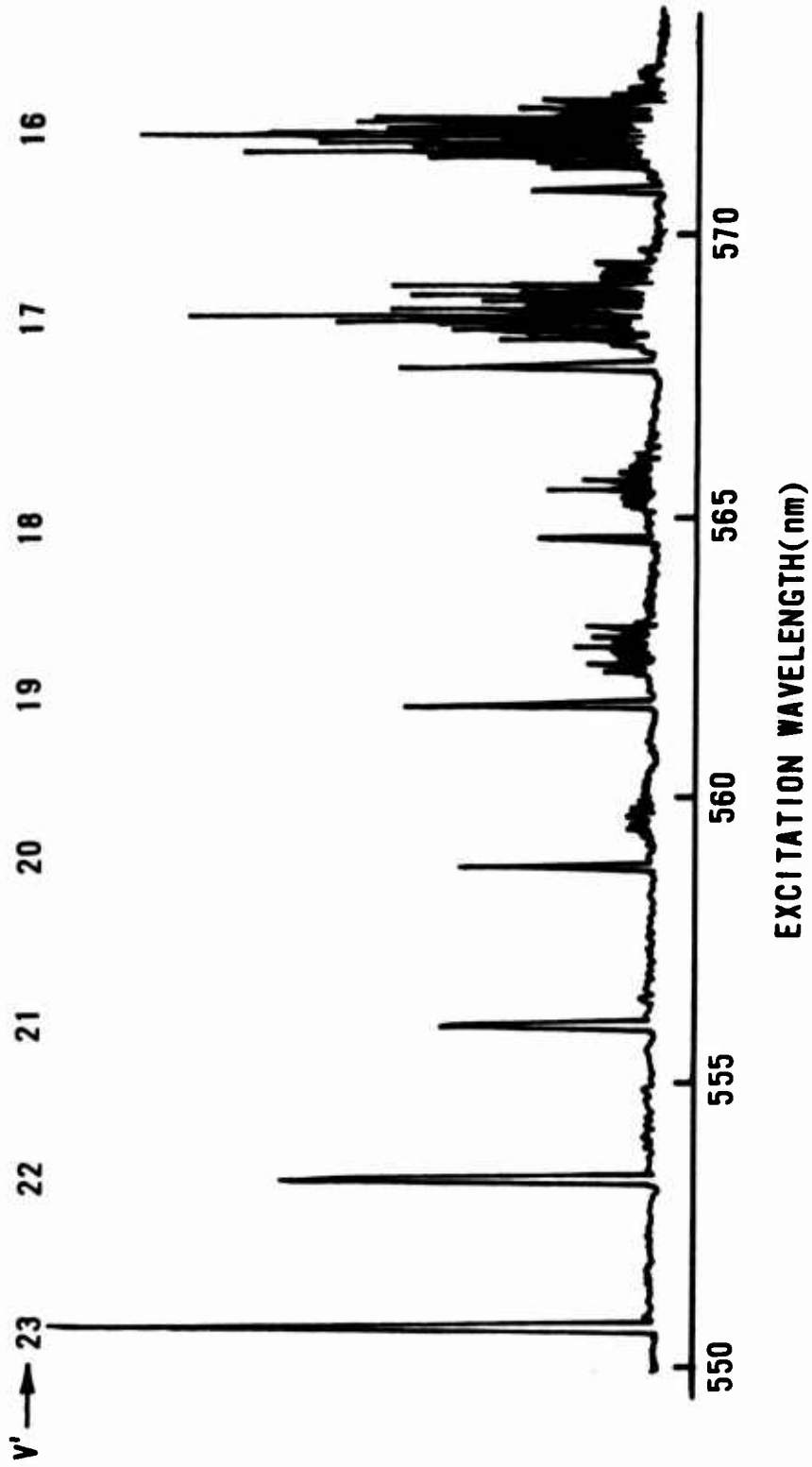
Figure 4.30 ASE Excitation with Helium Buffer Gas. Spectrum was taken at 200 mTorr Iodine and 7000 mTorr of He in the gain cell.

no normal excitation for $v' = 21$. The spiked excitation is less effected by the buffer. The (23,0) spike is the dominate feature of the spectrum in Figure 4.30.

The apparent quench immunity of the spiked excitation is due to the nature of CSE and the superlevel. Bimolecular collisions distribute molecular populations from a specific $v,J$ prepared state to many $v \pm \Delta v, J \pm \Delta J$. Consider rotational transfer only, with the selection rule for $I_2$ (B-X) of $\Delta J = \pm 2, \pm 4 \cdots$ [20]. Figure 4.31 depicts two cases: normal stimulated emission and CSE. For the normal case, a single rotational level is the upper state for the gain transition. Any collision which causes rotational transfer will deplete the inversion, thus reduce the gain. For the case of CSE, a superlevel (many adjacent rotational levels) exists for the gain transition. As shown in the figure, many of the collisions simply redistribute the population within the superlevel. This action does not reduce the population of the superlevel, hence is not a loss mechanism. Only those collisions that remove population from the superlevel will reduce the gain. As Figure 4.30 shows, for some transitions a significant fraction of the rotational collisions simply redistribute the population within the superlevel. This observed quench immunity is another confirmation of CSE and the superlevel as the explanation for the spiked excitation. The degree of quench immunity should be related to the number of individual levels that make up the superlevel and

108
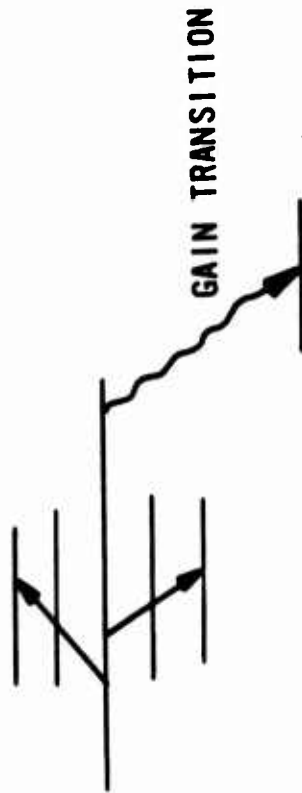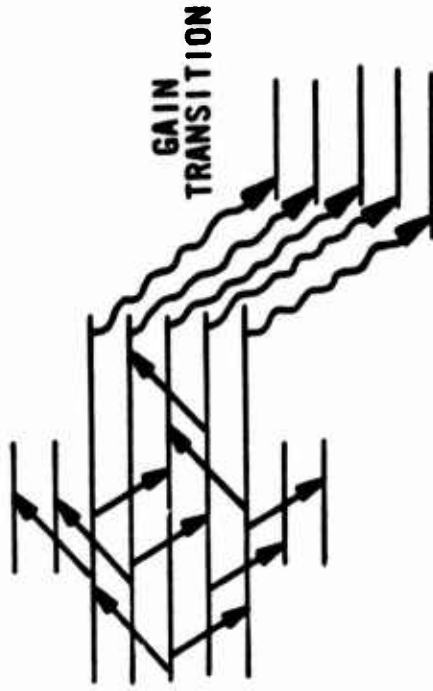
Figure 4.31 Collisional Rotational Transfer. Single level (a) and superlevel (b) systems are shown. Collisional transfer is shown by straight lines.

the total population that contributes to gain. This hypothesis will be discussed quantitatively in the next section.

C.Buffer Gas Studies

1.Relative Collisional Transfer

This section quantitatively investigates the spectroscopically observed quench resistance of spiked emission. The experiment consisted of pumping both the spiked and normal regions of various vibrational bands. A buffer gas was incrementally introduced into the gain cell, and the ASE signal was recorded as a function of buffer gas pressure.

From the theoretical discussion presented earlier, a graph of $\ln(N_2(t_D)/N_2(0))$ verses buffer pressure P should yield a straight line whose slope is related to the rate constant for collisional losses from the upper gain level. Experimentally the total energy per pulse is measured. The total energy per pulse is proportional to the upper state population, so a graph of $\ln(I/I_0)$ verses buffer pressure P should yield a straight line where I is the total energy per pulse and $I_0$ is the zero buffer pressure energy.

For the purposes here, one need only be concerned with the difference between the rotational losses for the

superlevel and the single level, as described by
Figure 4.31. Then for the same vibrational band, all other
losses (vibrational transfer, quenching, predissociation)
should be the same for both the spiked and normal region.
Spontaneous predissociation is a function of J, but its
effect is negliable in the present study, as Appendix I
explains. So a comparison between the spiked and normal
emission will reveal the difference between the superlevel
rotational quenching and normal rotational quenching (as
shown in Figure 4.30).

2.Collisional Quench Immunity

The buffer gas experiments were performed for v'= 16,
23, 27, and 34. The v'= 16 and 23 bands were chosen because
they represent the extremes of Figure 4.30. The v'= 27
and 34 bands were chosen to allow larger superlevels to be
investigated. Typical results are shown in Figures 4.32,
4.33, and 4.34. The complete results are shown in
Appendix J. Each data point represents the average total
energy per pulse of several hundred ASE pulses. Even so,
there is much scatter in the data. This is largely the
result of poor intensity stabilization of the pulsed dye
laser used as the pump. For accurate results, the laser
intensity should remain constant for the entire data run.
This was never the case though. The data was fit to the
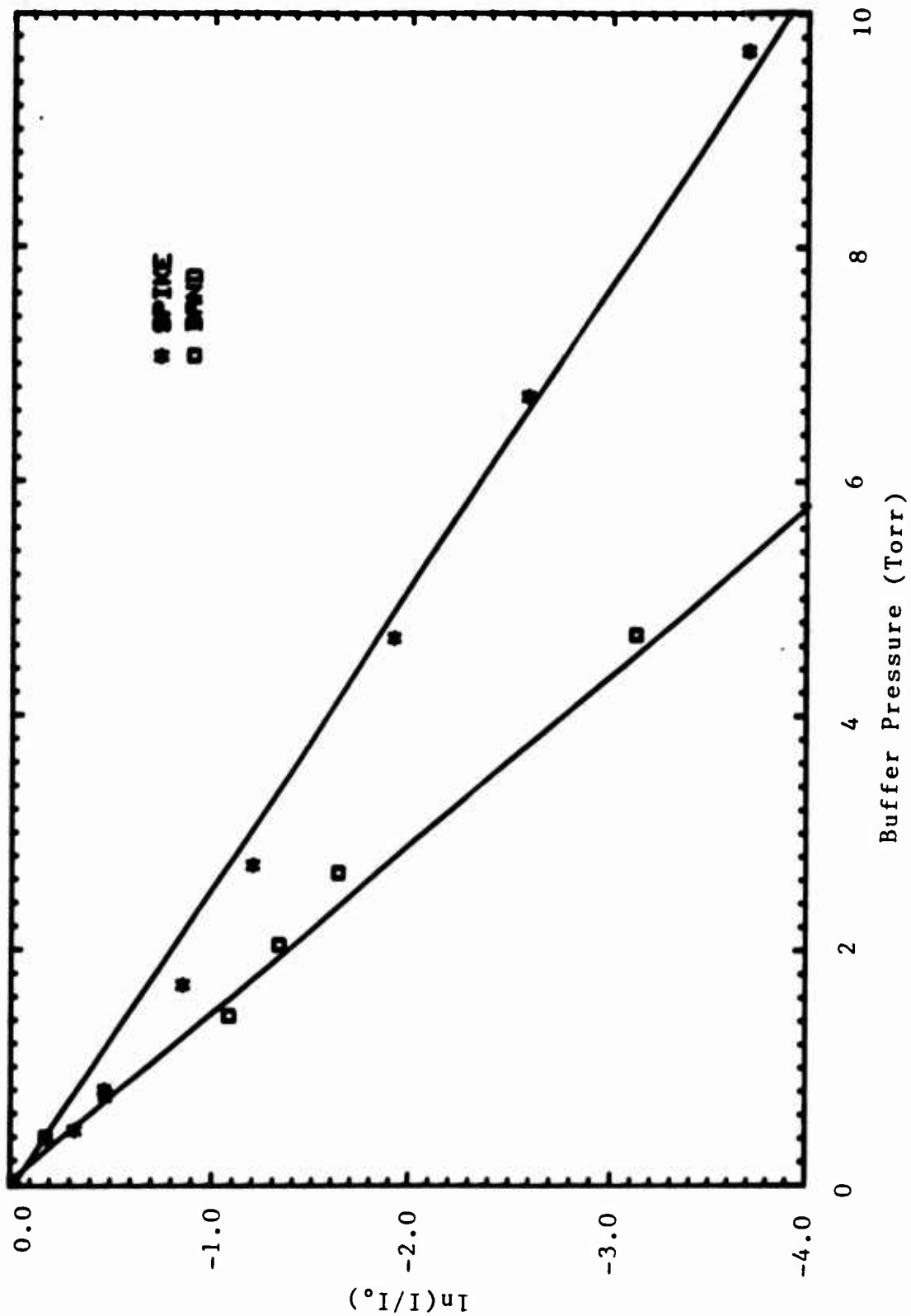
Figure 4.32 Helium Buffer Quenching of ASE for (23,0). Pump wavelengths for the spike and band are 550.7 and 551.7 nm respectively.

112

Figure 4.33 Heluim Buffer Quenching of ASE for (27,0). Pump wavelengths for the spike and band are 541.2 and 542.2 nm respectively.

113
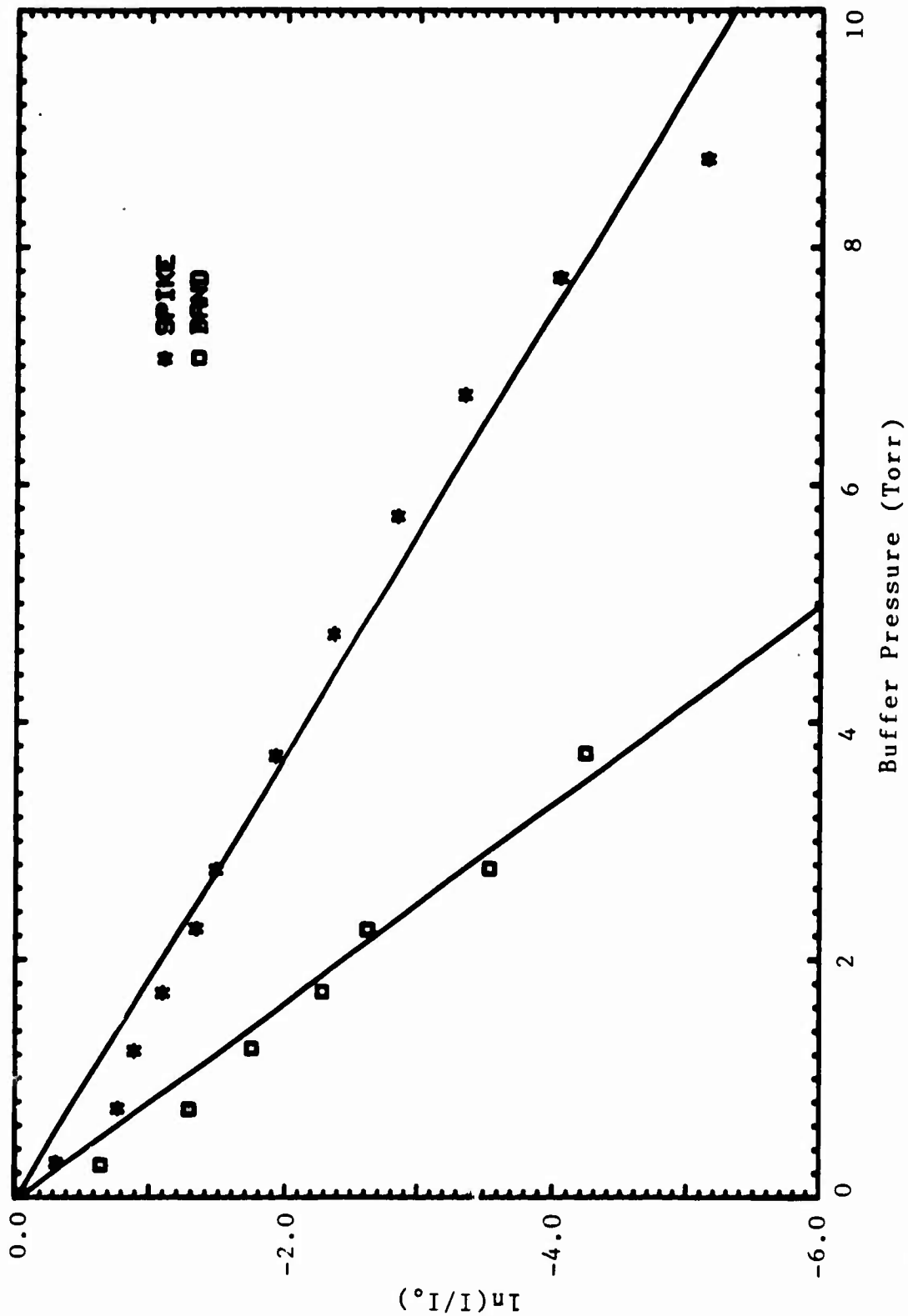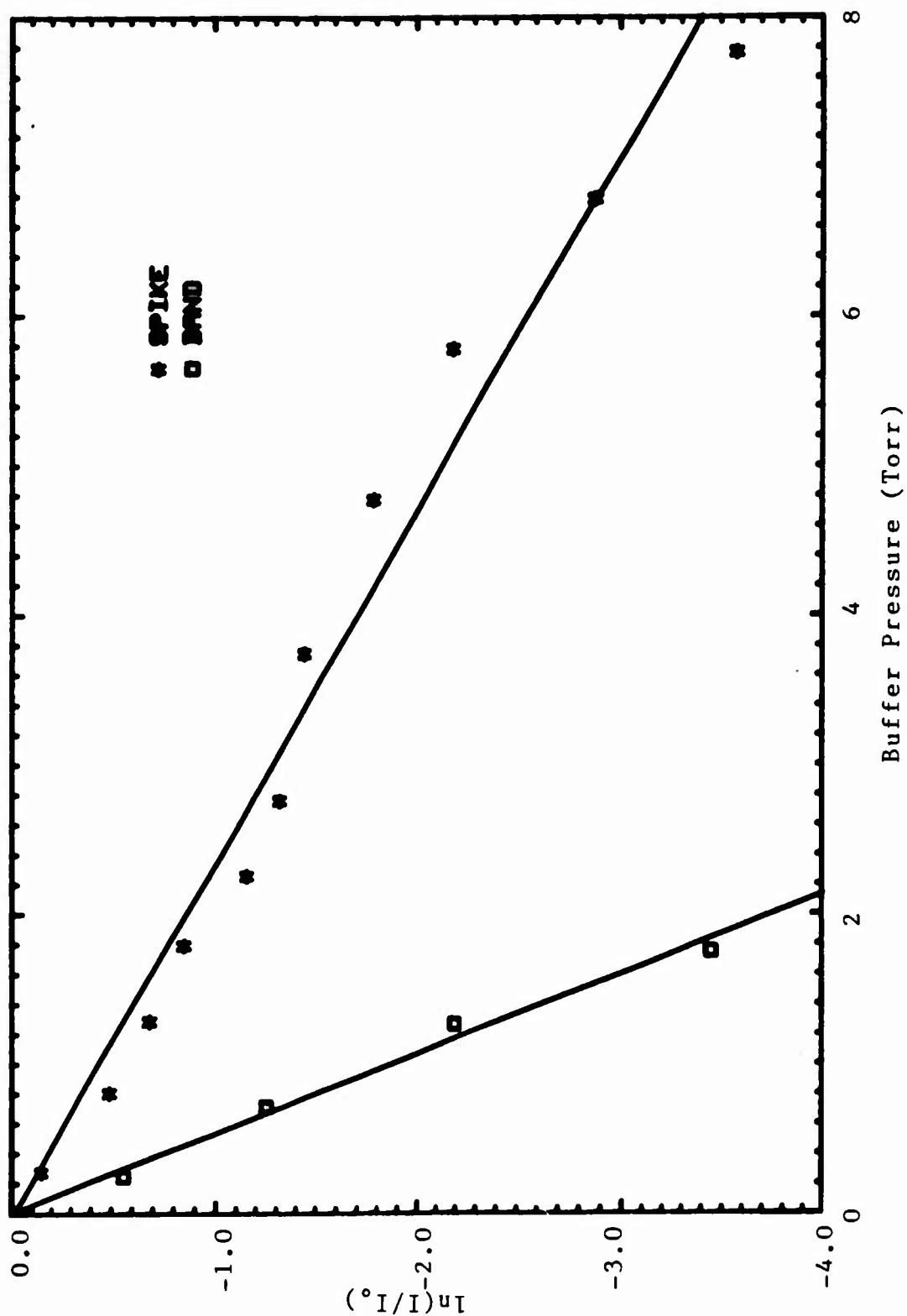
Figure 4.34 Helium Buffer Quenching of ASE for (34,0). Pump wavelengths for the spike and band are 527.4 and 528.2 nm respectively.

equation y = mx using a linear least squares analysis. The slope of the line represents the effective quenching rate of the upper gain level(s) during the ASE pulse length.

In the current work, a comparison of the relative effectiveness of collisionally quenching of the ASE signal between a single emitting rotational level and a superlevel is the goal. Therefore, the quenching rates, i.e. the slopes for the spike and band quenching from the graphs shown in Appendix J, for one vibrational number v' are compared relative to one another by dividing the band quenching rate to the spike quenching rate. This results in a dimensionless number that allows the desired comparison. Call this ratio of rates (or ratio of the slopes) the Quench Immunity Enhancement (QIE) factor. If the QIE is greater than one, then the superlevel is more difficult to collisionally quench than a single rotational level. For example, if the slope of the spike quenching curve is half that of the band quenching curve, then the QIE = 2. This means that the superlevel will require twice as many collisions as a single rotational level to reduce the ASE signal by the same factor. That is, the superlevel posesses an immunity to collisional quenching by an enhancement factor of 2.

A graph of the Quench Immunity Enhancement for all the data is shown in Figure 4.35. As shown, for v' = 34, the enhancement is greater than 4, making the v' = 34 superlevel

115
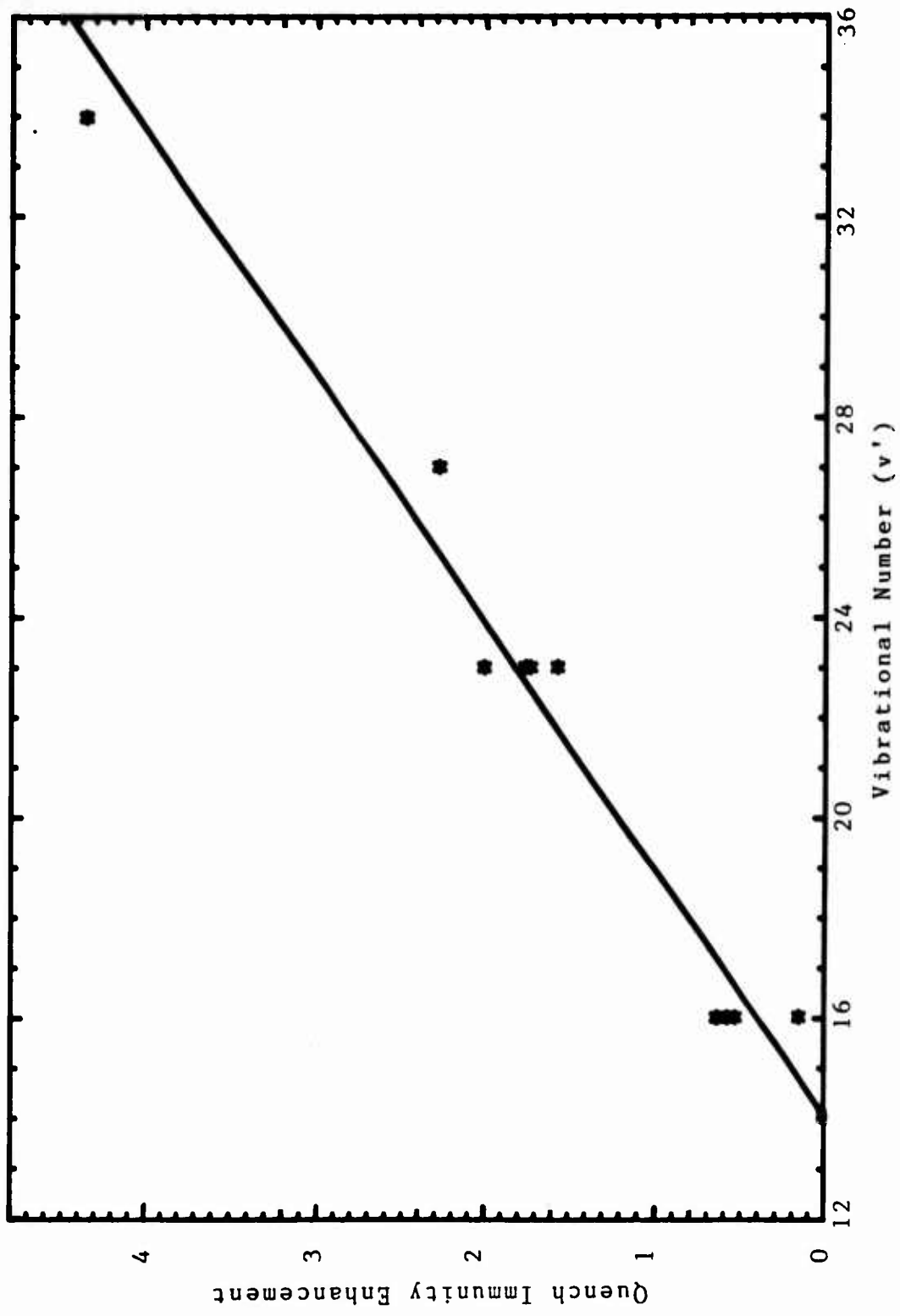
Figure 4.35 Quench Immunity verses Vibrational Excitation. An enhancement of greater than 1 means that the superlevel posesses a degree of quench immunity.

116

4 times as difficult to collisionally quench that any v'= 34 single rotational level. A straight line is drawn through the data, suggesting a relationship between quench immunity and the vibrational excitation level. The fact that the v'= 16 data all fall below one is a potential inconsistancy. A quench immunity factor below one means that the superlevel quenches easier than a single rotational line. One would assume that the QIE of one would be the limiting value. Further investigation in this area is warrented.

D. Performance Investigation

1. ASE Output Variation with Pressure and Gain Length

In an earlier section, the wavelength conversion properties of iodine ASE were discussed. This system could serve as a simple, discretely tuneable, near-infrared mirrorless laser for various spectroscopic applications [101]. Such a device would be useful if sufficient output energy was available for experimental use. Therefore the ASE output characteristics were investigated in detail.

The ASE output energy per pulse was studied parametrically as a function of gain cell length and iodine pressure. For each length-pressure condition, the pump energy was increased until the ASE output energy reached a steady value, independent of further pump energy increase.

117

At this point, the ASE pump transition was completely saturated, with half of the ground state population pumped to the upper ASE level. This condition represents the maximum possible ASE output for the given length-pressure condition. The results of this study on the (21,0) spike transition are shown in Figure 4.36. The (21,0) band was choosen because the Franck-Condon factors for the $v'=21$ progression have been published [38]. Figure 4.36 shows cell length variation from 124 to 204 cm with iodine pressure variation from 150 to 320 mTorr.

The ASE energy curves shown in Figure 4.36 increase with both cell length and iodine pressure with no leveling off observed. The greater the number of excited molecules that are present, the greater the total gain of the system. The limiting factor in this work was pump energy, not enough pump energy was available to saturate the pump transition for very large length-pressure conditions.

2.Gain Calculation

The determination of gain for a pulses amplified spontaneous emission system may be more subtle than one may realize. An ASE signal is generated out of the spontaneous emission noise, and the amplification of that signal via stimulated emission may follow different models. ASE may be generated from different initiation locations within the

118
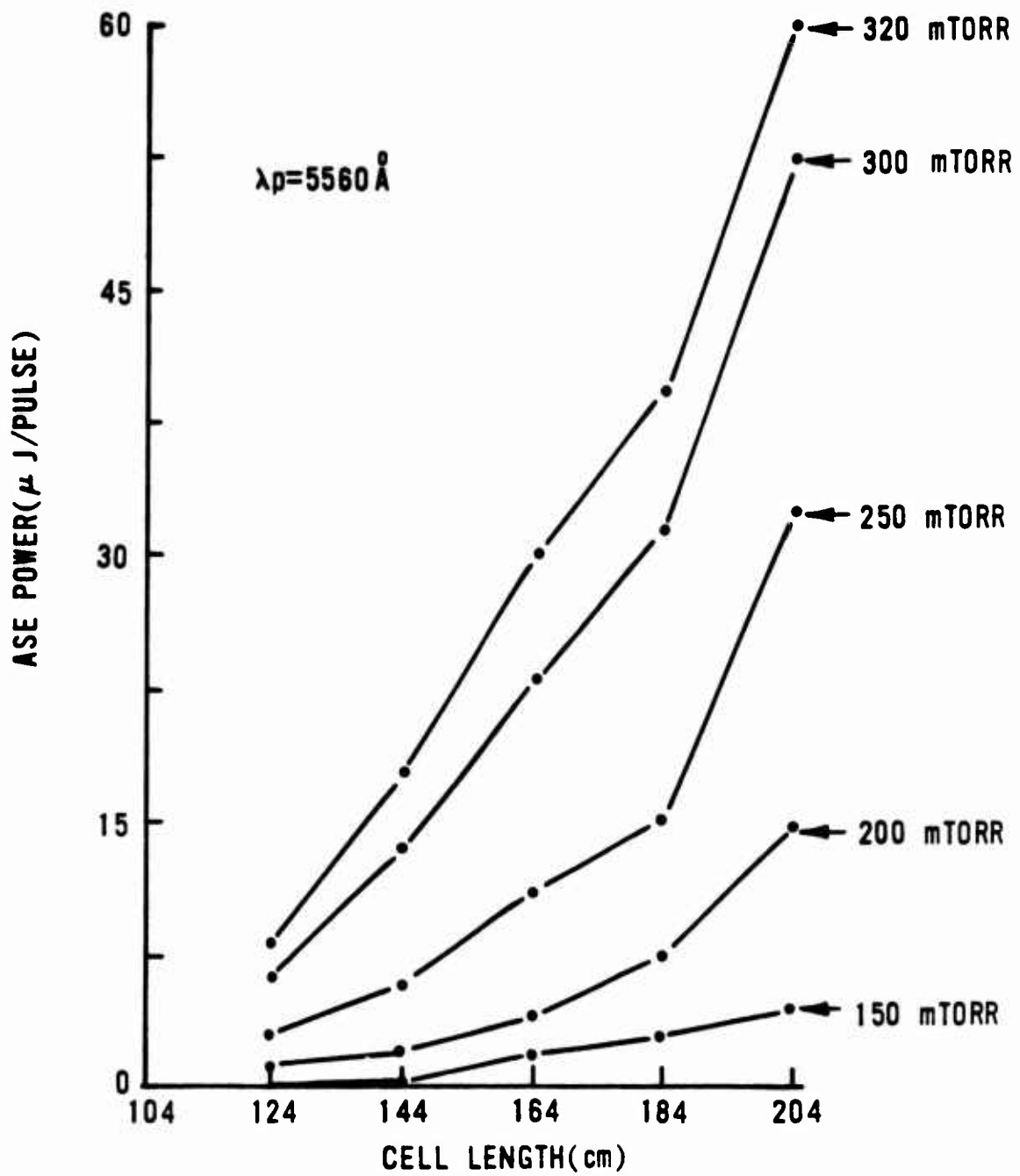
Figure 4.36 ASE Output Energy.

gain medium, such that independent radiation fields are what are actually observed. Or, a single photon may initiate ASE, sweeping out the gain of the entire medium in one radiation field. Whatever the process, the gain itself most likely varies from a small signal gain early on in the amplication, to a saturated gain later in the amplification process. The final output can be thought of as the result of some average gain.

Amoung this uncertainty, it is reasonable to assume that the upper limit to the gain can be calculated using the model that the output is initiated by a single photon. Since the energy per photon is simply $hc/\lambda$, the number of photons n in the observed ASE signal of energy E are related by

$$E = nhc/\lambda \qquad (4.1)$$

Using the 320 mTorr data set from Figure 4.36 and the equation above, the upper limit gains for the various gain cell lengths are calculated and presented in Table 4.6. The total gains are on the order of 30, increasing with increasing gain cell length. The gain coefficients (total gain divided by cell length) increase with decreasing gain length. This is to be expected since for shorter gain lengths, the average gain experiences less saturation effects. The gain coefficients are very high, when compared

Table 4.6

ASE Gain

| Gain Length | Output Energy | Photons | Total Gain | Gain Coef. |
|---|---|---|---|---|
| $\ell$ (cm) | E ($\mu$Joules) | $n(10^{14})$ | $\ln(n)$ | ($\%$ cm$^{-1}$) |
| 204 | 60 | 3.78 | 33.6 | 16.5 |
| 184 | 40 | 2.52 | 33.2 | 18.0 |
| 164 | 32 | 2.01 | 33.0 | 20.1 |
| 144 | 20 | 1.26 | 32.5 | 22.5 |
| 124 | 10 | 0.63 | 31.8 | 25.6 |

ASE from (21,59) at 1.2607 $\mu$m. Iodine pressure 320 mTorr.

to 3 % cm$^{-1}$ for iodine OPL as reported in the literature
[6]. But the gain reported here results from pumping the
(21,0) spike transitions, i.e. the gains reported here are
"superlevel gain". It is expected that the gain for a
superlevel to be greater than a single level due to the
nature of CSE.

### 3.Amplifier Performance

An experiment was performed to use an ASE cell as an
amplifier for an iodine laser, as described in an earlier
section. The iodine laser signal acts as the initial
intensity $I_O$ for the ASE gain cell. Figure 4.37 shows the
amplified signal strength as a function of ASE gain cell
pressure. Also shown is the intensity verses pressure curve
for a pure ASE configuration. Much greater output powers
are realized with the amplifier. For the laser-amplifier
set-up, no threshold is required as is the case with the ASE
only configuration.

Since there is a known initial intensity, a graph of
$\ln(I/I_O)$ = gain verses pressure can be generated directly.
Using the cell length, the gain per length is calculated.
Figure 4.38 displays the results. The gain increases with
pressure, with a maximum value of 1 % cm$^{-1}$ at 240 mTorr.
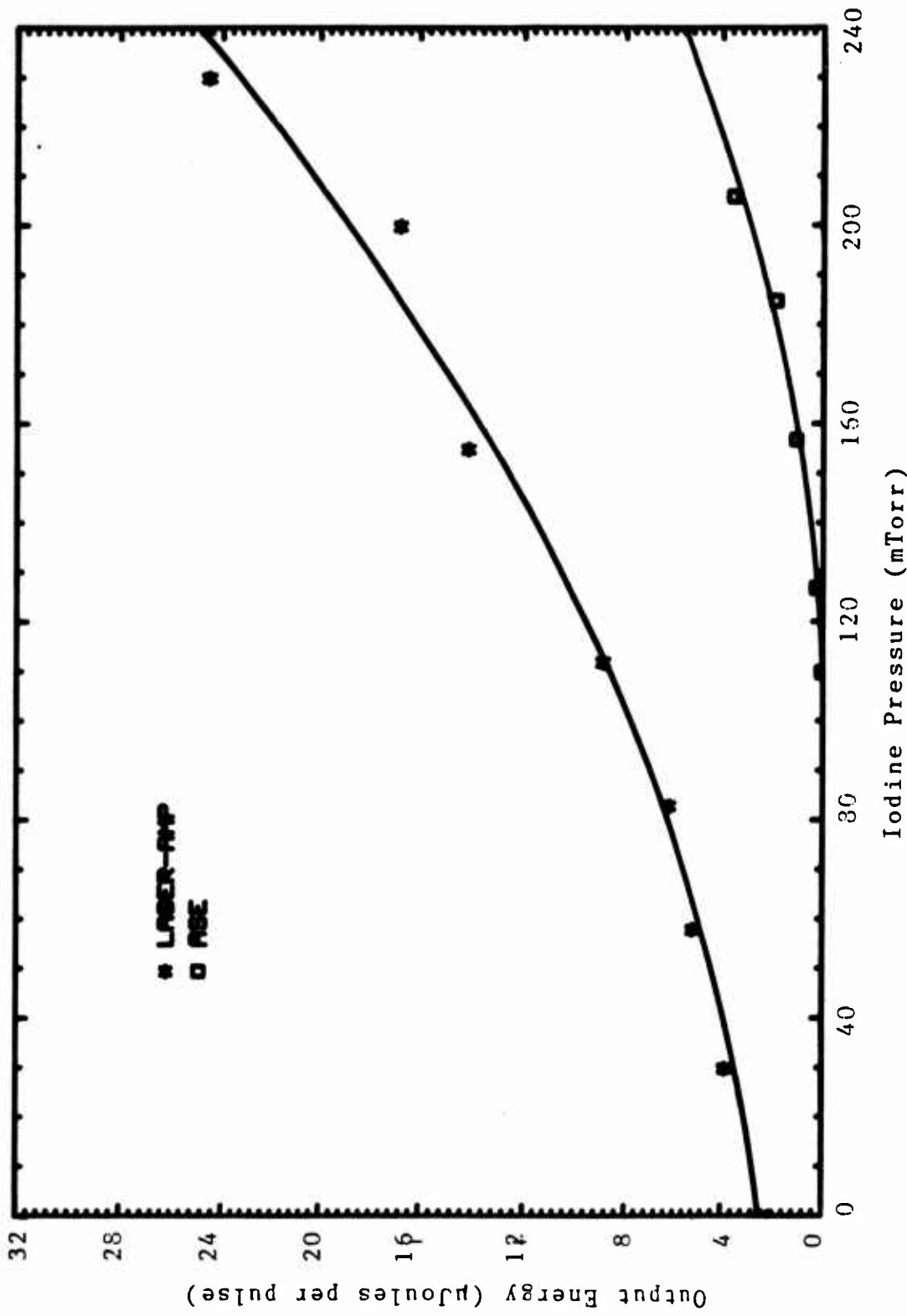
Figure 4.37 Gain Cell Output. Both the output as an amplifier and ASE output is shown. Cell length is 239 cm. Pump wavelength is 565 nm pumping the (18,0) band.
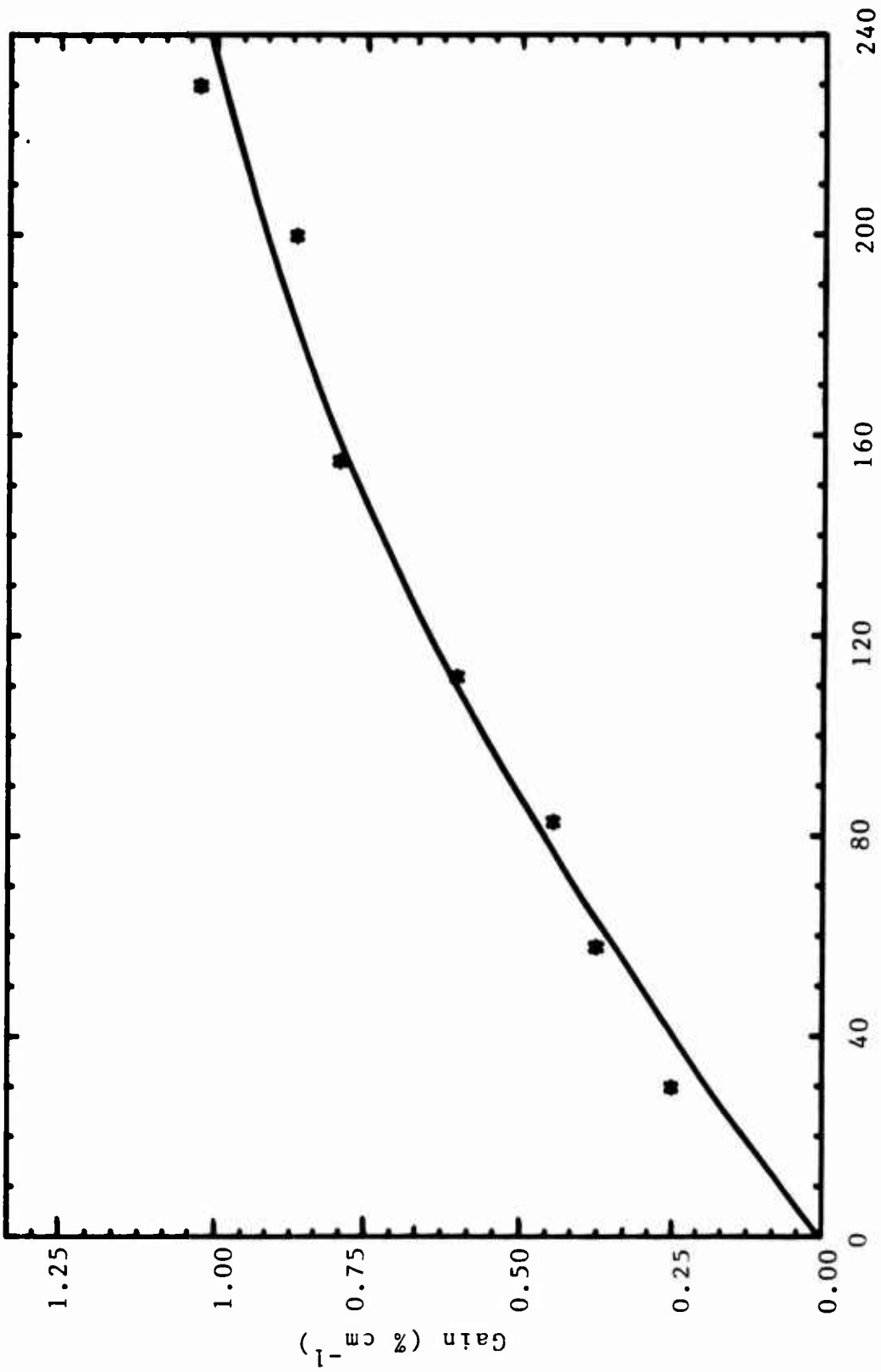
Figure 4.38 Gain verses Pressure for the Amplifier Configuration.

124

E.Miscellaneous Results


1.Near Threshold Performance


The behavior of the ASE output signal near threshold as
a function of pump intensity is shown in Figure 4.39. The
graph reveals that the ASE output is linearlly dependent on
the pump intensity. This behavior confirms that ASE is the
actual physical process and not superradiance. As the
Theory section explained, the superradiant intensity is
proportional to the square of the number of radiators. The
number of radiators is proportional to the pump intensity,
therefore superradiant intensity is proportional to the
square of the pump intensity. Although there is a high
degree of scatter, the relationship between output intensity
and pump intensity is clearly linear. Therefore, ASE is
occuring, not superradiance.


2.Absorbed Pump Energy


Another plot of ASE output verses pump input is shown
in Figure 4.40. Curves for 200 and 150 mTorr are displayed.
Both curves show that the ASE output levels off at pump
energy of about 10 mJ/pulse. This is an indication that the
pump transition for the ASE is saturated. With no more
molecules available for pumping, ASE output no longer
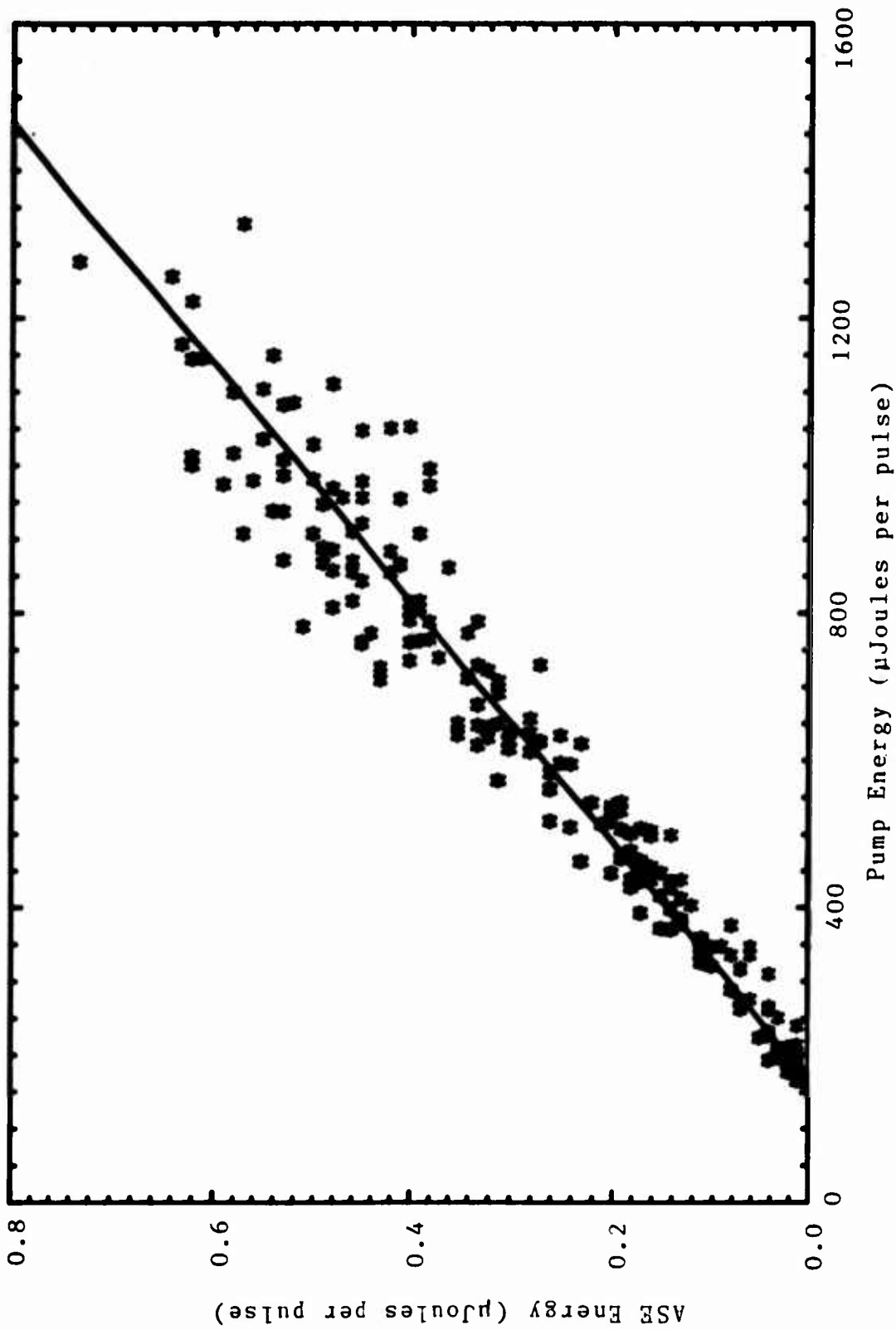
Figure 4.39 ASE Energy verses Pump Energy Near ASE Threshold. Cell length is 239 cm. Iodine pressure is 200 mTorr. Pump wavelength is 527.3 nm, exciting the (34,0) spike.
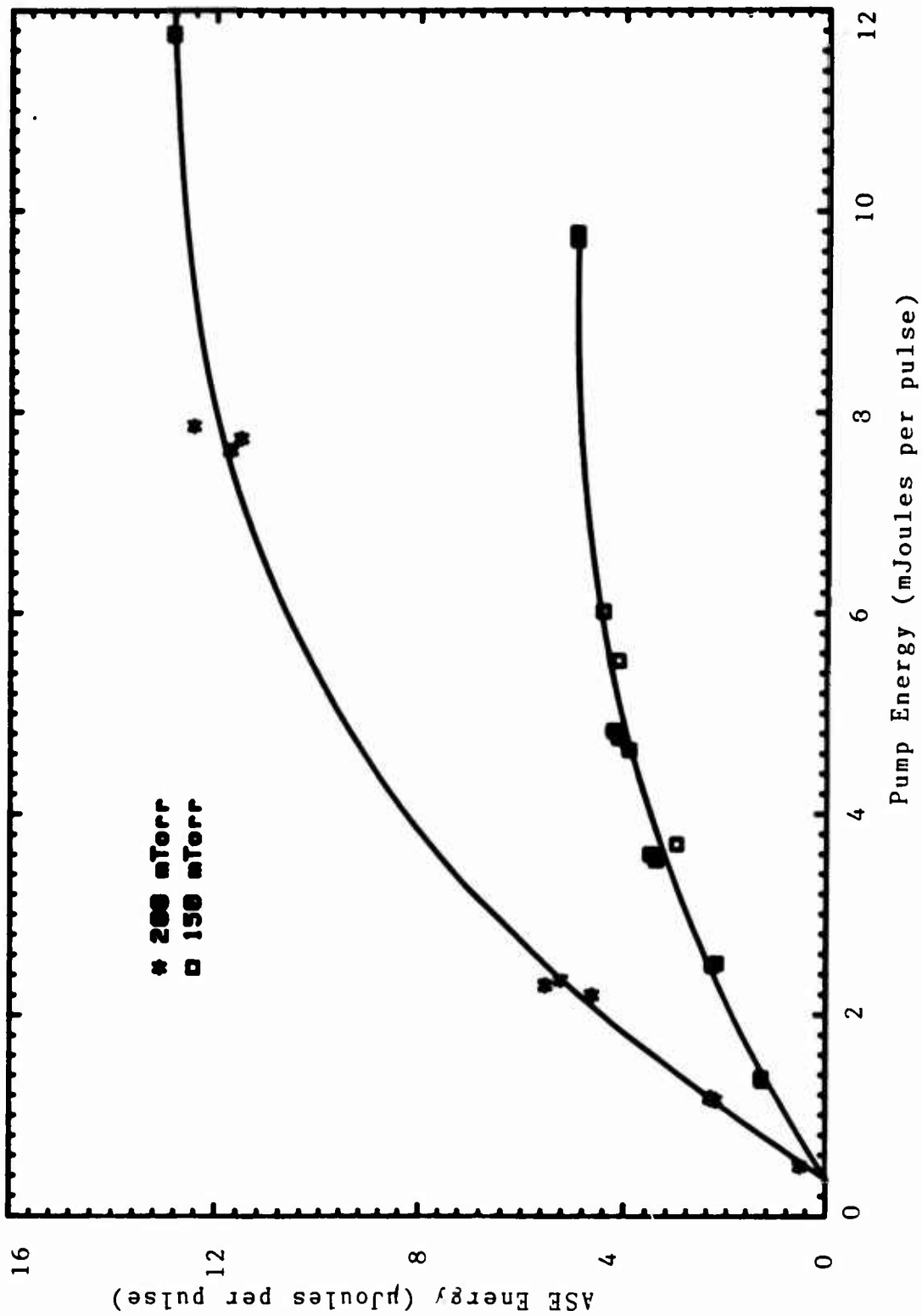
Figure 4.40 ASE Energy verses Pump Energy. Cell length is 223 cm. Pump wavelength is 556 nm, exciting the (21,0) spike.

increases with pump energy.                    ,

Not all of the input energy is absorbed by the iodine
gas, as Figure 4.41 reveals.  Here, the transmitted
intensity is plotted against the input intensity.  The
transmitted intensity includes pump and ASE energy.  But the
ASE signal is very small compared to the pump, so the error
introduced can be ignored in this case.  The graph shows
that only 35% of the pump energy is actually absorbed by the
iodine gas molecules.  This fraction is very nearly constant
over the pump range of 2-25 mJ input intensity.

3.Conversion Efficiency

Using the results of the above section, the ASE
conversion efficiency can be calculated.  Consider two
cases, one far from saturation (CASE 1) and the other at
saturation (CASE 2) with

|                  | CASE 1      | CASE 2      |
|------------------|-------------|-------------|
| Iodine pressure  | 200 mTorr   | 200 mTorr   |
| Pump input       | 1.0 mJ      | 12 mJ       |
| Absorbed pump    | 35 %        | 35 %        |
| ASE output       | 1.8 µJ      | 13 µJ       |

128
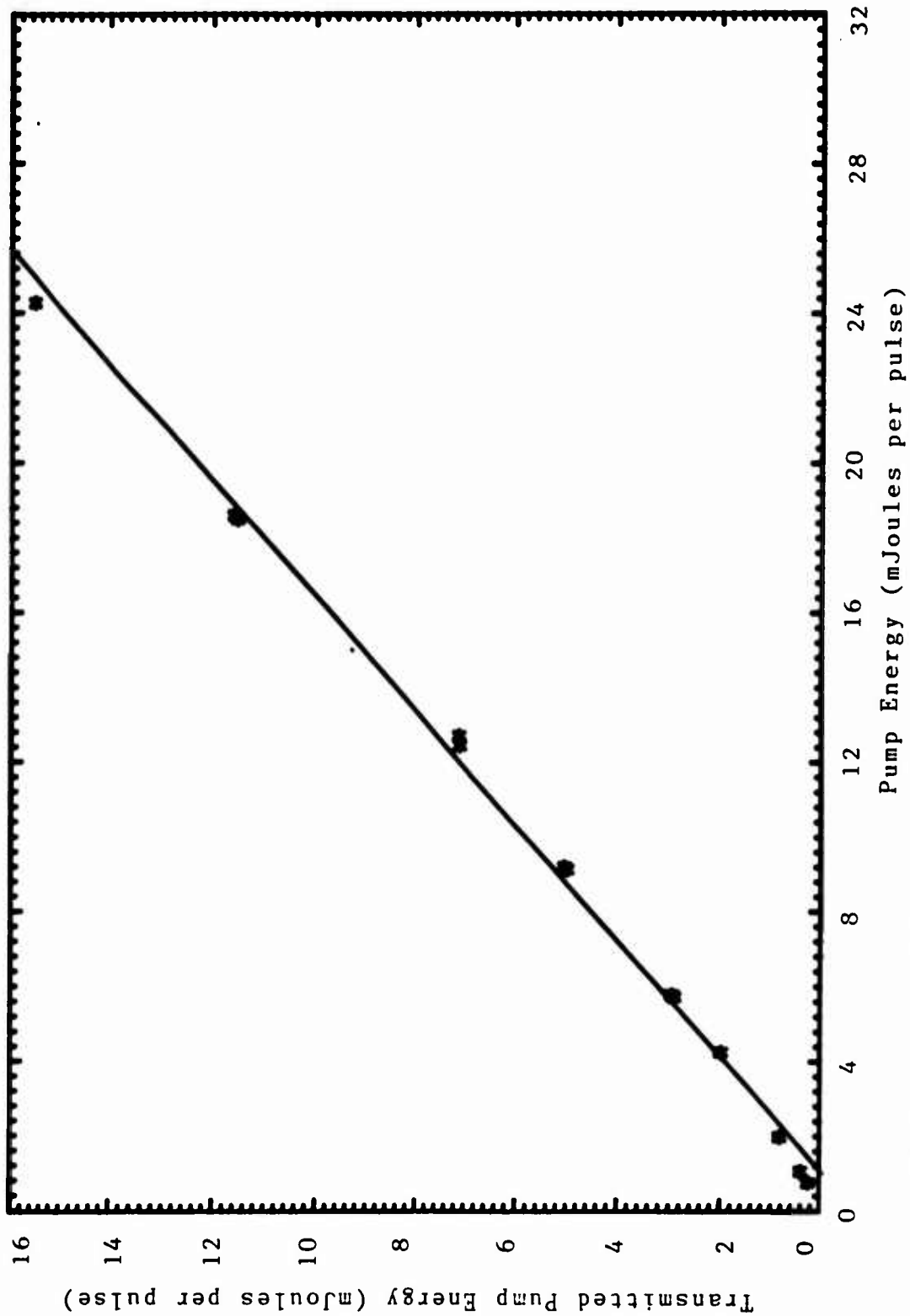
Figure 4.41 Transmitted Pump energy. Iodine pressure is 260 mTorr. Cell length is 223 cm. Pump wavelength is 556 nm, exciting the (21,0) spike. The slope of the curve indicates that 65% of the pump energy is transmitted.

Energy is related to number density n of molecules by the relation

$$E = nhcv/\lambda \qquad (4.2)$$

where v is gain volume. The gain volume with a converged pump laser beam of radius of 2 mm is

$$v = \ell/8 \text{ cm}^3 \qquad (4.3)$$

Using the (21,59) emission wavelength of 12607 Å, then

$$n = 5 \times 10^{13} E/\ell \text{ cm}^{-3} \qquad (4.4)$$

where E is in $\mu J$ and $\ell$ in cm. Note that the calculation is very sensitive to the beam radius. A factor of 2 error is possible with a 40% variation of radius. Experimentally, the measurement of the radius was approximate at best. Using the ASE intensity in Equation 4.4, the number of molecules contributing to ASE can be calculated. And using the absorbed pump intensity, the number of molecules pumped can be calculated. Taking ratios of these values allows the efficiency of ASE to be calculated. From the above information, the following is calculated

130

|                                        | CASE 1 | CASE 2 |
| -------------------------------------- | ------ | ------ |
| molecules pumped $(10^{13} cm^{-3})$   | 3.5    | 40     |
| molecules ASE $(10^{11} cm^{-3})$      | 4.0    | 29     |
| quantum efficiency (%)                 | 1.2    | 0.7    |

The efficiencies calculated above compare to a 0.5% conversion efficiency reported by Byer, et al. [4].

4.Heated Cell Performance

In an effort to increase ASE output intensity and efficiency, the vapor pressure of iodine was raised by heating a 98 cm sealed cell in an oven.  By raising the vapor pressure, the number density of molecules is increased and the percentage of pump energy absorbed is increased as the cell becomes optically dense.  Both of these effects should increase the inversion density, hence increase the gain.  Figure 4.42 shows (19,0) spike intensity verses temperature.  The output energies plotted indicate an order of magnitude increase over the room temperature measurements shown earlier.  For this case, the ASE energy peaks at $65^{\circ}c$, then decreases with increasing temperature.  This could be due to collisional losses greatlv increasing at high number densities, and to insufficient pump energy to achieve a population inversion over the entire gain length.
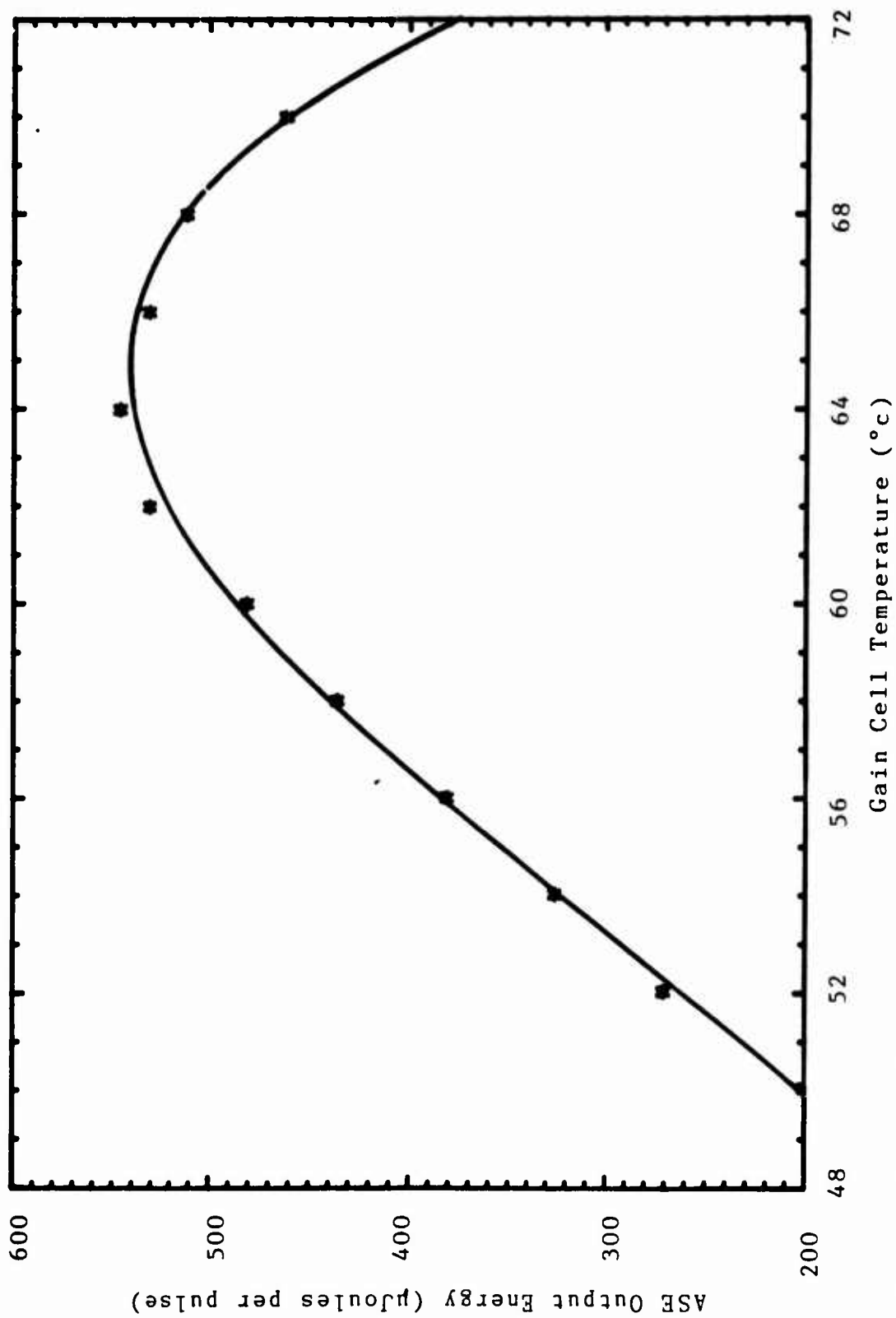
Figure 4.42 ASE Output Energy verses Temperature. Cell length is 98 cm. Pump wavelength is 561.7 nm, exciting the (19,0) spike.
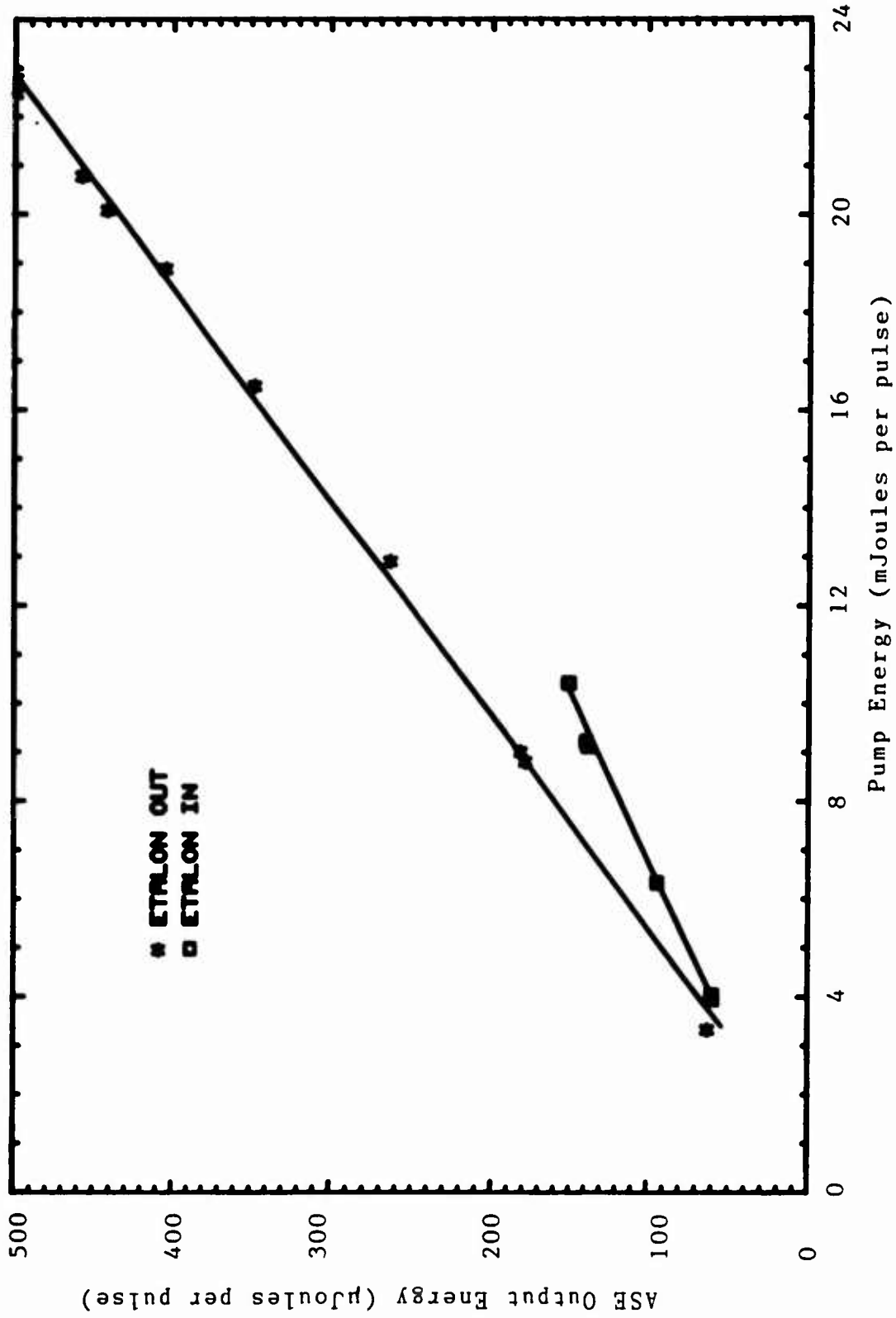
Figure 4.43 Heated Cell ASE Output verses Input Energy. Cell length is 98 cm.
Pump wavelength is 556 nm, exciting the (21,0) spike. Cell temperature is 75°c.

Figure 4.43 shows that the high temperature ASE output is pump energy limited, as hypothesized above. The ASE output increases linearly with pump energy. The curve for the case where the pump dye laser's etalon is out shows a 2% energy efficiency or a 4.5% quantum efficiency.

The heated cell ASE does indeed yield greater performance over room temperature ASE. But this output energy increase is accompanied with multi-line spectral output. The emission spectrum for these high temperatures includes emission from many additional vibrational lines including hot band emission (emission from transitions pumped from $v'' = 1$). Appendix G includes high temperature excitation and emission spectra.

### 5. Variation of Pump Bandwidth

The pump dye laser has an intracavity etalon, which may be inserted or removed, to decrease the pump spectral linewidth by a factor of five. The overall pump energy decreases by about a factor of two when the etalon is in place, but the spectral energy density increases with the etalon in. In Figure 4.43, two curves are shown, with and without the etalon. The addition of the etalon decreases the ASE spike intensity even though the spectral pumping power has been increased. It is the spectral narrowing of the pump that causes the reduction of output. With a narrow

134

bandwidth pump, fewer rotational levels are pumped in the superlevel, resulting in less CSE intensity. This is an unusual situation because narrow bandwidth pump lasers are usually prefered in spectroscopic applications. But for best CSE performance, the pump laser should be as wide as the manifold of transitions that excite the complete superlevel. This can be very wide, as in the case of the (44,84) superlevel which has a pump manifold 25 Å wide.

A final performance study used a wide pump source to populate a larger superlevel than possible with the Quanta-Ray laser. A Phase-R flashlamp pumped dye laser was used to pump v'= 42, 43, and 44 with a 4 Å wide source. Table 4.7 shows some results of this work, and for comparison, results with the Quanta-Ray. ASE output intensities were very high when the wide pump was used, as compared to the narrower pump. These vibrational levels have the widest pump manifold for the superlevel, and take advantage of the wide bandwidth of the Phase-R laser to achieve very high output energies that approach the heated cell performance.

**Table 4.7**

Selected Output Performance

| $\lambda$pump (Å) | Input (mJ) | ASE (µJ) |
|---|---|---|
| Phase-R[1] | | |
| 100 Pulse Averages | | |
| 5145 | 22 | 18 |
| 5152 | 22 | 30 |
| 5158 | 22 | 50 |
| 5162 | 22 | 40 |
| Single Pulse High | | |
| 5170 | 20.4 | 97.5 |
| Quanta-Ray[2] | | |
| 5152 | 2 | 1 |

1. Pump bandwidth $\Delta\lambda$ = 4 Å, iodine pressure 250 mTorr, 171 cm gain cell length.
2. Pump bandwidth $\Delta\lambda$ = 0.2 Å, iodine pressure 250 mTorr, 204 cm gain cell length.

136

# V.CONCLUSION

## A. Summary

Amplified spontaneous emission (ASE) via optical excitation of the $B^3\Pi(0_u^+)-X^1\Sigma(0_g^+)$ system of molecular iodine has been studied. Rotationally resolved excitation and emission spectroscopy over the entire B-X manifold was investigated. The relative efficiency of gain degradation through collisional losses was studied for various buffer gases. A parametric study of output performance, including gain and conversion efficiency, was also performed.

ASE was observed for the pump wavelength range 604-514 nm. This wavelength range produced excited $I_2(B)$ with vibrational excitation of v'= 7-44. Subsequent emission to the $I_2(X)$ state occured to the vibrational levels v"= 38-84. Emission for these transitions occured in the wavelength range of 1.07-1.34 μm. With pumping of one excited state vibrational level (v'), emission was observed to (at most) three adjacent vibrational levels (v"). These emission transitions had the highest Franck-Condon factors of the v" progression. The total emission series (v',v") mapped out the Franck-Condon parabola.

The rotational dependence of the ASE showed two distinct regions:normal and spiked. These regions showed markedly different characteristics.

137

The normal emission intensity varied as expected from the rotational Boltzmann population distribution with a threshold condition. Intensity peaked at the Boltzmann population maximum, $J = 52$, for transitions from each vibrational level, with observed emission over the general region of $25 < J < 85$. The normal emission occured for $7 \leq v' \leq 30$. Also the normal emission consisted of PR doublets consistent with rotational selection rules.

The so-called spike emission displayed an abnormally strong emission signal when rotational levels near the pump bandhead (whose populations are far below threshold as defined by the normal emission cutoff) were pumped. Spike emission occured for $11 \leq v' \leq 44$. The spike excitation envelope was $\sim 1$ Å wide, except where near $\lambda_{pump} = 515$ nm when the single spike separated into multiple spikes before abruptly terminating for $v' \geq 45$. Also, spike emission consisted of a single line rather than doublet emission.

The spike is the result of a cooperative stimulated emission (CSE) of several, simultaneously populated rotational levels whose emission occurs within the Doppler width of any one of the levels involved (called a superlevel). A superlevel is formed of rotational levels that emit at the emission bandhead in the R branch. For the vibrational transitions observed, several rotational levels emit to within the Doppler width at the bandhead. So through stimulated emission, independent rotational levels

138

combine their subthreshold populations to exceed threshold
and emit as one superlevel. CSE results in emission of a
single line, the bandhead transition. This fact explains
the observations of Hanko et al.[64], who first observed
iodine CSE for $\lambda_{pump}$= 5154 and 5161 $\overset{\circ}{A}$.

Superlevel CSE explains the odd behavior of the spike
excitation for $\lambda_{pump} \simeq 515$ nm as the natural result of
bandhead formation at increasingly higher rotational levels,
and the merging of ordinary and extraordinary bandheads in
the R branch for the (44,84) transition. ASE does not reach
threshold for $v' \geq 45$ because the bandhead formation shifts
to the P branch at very high, hence weakly populated,
rotational levels, $J > 100$.

Synthetic excitation spectra were generated by use of a
computer program which incorporated the concept of CSE, the
pump laser characteristics, spectroscopic properties and
constants of iodine, and the Boltzman population
distribution. The synthetic spectra showed excellent
qualitative agreement with good quantitative agreement with
the actual spectra.

Through a simple model, the superlevel was shown to
possess a degree of rotational quench resistance which
increased as the size of the superlevel increased. That is,
rotational transfer within the superlevel does not quench
CSE. This was varified by using buffer gases to study the
relative quenching of the ASE in both the spiked and normal

139

band regions. Buffer gases included He, Ar, Xe, and $N_2$. When pumping v'= 34, the spike emission persisted beyond 8 Torr of He buffer, while the normal band emission quenched at 2 Torr of He buffer.

The ASE output energy was studied as a function of iodine pressure, gain cell length, and pump energy. Output powers as high as 60 μJo: 'es per pulse were recorded at 320 mTorr pressure and 204 cm cell length. Using the model that a single photon initiates ASE, a total gain of 33.6, or 16 % per cm, was calculated from the above conditions. Energy conversion efficiencies of up to 2 % were calculated, with 4.5 % quantum efficiency.

ASE performance was greatly increased when a iodine cell was heated. Peak output energies of 0.5 mJoules per pulse were realized at $65^{\circ}$c for a 98 cm cell for pumping the (19,0) spike. Also, at high temperatures, hot band emission was detected. With the good performance demonstrated here, iodine ASE has potential application for a visible to near-infrared wavelength converter [101] for various spectroscopic uses.

B. Conclusions

Some general conclusions can be drawn from the work presented as outlined in this dissertation. Although LIF is a widely used technique, and OPLs have been the subject of

140

keen interest, it is curious that monitoring stimulated emission as a function of excitation wavelength is sparcely reported. This experimental technique, as this work reports, reveals features that are difficult if not impossible to observe using traditional LIF methods. Understanding the $I_2$ B-X ASE excitation spectra was the crux of this thesis and the key to the discovery of the cooperative process involved. Researchers should give more thought to employing this experimental technique.

Observing ASE rather that traditional lasing is a novel approach, also practically unreported in the literature as a spectroscopic technique. It's key strong points rest in the ease of the experiment (no cavity optics) and the response of the medium is totally unhindered by external devices (wavelength dependence of mirror reflectivity, etalons, gratings, cavity geometry, etc.). ASE allows fundamental spectroscopic and kinetic information about the medium to be studied with little external "complications". Iodine ASE has also shown itself to have practical applications such as a simple, discretely tuneable wavelength converter. The near infrared output, with reasonable efficiency and energy, could lend itself for applications in spectroscopy and kinetics [101]. Where applicable, ASE deserves serious consideration as a spectroscopic tool and technique.

The cooperative stimulated emission (CSE) observed here has never been reported in such detail before. Indeed, CSE

could have been predicted with simple knowledge of molecular spectrocopy and from the spectroscopic constants of $I_2$. CSE could be observed in any molecule that satisifies two requirements; a) one must be able to simultaneously excite several J' levels, and b) this group of rotational levels must emit within a Doppler width of any one of its members. Other molecules should be investigated for possible cooperative emission transitions. The rotational quench resistence and the enhanced optical gain properties, makes CSE an attractive process, and one that merits future research.

## C. Future Work

Further studies of superlevel CSE are necessary to better understand this process. Examination of the CSE emission with sufficient resolution to measure the linewidth would yield information as to the range of the cooperation, and the relative amount of population that is contributed by each member of the superlevel. Precise quenching studies would also be desired, to use the superlevel to test current quenching models and data and supply a unique dataset as well. An extension of ASE to pump wavelengths shorter than 515 nm has been achieved, but assignment of the transitions has not been made [102]. The assignments need to be made. Work here may lead to improved spectroscopic constants for

high lying vibrational levels for both the B and X states. For very long cell lenghts (up to 4 meters) visible ASE from several bands was observed, as well as the typical infrared emission [103]. Studies of high gain configurations such as this could be useful to examine gain, saturation, and competition between vibrational bands in stimulated emission.

The time resolved ASE output as described in Appendix K needs to be explained. More parametric and spectroscopic time resolved information is needed. Theoretical modeling of ASE would most likely be required to understand the temporal behavior. Such a modeling attempt would have to examine the statistical nature of ASE, and include pressure, length, time, and buffer effects as variables.

# REFERENCES

1. J. Koffend, et al. "Pulsed and CW Optically Pumped Lasers for Novel Applications in Spectroscopy and Kinetics," Springer Series in Optical Sciences Vol. 7: Laser Spectroscopy III, Hall and Carlster ed., New York (1977).

2. B. Wellegehausen, IEEE J. Q. E.: QE-15, 1108 (1979).

3. G. Herzberg, Spectra of Diatomic Molecules, 2ed, (Reinhold, New York, 1950).

4. R. Byer, et al., App. Phys. Lett., 20, 463 (1972).

5. B. Hartman, et al., Opt. Comm., 21, 33 (1977).

6. J. Koffend and R. Field, J. App. Phys., 48, 4469 (1977).

7. B. Wellenghausen, et al., Opt. Comm., 23, 157 (1977).

8. F. Wodarczyk and H. Schlossberg, J. Chem. Phys., 67, 4476 (1977).

9. G. Perram and S. Davis, J. Chem. Phys., 84, 2526 (1986).

10. S. Davis and L. Hanko, App. Phys. Lett., 37, 692 (1980).

11. S. Davis, et al., J. Chem. Phys., 78, 172 (1983).

12. S. Davis, et al., J. Chem. Phys., 82, 4831 (1985).

13. M. Henesian, et al., J. App. Phys., 47, 1515 (1976).

14. H. Itoh, et al., Opt. Comm., 18, 271 (1976).

15. S. Leone and K. Kosnik, App. Phys. Lett., 30, 346 (1977).

16. B. Wellegehausen, Opt. Comm., 26, 391 (1978).

17. M. Burrows, et al., App. Phys. Lett., 46, 22 (1985).

18. S. Davis, App. Phys. Lett., 32, 656 (1978).

19. E. Schmitschek, et al., Conference on Laser Engineering and Applications, Washington, D. C. (1977).

20. R. Mulliken, J. Chem. Phys., 55, 288 (1971).

21. J. Hutson, et al., J. Mol. Spect., 96, 266 (1982).

22. P. Luc, J. Mol. Spect., 80, 41 (1980).

23. J. Tellinghuisen, et al., J. Mol. Spect., 82, 225 (1980).

24. M. Boyer, et al., J. Chem. Phys. 64, 4793 (1976).

25. M. Boyer, et al., J. Chem. Phys., 63, 5428 (1975).

26. J. Vigue, et al., J. Chem. Phys., 62, 4841 (1975).

27. J. Paisner and R. Wallenstein, J. Chem. Phys., 61, 4317 (1974).

28. J. Vigue, et al., J. Phys. B, 7, L158 (1974).

29. G. Capella and H. P. Broida, J. Chem. Phys., 58, 4212 (1973).

30. G. Chapman and P. Bunker, J. Chem. Phys., 57, 2951 (1972).

31. J. Tellinghuisen, J. Chem. Phys., 57, 2397 (1972).

32. R. Kurzel, et al., J. Chem. Phys., 55, 4822 (1971).

33. R. B. Kurzel and J. I. Steinfeld, J. Chem. Phys., 53, 3293 (1970).

34. E. O. Degenkolb, et al., J. Chem. Phys., 51, 615 (1969).

35. E. Wasserman, et al., J. Chem. Phys., 49, 1971 (1968).

36. A. Chutjian, et al., J. Chem. Phys., 46, 2666 (1967).

37. J. Tellinghuisen, J. Chem. Phys., 76, 4736 (1982).

38. J. Tellinghuisen, J. Spect. Rad. Trans., 19, 149, (1978).

39. M. Clyne, et al., J. Chem. Soc. Far. Trans. II, 76, 961, (1980).

40. M. Clyne and D. Smith, J. Chem. Soc. Far. Trans. II, 75, 704 (1979).

41. M. Clyne and I. McDermid, J. Chem. Soc. Far. Trans. II, 74, 935 (1978).

145

42. M. Clyne and I. McDermid, J. Chem. Soc. Far. Trans. II, 75, 280 (1979).

43. M. Clyne and I. McDermid, J. Chem. Soc. Far. Trans. II, 75, 1313 (1979).

44. M. Clyne and E. Martinez, J. Chem. Soc. Far. Trans. II, 76, 1561 (1980).

45. M. Clyne and I. Mcdermid, J. Chem. Soc. Far. Trans. II, 74, 1644 (1978).

46. P. Whitefield, et al., J. Chem. Phys., 78, 6793 (1983).

47. J. Birks, et al., Can. J. Phys., 57, 23 (1975).

48. P. Wolf, Collisional Dynamics of the B3 (0+) State of Iodine Monofluoride, Dissertation, Wright-Patterson AFB, Ohio, Air Force Institute of Technology (1985).

49. G. Holleman and J. Steinfeld, Chem. Phys. Lett., 12, 431 (1971).

50. S. Harris, et al., J. Chem. Phys., 70, 4215 (1979).

51. M. Havey and J. Wright, J. Chem. Phys., 68, 4754 (1978).

52. S. Hansen, et al., J. Chem. Soc. Far. Trans. II, 78, 1293 (1982).

53. M. Clyne and I. McDermid, J. Chem. Soc. Far. Trans. II, 72, 2242 (1976).

54. M. Clyne and M. Heaven, J. Chem. Soc. Far. Trans. II, 76, 49 (1980).

55. M. Clyne and I. McDermid, J. Chem. Soc. Far. Trans. II, 74, 644 (1978).

56. M. Clyne and I, McDermid, J. Chem. Soc. Far. Trans. II, 74, 664 (1978).

57. M. Clyne and I. McDermid, J. Chem. Soc. Far. Trans. II, 74, 1376 (1978).

58. M. Clyne and J. Liddy, J. Chem. Soc. Far. Trans. II, 76, 1569 (1980).

59. M. Clyne and I. McDermid, J. Chem. Soc. Far. Trans. II, 4, 807 (1978).

146

60. M. Clyne and I. McDermid, J. Chem. Soc. Far. Trans. II, 4, 789 (1978).

61. G. Perram, Collisional Dynamics of the B3 (0+) State of Bromine Monochloride, Dissertation, Wright-Patterson AFB, Ohio, Air Force Institute of Technology (1986).

62. J. Koffend, et al., J. Chem. Phys., 70, 2366 (1979).

63. K. Truesdell, et al., J. Chem. Phys., 73, 1117 (1980).

64. L. Hanko, et al., Opt. Comm., 37, 63 (1979).

65. J. Steinfeld, Molecules and Radiation, (MIT Press, Cambridge, 1981).

66. L. Hanko, private communication (1984).

67. J. Dunham, Phys. Rev., 41, 721 (1932).

68. W. Jarmin, J. Quant. Spect. Rad. Trans., 11, 421 (1971).

69. J. Coxon, J. Quant. Spect. Rad. Trans., 11, 443 (1971).

70. J. Tellinghuisen, J. Mol. Spect., 44, 194 (1972).

71. J. Tellinghuisen, Comp. Phys. Comm., 6, 221 (1974).

72. J. Tellinghuisen and S. Henderson, Chem. Phys. Lett., 91, 447 (1982).

73. W. Kosman and J. Hinze, J. Mol. Spect., 56, 93 (1975).

74. J. Koffend and R. Field, Laser Spectroscopy III, Springer Series in Optical Science, Vol. 7, 382 (Springer-Varlag, Berlin, 1980).

75. A. Shultz, et al., J. Chem. Phys., 57, 1354 (1972).

76. O. Svelto, Principles of Lasers, 2ed, (Plenum, New York, 1982).

77. R. Wood, Phil. Mag., 24, 673 (1912).

78. T. Balasubramanian, et al., J. Mol. Spect., 88, 259 (1981).

79. J. Tromp and R. LeRoy, J. Mol. Spect., 100, 82 (1983).

80. G. King, et al., Chem. Phys., 50, 291 (1980).

81. M. Danyluk and G. King, Chem. Phys., 25, 343 (1977).

82. J. Steinfeld, J. Phys. Chem. Ref. Data, 13, 445 (1984).

83. M. Borm and J. Oppemheimer, Ann. Phys., 84, 457 (1927).

84. J. Franck, Trans. Far. Soc.,21, 536 (1925).

85. F. Condon, Phys. Rev., 32, 858 (1928).

86. R. Loudon, The Quantum Theory of Light, 2ed., (Clarendon Press, Oxford, 1983).

87. W. Demtroder, Laser Spectroscopy, 2ed., (Springer-Verlag Series in Chemical Physics, Vol. 5, Berlin, 1982).

88. L. Allen. "Amplified Spontaneous Emission," Coherence and Quantum Optics, (edited by Mandel and Wolf, New York, Plenum Press, 1973)

89. R. Dicke, Phys. Rev., 93, 99 (1954).

90. F. Mattar, et al., 46, 1123 (1981).

91. F. Haake, et al., Phys. Rev. A, 23, 1322 (1981).

92. M. Gross and S. Haroche, Phys. Rep., 93, 301 (1982).

93. J. MacGillivray and M. Feld, Phys. Rev. A, 14, 1169 (1976).

94. D. Burnham and R. Chiao, Phys. Rev., 188, 667 (1969).

95. C. Hampel, The Encyclopedia of the Elements, (Reinhold, New York, 1968).

96. M. Kroll and K. Innes, J. Mol. Spect., 36, 295 (1970).

97. J. Tellinghuisen, et al., J. Chem. Phys., 64, 4796 (1976).

98. J. Tellinghuisen, et al., J. Chem. Phys., 68, 5177 (1978).

99. J. Tellinghuisen, et al., App. Phys. Lett., 41, 789 (1982).

100. J. Tellinghuisen and J. Ashmore, App. Phys. Lett., 40, 867 (1982).

101. J. Glessner, et el., Air Force Invention Disclosure #17046 (patent pending), (1985).

**102. Strong excitation features appear between 505-509 nm.** Rotational doublet splittings tend to indicate very high rotational excitation. The emission of these lines are all $13362 \pm 6$ Å. Attempts to assign transitions using the best available constants has been unsuccessful. This excitation is hypothesized to correspond to P branch bandhead(s), based upon the trends of the known ASE.

103. Visible ASE has been observed for pumping in the R590 dye region. Very long cells were used (4 meters) and low pump power was a limiting factor (the Quanta-Ray pump laser experienced a catastrophic failure that

# APPENDIX A

## Spectroscopic Term Values

The energy levels of a rotating vibrator are given in terms of the vibrational and rotational quantum numbers, v and J. The Dunham equation [67] is a convenient expression for the energy levels

$$F(v,J) = \sum Y_{jn}(v+0.5)^j J^n (J+1)^n \qquad (A.1)$$

The $Y_{jn}$'s are called Dunham coefficients. These coefficients can be calculated by use of a series in powers of the ratio $B_e^2/w_e^2$ where $w_e$ is the classical frequency of small oscillations and $B_e = h/(8\pi^2 m r_e^2 c)$ [65].

The connection between the Y's and the ordinary band spectrum constants are as follows:

$$\left.\begin{array}{llll}
Y_{1,0} = w_e & Y_{2,0} = -w_e x_e & Y_{3,0} = w_e y_e & Y_{4,0} = w_e z_e \\
Y_{0,1} = B_e & Y_{0,2} = D_e & Y_{0,3} = H_e & Y_{0,4} = L_e \\
Y_{1,1} = -\alpha_e & Y_{2,1} = \gamma_e & Y_{1,2} = \beta_e &
\end{array}\right\} \quad (A.2)$$

The equality bewteen the Y's and the ordinary spectroscopic constants is not truly exact, but differs by terms in $B_e^2/w_e^2$. This ratio is very small for heavy molecules so that the equality is adequate for most purposes. For iodine

thir ratio is of the order of $10^{-8}$.

Since the Dunham equation comes from an a priori analysis of the energy states of a molecule, a phenomenological approach is often used by spectroscopists to report the electronic, vibrational, and rotational levels corresponding to these energy states

$$T_e + G_v + F_J \qquad (A.3)$$

where

$T_e$ = electronic energy above the ground state

$G_v = w_e(v+0.5) - w_e x_e (v+0.5)^2 + w_e y_e (v+0.5)^3 + \ldots$

= vibrational energy

$F_J = B_v J(J+1) - D_v J^2 (J+1)^2 + H_v J^3 (J+1)^3 + \ldots$

= rotational energy

The energies are related as follows

$$T_e \gg G_v \gg F_J \qquad (A.4)$$

The various spectroscopic constants arise from the molecule's non-ideal behavior (centrifugal distortion and anharmonicity). The rotational constants include vibration-rotation interaction effects as shown in Equations A.5

$$
\left.\begin{array}{l}
B_v = B_e + \alpha_e(v+0.5) + \gamma_e(v+0.5)^2 + \ldots = \sum b_n(v+0.5)^n \\[2mm]
D_v = D_e + \beta_e(v+0.5) + \ldots = \sum d_n(v+0.5)^n \\[2mm]
H_v = H_e + \ldots = \sum h_n(v+0.5)^n
\end{array}\right\} \quad (A.5)
$$

The Equations A.5 are obtained from an expansion of the Dunham equation with a grouping of the spectroscopic constants which are used in place of the Dunham coefficients.

# APPENDIX B

## Band Head Formation

A simple graphical representation of the P and R rotational transitions of a vibrational band is given by a Fortrat Diagram, shown in Figure 2.1. The curve traced out by the transitions is called a Fortrat Parabola [3]. In a Fortrat parabola, the P and R branches are represented by a single formula

$$\nu = \nu_o + (B_{v'} + B_{v''})m + (B_{v'} - B_{v''})m^2 \qquad (B.1)$$

where $m = -J$ for the P branch and $m = J+1$ for the R branch. The above formula ignores higher order rotational constants for simplicity. Generally, one of the branches turns back on itself, giving rise to the characteristic shape of the curves in the visible and ultraviolet regions. The bandhead corresponds to the vertex of the Fortrat parabola.

The bandhead is a result of the quadratic term above, dominating the linear term at and above some value of m. Consider the case where $B_{v'} - B_{v''} < 0$. Here the linear and quadratic terms have opposite signs, and a maximum of $\nu$ occurs for some value of m designated $m_{vertex}$. The value for $m_{vertex}$ is found by setting $d\nu/dm = 0$. This gives

$$m_{vertex} = - \frac{B_{v'} + B_{v''}}{2(B_{v'} - B_{v''})} \qquad (B.2)$$

153

With $B_{V'} - B_{V''} < 0$ the bandhead is formed in the R
branch and the head lies on the short wavelength side of the
band origin. The bands are then said to be red shaded.
This is generally the case for the iodine B-X system. Note
that red shading implies $B_{V'} < B_{V''}$ so that $R_{V'} > R_{V''}$ since

$$B_V = \frac{\hbar}{4\pi c \mu} \langle v | R^{-2} | v \rangle \qquad (B.3)$$

That is the atoms in the upper state are further apart than
in the lower state. The iodine potential energy diagram
clearly shows this to be the case for the B-X system.

Bandhead formation occurs in the P branch when
$B_{V'} - B_{V''} > 0$, with shading toward the violet. Also, bands
can have more than one head. The extraordinary bandheads
occur when the effect of the higher order rotational
constants, $D_V$, $H_V$, etc, is not insignificant. This may
occur at high rotational levels, as the higher powers of m
allow these constants to dominate the analysis.

# APPENDIX C

Transition Strengths for Molecules


The intensity of electronic transitions for molecules can be derived from a quantum mechanical description first noting that the electric dipole transition strength is proportional to the square of the electric dipole matrix elememt D

$$D = \langle \psi^* |\bar{\mu}| \psi \rangle \qquad \text{(C.1)}$$

where $\psi$ is the molecular wavefunction with $\bar{\mu}$ the electric dipole transition moment for a transition between the primed and double-primed states [65]. The wavefunction $\psi$ is a function of the position of the electrons r and the internuclear separation R. Born and Oppenheimer separated the wavefunction into electronic, e, and nuclear vibrational, v, parts [83] by assuming that the nuclear motion is small, approximately constant, with respect to the electrons

$$\psi(r,R) = e(r;R)v(R) \qquad \text{(C.2)}$$

where R is a constant in the electronic wavefunction $e(r;R)$. The dipole moment can also be separated into electronic $\bar{\mu}_e$ and nuclear parts $\bar{\mu}_N$,

$$D = \langle e'v' | \ \overline{\mu}_e + \overline{\mu}_N | e''v'' \rangle \qquad (C.3)$$

The Hermitian conjugate of the wavefunctions in the bra is understood. Then

$$D = \langle e'v' | \overline{\mu}_e | \ e''v'' \rangle + \langle e'v' | \ \overline{\mu}_N | e''v'' \rangle \qquad (C.4)$$

Grouping terms

$$D = (\langle e' | \overline{\mu}_e | e'' \rangle) v' | v'' \rangle + \langle e' | e'' \rangle \langle v' | \overline{\mu}_N | v'' \rangle \qquad (C.5)$$

The second term above is 0 because of the orthognality of $\langle e' | e'' \rangle$. The electronic transition moment is the first term in parenthesis

$$D_e = \langle e' | \overline{\mu}_e | e'' \rangle \qquad (C.6)$$

By the Franck-Condon principle [84,85], the transition moment $D_e(R)$ is approximately constant with respect to nuclear motion, so

$$D_e(R) = \text{constant} = \overline{D_e(R)} \qquad (C.7)$$

Then

$$D = \overline{D_e(R)} \langle v' | v'' \rangle \qquad (C.8)$$

156

The transition strength is proportional to the above equation, and the quantity $|\langle v'|v''\rangle|^2$ is called the Franck-Condon Factor (FCF). FCF's are simply the overlap between the vibrational wavefunctions of the two states in the transition. Physically, the more the states overlap, the greater the propability of a transition, and the stronger the intensity of the resultant fluorescence.

Properties of $I_2$ $B^3\Pi(0_u^+)-X^1\Sigma(0_g^+)$

The spectroscopic and kinetic properties of iodine have been studied since the work of Wood early in this century [77]. Of all the work done, the most detailed and precise studies have been performed over the past two decades using LIF techniques. Mulliken's iodine review article presents an extensive summary of the information available for many excited states of iodine [20]. This appendix will briefly review the B-X system only.

Molecular spectroscopic constants are required in order to provide the information about the energies of the various vibrational and rotational levels of the electronic state of a molecule. The most accurate ground state constants for $I_2$ have been presented by Tellinghuisen, McKeever, and Sur in an analysis of the D-X spectrum [23]. In their analysis they used the expression

$$E(v,J) = G_v + B_vJ(J+1) - D_vJ^2(J+1)^2 + H_vJ^3(J+1)^3 \qquad (D.1)$$

The constants were given in terms of expansion parameters

$$\left.\begin{array}{l} G_v = \sum g_n(v+0.5)^n \\[4pt] B_v = \sum b_n(v+0.5)^{n-1} \\[4pt] \ln(D_v) = \sum d_n(v+0.5)^{n-1} \\[4pt] \ln(H_v) = \sum h_n(v+0.5)^{n-1} \end{array}\right\} (D.2)$$

The parameters are given in Table D.1.

The exhaustive Fourier Transform Spectroscopy work of Luc described the B state of iodine to a precision greater than the rotational transition linewidth [22]. Luc uses the standard relation

$$E(v,J) = T_e + G_v + B_v J(J+1) - D_v J^2 (J+1)^2 + H_v J^3 (J+1)^3 \quad (D.3)$$

where the rovibrational constants are defined by the expansion parameters

$$\left.
\begin{aligned}
G_v &= \sum g_n (v+0.5)^n \\
B_v &= \sum b_n (v+0.5)^n \\
D_v &= \sum d_n (v+0.5)^n \\
H_v &= \sum h_n (v+0.5)^n
\end{aligned}
\right\} \quad (D.4)$$

These parameters are given in Table D.2.

An extensive calculation of Frank-Condon factors for the B-X system has been published by Tellinghuisen [38]. The electronic transition moment has been determined over a range of R-centroids from 2.6 < R < 4.8 Å [37,38,62,78]. There has been great interest in the B state near the dissociation limit [79-81], as researchers try accurately to characterize the potential curve near the dissociation limit, and to determine the number of bound vibrational levels. The dissociation limit $D$ • has been found to be 20043.16 (±0.02) $cm^{-1}$ and the vibrational index at

159

dissociation is $v_D$ = 87.32 [79]. The visible and infrared absorption spectrum of $I_2$ has had inconsistencies in the three transitions generally felt to contribute to total absorption, B-X, A-X, and $1u(\Pi)$-X. Tellinghuisen gives a thorough analysis of the transition strengths of these electronic states and explains how they relate to the absorption spectrum of $I_2$ [37].

Lifetime, quenching, and energy transfer studies of the B-X system have been most numerous and enlightening. Lifetime studies have confirmed natural [25], magnetic [30], and hyperfine [24] predissociations for this system. A typical fluorescent collision free lifetime for B-X emission is 0.5-1 μs [24,25,30]. A study of predissociations has been used to locate curve crossings between the B state and various repulsive potentials. Quenching studies via lifetime measurements have yielded self-quenching and various buffer gas quenching cross sections and these results have been summarized and tabulated by Steinfeld [82]. Vibrational and rotational energy transfer studies have shown multiquantum transfer effects and the persistance of the rotational state [32,33].

Table D.1

Iodine $X^1\Sigma(0_g^+)$ State Molecular Expansion Parameters

| $G_v$ | $B_v$ | $\ln(D_v \times 10^9)$ | $\ln(-H_v \times 10^{16})$ |
|---|---|---|---|
| 2.14538660E-2 | 3.736849E-2 | 1.5206 | 1.8648 |
| -6.18970919E-1 | -1.146334E-4 | 3.8326E-3 | -1.2164E-2 |
| 1.61204430E-3 | -7.361611E-8 | 8.7000E-5 | 2.5915E-3 |
| -4.10109637E-4 | -2.745772E-8 | 1.9422E-6 | -3.7770E-5 |
| 3.38088677E-5 | 9.539462E-10 | | 2.1678E-7 |
| -1.78986530E-6 | -1.827290E-11 | | |
| 6.01983892E-8 | 1.353723E-13 | | |
| -1.25300668E-9 | -3.588030E-16 | | |
| 1.35425963E-11 | | | |
| 1.77848866E-14 | | | |
| -2.87954337E-15 | | | |
| 4.36352676E-17 | | | |
| -3.32846207E-19 | | | |
| 1.33752148E-21 | | | |
| -2.25287105E-24 | | | |

All constants are in $cm^{-1}$. Results are good to 0.01 $cm^{-1}$. Constants are valid for v<100 and J<100. Source is [23].


Table D.2

Iodine $B^3\Pi(0_u^+)$ State Molecular Expansion Parameters

| $G_v$ | $B_v$ | $D_v$ | $H_v$ |
|---|---|---|---|
| 1.256724E+2 | 2.8993694599E-2 | 6.125767E-9 | -2.15004734 E-15 |
| -0.752677 | -1.406799398 E-4 | 1.418420E-10 | 7.915679522E-15 |
| -3.246282E-3 | -5.088972976 E-6 | -2.825041E-12 | -1.02396618 E-14 |
| 1.875736E-5 | 8.7511454030E-7 | 5.544495E-13 | 4.852619270E-15 |
| -3.414124E-6 | -1.171736403 E-7 | -2.644252E-14 | -1.19975156 E-15 |
| 2.004998E-7 | 9.7025967839E-9 | 9.539521E-16 | 1.792143124E-16 |
| -6.950414E-9 | -5.304859892 E-10 | -1.864100E-17 | -1.75575349 E-17 |
| 1.517899E-10 | 1.9571123281E-11 | 1.813907E-19 | 1.185081818E-18 |
| -1.899790E-12 | -4.894864050 E-13 | -6.053203E-22 | -5.67595443 E-20 |
| 1.226941E-14 | 8.1736417235E-15 | | 1.958960707E-21 |
| -3.137312E-17 | -8.715621632 E-17 | | -4.88849274 E-23 |
| | 5.3609973831E-18 | | 8.739722535E-25 |
| | -1.445945450 E-21 | | -1.09126306 E-26 |
| | | | 9.034911061E-29 |
| | | | -4.45560254 E-31 |
| | | | 9.904029815E-34 |

Te = 15769.0485 $cm^{-1}$. Constants are in $cm^{-1}$. Valid for v<63. Results are good to 0.01 cm-1. Source is [22].

161

Molecular Population Distributions


Given a gas phase molecular species at pressure P corresponding to number density n, the internal energy is partitioned between electronic, vibrational, rotational, and nuclear hyperfine population groups

$$n(e,v,J,f) = n_e n_v n_J n_f \qquad \text{(E.1)}$$


For most diatomics all of the population resides in the ground electronic state at room temperature, so define $n_e = n_o$ where $n_o$ is the total number density of the gas.

The vibrational population is partitioned according to vibrational energy

$$n_v = \exp\left(-\frac{E_v - E_o}{kT}\right) \qquad \text{(E.2)}$$


where

$$E_v = w_e(v+0.5) - w_e x_e (v+0.5)^2 + \ldots$$


with the normalization

$$\sum n_v = 1 \qquad \text{(E.3)}$$

For molecular iodine at room temperature the vibrational population distribution is given in Figure E.1.

Within a vibrational level, populations are further partitioned according to rotational energy via the Boltzmann distribution

$$n_J = (2J+1)\exp\left(-\frac{E_J}{kT}\right) \qquad (E.4)$$

where

$$E_J = B_v J(J+1) - D_v J^2 (J+1)^2 + \ldots \qquad (E.5)$$

with the fraction of molecules that reside in any one rotational level $f_J$ as

$$f_J = \frac{n_J}{\sum n_J} \qquad (E.6)$$

The rotational populations given by Equation (E.4) is incomplete, however. This is because of symmetry restrictions on nuclear-spin states, which must be considered now. In a homonuclear diatomic molecule, like $I_2$, it is required that the total wavefunction be antisymmetric with respect to nuclear interchange if the nuclei are fermions [65]. Iodine has a nuclear spin I of 5/2, therefore it obeys Fermi-Dirac statistics and is a fermion [65]. Of the $(2I+1)^2$ possible nuclear spin states, $(2I+1)(I+1)$ are symmetric and $(2I+1)I$ are antisymmetric

163
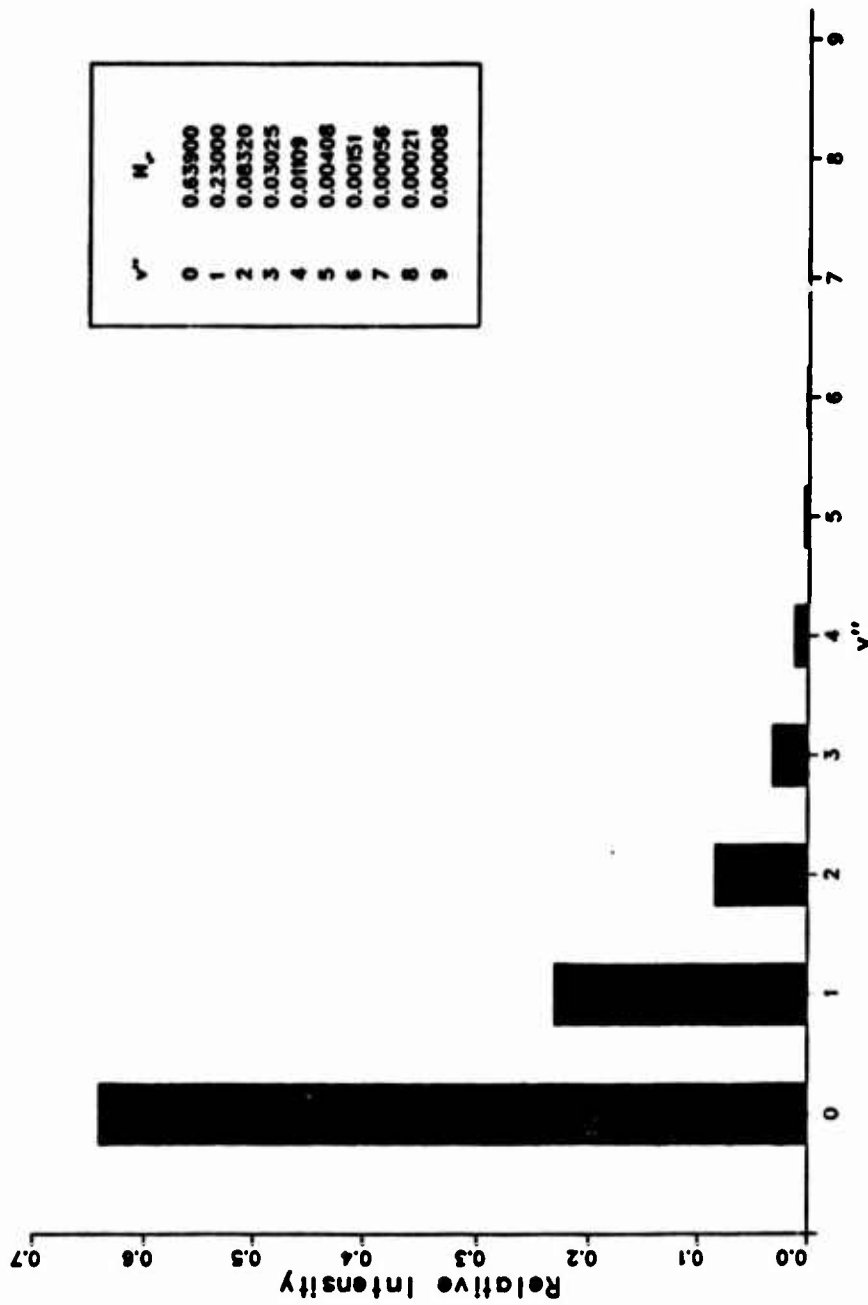
Figure E.1 Vibrational Population Distribution for the Ground Electronic State of Iodine at 300°K.

[65].

The basic symmetry for rotational levels is that even-J levels are symmetric and odd-J levels are antisymmetric [65]. Under a nuclear interchange operation, an even function does not change sign, while an odd function will.

Now the total wavefunction $\Psi$ must be antisymmetric where

$$\Psi = \psi_e \, \psi_J \, \psi_f \tag{E.7}$$

The ground electronic state of iodine $X^1\Sigma_u^+$ is symmetric. Therefore, the odd-J states must combine with the even nuclear-spin states (and visa versa) to maintain an overall antisymmetric wavefunction. This means that odd-J states have a weight of $(2I+1)(I+1) = 21$ for iodine. And even-J states have a weight of $(2I+1)I = 15$ for iodine. A 7:5 intensity alternation is predicted for the ground state of $I_2$ and it is indeed observed [65].

So now the rotational populations are modified by a nuclear-spin factor $f_{NS}$

$$n_J = f_{NS} (2J+1) \exp\left(- \frac{E_J}{kT}\right) \tag{E.8}$$

and

$$f_{NS} = \begin{cases} 7/6 & \text{for odd } J \\ 5/6 & \text{for even } J \end{cases}$$

For the ground state of iodine the rotational population

distribution is given by Figure E.2.
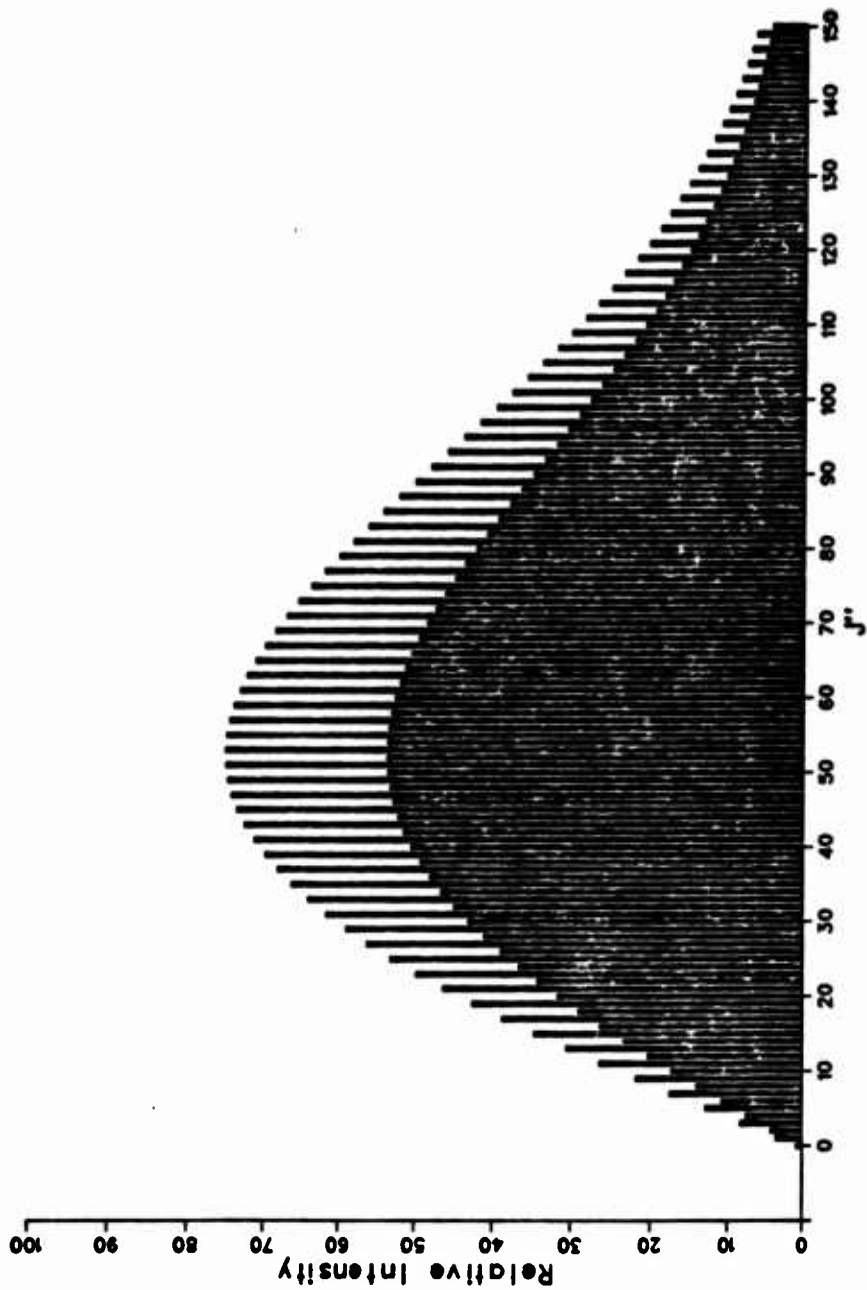
Figure E.2 Rotational Population Distribution for the Ground Vibrational State of Iodine at 300°K.

167

## Stimulated Emission and Gain

The quanitity of fundamental importance in a system involving optical gain is the gain coefficient. The gain coefficient is related to the stimulated emission cross section $\sigma$ by

$$g = \sigma \, \Delta n \qquad\qquad (F.1)$$

where $\Delta n$ is the inversion density, $\Delta n = n_u - \frac{g_u}{g_l} n_l$, where u refers to the upper state and l refers to the lower state and the g's are the degenercies. The cross section is related to the Einstein B coefficient by

$$\sigma = \frac{h\nu}{c} \, Bf(\nu - \nu_o) \qquad\qquad (F.2)$$

where $f(\nu - \nu_o)$ is the lineshape function. With the B coefficient given by

$$B = \frac{2\pi^2}{3\epsilon_o \hbar} \, |\mu|^2 \qquad\qquad (F.3)$$

then

$$\sigma = \frac{2\pi^2 \nu}{3\epsilon_o c h} |\mu|^2 f(\nu - \nu_o) \qquad\qquad (F.4)$$

where $|\mu|$ is the dipole moment. For a molecular transition
between electronic states

$$|\mu|^2 = |R_e|^2 q_{v'v''} \frac{S_{J',J''}}{2J'+1} \qquad \text{(F.5)}$$

where $|R_e|^2$ is the average electronic transition moment,
$q_{v'v''}$ is the Franck-Condon factor, and $S_{J'J''}$ is the
Hönl-London factor, or the rotational line strength.

For Doppler broadened transitions the lineshape
function is

$$f(\nu-\nu_0) = \frac{1}{\Delta\nu} \sqrt{\frac{4\ln 2}{\pi}} \exp\left[\frac{1}{\ln 2}\left(\frac{\nu-\nu_0}{2\Delta\nu}\right)^2\right] \qquad \text{(F.6)}$$

where $\Delta\nu$ is the FWHM

$$\Delta\nu = \nu \sqrt{\frac{8kT\ln 2}{mc^2}} \qquad \text{(F.7)}$$

So for a diatomic molecule, gain on line center is expressed
as

$$\sigma = \frac{2\pi^2}{3\varepsilon_0 hc} \sqrt{\frac{4\ln 2}{\pi}} \frac{\nu_0}{\Delta\nu} |R_e|^2 q_{v',v''} \frac{S_{J',J''}}{2J''+1} \qquad \text{(F.8)}$$

in MKS units or in CGS units as

$$\sigma = \frac{8\pi^3}{3hc} \sqrt{\frac{4\ln 2}{\pi}} \frac{\nu_0}{\Delta\nu} |R_e|^2 q_{v',v''} \frac{S_{J',J''}}{2J'+1} \qquad \text{(F.9)}$$

169
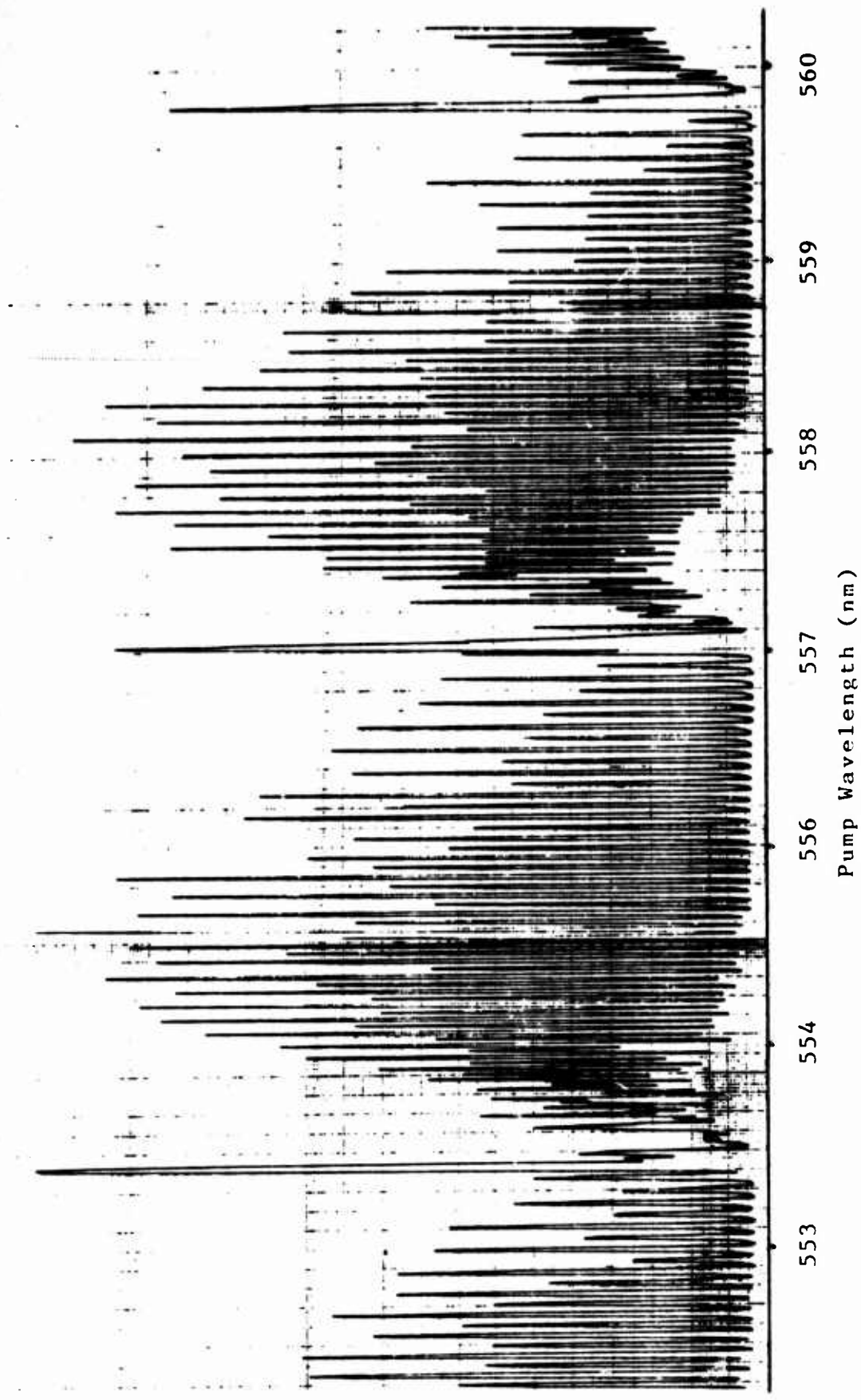
Figure G.1 Moderate Resolution Spectrum with F548 Dye. The (22,0) and (21,0) bands are shown.

Pump Wavelength (nm)

171
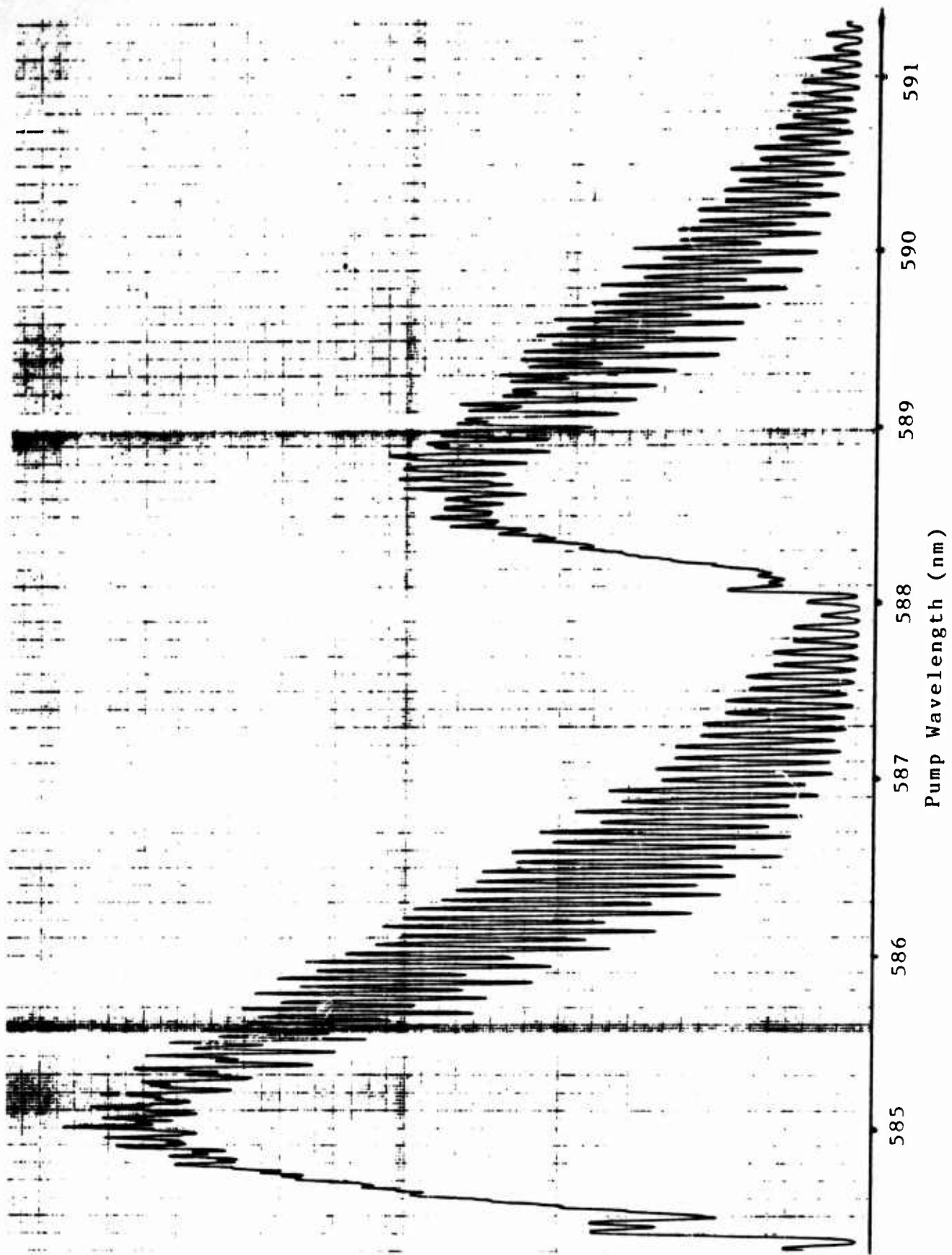
Figure G.2 Moderate Resolution Spectrum with KR620 Dye. The (21,0) and (11,0) bands are shown.
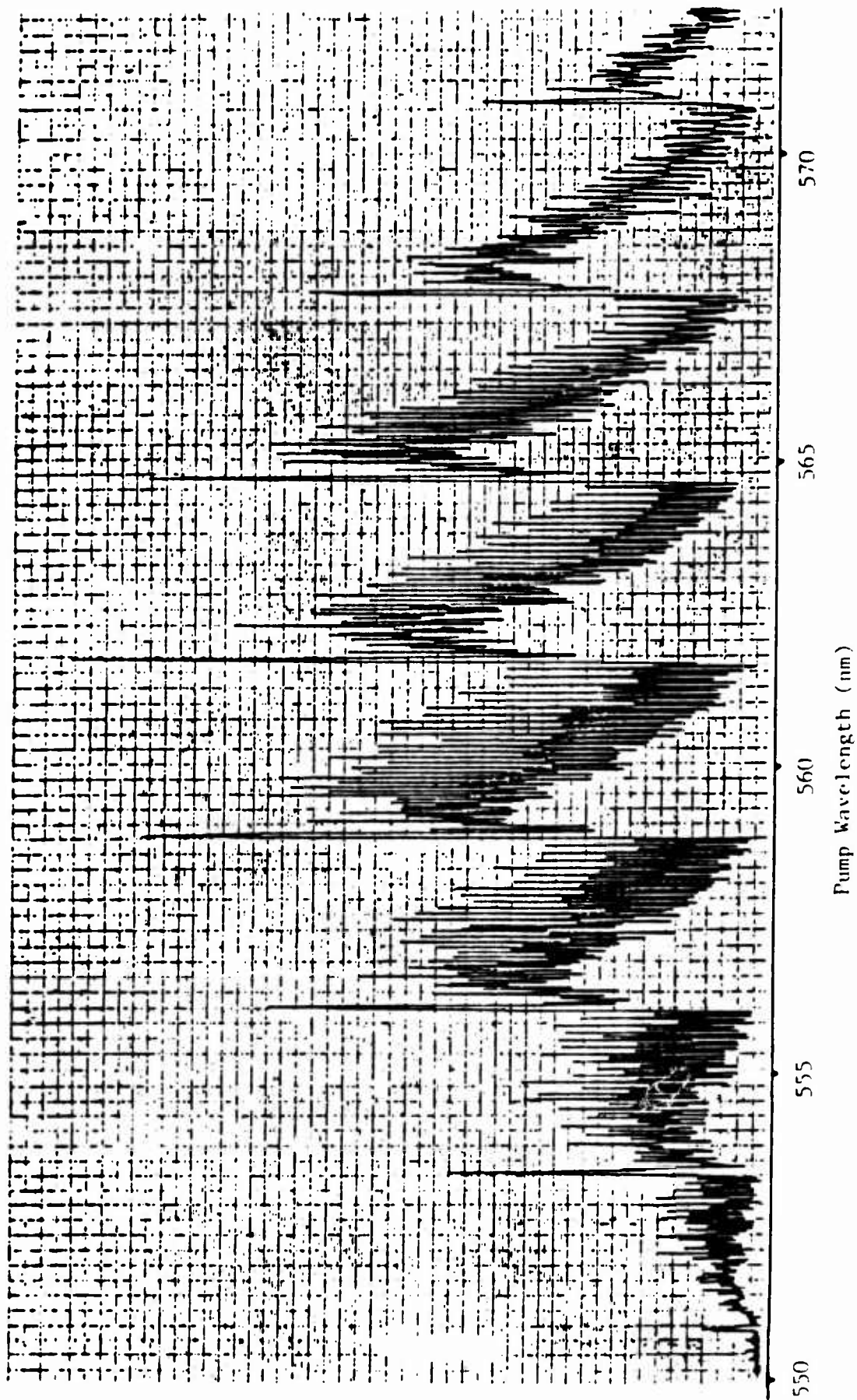
Figure G.3 ASE Excitation at 39°c Cell Temperature.   Iodine vapor pressure is 939 mTorr.

173
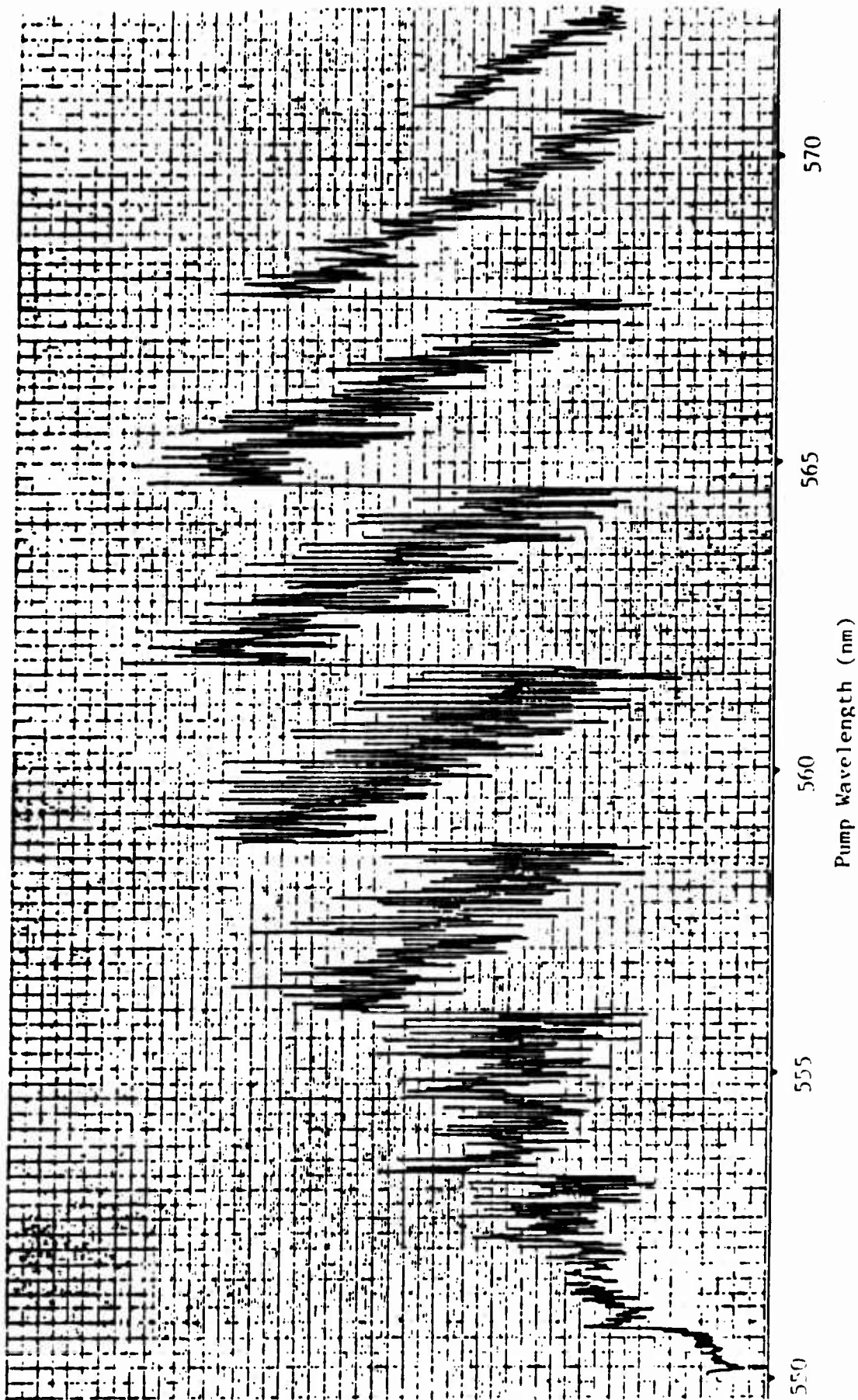
Figure G.4 ASE Excitation at 61°c Cell Temperature. Iodine vapor pressure is 4506 mTorr. Hot band excitation is evident.
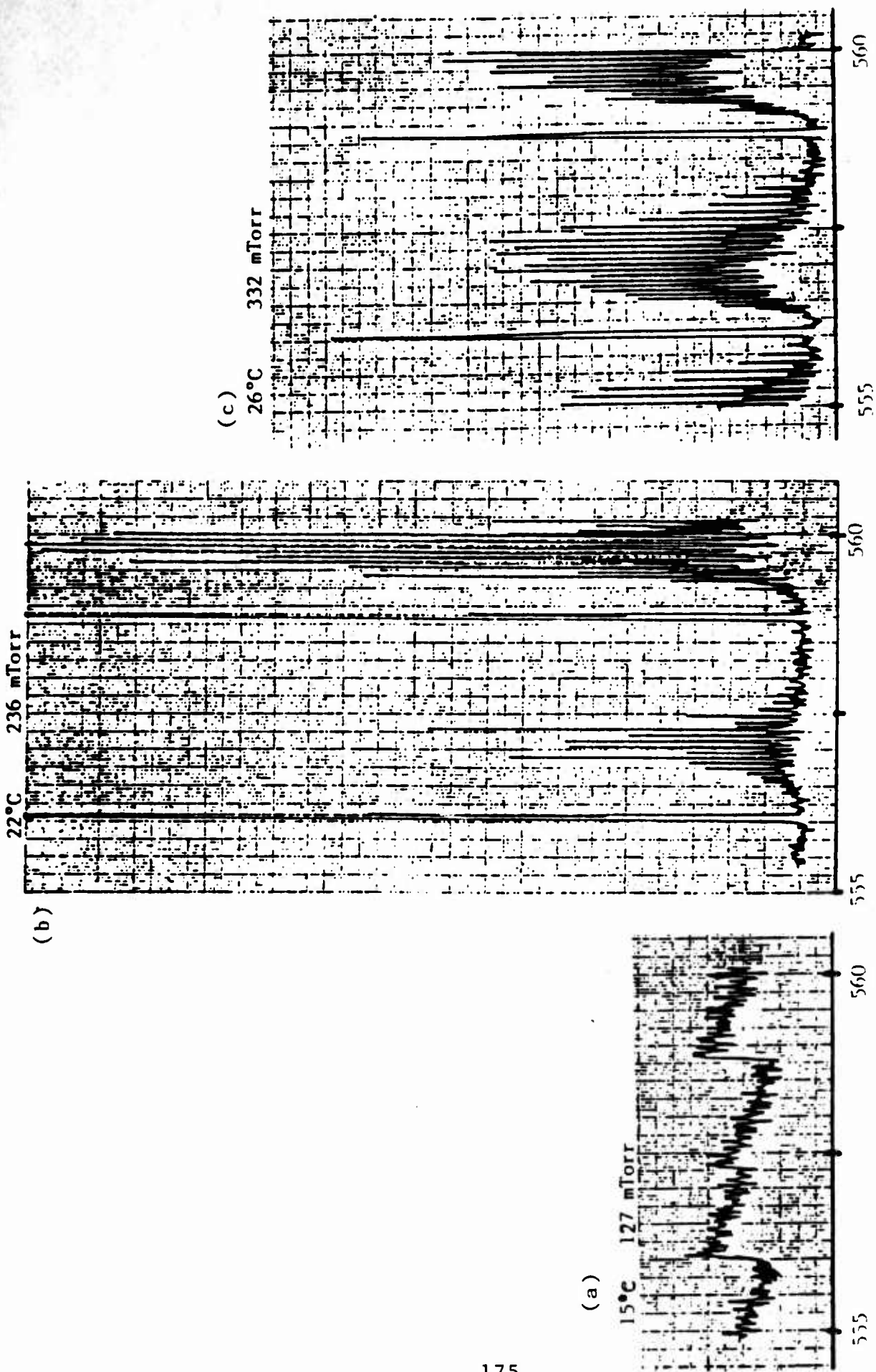
Figure G.5 Low Temperature ASE Excitation of (21,0).
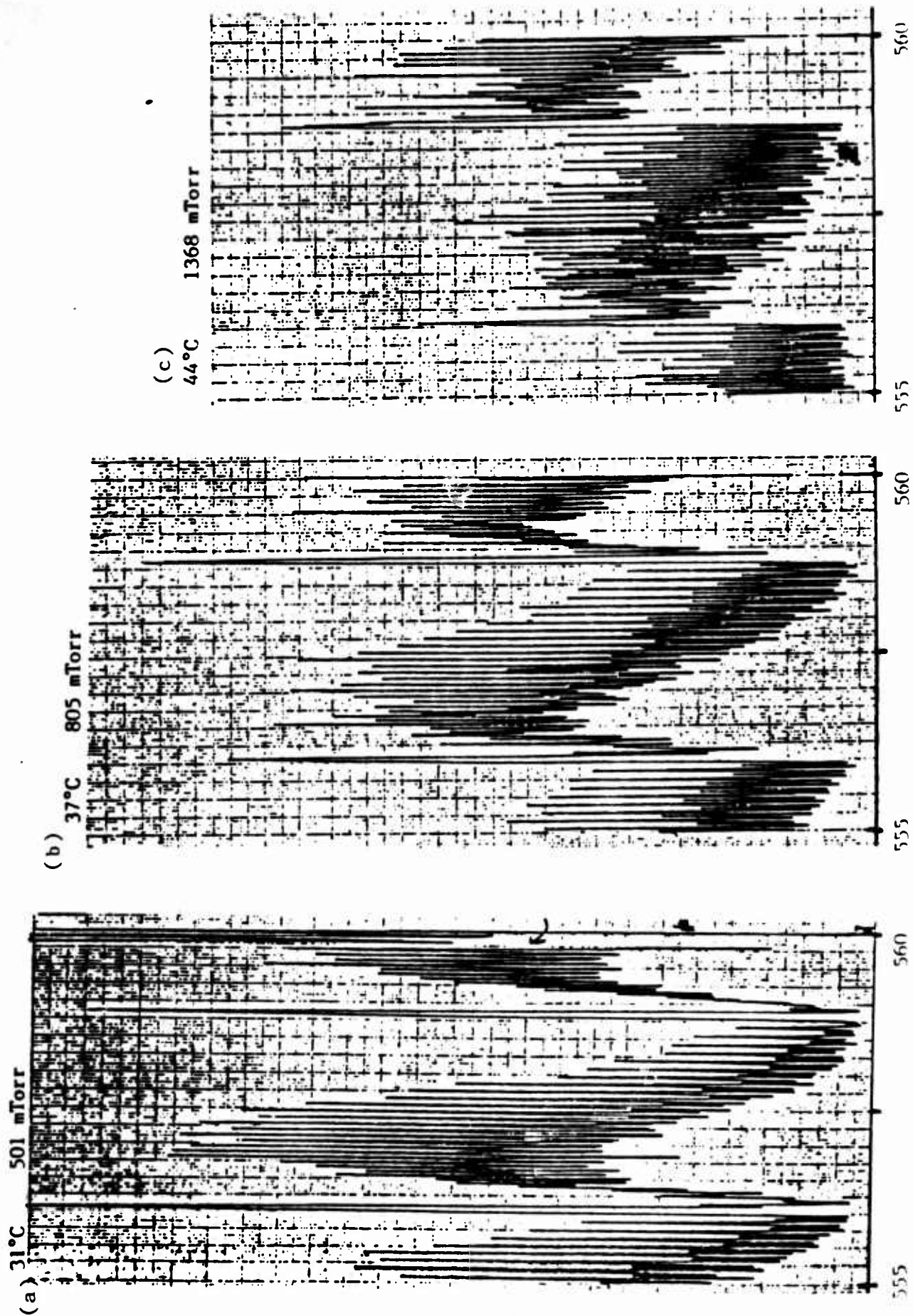
Figure G.6 Moderature Temperature ASE Excitation of (21,0).
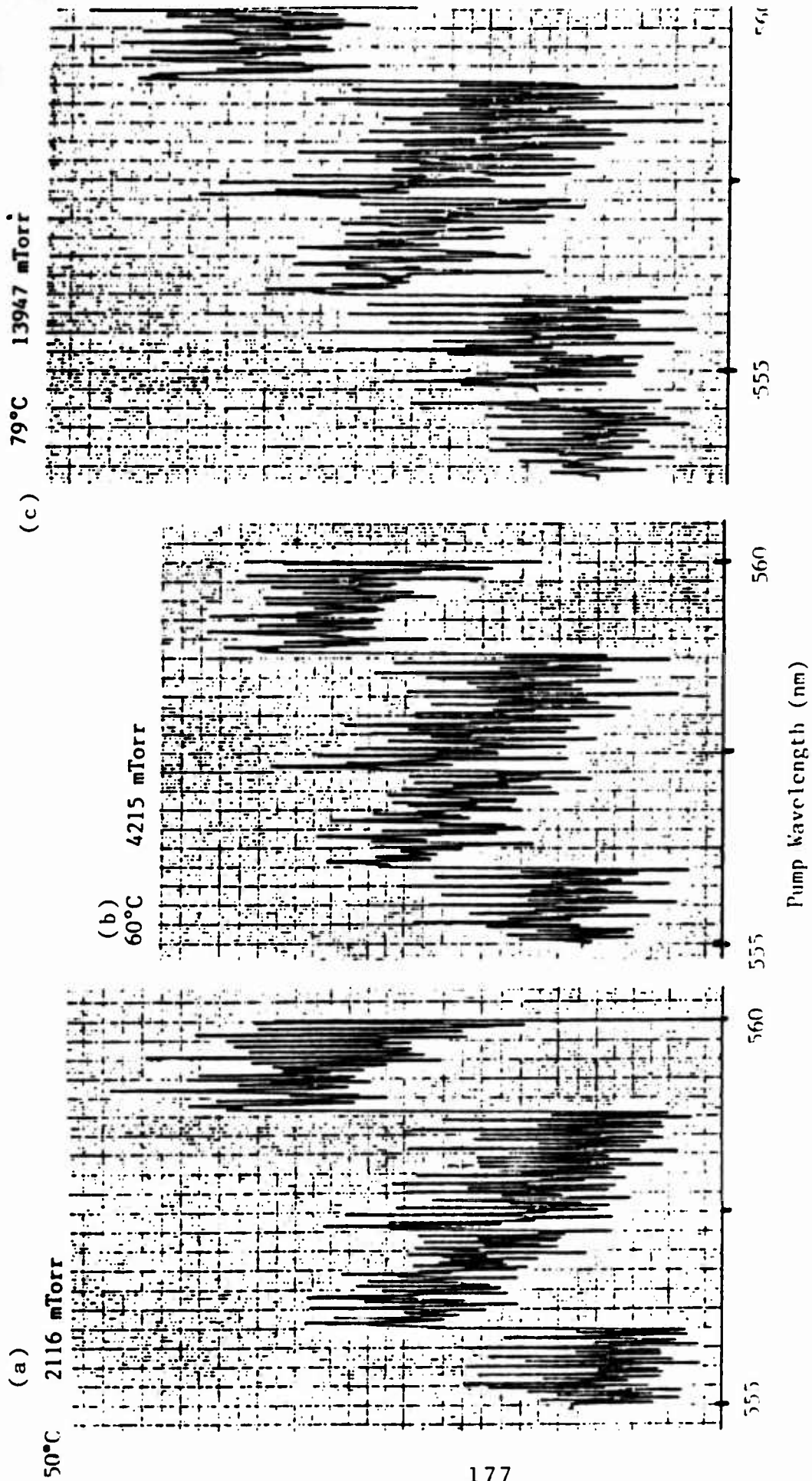
Figure G.7 High Temperature ASE Excitation of (21,0).
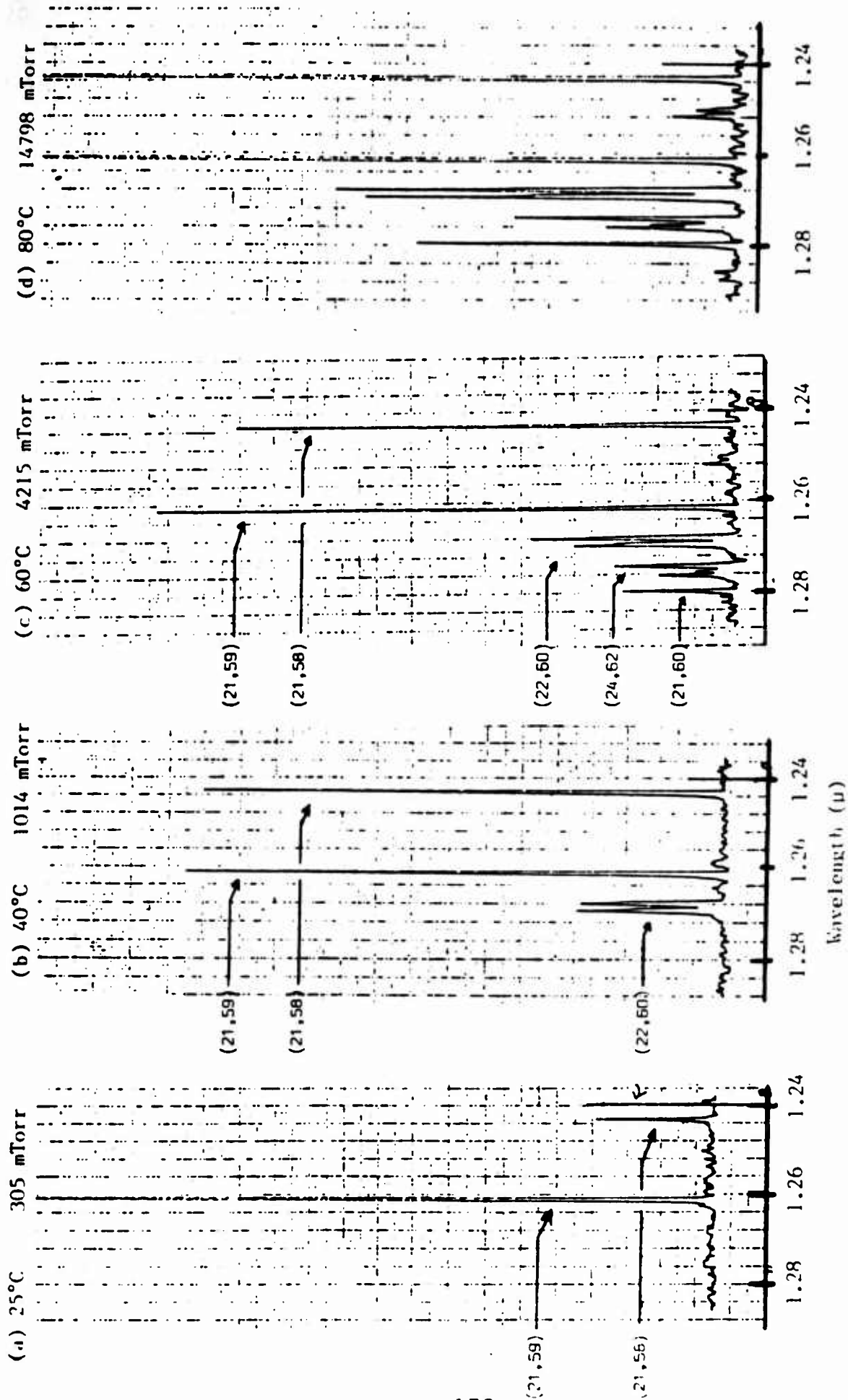
Figure G.8 ASE High Temperature Emission Spectra. Hot band emission is observed. Pump wavelength is 556 nm. A 0.3 m monochromator with 50μm slit width was used.

178

Synthetic Spectrum Computer Code

The following computer listing is the FORTRAN V code
used to generate synthetic excitation spectra.  The code
incorporates the concept of cooperative stimulated emission.
See text for a detailed description of the program.

```
Xfile name=iodine
      program iodine  (input,output,tape5=input,tape6=output,tape99)
c
c        this program generates a synthetic ase excitation
c        spectrum of iodine for plotting and in doing so
c        this program calculates the p and r transition
c        energy in vacuum, wavelength in air, and the
c        intensity of the line using the constants of
c        tellinghuisen (j mol spect 82 p.225 1980) and
c        luc (j mol spect 80 p.41 1980)
c        constants are reliable for v"=0-99 and v'=0-62
c
      dimension a(200,4),b(50,3),c(100,2),w(3000),xaxis(3000),em(1000)
      dimension gp(16),gdp(16),bp(13),bdp(13)
      dimension dp(9) ddp(9),hp(16),hdp(9)
c
      num=3000
      vp=21.
      vdp=0.
      vddp=59.
      wlo=5558.
      wlinc=0.01
      wlend=5588.
      th=12.5
c
      do 10 i=1,200
      do 10 j=1,4
   10 a(i,j)=0.0
c
      do 15 i=1,1000
   15 em(i)=0.0
c
c
c
c        calculate transition wavelengths and intensities
c
c
      do 50 icontrol=1,2
      e=0.
      bvp=0.
      bvdp=0.
      dvp=0.
      dvdp=0.
      hvp=0.
      hvdp=0.
      t=300.
c
c        constants for iodine x and b states
c
c        b state,electronic and vibrational
c
      data (gp(i),i=1,16)/15769.0485,125.6724,-0.752677,
     c-3.246282e-3,1.875736e-5,-3.414124e-6,2.004998e-7,
     c-6.950414e-9,1.517899e-10,-1.899790e-12,
     c1.226941e-14,-3.137312e-17,0.,0.,0.,0./
c
c        x state,electronic and vibrational
c
      data (gdp(i),i=1,16)/0.,2.1453866e+2,-6.18970919e-1,
     c1.6120443e-3,-4.101096637e-4,3.38088677e-5,-1.7898653e-6,
```

```
      c6.01983892e-8,-1.25300668e-9,1.35425963e-11,1.77848866e-14,
      c-2.87954337e-15,4.36352676e-17,-3.32846207e-19,
      c1.33752148e-21,-2.25287105e-24/
c
c        b state,rotational
c
        data (bp(i),i=1,13)/0.028993694599,-0.1406799398e-3,
      c-0.5088972976e-5,0.87511454030e-6,-0.1171736403e-6,
      c0.97025967839e-8,-0.5304859892e-9,0.195711232281e-10,
      c-0.4894864050e-12,0.81736417235e-14,-0.8715621632e-16,
      c0.53609973831e-18,-0.1445945450e-20/
c
        data (dp(i),i=1,9)/6.125767e-9,1.418420e-10,
      c-2.8525041e-12,5.54495e-13,-2.644252e-14,9.539521e-16,
      c-1.864100e-17,1.813907e-19,-6.053203e-22/
c
        data(hp(i),i=1,16)/-0.215004734e-14,0.7915679522e-14,
      c-0.102396618e-13,0.485261927e-14,-0.119975156e-14,
      c0.1792143124e-15,-0.175575349e-16,0.1185081818e-17,
      c-0.567595443e-19,0.1958960707e-20,-0.488849274e-22,
      c0.8739722535e-24,-0.109126306e-25,0.9034911061e-28,
      c-0.445560254e-30,0.9904029815e-33/
c
c        x state,rotational
c
        data (bdp(i),i=1,13)/3.736849e-2,-1.146334e-4,
      c-7.361611e-8,-2.745772e-8,9.539462e-10,-1.82729e-11,
      c1.353723e-13,-3.58803e-16,0.,0.,0.,0.,0./
c
        data (ddp(i),i=1,9)/1.5206,3.8326e-3,8.7e-5,1.9422e-6,
      c0.,0.,0.,0.,0./
c
        data (hdp(i),i=1,9)/1.8648,-1.2164e-2,2.5915e-3,-3.777e-5,
      c2.1678e-7,0.,0.,0.,0./
c
c        calculate the band origin
c
        do 60 j=1,16
        i=j-1
        e=e+gp(j)X(vp+0.5)XXi-gdp(j)X(vdp+0.5)XXi
   60 continue
c
c        calculate rotational constants
c
        do 70 i=1,13
        j=i-1
        bvp=bvp+bp(i)X(vp+0.5)XXj
        bvdp=bvdp+bdp(i)X(vdp+0.5)XXj
   70 continue
        do 80 i=1,9
        j=i-1
        dvp=dvp+dp(i)X(vp+0.5)XXj
        dvdp=dvdp+ddp(i)X(vdp+0.5)XXj
        hvdp=hvdp+hdp(i)X(vdp+0.5)XXj
   80 continue
        dvdp=1.0e-9Xexp(dvdp)
        hvdp=-1.0e-16Xexp(hvdp)
        do 90 i=1,16
        j=i-1
        hvp=hvp+hp(i)X(vp+0.5)XXj
```

```fortran
   90 continue
c
      if(icontrol.eq.2) goto 120
c
c       calculate energy of the p and r branches
c
      do 100 i=1,100
      ii=i+100
      j=i-1
      k=i+1
      a(i,1)=e+i*(bvp*k-bvdp*j)-(i**2)*(dvp*k**2-dvdp*j**2)+
     c(i**3)*(hvp*k**3-hvdp*j**3)
      a(ii,1)=e+i*(bvp*j-bvdp*k)-(i**2)*(dvp*j**2-dvdp*k**2)+
     c(i**3)*(hvp*j**3-hvdp*k**3)
c
c       calculate intensity of the p and r branches
c
      ejdp=bvdp*j*i-dvdp*((j*i)**2)
      eidp=bvdp*i*k-dvdp*((i*k)**2)
      ins=(-1)**j
      s=5./6.
      if (ins.lt.0) s=7./6.
      ss=7./6.
      if (ins.lt.0) ss=5./6.
      a(i,2)=s*i*exp(-ejdp/(0.695*t))
      a(ii,2)=ss*i*exp(-eidp/(0.695*t))
  100 continue
c
      vdp=vddp
   50 continue
  120 continue
      do 130 i=1,100
      ii=i+100
      j=i-1
      k=i+1
      il=i-1
      a(i,3)=e+i*(bvp*k-bvdp*j)-(i**2)*(dvp*k**2-dvdp*j**2)+
     c(i**3)*(hvp*k**3-hvdp*j**3)
      a(ii,4)=e+i*(bvp*j-bvdp*k)-(i**2)*(dvp*j**2-dvdp*k**2)+
     c(i**3)*(hvp*j**3-hvdp*k**3)
      if(il.le.0) goto 130
      a(ii,3)=a(il,3)
  130 continue
      do 135 i=1,100
      ii=i+101
      if(ii.gt.200) goto 135
      a(i,4)=a(ii,4)
  135 continue
c
c       convert to wavelength
c
      do 140 i=1,200
      do 140 j=1,4
      if(j.eq.2) goto 140
      if(a(i,j).eq.0.0) goto 140
      a(i,j)=a(i,j)*(1.+1.0e-7*(2726.43+12.288e-8*a(i,j)**2+
     c0.3555e-16*a(i,j)**4))
      a(i,j)=1.0e+8/a(i,j)
  140 continue
c
```

```
c
c
c          compute the excitation spectrum
c
c
      do 300 n=1,num
      w(n)=0.0
      pump=wlo+wlinc*float(n)
      xaxis(n)=pump
      do 312 i=1,50
      do 312 j=1,3
  312 b(i,j)=0.0
      do 314 i=1,100
      do 314 j=1,2
  314 c(i,j)=0.0
c
c          calculate pumping intensities
c
      icontrol=1
      do 310 m=1,200
      str=exp(-((a(m,1)-pump)/0.10)**2)
      str=str*a(m,2)
      if(str.lt.0.01) goto 310
      b(icontrol,1)=str
      do 320 mx=3,4
      my=mx-1
      b(icontrol,my)=a(m,mx)
  320 continue
      icontrol=icontrol+1
  310 continue
      ib=icontrol-1
      if(ib.eq.0) goto 300
c
c          load new matrix
c
      do 330 i=1,ib
      ic=2*i
      id=2*i-1
      c(id,1)=b(i,1)/2.
      c(id,2)=b(i,2)
      c(ic,1)=b(i,1)/2.
      c(ic,2)=b(i,3)
  330 continue
      icc=2*ib
c
c          compute emission gain profile
c
      emax=0.0
      do 340 i=1,icc
      if(c(i,2).gt.emax) emax=c(i,2)
  340 continue
      emin=emax-7.
      emax=emax+0.05
      emin=emin-0.05
      inc=int((emax-emin)*100.)
c
      do 350 i=1,inc
      ai=0.0
      do 355 j=1,icc
      value=abs((c(j,2)-emin-float(i)*0.01)/0.02)
```

```fortran
      if(value.gt.5.0) value=5.0
      ai=ai+c(j,1)*exp(-(value**2))
  355 continue
      em(i)=ai
  350 continue
c
c     subtract off threshold and sum result
c
      do 360 i=1,inc
      em(i)=em(i)-12.5
      if(em(i).lt.0.0) em(i)=0.0
      w(n)=w(n)+em(i)
  360 continue
  300 continue
c
c     find the max intensity for the plots
c
      wmax=1.0
      do 500 i=1,num
      if(w(i).gt.wmax) wmax=w(i)
  500 continue
c
c
c     plot the excitation spectra
c
c
      call meta
      call bgnpl(0)
      call duplx
      call basalf('l/cstd')
      call mx3alf('inst','x')
      call mixalf('standard')
      call grace(0.0)
      call xticks(10)
      call yticks(5)
      call yintax
      call title('(iodine ase) 21,0 (excitation spectrum)$',-100
     c,'(wavelength)$',100,'(intensity)$',100,9.0,6.0)
      call graf(wlo,1.,wlend,0.0,'scale',wmax)
      call curve(xaxis,w,num,0)
      call endpl(0)
      call donepl
      stop
      end
*cft I=iodine
*ldr lib=disspla,go
*dispose dn=tape99,mf=fa,df=sb,dc=st,sdn=aaa,id=jwg,wait
```

Spontaneous Predissociation and ASE

The $B^3\Pi(0_u^+)$ state of iodine has long been known to possess a natural, rotationally dependent spontaneous predissociation [6]. The inverse collision free lifetime $\Gamma$ of any particular rovibronic state takes the form

$$\Gamma = \Gamma_0 + K_{v'}J'(J'+1) \tag{I.1}$$

where $\Gamma_0$ is the radiative lifetime and $K_{v'}$ is the spontaneous predissociative rate constant that depends on $v'$. The $K_{v'}$ values vary greatly but are small, generally less than 30 $s^{-1}$ [6].

How important is the predissociative loss from the upper ASE level, during the time it takes ASE to occur? To answer this question, consider the following conditions [6]

$$K_{v'} = 30 \ s^{-1}$$
$$\Gamma_0 = 10^6 s^{-1}$$
$$J' = 10 \text{ and } 50$$
$$t = 30 \text{ ns}$$

which are used to calculate the fraction F of molecules in the excited state after the time t

$$F = \exp(-t\Gamma) \qquad (I.2)$$

where the time t = 30 ns is the typical ASE pulse length
from Appendix K.  The results from the calculations are

$$F = 0.970 \text{ for } J' = 10$$
$$F = 0.968 \text{ for } J' = 50$$

The difference between the two cases is 0.2%, which is
insignificant compared to other sources of error in the
buffer gas studies.  Therefore, the rotationally dependent
spontaneous predissociation has no measurable effect on the
buffer gas results.

Buffer Gas Quenching Curves

The following is a complete list of buffer gas quenching data for He, Ar, Xe, and $N_2$ buffer gases. The pumped vibrational levels include $v' = 16$, $21$, $27$, and $34$. There are two curves per graph: one for the spiked emission and one for the normal band emission. See the text for the discussion of this data.
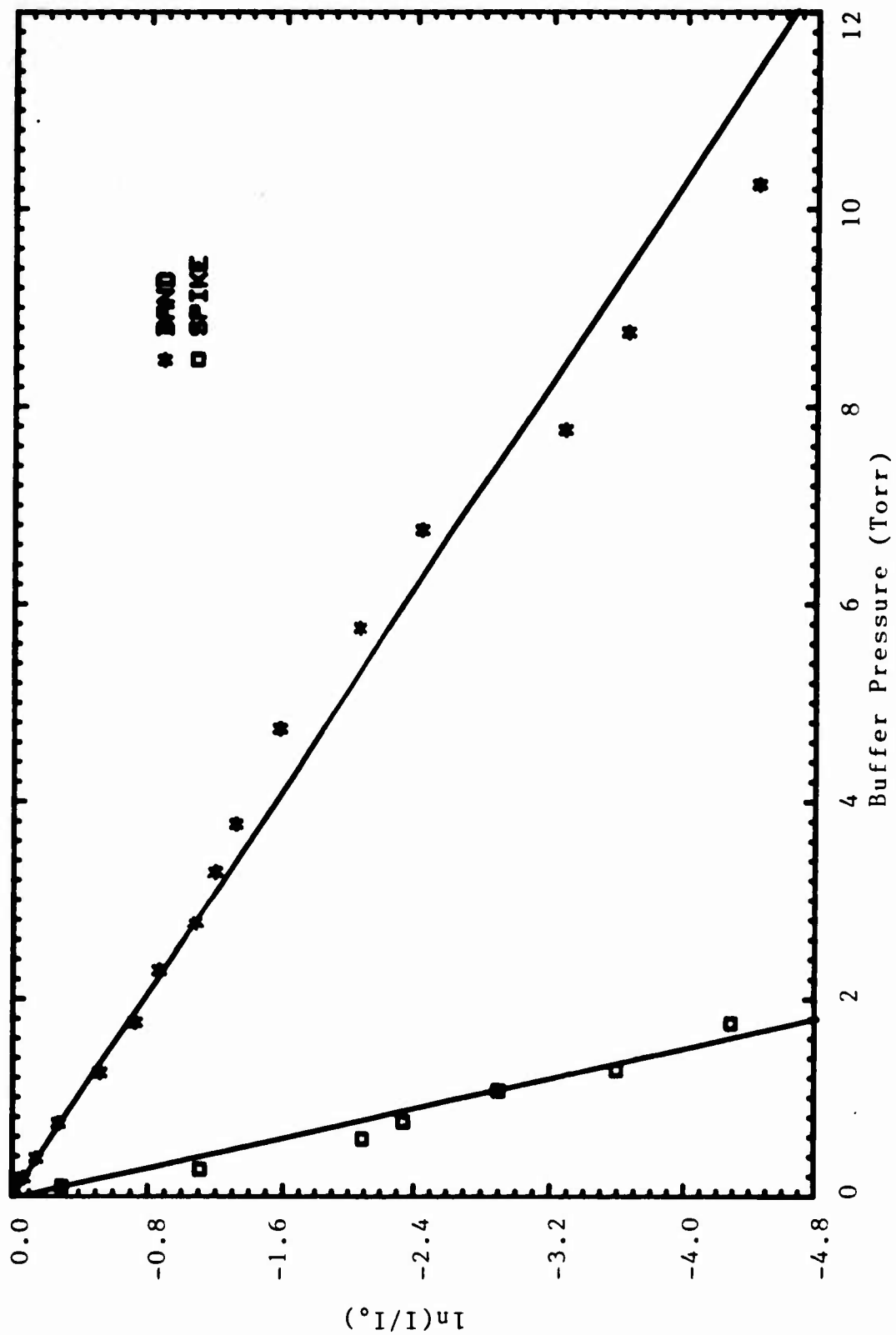
Figure J.1 Helium Buffer Quenching of ASE for (16,0). Pump wavelengths for the spike and band are 570.9 and 571.9 nm respectively.

188
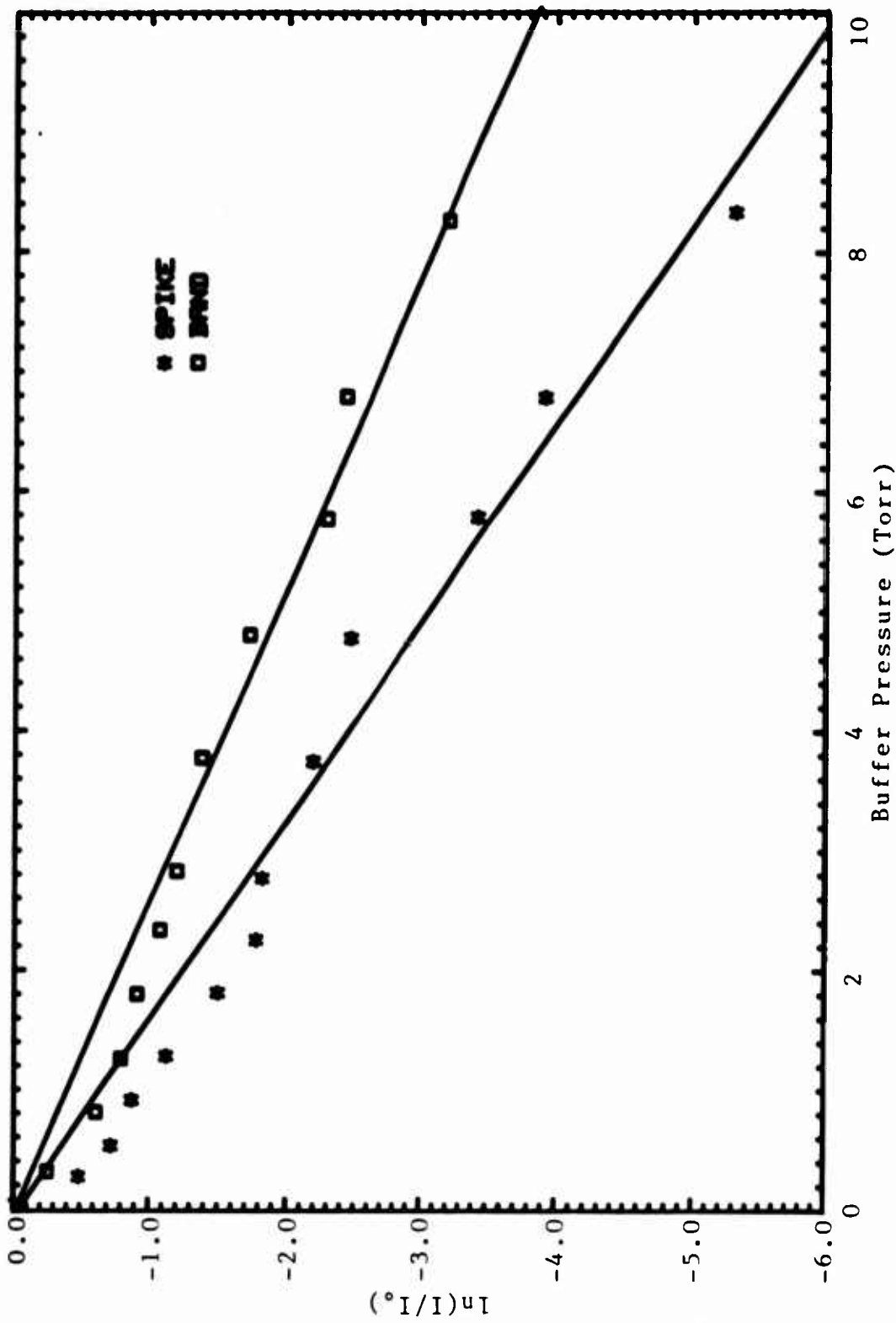
Figure J.2 Argon Buffer Quenching of ASE for (16,0). Pump wavelengths for the spike and band are 570.9 and 571.9 nm respectively.

189
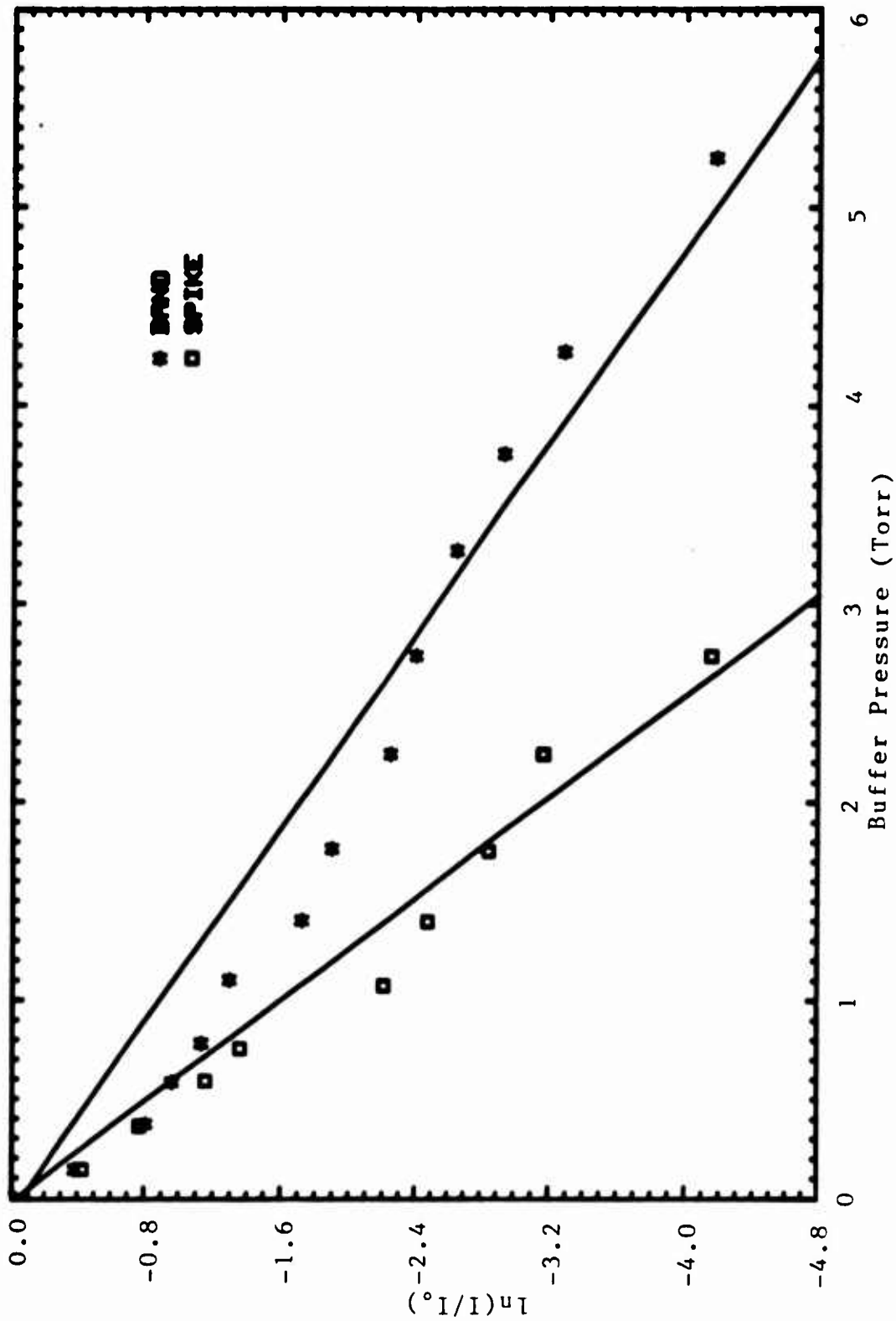
Figure J.3 Xenon Buffer Quenching of ASE for (16,0). Pump wavelengths for the spike and band are 570.9 and 571.9 nm respectively.

190
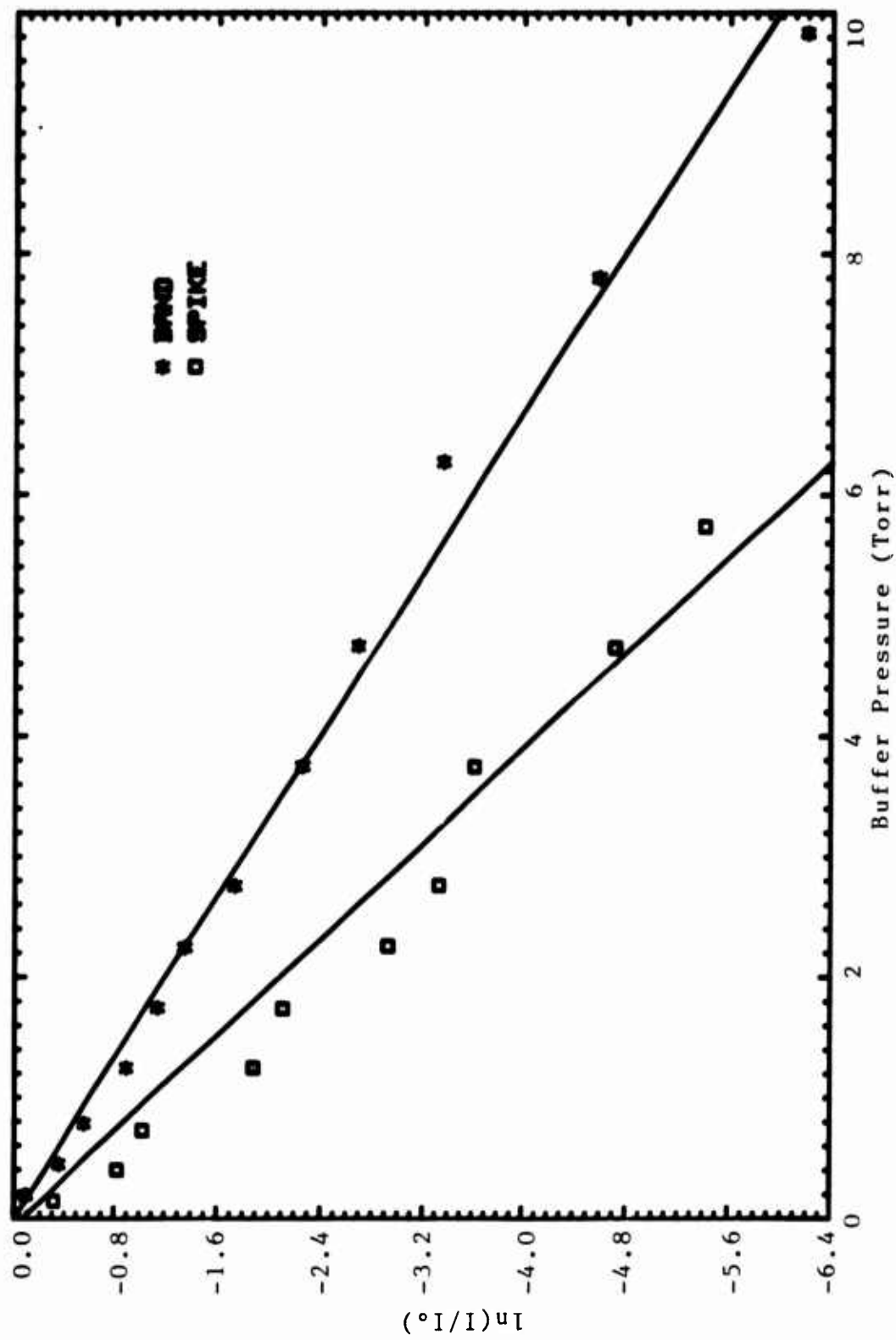
Figure J.4 Nitrogen Buffer Quenching of ASE for (16,0). Pump wavelengths for the spike and band are 570.9 and 571.9 nm respectively.

191
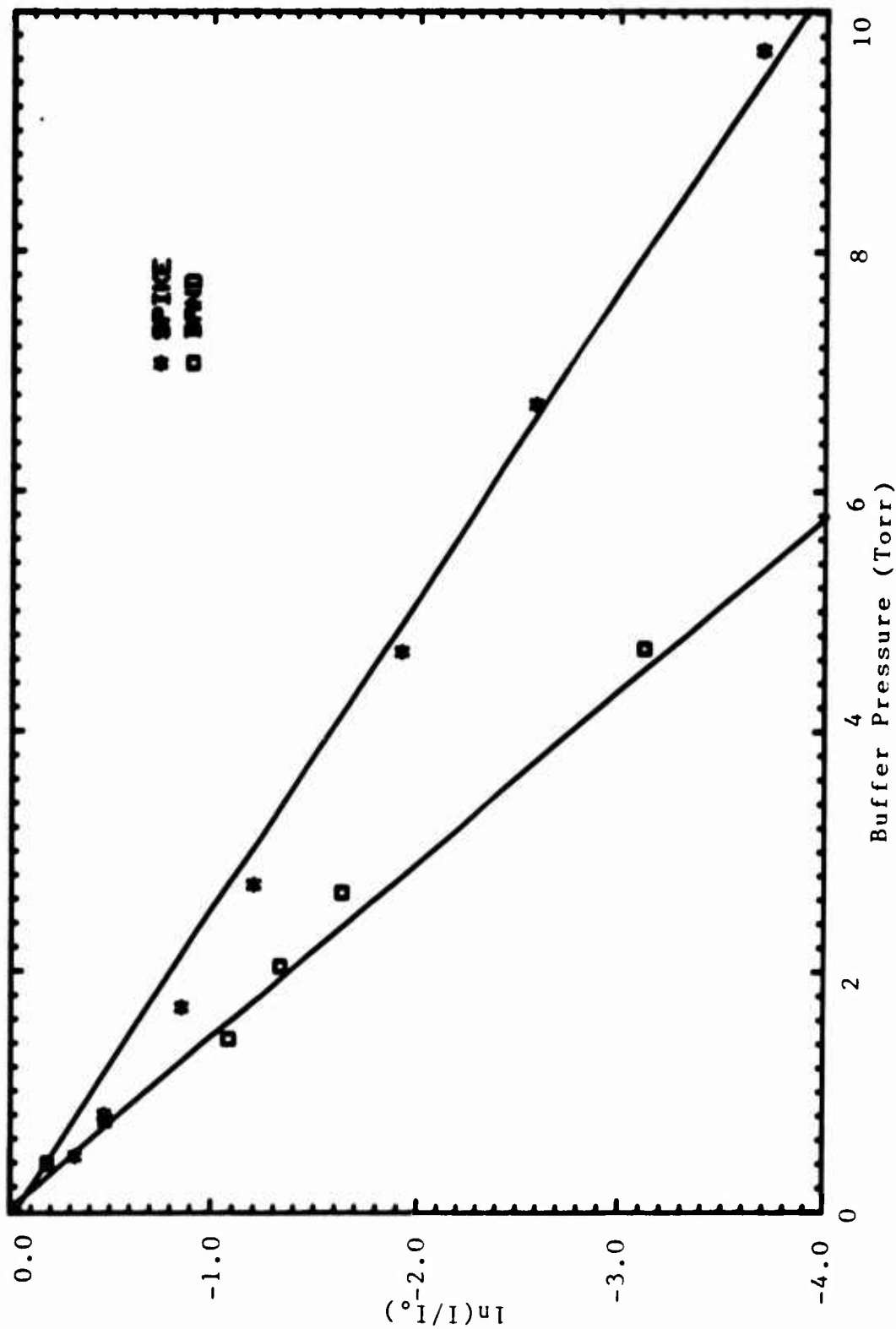
Figure J.5 Helium Buffer Quenching of ASE for (23,0). Pump wavelengths for the spike and band are 550.7 and 551.7 nm respectively.
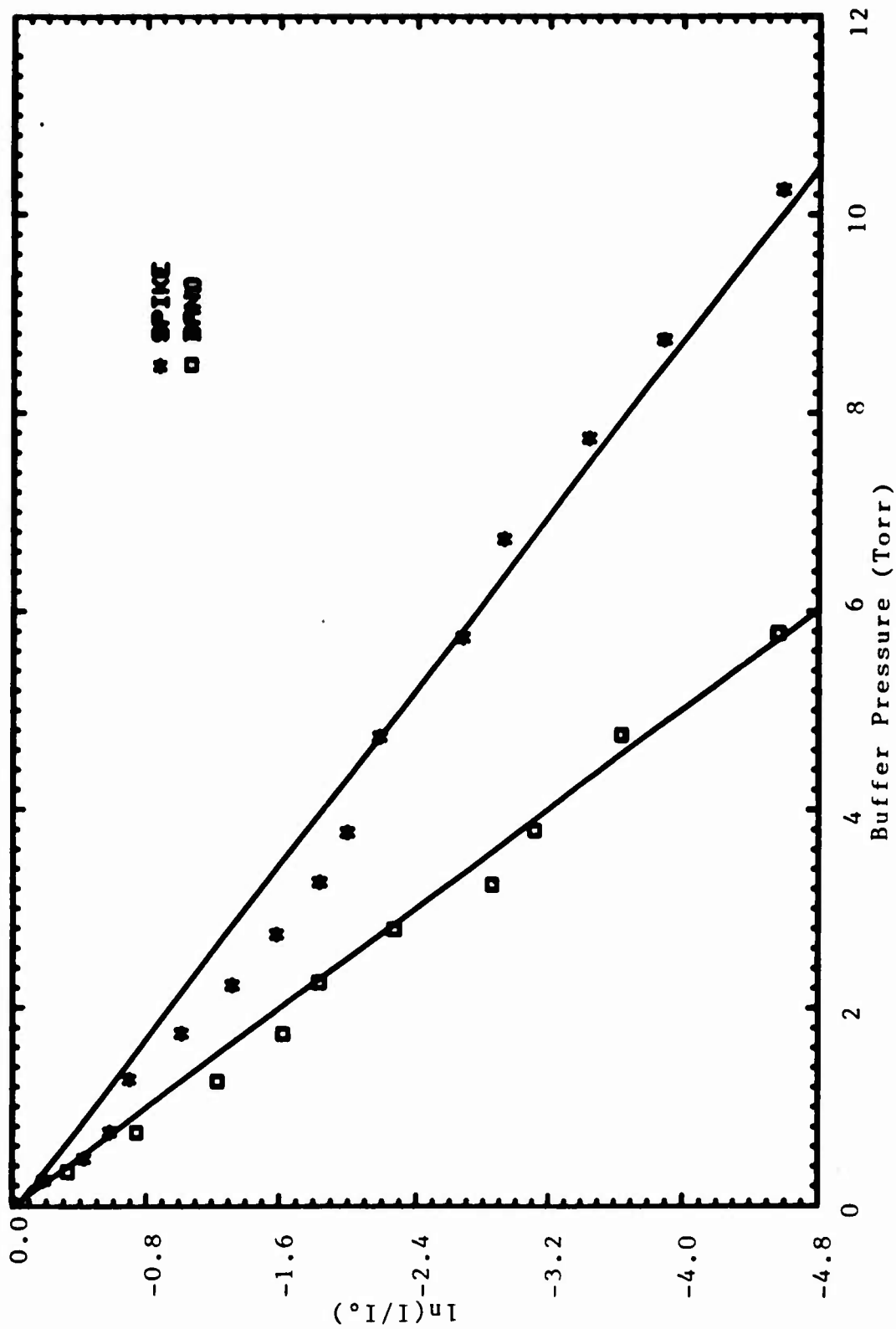
Figure J.6 Argon Buffer Quenching of ASE for (23,0). Pump wavelengths for the spike and band are 550.7 and 551.7 nm respectively.

193
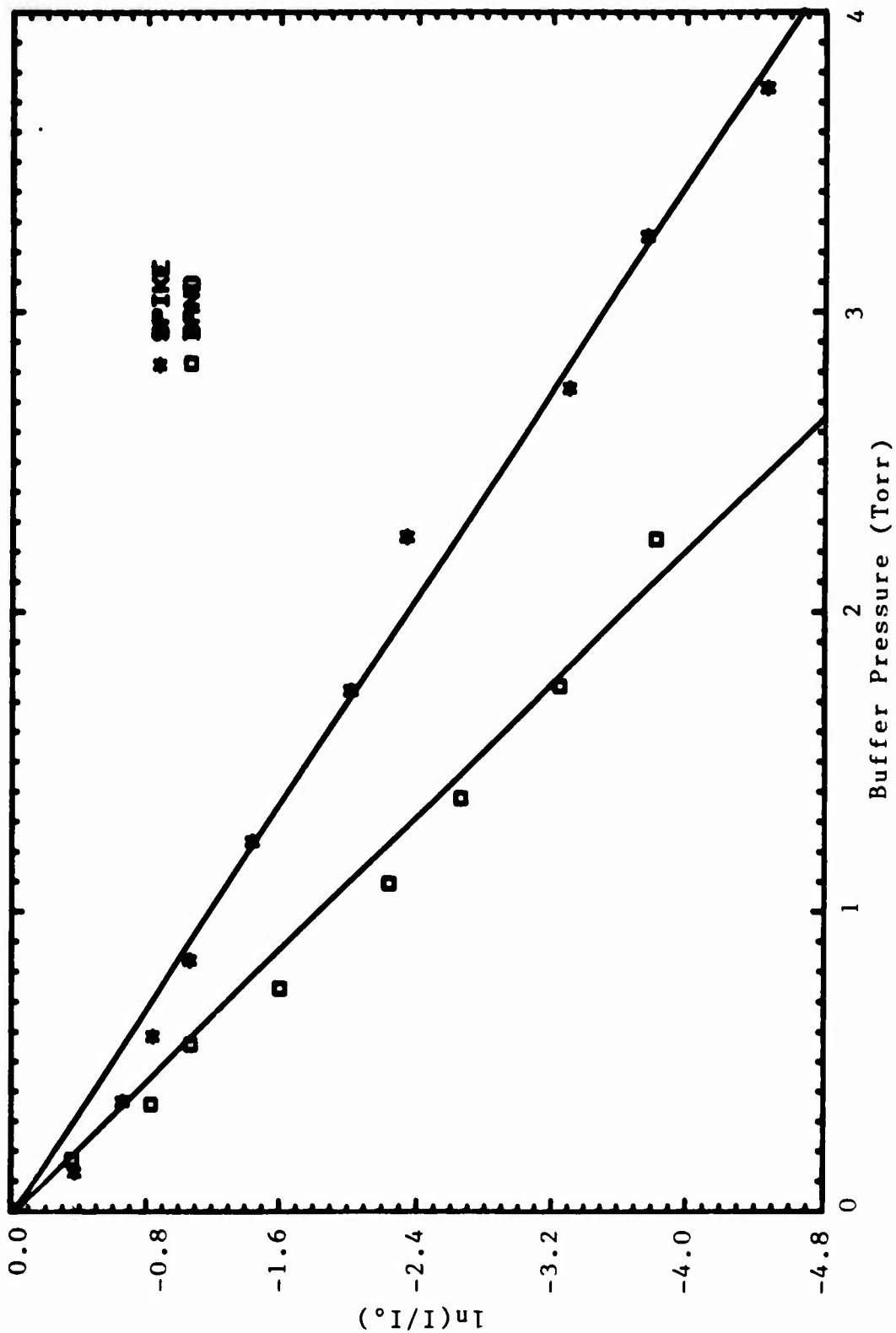
Figure J.7 Xenon Buffer Quenching of ASE for (23,0). Pump wavelengths for
the spike and band are 550.7 and 551.7 nm respectively.

194
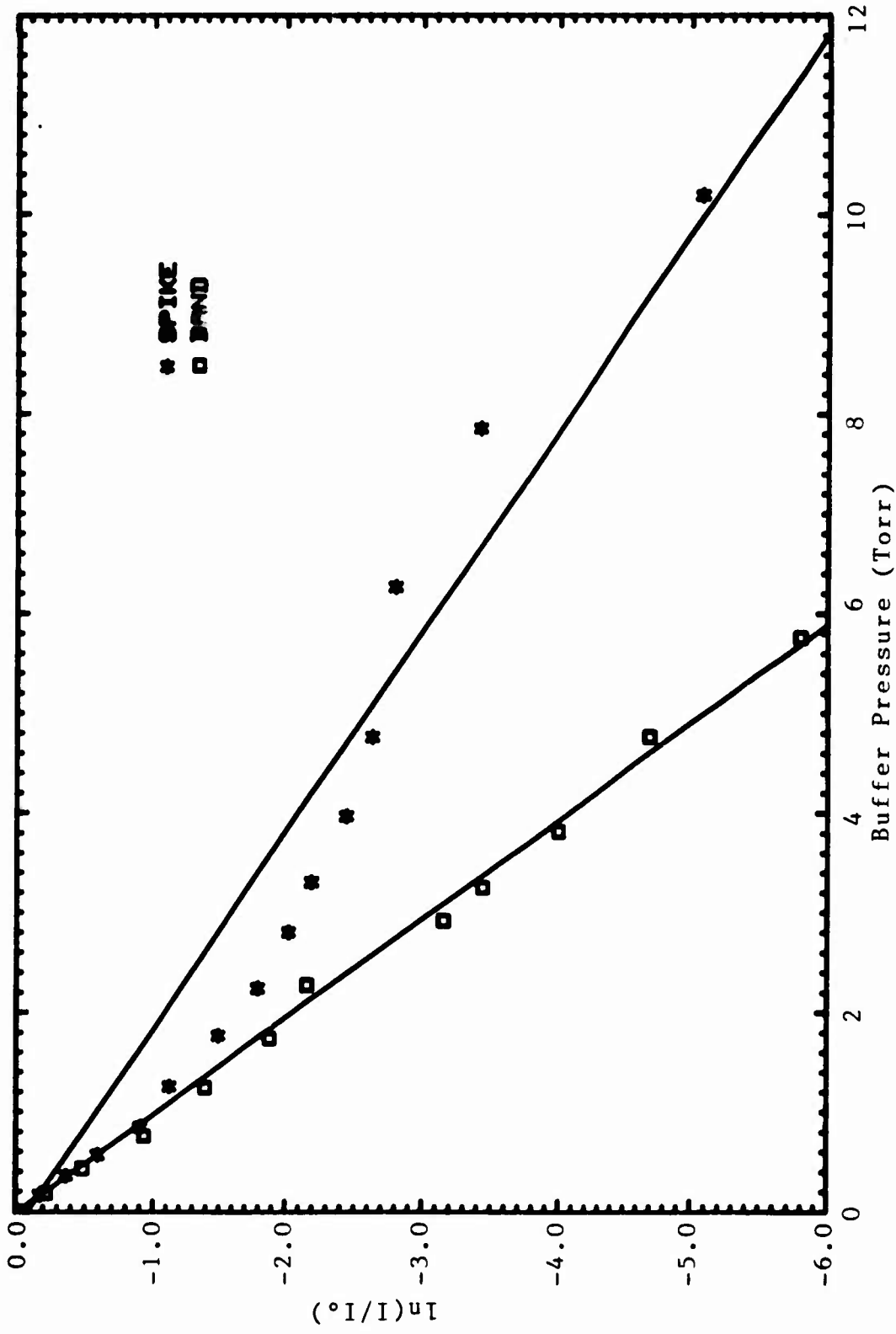
Figure J.8 Nitrogen Buffer Quenching of ASE for (23,0). Pump wavelengths for the spike and band are 550.7 and 551.7 nm respectively.

195
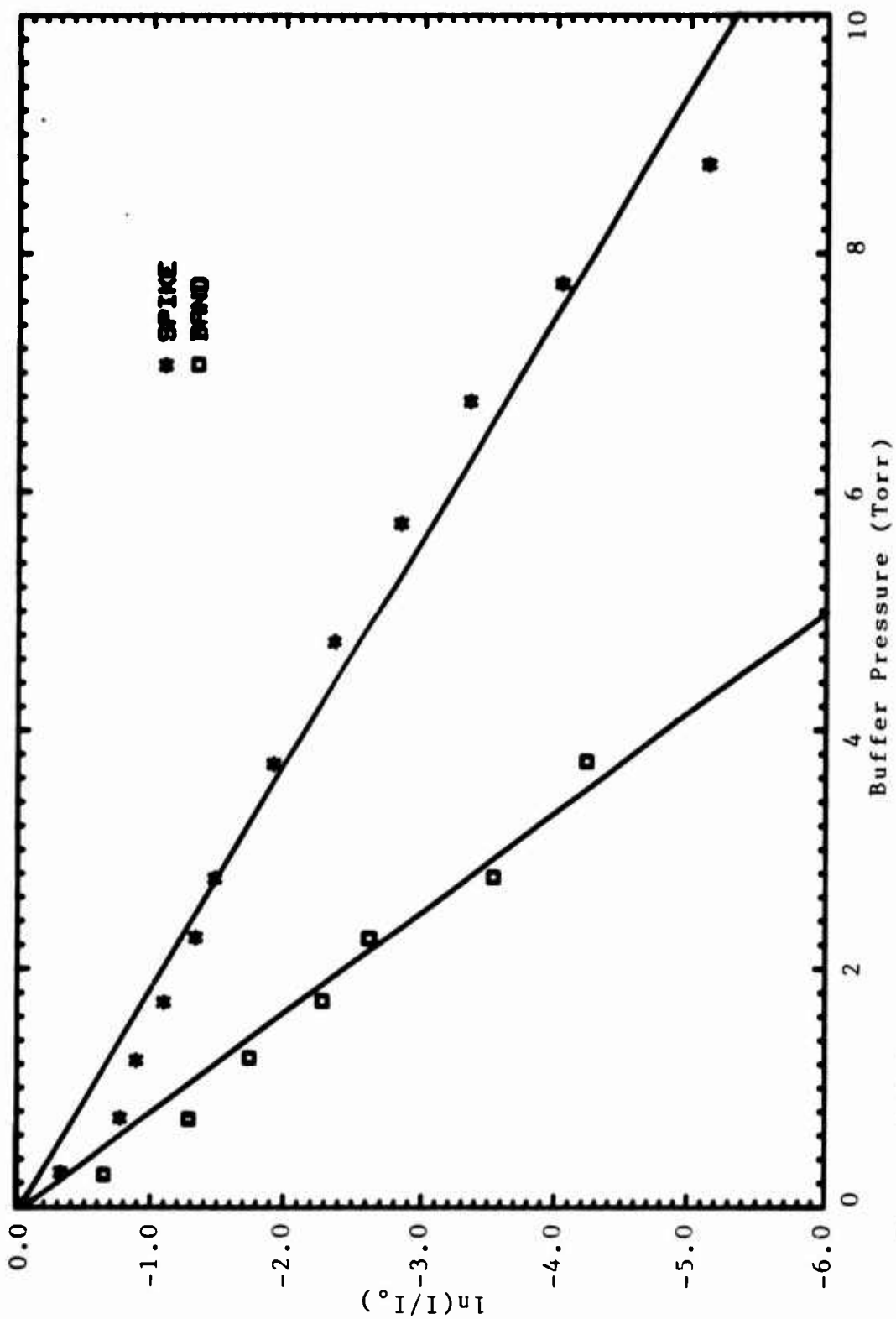
Figure J.9 Helium Buffer Quenching of ASE for (27,0). Pump wavelengths for the spike and band are 541.2 and 542.2 nm respectively.
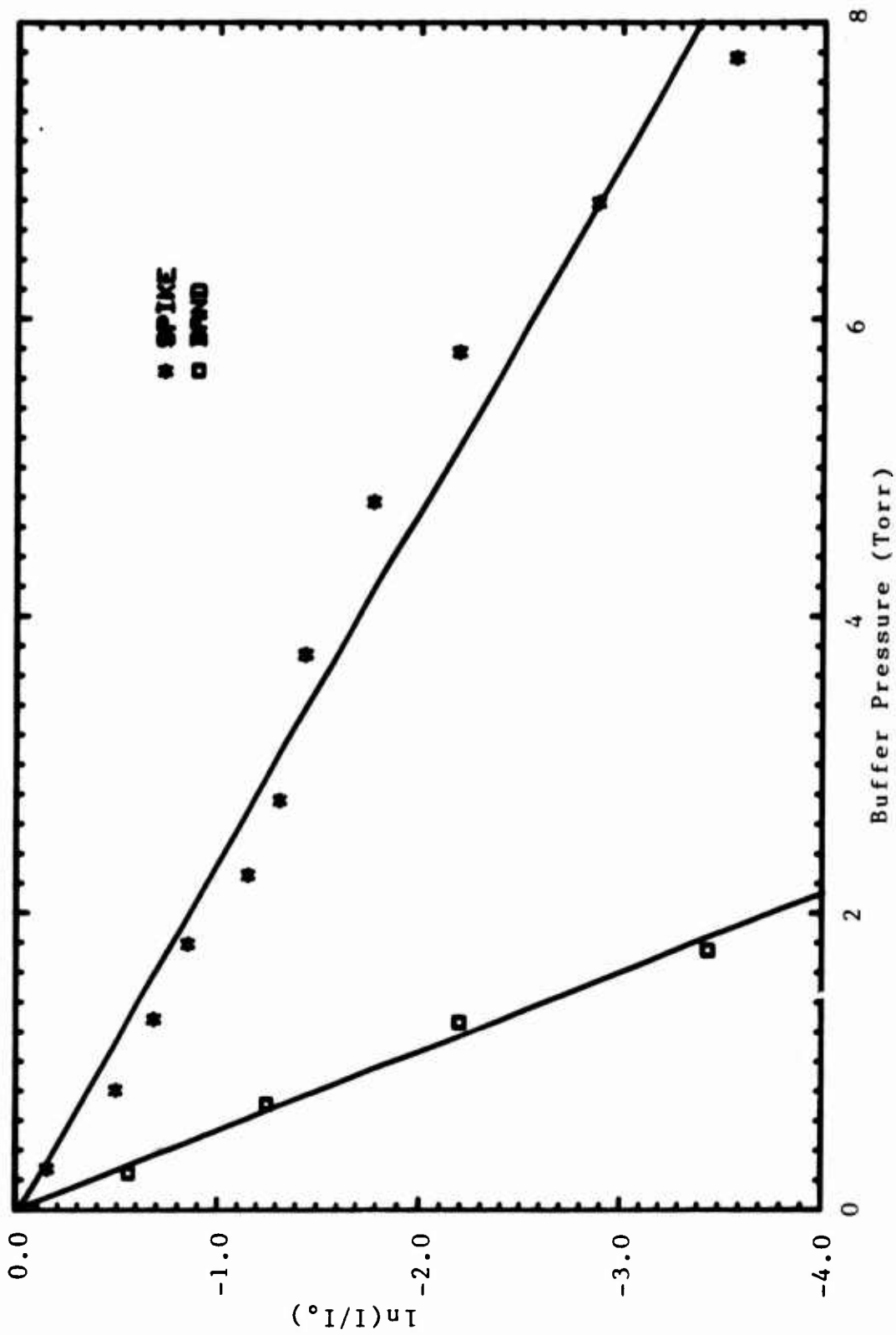
Figure J.10 Helium Buffer Quenching of ASE for (34,0). Pump wavelengths for the spike and band are 527.4 and 528.2 nm respectively.

APPENDIX K

Time Resolved ASE

The temporal profile of the ASE pulses was obtained by
using an Opto-Electronics high speed germanium photodiode
detector (PD 20-01). Signals were monitored on two
different oscilloscopes. An HP 7844 dual beam scope with
7A19 amplifiers was used for its fast responce time (1 ns).
Only multiple exposure photographs of the traces were
possible with this system (using Polaroid Type 612
Ultra-High Speed film, ASA 20,000). An HP 7633 storage
oscilloscope with 7A19 amplifier was also used with responce
time of 4 ns. The slower responce time was offset by the
ability to display and store one trace. ASE pulses were
observed under a wide variety of pump wavelengths, iodine
pressures, gain cell lengths, and buffer gases. Spectral
resolution of the temporal signal was also attempted.

The typical ASE pulse profile is shown in Figure K.1.
This figure is a tracing from a photograph of an
oscilloscope trace. Two peaks are generally observed in an
ASE pulse, with the relative heights of the peaks varing
somewhat on a shot-to-shot basis. The ASE signal begins
near the peak of the pump pulse. This compares with delay
times between the pump pulse and an iodine lasing pulse of
about 100 ns [20]. The laser delay time is due to the
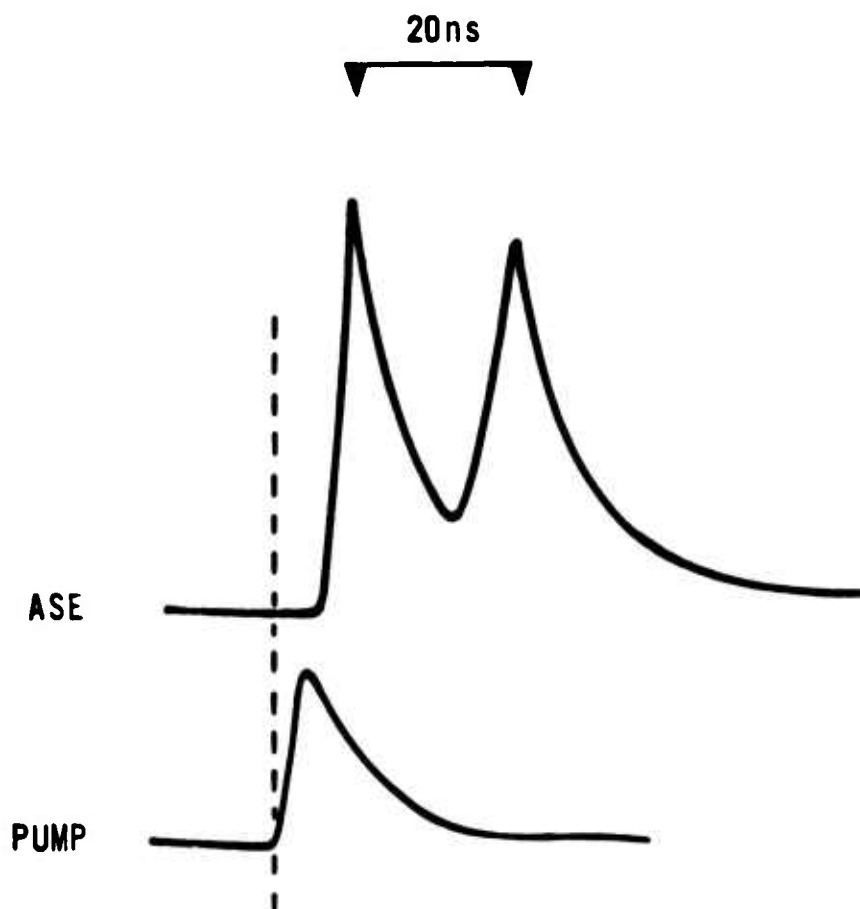
Figure K.1 Typical ASE Time Resolved Pulse. Also
shown is the pump pulse.
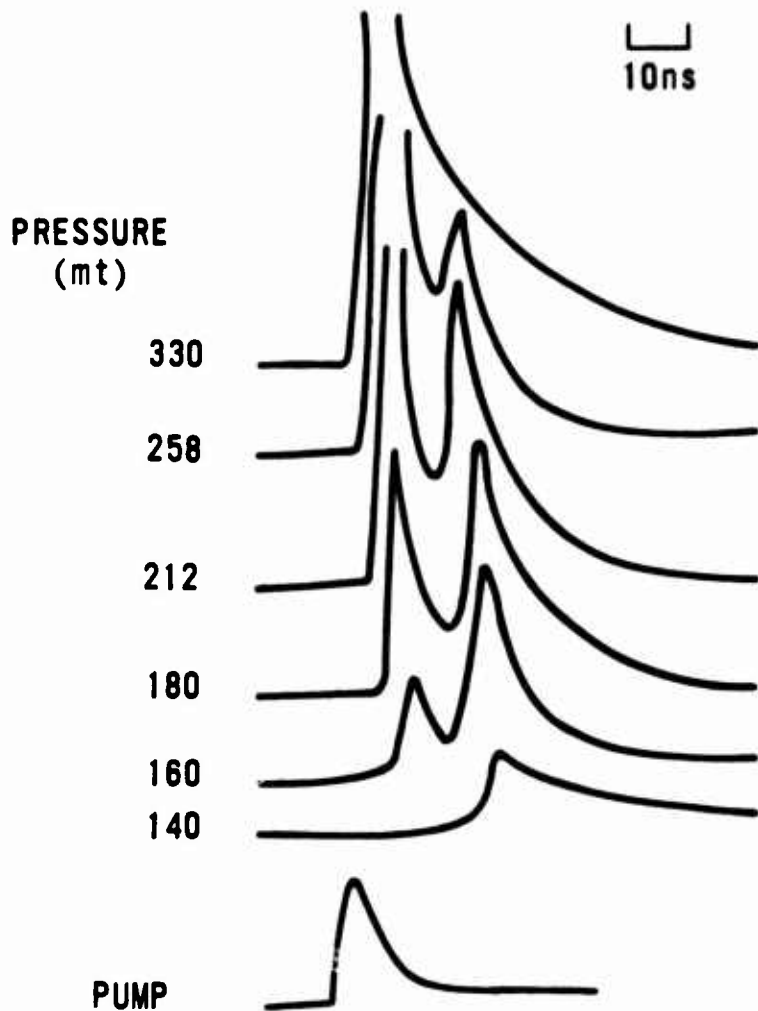
Figure K.2 ASE Time Resolved Pulse Variation with Iodine Pressure. Cell length is 223 cm. Pump Wavelength is 566.2 nm.

pulse and the start of the ASE pulse decreases as the iodine pressure increases.

The ASE temporal profile also reveals an unusual behavior when buffer gas is introduced. Figure K.3 shows an overlay of four tracings of increasing helium buffer gas pressure. As the buffer gas is introduced, the late pulse intensity is quickly reduced, while the early pulse shows little change. Only at very high buffer pressure does the early pulse lose intensity. The effect of the buffer gas is to introduces collisional losses of the initially pumped rotational levels, reducing the inversion. The results indicate that the late pulse is most sensitive to collisional losses. This is odd, when one considers that the late pulse is the first to appear at low iodine pressures. One would think that the effect of the buffer is simply to reduce the net gain, which is the same effect as reducing the iodine pressure. But the results here show the early and late pulses behaving differently under these two conditions.

In summary, the time resolved ASE output occurs for about 40 ns and is composed of two pulses about 15 ns apart. The qualitative behavior of these pulses, called the early and late pulse respectively, is summarized in Figure K.4. As the system gain is increased, the late pulse appears first and rapidly reaches its maximum value. The early pulse appears when the gain is well above threshold, and

202
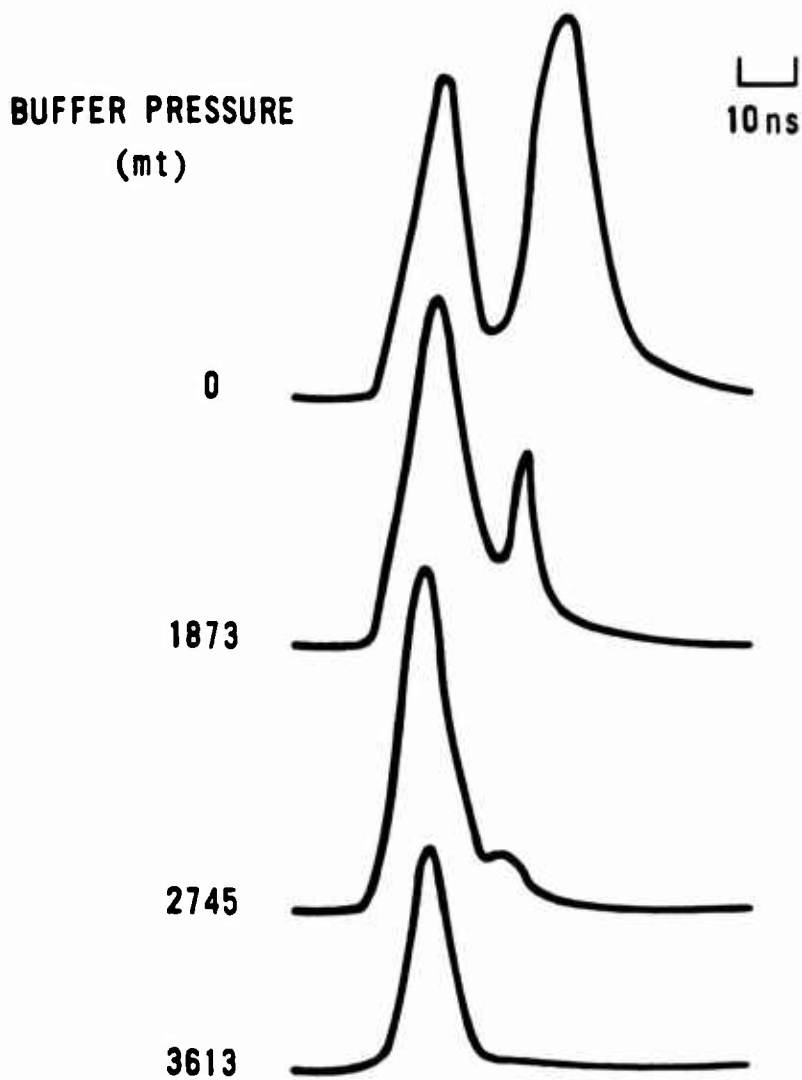
Figure K.3 ASE Time Resolved Pulse Variation with
Buffer Gas Pressure. Iodine pressure is 150 mTorr.
Cell length is 223 cm. Pump wavelength is 550.7 nm.
Buffer gas is helium.

203
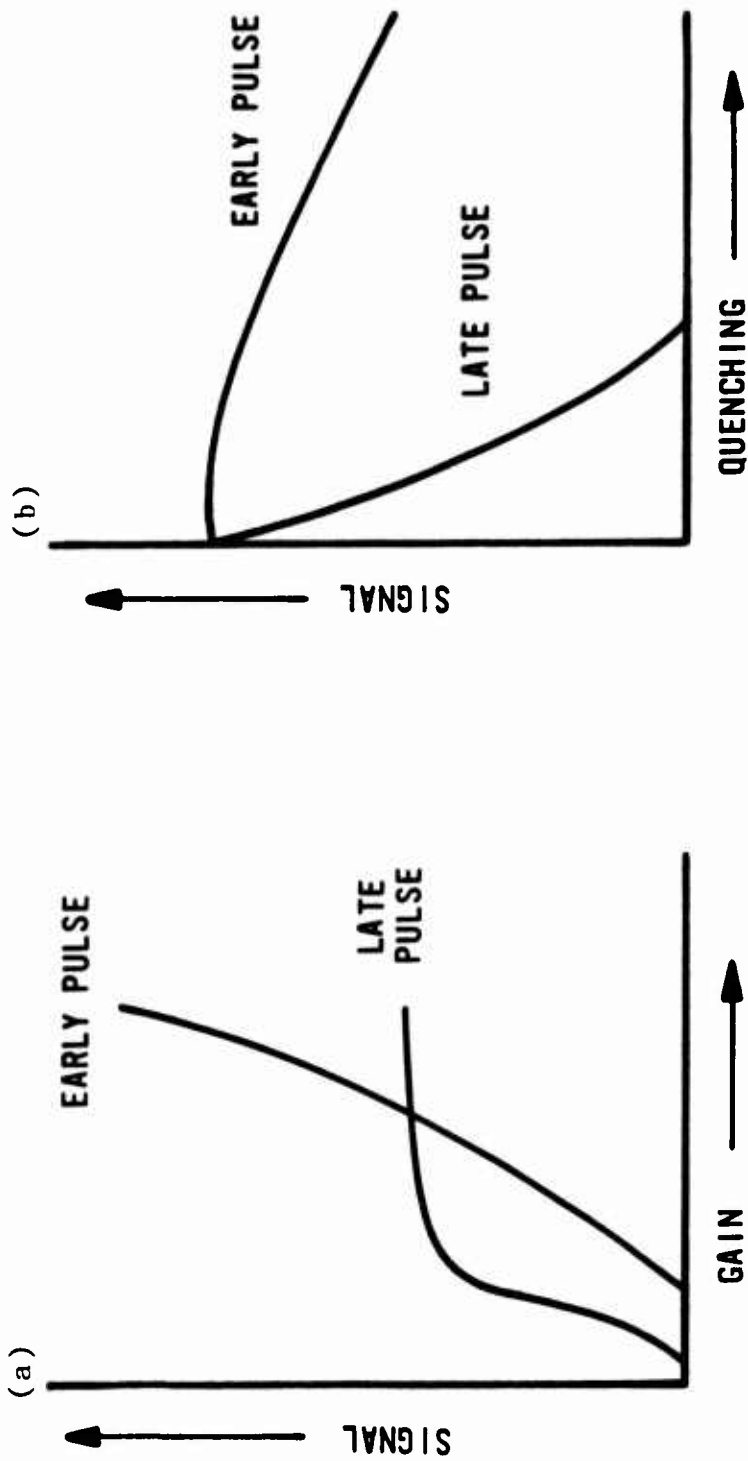
Figure K.4 Qualitative ASE Time Resolved Pulse Behavior. Variation with iodine pressure corresponds to a variation in gain, shown in (a). Variation with buffer gas pressure corresponds to a variation in collisional quenching, shown in (b).

204

continues to grow as gain is increased.  Buffer gas
quenching quickly diminishes the late pulse, while the early
pulse is little effected until the buffer gas pressure is
greatly increased.  The ASE temporal behavior is independent
of the gain cell length (for the 1 to 2.5 meters
investigated), spectroscopy, and spiked verses normal band
emission.  The reasons for the above behavior have not been
determined, and further work in this area is required.

# VITA

John Warren Glessner was born on ███████████████ ███████████████ He graduated with honors from ██████████████ ███████████████████████████████████████ and attended the University of Lowell from which he received a Bachelor of Science degree in Physics, Magna Cum Laude, in May 1979. Upon graduation, he was commissioned a Second Lieutenant in the United States Air Force through AFROTC. He then reported to duty at the Air Force Rocket Propulsion Laboratory, Edwards AFB, California. While there he worked on Pulsed Plasma Electric Propulsion in the Satellite Propulsion Branch. He then entered the Air Force Institute of Technology, Wright-Patterson AFB, Ohio from which he received a Master of Science degree in Engineering Physics in December 1982. Selected by the Air Force to continue his education, he was enrolled in the doctorate program at AFIT where he completed his course work for a Doctorate of Philosophy degree in Chemical Physics. He completed his dissertation at the Air Force Weapons Laboratory, Kirtland AFB, New Mexico in the Advanced Laser Technology Division. He is currently assigned to the Quantum Optics Branch of AFWL.

# REPORT DOCUMENTATION PAGE

| 1a. REPORT SECURITY CLASSIFICATION | 1b. RESTRICTIVE MARKINGS |
|---|---|
| Unclassified | N/A  A182570 |

| 2a. SECURITY CLASSIFICATION AUTHORITY | 3. DISTRIBUTION / AVAILABILITY OF REPORT |
|---|---|
| N/A | Approved for public release; distribution |
| 2b. DECLASSIFICATION / DOWNGRADING SCHEDULE | unlimited. |
| N/A | |

| 4. PERFORMING ORGANIZATION REPORT NUMBER(S) | 5. MONITORING ORGANIZATION REPORT NUMBER(S) |
|---|---|
| AFIT/DS/PH/87-2 | N/A |

| 6a. NAME OF PERFORMING ORGANIZATION | 6b. OFFICE SYMBOL (If applicable) | 7a. NAME OF MONITORING ORGANIZATION |
|---|---|---|
| Air Force Institute of Tech Wright-Patterson AFB, Oh 45433 | AFIT/ENA | N/A |

| 6c. ADDRESS (City, State, and ZIP Code) | 7b. ADDRESS (City, State, and ZIP Code) |
|---|---|
| Wright-Patterson AFB, Ohio 45433 | N/A |

| 8a. NAME OF FUNDING / SPONSORING ORGANIZATION | 8b. OFFICE SYMBOL (If applicable) | 9. PROCUREMENT INSTRUMENT IDENTIFICATION NUMBER |
|---|---|---|
| Air Force Weapons Laboratory | AFWL/AR | N/A |

| 8c. ADDRESS (City, State, and ZIP Code) | 10. SOURCE OF FUNDING NUMBERS | | | |
|---|---|---|---|---|
| | PROGRAM ELEMENT NO. | PROJECT NO. | TASK NO. | WORK UNIT ACCESSION NO. |
| Kirtland AFB, New Mexico 87117 | - | - | - | - |

**11. TITLE (Include Security Classification)**
Amplified Spontaneous Emission of the Iodine $B^3\Pi(0^+_u) - X^1\Sigma(0^+_g)$ System

**12. PERSONAL AUTHOR(S)**
John W. Glessner, Capt, USAF

| 13a. TYPE OF REPORT | 13b. TIME COVERED | 14. DATE OF REPORT (Year, Month, Day) | 15. PAGE COUNT |
|---|---|---|---|
| PhD dissertation | FROM 84/4/1 TO 87/5/20 | 87/5/20 | 218 |

**16. SUPPLEMENTARY NOTATION**

None

| 17. | COSATI CODES | | 18. SUBJECT TERMS (Continue on reverse if necessary and identify by block number) |
|---|---|---|---|
| FIELD | GROUP | SUB-GROUP | iodine          molecular spectroscopy |
| | | | amplified spontaneous emission |
| | | | cooperative emission |

**19. ABSTRACT (Continue on reverse if necessary and identify by block number)**

Amplified spontaneous emission (ASE) via optical pumping of the $I_2$(B-X) system has been studied. ASE was observed for v'=7-44 and v'=38-84 with excitation from 514-605 nm followed by emission from 1.07-1.34 um. The rotational dependence of the ASE displayed a cooperative stimulated emission (CSE) for excitation where several, simultaneously populated rotational levels emit within the Doppler width of any one of the levels involved. The emission occurs at a single frequency, centered on the emission bandhead transition frequency. The CSE was found to be remarkably immune to collisional quenching. The ASE output energy was studied as a function of iodine pressure, gain length, and pump energy. Output energies as high as 60 uJoules per pulse were recorded at 320 mTorr pressure and 204 cm cell length. Using the model that a single photon initiates ASE, a total gain of 33.6, or 16.5% per cm, was calculated from the above conditions. Energy conversion efficies of 2% were calculated. High temperature, up to 80°c, operation improved both output energy and efficiency. Possible application of iodine ASE as a wavelength converted was discussed.

| 20. DISTRIBUTION / AVAILABILITY OF ABSTRACT | 21. ABSTRACT SECURITY CLASSIFICATION |
|---|---|
| ☒ UNCLASSIFIED/UNLIMITED ☐ SAME AS RPT. ☐ DTIC USERS | Unclassified |

| 22a. NAME OF RESPONSIBLE INDIVIDUAL | 22b. TELEPHONE (Include Area Code) | 22c. OFFICE SYMBOL |
|---|---|---|
| Capt John W. Glessner | (505) 844-0475 | AFWL/ARBM |

DD FORM 1473, 84 MAR          83 APR edition may be used until exhausted          SECURITY CLASSIFICATION OF THIS PAGE
All other editions are obsolete.